A harmonic domain model for the interaction of the HVdc convertor with ac and dc systems

Bruce C. Smith

A thesis presented for the degree of
Doctor of Philosophy
in
Electrical and Electronic Engineering
at the
University of Canterbury,
Christchurch, New Zealand.

19 February 1996

ABSTRACT

This thesis describes a new steady state analysis of the HVdc convertor. Previous work is reviewed, and problems with accurate modelling of the convertor, and poor solution methods are discussed. A set of equations are derived that fully model the convertor in the steady state. The analysis of the convertor employs positive frequency harmonic phasor equations, and harmonic sampling using the discrete convolution. The equations so obtained are differentiable when decomposed to real and imaginary parts.

A fast and robust sparse Newton solution of the convertor equations is developed. Solutions are then obtained for a variety of unbalanced and resonant test systems, which are validated against time domain simulations. Since the ac/dc system and switching instant interactions are unified in a single unified solution, rapid convergence is obtained in all cases. Several other implementations of the Newton solution are investigated, and a sequence components solution is found to offer greater sparsity.

The Jacobian matrix of the Newton solution is used to derive linearised relationships between convertor variables. Of particular interest is the direct calculation of the convertor impedance, at an operating point, including the effect of control, commutation, and unbalance. Since the convertor impedance can be phase dependent, a new tensor representation of impedance is proposed, interpreted, and utilised in a tensor nodal analysis.

ACKNOWLEDGEMENTS

It is hard to imagine a more friendly and supportive environment within which to work and study for three years, and there are many people that I would like to thank for this. Sincere thanks must go to Dr Neville Watson and Prof. Jos Arrillaga, my supervisors, for inexhaustable and enthusiastic support, advice, and encouragement. Thank you Neville for capturing my interest in power systems analysis in 3rd Pro, with a project that has been the catalyst of much challenge and learning for me for four years now.

Dr Alan Wood has patiently endured countless discussions and advice giving sessions. Your lucid advice has rescued and inspired me on many occasions, and I am very grateful for your time and friendship.

I would also like to thank Maria-Luiza Lisboa, Simon Todd, Dave Waterworth, Du Zhen-Ping, Chen Shiun, Dinh Nhut-Quang, Dr. Stu Macdonald, Wade Enright, Roger Brough, Graeme Bathurst, Suo Li, and Chen Zheng-Hong for many refreshing discussions and distractions.

Finally, I would like to acknowledge the financial support I received through the University of Canterbury Doctoral Scholarship, and the William and Ina Cartwright Scholarship.

CONTENTS

LIST OF FIGURES

LIST OF TABLES

GLOSSARY

In order to simplify notation in this thesis, subscripts and superscripts are used to narrow the descriptive range of a symbol only were necessary. For example the range of the terminal voltage symbol, V, is successively narrowed as follows:

- V_P^D Three phase line to ground voltage harmonics across the equivalent star-g/delta transformer primary winding.
- V_{Pa}^D Phase 'a' line to ground voltage harmonics on the primary winding of the equivalent star-g/delta transformer.
- V_{Pak}^D kth harmonic phase 'a' line to ground voltage on the primary winding of the equivalent star-g/delta transformer.
- $\mathcal{I}\{V_{Pak}^D\}$ Imaginary part of the kth harmonic phase 'a' line to ground voltage on the primary winding of the equivalent star-g/delta transformer.

SUBSCRIPTS

$+, -$	Phases connected to positive and negative dc rails respectively
$0, -, +$	Three sequence labels
a, b, c	Three phase labels
(a, b)	Coordinates of centre of circular impedance locus
b	Phase beginning conduction
e	Phase ending conduction
i	Firing Number, $i = 1, 2, 3, 4, 5, 6$
I	Imaginary part of
k	Harmonic order
l	Harmonic order
m	Harmonic order
M	Magnitude
o	The phase not participating in a commutation
p	Conduction interval number, $p = 1 \cdots 12$
P	Primary side

R	Real part of
S	Secondary side
θ	Argument of

SUPERSCRIPTS

D	Associated with star-g/delta group
m	Measured quantity
S	Associated with star-g/star group
$\bar{X}$	X is a vector or a tensor
$\bullet$	Converged value

SYMBOLS

$\otimes$	Convolution operator
$*$	Conjugation operator
a	Angles of conduction interval beginnings
a_1, a_2	Off nominal tap ratios
b	Angles of ends of conduction intervals
C	Total time derivative of a static nonlinearity
D	Commutating current initial offset
$f(v(t))$	Arbitrary static function
F	Full mismatch vector in Newton's method
F_I	Ac side harmonic current mismatches
F_{Id}	Direct current harmonic ripple mismatches
F_S	Rectified power mismatch
F_V	Ac terminal harmonic voltage mismatches
F_{Vd}	Dc side harmonic voltage mismatches
F_W	Sequence components ac side harmonic voltage mismatches
$F_{\alpha 0}$	Average delay angle mismatch
F_θ	Firing mismatches
F_ϕ	End of commutation mismatches
$g(v(t), t)$	Arbitrary dynamic function
G	Current transducer gain
$i(t)$	Time domain current waveform
$i_c(t)$	Time domain commutatin current waveform
$\mathcal{I}$	Imaginary part of
I	Convertor three phase ac side harmonic currents
I_c	Commutating current harmonics
I_d	Convertor dc side harmonic currents

j	$\sqrt{-1}$
J	Jacobian Matrix
L	Commutating inductance
n_h	Highest harmonic order to be solved
$\mathcal{R}$	Real part of
P	Current controller proportional gain
P	Linear voltage sample matrix
P	Real power
$P_{measured}$	Measured dc side power
P_{order}	Power order
Q	Reactive power
r	Radius of circular impedance locus
R_{ac}	Total commutating resistance referred to ac system
R_c	Transformer conduction resistance
R_t	Thyristor conduction resistance
S	Complex power
t	Time
T	Current transducer time constant
T	Sequence transform matrix
T_D	Current transfer matrix across star-g/delta transformer
T_I	Current controller integral time constant
$v(t)$	Time domain voltage waveform
V	Convertor three phase ac side harmonic voltages
V_d	Convertor dc side direct voltage harmonics
V_{dc}	Dc system direct voltage source
V_{dp}	pth direct voltage sample harmonics
V_{fwd}	Constant forward voltage drop of thyristor stack
V_{th}	Ac system Thevenin voltage source harmonics
W	Convertor ac side terminal voltage in sequence components
X	Commutating reactance at fundamental frequency
X	Solution vector in Newton's method
Y_{cc}	Total ac side admittance
Y_d	DC system equivalent admittance
Y_D	Zero sequence shunt associated with star-g/delta transformer
Y_{filter}	Filter admittance
Y_l	Equivalent harmonic admittance of a $P + jQ$ load
Y_{tc}	Ac system Thevenin series admittance
α	Time domain firing order waveform
β	Equidistant timing references
η	Magnitude tolerance for sparse impedance calculation

θ	Firing instants
γ	Orientation of circular impedance locus
λ	Convergence factor
μ	Average commutation duration
ϕ	End of commutation instants
ω	Fundamental angular frequency
ψ	Periodic square pulse sampling function
Ψ	Harmonic components of square pulse sampling function

Chapter 1

INTRODUCTION

1.1 POWER QUALITY

The increasing use of power electronic devices in the power system requires that methods are available to calculate the effect of the harmonic currents that they inject. Harmonic currents are a type of pollution in the power system, as they propagate throughout the power system affecting other users adversely, by degrading power quality. Harmonic currents can cause telecommunications interference, overheating of filters and machines, increased current and voltage levels, and a reduction in the lifetimes of power system components.

The propagation of harmonic currents throughout the system due to several injecting sources is well modelled at present. The HVdc convertor, which is one of the largest harmonic sources in the power system, has been modelled best in isolation from its interaction with the ac system. Combining an accurate convertor model with a full ac system model is quite challenging, as the combined interaction does not fit naturally into either time or frequency domain analysis methods. This is because a time domain simulation of the full ac system is not feasible.

1.2 THESIS OBJECTIVES

This thesis is primarily concerned with the numerical modelling of convertor plant in the steady state. The objective is to improve on existing convertor models by developing a method for solving the convertor steady state quickly and accurately.

Existing models either ignore some important aspects of convertor operation, suffer convergence problems, or are slow. A robust and fast solution is developed in this thesis by the use of Newton's method with sparsity. The issue of accuracy, as always, requires a decision on the relative merits of speed and simplicity, against complexity and accuracy. There are several arguments against modelling power system components accurately; there are too many of them, the required component information is rarely

available, the system is never in the steady state, the system configuration is highly variable.

The first two points raised above are generally dealt with by lumping many components into electrical equivalents, using an empirical rule to calculate the electrical equivalent parameters. For example in harmonic penetration studies, load centres are modelled by a shunt admittance based upon the complex power and the likely make-up of the load. The effect of such approximations can be determined by a sensitivity analysis if necessary, which requires that several system solutions be obtained. Uncertainty in component parameters can also be accounted for by considering the range of parameter values to be a type of system variability; for instance the filter capacitance values can be considered to vary independently over a 5% range.

Engineers typically deal with system variability by designing for the worst case. This is a conservative approach, which leads to greater investment in plant, for example convertor filters. The availability of fast and accurate solutions to the system steady state would allow an extension of reliability analysis to calculate harmonic compliance indices. Thus, by iterating over many system steady states, each accurately solved, probability density functions (p.d.f.) for the harmonic voltages at a convertor bus could be calculated. The objective of the filter design would then be to ensure that the integral of the pdf for each harmonic over an interval on the complex plane defined by the harmonic legislation was greater than 95%. This approach to design is merely the logical extension of the existing use of computer models, whereby many different system configurations and operating points are analysed.

An important objective of the research reported in this thesis was to develop a convertor model fast and accurate enough to be integrated with a load flow and a reliability program. Combined with other component models, this will provide a platform for the investigation of stochastic harmonic processes in the power system. Such processes include arc furnaces, background harmonics, and the distributed switchings that mean the system is only in a quasi-steady state. In a stochastic harmonic program, these processes can be represented by the convolution of the harmonic probability density functions with point spread functions, or by an appropriately described random injection at each system solution.

A secondary objective of the research was to efficiently linearise the convertor around an operating point. This has relevance to resonance analysis, and the calculation of stability factors. A linearisation can also give greater insight into interactions between the convertor, ac, and dc systems.

1.3 THESIS OUTLINE

Chapter 2 surveys existing methods for steady state analysis of the power system, with particular regard to convertor modelling, and the solution methods used.

Chapter 3 develops a new convertor model in the harmonic domain. The model is expressed in terms of equations in variables that fully describe the convertor in the steady state, particularly the harmonic transfer between the ac and dc systems. Particular attention is paid to the modelling of unbalance in the convertor transformers, and the commutation process.

Chapter 4 extends the convertor steady state equations to encompass a description of the harmonic interaction with Thevenin equivalents of the ac and dc systems. A reduced set of equations and variables suitable for solution by Newton's method is obtained. The Newton solution in terms of phase components on the ac side is implemented, and the Jacobian is shown to exhibit a high degree of sparsity, upon elimination of small terms. The solution of a controlled twelve pulse rectifier under various unbalanced and resonant conditions is verified against a time domain simulation.

Chapter 5 explores other possible implementations of the Newton solution. A solution in polar coordinates is found to be poorly conditioned and is not implemented. A solution that decouples interactions between switching instant variation and terminal harmonic variation is implemented, and found to diverge if even order harmonic sources are present in the ac system. A much higher degree of sparsity in the Jacobian is obtained if the Newton mismatch equations and variables are written in sequence components on the ac side.

Chapter 6 develops a tensor representation of the convertor admittance that is able to linearise phase dependence. Properties of the tensor are explored, and related to the complex admittance. A nodal analysis of the convertor and ac system using the tensor admittance is proposed, and then implemented to calculate the equivalent impedance of the convertor and ac system at the convertor bus. The impedance obtained is verified against that obtained by a perturbation method. A sparse calculation of the impedance tensor on the dc side is also implemented, and verified against a frequency domain model. Finally, the variation in the convertor impedance with operating point and ac terminal distortions is investigated.

Chapter 7 summarises the research described in the thesis, and discusses the proposed direction of future research and development.

Chapter 2

A REVIEW OF STEADY STATE CONVERTOR MODELLING

2.1 INTRODUCTION

On the assumption of a balanced, undistorted ac terminal voltage, and infinite smoothing reactance, the convertor is readily analysed by Fourier methods. Closed form expressions can be obtained for the firing angles, commutation duration, characteristic phase current harmonics, and dc voltage harmonics [Arrillaga 1983].

Nonideal convertor behaviour causes a divergence from these values, as well as a multiplication in the number of unknowns. It no longer suffices to specify one delay angle and commutation duration, as they are all different. Additional harmonics also appear on the ac and dc sides of the convertor. Early extensions to the ideal convertor model were primarily concerned with explicating a mechanism of harmonic instability associated with the individual firing control [Ainsworth 1967]. It was shown by Ainsworth that terminal voltage harmonics can modulate the firing instants in such a way as to cause the injection of harmonic currents into the ac system that reinforces the originating terminal voltage distortion. The solution to the problem was the equidistant firing control [Ainsworth 1968]. Several other authors also investigated the generation of noncharacteristic harmonics due to control errors, namely Phadke and Harlow [1968] and Reeve and Krishnayya [1968]. Since that time a number of harmonic problems have been encountered that are due to different mechanisms, some of which are listed below:

- The Intermountain Power Project dc side resonances were found to be a function of the ac system impedances [Bahrman *et al.* 1986].

- High levels of geomagnetically induced current (GIC) excited a 5th harmonic resonance involving the parallel combination of ac system and convertor impedances [Dickmander *et al.* 1994]. This occurred at the Radison terminal of the Quebec-New England Phase II HVdc Transmission.

- High levels of 9th harmonic in the New Zealand HVdc link caused by imbalance at the fundamental, and a parallel resonance in the ac system at the 9th harmonic.
- Harmonic instability of the 2nd harmonic in the Chateauguay scheme due to controller, ac and dc system impedances, and transformer saturation [Hammad 1992]
- Non-characteristic dc side harmonics subsequent to transformer energisation or system disturbances caused current and voltage overloading of dc side filters causing them to trip. This occurred at the Nelson River Scheme dc convertor at Radison [Mathur and Sharaf 1977].
- Second harmonic instability occurred in the Blackwater 200MW back to back link [Stemmler 1987]

Harmonic problems similar to those mentioned above are bound to proliferate as convertors and FACTs become more common, and as the power handled by them increases as a proportion of the ac system short circuit power. A general purpose tool for solving harmonic interactions between the convertor and the ac and dc systems has been slow to emerge, because of the large number of interrelated phenomena that must be solved. A particular problem is the relationship between time domain switching actions in the convertor, and the frequency dependence of the ac and dc systems. The frequency dependence of the ac system is itself variable, depending upon load conditions, generation dispatch, and system configuration. Ideally, all of the following should be modelled:

- Unbalance in the ac system, convertor filters, and transformers.
- Frequency dependence of the ac and dc system impedances. In general the ac system impedance will be unbalanced at harmonic frequencies [Arrillaga *et al.* 1987].
- Injection of harmonic currents by the convertor causing harmonics in the terminal voltage. The direct current will also contain harmonic ripple.
- Parallel resonances on the ac side, and series resonances on the dc side.
- Response of the convertor controller to terminal voltage and direct current harmonics, resulting in firing angle modulation.
- The effect of dc ripple and terminal voltage harmonics on the commutation process.
- Effect of harmonic modulation of the firing and end of commutation instants on the transfer of harmonic distortions across the convertor.
- A comprehensive range of convertor controls.

- Saturation of the convertor transformer and the resulting harmonic current injections.
- Interaction of the convertor, ac and dc systems at non-harmonic frequencies.

Convertor models developed to date can be divided into two broad categories; time domain and frequency domain models. Time domain models of the convertor have generally been more detailed, but can only approximately represent the frequency dependence of the ac system, and are computationally intensive as the convertor model must be simulated to the steady state. Frequency domain models have been much faster, have modelled frequency dependence in the ac and dc systems accurately, but representation of the convertor switchings has been restrictive. More detailed harmonic domain convertor models are iterative, and have suffered convergence problems. Because of the ability to represent the ac system accurately, frequency domain models have progressed further toward steady state modelling of the power system as a whole.

2.2 TIME DOMAIN MODELLING

Time domain simulation of a convertor to the steady state is the most mature method of convertor modelling, being widely available in programs such as EMTDC [Woodford *et al.* 1983] and EMTP [Dommel *et al.* 1980]. Both of these programs are modular and general purpose, and employ the time domain simulation method using nodal admittance matrices proposed by Dommel [1969]. Early transient convertor models used a numerical integration of the state variable equations, with variable step length interpolated to coincide with switching instants [Arrillaga 1983] [Htsui. and Shepherd 1971], [Reeve and Subba Rao 1973], and [Kitchin 1981]. The program EMTDC also interpolates switching instants, allowing longer time steps to be used.

Much research has been directed toward reducing the number of cycles required to be simulated before the steady state is achieved. The review paper by Skelboe [1982] is an excellent and detailed summary of the main techniques developed for time domain steady state simulation, which, at the time of writing, were the Newton's, optimisation, and extrapolation methods. The Newton's method was first described by Aprille and Trick [1972] for simple nonlinear circuits and has been recently applied to the static convertor. The method involves calculating the state transition matrix relating the state variables from time t to time $t+T$, where T is the steady state period. Newton's method is applied to satisfy the requirement that the state variables are periodic, with period T. This requires the calculation of the derivative of the state transition matrix, to be used as the Jacobian.

When applied to the convertor, additional boundary conditions are applied at each switching to link each circuit topology. Since each circuit is linear, the state transition matrix over each conduction interval can be written in analytic form, and Newton's

method is applied to solve the switching instants and the state variables. This approach has been applied to a single phase rectifier [El-Bidweihy and Al-Badwaihy 1982], and a Graetz bridge attached to a balanced ac system [Ooi *et al.* 1980]. More recently a very fast solution of a Buck convertor has been obtained by approximating the state transition matrix, an exponential, with Chebyshev polynomials [Luciano and Strollo 1990]. Clearly these methods are still in development, but may yield fast and detailed solutions of the convertor and other nonlinearities attached to simple RLC equivalents of the ac and dc systems.

2.3 FREQUENCY DOMAIN MODELLING

Many authors assume that since the convertor exhibits a strong coupling between harmonics, it must be strongly nonlinear. This is not the case, as in the absence of firing angle and commutation duration variation, the convertor is completely linear in the frequency domain [1]. By linearising the effects and variation of switching angles due to control and commutation, powerful linearised convertor models are possible. Although they cannot be exact, such models are in the form of direct analytic expressions that can model the effect of any frequency of distortion, not just harmonics. An additional benefit of such modelling is the insight into convertor operation they can provide.

The first comprehensive linearised model, developed by Persson [1970], included a linearisation of the effect of firing angle variation, but not commutation variation. The analysis was by means of conversion functions, which linearised the transfer of distortion around the convertor. The objective was to calculate the frequency response of the current control loop on the dc side, for which the effect of commutation variation is not so important [Wood and Arrillaga 1994].

A more recent and less accurate model [Hu and Yacamini 1992] [1993] uses switching functions in a similar manner, but does not represent the controller or commutation variation. Nearly exact agreement with time domain simulation is obtained by using a test system with no commutating reactance or control, and an infinite ac system. The close agreement obtained effectively verifies that the convertor is linear in the absence of the above mentioned mechanisms.

The linearised effect of commutation period and firing angle variation has been modelled recently by Wood and Arrillaga [1994], using modulation theory. In this approach the conduction periods are described by switching functions, which are position and duration modulated as a result of applied distortions. The importance of modelling accurately the commutation shape and duration variation is clearly demonstrated, and close agreement with time domain simulation of the CIGRE benchmark rectifier is obtained for most frequencies below the 11th harmonic, despite a piecewise

[1] The fact that a device linear in the frequency domain can exhibit frequency coupling and phase dependence is discussed in Chapter 6

linear approximation to the commutation current waveform. This model predicts and explains the phase dependence of many of the distortion transfers, and prompted the development of a tensor impedance representation described in Chapter 6.

2.4 HARMONIC DOMAIN MODELLING

A diverse range of harmonic domain convertor models are described in the literature, developed in accordance with differing intended applications. The extent of modelling covers a wide range, determined by the number of variables that are assumed known. Thus, some authors have assumed that the dc current and terminal voltage are known, and that it is desired to calculate the phase currents, perhaps for filter design purposes. Many convertor models described recently are less general than earlier ones, but employ better numerical methods in the solution process. Lack of computing power was often reported as a factor limiting the extent of modelling in earlier harmonic analyses of the convertor. Harmonic domain convertor models developed to date can be classified into two main types; those that assume predetermined terminal voltage and dc current harmonics, and those that solve the convertor interaction with the ac and dc systems.

2.4.1 Predetermined Terminal Voltage and Dc Current Harmonics

The 'standard' convertor analysis is included in this classification under the assumptions of ripple free dc current and balanced sinusoidal terminal voltage [Arrillaga 1983]. Using Fourier analysis, Reeve and Krishnayya [1968] calculated the abnormal dc side voltage harmonics due to firing error and ac side terminal voltage unbalance, assuming ripple free direct current. The model was later extended to calculate line current harmonics [Reeve *et al.* 1969], and the effect of harmonics in the terminal voltage [Reeve and Baron 1970]. Yacamini and de Oliveira [1980] developed a very similar model assuming ripple free direct current, and showed how to model unbalanced convertor transformers with any desired phase shift. This generalised convertor transformer representation permits the modelling of high pulse number convertors, but is incorrect for unbalanced star-g/delta transformers.

The effect of direct current ripple was investigated by Cavallini *et al.* [1994]. They compared the ac side characteristic harmonic currents calculated by several models which take as input a parameterised description of the dc ripple waveshape. Grötzbach and Draxler [1993] modelled the effect of commutation on ac side currents, again utilising a parameterised description of the dc ripple waveshape. This analysis employed a Newton method to calculate the average delay and commutation angles, with a trapezoidal approximation to the commutation shape. Finally, Rice [1994] calculated the dc ripple given a constant delay angle, and assuming no commutating reactance or ac side terminal voltage distortion.

2.4.2 Iterative Harmonic Analysis

If the ac terminal voltage or direct current harmonics are not known an iterative solution is necessary, and the convertor controller must be modelled. The simplest iterative solution method is a fixed point iteration, which is known to have poor convergence. Reeve and Baron [1971] were the first to implement a fixed point iterative solution, a method subsequently termed *Iterative Harmonic Analysis* (IHA), and applied to transformer saturation analysis as well [Dommel *et al.* 1986]. Reeve's IHA consisted of using a Fourier analysis to calculate the direct voltage and phase currents, given the terminal voltage and direct current. By applying the calculated direct voltage and phase currents to the appropriate systems, updates to the terminal voltage and direct current were obtained. The iteration was found to diverge in some cases, and Reeve incorrectly used the divergence to infer harmonic instability in a real system.

A more detailed IHA convertor model was developed which included control representation [Yacamini and de Oliveira 1980] [1986]. A simplifying assumption that dc ripple has no effect on the commutation and or direct voltage was made. Yacamini and de Oliveira [1980] also inferred knowledge about the test system behaviour, based upon divergence of the iterative method.

Utilising an expression derived by Yacamini and de Oliveira [1980] for the time evolution of the commutation current, Callaghan and Arrillaga [1989] implemented an IHA of the convertor that avoided both complicated Fourier analysis, and solution of the switching instants. They constructed time domain waveforms for the direct voltage and ac side phase currents by evaluating analytic expressions for those quantities on a point by point basis. Application of the FFT then yielded the desired harmonic information. Convergence of the fixed point iteration was then investigated, and sufficient criteria for convergence was derived analytically [Callaghan and Arrillaga 1990].

Analysis of the convergence indicated divergence when the ac system impedance was large, and the commutating reactance was small. Callaghan showed that divergence could sometimes be avoided, or convergence improved, if a *matched reactance* pair was inserted between the convertor transformer primary, and the filter bus. The matched reactance pair consisted of a series combination of a reactance, and its negative, with the midpoint voltage being the new voltage to be solved by the IHA. The reactance value was chosen to cancel the ac system reactance, and to increase the commutating reactance.

Arrillaga *et al.* [1987] compared solutions for a convertor attached to an ac system using both IHA, and a transient convertor simulation to the steady state. The two methods showed close agreement when the ac system could be fully represented in the time domain simulation. If the ac system was weak, the IHA frequently diverged despite the time domain simulation converging to a solution representing an acceptable operating state of the convertor. This proved that divergence of the IHA is not

indicative of harmonic instability, and cannot be used to analyse the real system it models.

Noting that a matched reactance pair cannot cancel high impedance in the ac system due to parallel resonances, several authors have proposed the use of a matched impedance pair to further improve the convergence of IHA. The impedance is chosen to mirror quite closely the frequency dependence of the ac system impedance, and consists of a simple RLC network. This approach complicates the commutation analysis considerably, so much so that Carbone *et al.* [1992] solve the convertor at each iteration by time domain simulation to the steady state. The IHA is therefore used only to solve the interaction of the convertor with that portion of the ac system impedance that cannot be represented by a simple RLC network. Carpinelli *et al.* [1993] [1994] have taken the alternative approach of developing a methodology for deriving analytic expressions for the commutation current and dc voltage, given a commutating RLC network.

The main problem with the matched impedance pair method is the added complexity. Selection of the RLC network is by no means straightforward, and the resulting commutation process is formidably difficult to solve. Most recent work has been directed toward improving the solution method itself, rather than improving the fixed point iteration.

2.4.3 The Method of Norton Equivalents

In the iterative harmonic method, the convertor is represented in the ac system solution at each iteration by a constant current source. Far better convergence can be expected if the convertor is represented by a Norton equivalent, with the Norton admittance representing a linearisation, possibly approximate, of the convertor response to variation in terminal voltage harmonics.

Such a model has been developed for the Multiphase Harmonic Load Flow program by Xu *et al.* [1990] [1994]. This program iterates between a three phase load flow, and a direct solution of the harmonic interaction between nonlinear current injections. The harmonic interaction is solved by injecting harmonic currents, calculated by nonlinear models, into an admittance matrix. The admittance matrix does not contain cross harmonic coupling, but does include terms which represent a linearisation of the nonlinear devices. The convertor model in MHLF assumes a predetermined firing angle and dc current. Only the contribution of the commutation current to the phase currents is linearised.

As discussed in Chapter 6, a full linearisation of the convertor requires either an admittance tensor, or a complex conjugate cross harmonic admittance matrix representation. Several authors have taken the latter approach in connection with the modelling of transformer and synchronous machine nonlinearities [Semlyen *et al.* 1988], [Arrillaga

et al. 1994]. The method is called Harmonic Domain Analysis (HDA), and is a variant of Newton's method. Clearly there are two important aspects to HDA; evaluation of the voltage controlled current injections at each nonlinearity, and calculation of the Norton admittances. The HDA method has been well developed in connection with devices that can be described by a static (time invariant) voltage-current relationship,

$$i(t) = f(v(t)), \tag{2.1}$$

in the time domain. For such devices, both the current injection and the Norton admittance can be calculated by an elegant procedure involving an excursion into the time domain. At each iteration, the applied voltage harmonics are inverse Fourier transformed to yield the voltage waveshape. The voltage waveshape is then applied point by point to the static voltage- current characteristic, to yield the current waveshape. By calculating the voltage and current waveshapes at 2^n equi-spaced points, a FFT is readily applied to the current waveshape, to yield the total harmonic injection. To calculate the Norton admittance, the waveshape of the total derivative

$$\frac{dI}{dV} = \frac{di(t)}{dt}\frac{dt}{dv(t)}, \tag{2.2}$$

$$= \frac{\frac{di(t)}{dt}}{\frac{dv(t)}{dt}} \tag{2.3}$$

is calculated by dividing the point by point changes in the voltage and current waveshapes. Fourier transforming the total derivative yields columns of the Norton admittance, which is Toeplitz in structure. The Norton admittance calculated in this manner is actually the Jacobian for the source. This is proven below.

Derivation of the Toeplitz Jacobian Matrix

The Jacobian elements for a VI linearisation are

$$J_{lm} = \frac{\partial I_l}{\partial V_m}, \tag{2.4}$$

where

$$i = \sum_{k=-\infty}^{\infty} I_k e^{jk\omega t}, \tag{2.5}$$

$$v = \sum_{k=-\infty}^{\infty} V_k e^{jk\omega t}, \tag{2.6}$$

$$i = f(v). \tag{2.7}$$

By the chain rule

$$\frac{\partial I_l}{\partial V_k} = \frac{dI_l}{dv}\frac{\partial v}{\partial V_k}. \tag{2.8}$$

Differentiating equation 2.6 yields

$$\frac{\partial v}{\partial V_k} = e^{jk\omega t}. \tag{2.9}$$

Substituting this into equation 2.8 yields

$$\frac{\partial I_l}{\partial V_k} = \frac{dI_l}{dv}e^{jk\omega t}. \tag{2.10}$$

Thus

$$\frac{dI_l}{dv} = \frac{\partial I_l}{\partial V_k}e^{-jk\omega t} \tag{2.11}$$

Differentiating equation 2.5,

$$\frac{di}{dv} = \sum_{l=-\infty}^{\infty}\frac{dI_l}{dv}e^{jl\omega t}, \tag{2.12}$$

and substituting 2.11 into 2.12 yields

$$\frac{di}{dv} = \sum_{l=-\infty}^{\infty}\frac{\partial I_l}{\partial V_k}e^{j(l-k)\omega t}. \tag{2.13}$$

Considering now the mth spectral component of the total derivative $\frac{dI}{dV}$,

$$C_m = \left[\frac{di}{dv}\right]_m = \frac{\partial I_{k+m}}{\partial V_k}. \tag{2.14}$$

This was obtained by finding l such that $l-k$ in the exponential is equal to m. The subscript k is arbitrary, and setting $p = k+m$ yields

$$\frac{\partial I_p}{\partial V_k} = C_m = \frac{\partial I_{p+n}}{\partial V_{k+n}}, \tag{2.15}$$

for any n. This means that all the elements in any diagonal of the Jacobian are equal. The Jacobian is thus Toeplitz in structure. This also proves that the method of taking the FFT of the time domain total derivative, and assembling a Toeplitz matrix from the spectral components, is correct for this type of nonlinearity.

Time Stepping for Frequency Dependent Nonlinearities

It has been claimed that the time stepping and FFT method of obtaining a Norton equivalent is applicable to any type of nonlinearity [Semlyen *et al.* 1988]. This is not

always the case if the voltage-current relationship depends upon the voltage rate of change:

$$i(t) = g(v(t), \dot{v}) \tag{2.16}$$

In the case of a shunt capacitor,

$$i(t) = C\dot{v}, \tag{2.17}$$

so that

$$I_k = jk\omega V_k. \tag{2.18}$$

This relationship defines a non-Toeplitz admittance, since

$$\frac{\partial I_{(k+1)}}{\partial V_{(k+1)}} = \frac{k+1}{k}\frac{\partial I_k}{\partial V_k}. \tag{2.19}$$

To date this has not been a problem in the time stepping method, since RLC circuits are linear, with a readily calculated admittance. The circuit elements have always been seperated into those which are frequency dependent, but linear, and those which are static, but nonlinear. When the voltage current relationship is static, as in equation 2.1, the returned current waveform shape will be independent of the fundamental frequency. This is not the case for the convertor however, as every conduction state involves frequency dependent elements. It is therefore not possible to seperate the convertor current injection into the above two components for the time stepping method. This situation corresponds to a current injection which is a nonlinear function of both v, and $\dot{v}$, with the Norton admittance no longer Toeplitz. In general the Norton admittance matrix contains $n_h \times n_h$ unknowns, which cannot be obtained from the n_h components yielded by the FFT.

The problem with modelling the convertor and ac system by Norton equivalents is that the convertor is really an interface between the ac and dc systems, with only the ac system represented in the overall solution process. If the convertor controller is modelled, a separate iterative procedure is required to solve the convertor interaction with the dc system at each iteration. Such a model is described in the second paper in Appendix E, and, if combined with the Norton admittance tensor derived in Chapter 6, a convertor model suitable for use in the HDA could be constructed. Recently, several authors have proposed the more efficient approach of linearising the interaction between the ac and dc systems, and solving both together using ABCD parameter matrices.

2.4.4 ABCD Parameters Modelling

The use of an ABCD parameters matrix to linearise the harmonic transfer across a convertor was first proposed by Larson *et al.* [1989]. The matrix equation is

$$\begin{bmatrix} \Delta I \\ \Delta V_d \end{bmatrix} = \begin{bmatrix} A & B \\ C & D \end{bmatrix} \begin{bmatrix} \Delta V \\ \Delta I_d \end{bmatrix}, \tag{2.20}$$

where $\Delta I, \Delta V_d, \Delta V, \Delta I_d$ are vectors of harmonic perturbations. The ABCD matrix therefore links harmonics of different orders, on both sides of the convertor. To be fully general, both positive and negative harmonics must be included, or the matrix should be a tensor. Larson *et al.* [1989] used only positive order harmonics in their formulation, but noted that the matrix has a sparse lattice like structure [2]. The ABCD matrix was obtained by harmonic perturbations of a time domain simulation, and used to investigate composite ac/dc resonances.

If the effects of control and commutation variations are neglected, the convertor is linear in the harmonic domain, and the Δs in equation 2.20 can be dropped. Jalali and Lasseter [1991] [1994] iterated between a direct solution of the ac/dc system interaction described by an ABCD matrix, and an update to the commutation durations, without control. The method was implemented for a single phase rectifier, and the large ABCD matrix was updated at every iteration by evaluating the harmonic domain convolutions of terminal voltage and direct current spectra with switching functions. This approach was later extended by Rajagopal and Quaicoe [1993] to a six pulse three phase rectifier, but only by assuming no resistive component in the ac system impedance.

The decoupled solution developed in Chapter 5 is similar to this model, iterating between a linear solution of the ac/dc system interaction, and a Newton solution for the switching angles. This method was found to diverge in cases where even order harmonic sources were present in the ac system. There is thus a motivation to linearise switching angle variation with terminal harmonic variation, and develop a full Newton solution, dispensing with purely electrical equivalents.

2.4.5 Newton's Method

The only Newton type solution of the interaction of the convertor with the ac system is the well known Harmonic Power Flow developed by Xia and Heydt [1982]. In this model the load flow, harmonic interaction between nonlinear loads, and firing angle for convertors are linearised together in a unified Jacobian. This single phase program was extended to three phases by Valcárcel and Mayordomo [1993]. However the solution method described by Valcárcel and Mayordomo [1993] is a fixed point iteration of three separate Newton procedures; one each for the load flow, ac system harmonic interaction,

[2] The lattice structure and nodal tensor analysis are discussed in detail in Chapter 6

and commutation angles. The direct current is assumed ripple free, and in common with Xia, the convertor operating point is specified in terms of real and apparent power, rather than current order or dc power.

The decoupling between load flow solution and harmonic interaction proposed by Valcárcel and Mayordomo [1993], precludes the linearisation of an important interaction between the convertor and the load flow. Unbalance in loads near the convertor introduces a negative sequence component into the convertor terminal voltage. This is then converted into a positive sequence third harmonic phase current, which leads to a corresponding component in the terminal voltage. Positive sequence third harmonic terminal voltage is then converted back to negative sequence fundamental. In addition, negative sequence fundamental in the terminal voltage modulates the end of commutation angles at the second harmonic. This commutation variation in turn directly modulates the full dc current to produce a large negative sequence fundamental component on the ac side. A strong interaction of this sort, although involving small distortion levels, may not be solvable by a fixed point iteration.

2.5 CONCLUSION

Although an exact classification of existing techniques for steady state analysis of the convertor is not possible, most convertor models fall into three main categories; time domain, frequency domain, and harmonic domain. Time domain simulation to the steady state is the most developed, but is computationally intensive, and cannot easily model the frequency dependent impedance of the ac system. Methods for accelerating the convergence of time domain simulation to the steady state have been proposed, and of these, Newtons method has been applied to fairly restrictive convertor models with some success.

Frequency domain convertor models have been developed, which although not exact, are direct, can calculate the effect of any frequency of distortion, and give insight into the transfer of distortions around the convertor.

Harmonic domain convertor models have suffered convergence problems when the solution method is a fixed point iteration, but can model frequency dependence in the ac system with ease. Harmonic domain models have also suffered from restrictive modelling of the switching process in the convertor. More recently, improved solution methods have been proposed for harmonic domain modelling, based upon electrical equivalents that linearise the harmonic sources.

A full linearisation of the convertor requires that variables other than electrical quantities are linearised in the same Jacobian matrix. As discussed in Chapters 3 to 5 this implies a Newton solution in real variables, and positive harmonics only.

Chapter 3

A HARMONIC DOMAIN CONVERTOR MODEL

3.1 INTRODUCTION

This chapter describes a new analysis of the controlled six pulse bridge in the steady state, and under non ideal conditions. In order that the analysis be general, the ac terminal voltage is considered in the phase frame of reference, and furthermore, that it is distorted by unbalance at fundamental and harmonic frequencies. Although perfect equidistant firing is assumed, the constant current controller is likely to be responsive to low order harmonic currents on the dc side. It is therefore necessary to model the individual firing instants of the bridge, and since the terminal voltage is distorted, the individual commutation processes must be modelled also. Finally, the steady state solution must be compatible with the current or power order for the convertor.

Central to any analysis of a six pulse bridge is the commutation process. The presence of inductance between the convertor terminal voltage and the six pulse bridge means that the dc current cannot immediately transfer from one switch to another. An analysis of the commutation under non ideal conditions is complicated [de Jesus 1982]. In particular, the presence of resistance in the commutation circuit needlessly complicates the analysis if the interaction with the ac system is to be solved as well. Consequently, section 3.3 presents a commutation analysis with reactance only in the commutation circuit, but allowing for unbalance and harmonic distortion in the terminal voltage and dc current. The effect of commutation resistance will be accounted for in chapter 4 by placing it between the ac system terminal and the convertor transformer primary windings.

The effect of dc current harmonic ripple on the firing controller is analysed in section 3.4, while sections 3.5 and 3.6, deal with the transfer of voltage and current distortions across the bridge. Section 3.7 provides a new transfer analysis of unbalanced transformers, and correctly models the sequence transformation effect in an unbalanced star-g/delta transformer bank. The remaining sections develop equations for the constant current and power control loops, the presence of a load flow constraint at the convertor bus, and the representation of the ac and dc systems.

The outcome of this chapter is a set of equations that fully describe all the relationships that hold between the ac and dc systems, the convertor transformer, and the convertor switches. The solution of these equations is left to Chapter 4.

3.1.1 Angle Reference

The angle reference used throughout this thesis is an arbitrary angle, possibly unrelated to the convertor at all. For example, all angles may be referenced to the most recent positive zero crossing of the fundamental internal emf of the slack bus generator. At present, the first equidistant timing reference has arbitrarily been assigned an angle of zero. All firing angles and end of commutation angles are referenced to this angle, as opposed to the convertor terminal voltage fundamental frequency component, as is the usual practice.

3.1.2 Phasor Representation

Much of the analysis in this thesis has been expressed in terms of complex harmonic phasors. A harmonic phasor is a convenient and powerful representation of a sinusoidally varying quantity. Two types of harmonic phasor representation are in common use; positive frequency and complex conjugate. In the positive frequency representation, the time domain quantity is equal to the real or imaginary part of an anticlockwise (positive frequency) rotating phasor. The real part yields a cosine referenced waveform, whereas the imaginary part yields a sine wave referenced waveform. Positive frequency sine referenced phasors are used throughout this thesis.

In the complex conjugate phasor representation, the time domain waveform is equal to the sum of two counter-rotating phasors with conjugate angles. This representation has been used frequently for harmonic analysis as it is directly compatible with the FFT, however it is not suitable for the real variable Newton solution developed in this thesis.

General periodic functions of any wave shape can be represented by a Fourier sum of complex harmonic phasors. A more detailed description of harmonic phasors, and the relationship between harmonic phasor sums and the discrete Fourier series is given in Appendix A.

3.2 THYRISTOR MODEL

The thyristor voltage-current characteristic is approximated by an open circuit in the reverse direction, and a constant dc voltage drop and conduction resistance in the forward direction. This yields the equivalent circuits of figures 3.1 and 3.2 during two and three valve conduction states.

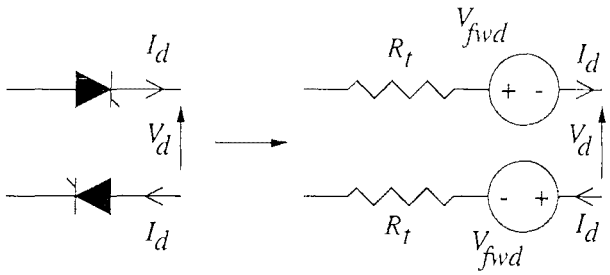

Figure 3.1 Equivalent thyristor circuit during double conduction

It is evident from these figures that the thyristor resistance can be lumped with the transformer series impedance (after transforming through any off nominal tap on the secondary), whereas the constant forward voltage drop can be represented by a constant voltage drop on the dc side.

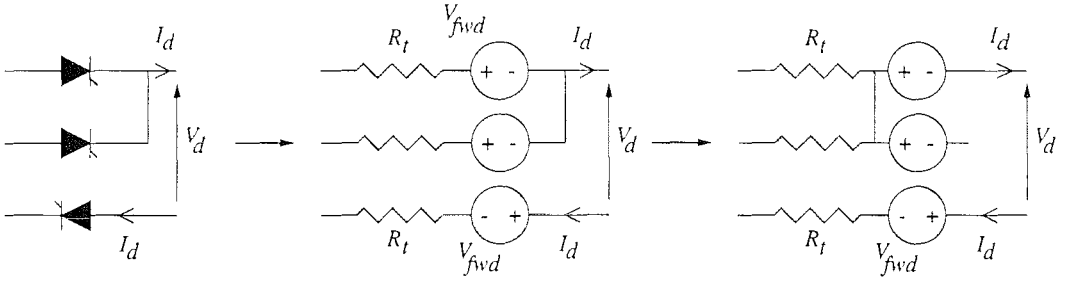

Figure 3.2 Equivalent thyristor circuit during triple conduction

The resulting equivalent circuit is shown in figure 3.3. The principal effect of these two energy loss mechanisms is to cause the convertor controller to slightly advance the firing angle. This phase shifts the convertor phase currents by an angle proportional to the harmonic order, which can be significant at the 50th order harmonic.

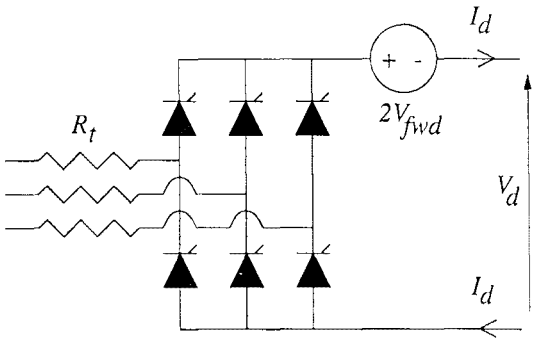

Figure 3.3 Lumped model of non-ideal thyristor effects.

3.3 THE COMMUTATION PROCESS

Two separate analyses of the commutation process are given here. One for a bridge connected to a star star transformer, and the other for a bridge connected to a star-g/delta transformer. Previously the star-g/delta connected bridge has been represented by phase shifting voltages and currents across the transformer by 30° and analysing as for a star-g/star transformer [Yacamini and de Oliveira 1980]. This process is valid for balanced transformers, since although it ignores the effect of circulating current entirely, the convertor is not affected by balanced voltage drops due to circulating current. It is possible to model the unbalanced effect by moving the unbalanced component of the leakage reactance through the star-g connection into the ac system, however this increases the ac system impedance at high order harmonics. The best method is to model all resistance in the ac system, and to write new equations for the six pulse group attached to the delta connected source, with unbalanced reactance.

3.3.1 Star Connection Analysis

The commutation circuit to be analysed is that of figure 3.4. Where V_a, V_b, I_c and I_d are sums of harmonic phasors. In this diagram phase 'a' is commutating off, whilst phase 'b' is commutating on. The commutation ends when $I_c = I_d$. Assuming the

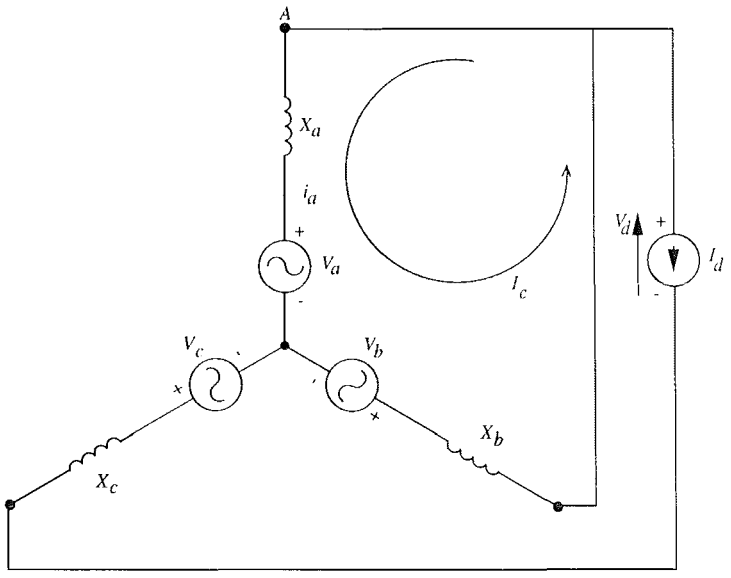

Figure 3.4 Circuit for star-g/star commutation analysis.

periodic steady state, and summing voltage drops around the commutation loop at harmonic order k:

$$V_{ak} + jkX_aI_{ck} - jkX_aI_{dk} + jkX_bI_{ck} - V_{bk} = 0. \tag{3.1}$$

Solving equation 3.1 for the commutation current:

$$I_{c_k} = \frac{jkX_a I_{d_k} - V_{ab_k}}{jk(X_a + X_b)}. \tag{3.2}$$

The periodic commutation current in the time domain is therefore

$$I_c(t) = D + \mathcal{I}\{\sum_{k=1}^{n_h} I_{c_k} e^{jk\omega t}\}, \tag{3.3}$$

where

$$D = -\mathcal{I}\{\sum_{k=1}^{n_h} I_{c_k} e^{jk\theta_i}\}. \tag{3.4}$$

D can be considered to be either a constant of integration, an initial condition, or equivalently a circulating dc current in the commutation loop. Assigning this value to D ensures that at the moment of firing a valve, θ_i, the current in it is zero.

The solution obtained for the commutation current is the steady state solution of the commutation circuit. Since there is no resistance in the circuit, the steady state is achieved instantaneously when the appropriate valve is fired. The commutation ends when the instantaneous commutation current is equal to the instantaneous dc current. This angle, the end of commutation ϕ_i, cannot be solved directly, as equation 3.3 is transcendental. Instead, the end of each commutation is determined by the zero crossing of a differentiable mismatch equation, solvable by Newtons method. The mismatch equation is easily constructed by substituting $\omega t = \phi_i$ into the Fourier series for the dc and commutation currents, and taking the difference:

$$F_{\phi_i} = \mathcal{I}\left\{ j(I_{d_0} - D) + \sum_{k=1}^{n_h} (I_{d_k} - I_{ci_k}) e^{jk\phi_i} \right\}. \tag{3.5}$$

Equation 3.5 completes the commutation analysis for a bridge connected to a star connected source via an inductance. This equation is suitable for modelling the connection to an unbalanced star-g/star connected transformer, if the leakage reactances and terminal voltages are referred to the secondary side after scaling by off-nominal tap ratios on the secondary or primary windings. This issue is addressed fully in section 3.7.

3.3.2 Delta Connection Analysis

The circuit to be analysed is that of figure 3.5, which corresponds to a particular commutation. The objective is to solve for the commutation current I_c, in terms of the sources. Proceeding directly with a phasor analysis in the steady state, a series of loop

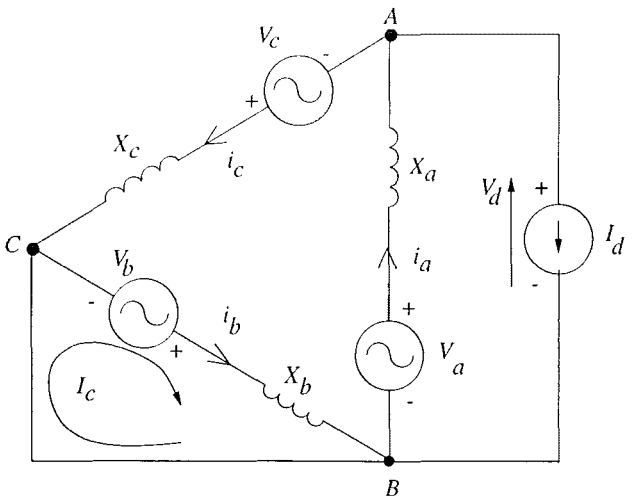

Figure 3.5 Circuit for star-g/delta commutation analysis.

and nodal equations can be obtained for this circuit at each harmonic k:

$$\begin{aligned} I_{dk} - I_{ck} + i_{bk} - i_{ak} &= 0 \\ I_{ck} + i_{ck} - i_{bk} &= 0 \\ i_{ak} - i_{ck} - I_{dk} &= 0 \\ V_{bk} - j i_{bk} X_{bk} &= 0 \\ V_{ck} - j i_{ck} X_{ck} + V_{dk} &= 0 \\ V_{ak} - j i_{ak} X_{ak} - V_{dk} &= 0, \end{aligned} \tag{3.6}$$

where for an inductance $X_k = kX_1$. This set of equations is readily solved to yield the dc voltage during the commutation, and the commutation current itself:

$$V_{dk} = \frac{V_{ak}X_{ck} - V_{ck}X_{ak} + jI_{dk}X_{ck}X_{ak}}{X_{ak} + X_{ck}} \tag{3.7}$$

$$I_{ck} = \frac{V_{bk}}{jX_{ck}} - \frac{V_{ck} + V_{dk}}{jX_{ck}} \tag{3.8}$$

A similar analysis holds for every separate commutation, with appropriate modifications to the phase subscripts, and the direction of the dc current. The end of commutation mismatch equation for the star-g/delta connection is obtained as for the star-g/star connection above.

3.4 THE VALVE FIRING PROCESS

There are two aspects to modelling the valve firing process; the firing controller, and the convertor controller. In modern schemes, the firing controller consists of a phase locked oscillator (PLO) tracking the fundamental component of the terminal voltage, and generating essentially equi-spaced timing references. A well designed phase locked oscillator is unaffected by harmonics in the terminal voltage, since its time constant is of the same order as the fundamental. Consequently, the PLO is not modelled, and the timing pulses are assumed perfectly equidistant, spaced by 60°.

In general the effect of a nonideal PLO would be to introduce a coupling between terminal voltage harmonics, and the firing mismatch equation to be derived below. A description of how this would be implemented is given in Chapter 7. The convertor controller described here is of a simple PI type, which is simpler than what would be encountered in practice. The analysis of the valve firing given here requires a frequency transfer function description of the controller, which is easily obtained for the P+I controller, and which is readily extended to any other linear controller. A nonlinear control characterisitic would require a linearisation around an operating point.

A valve firing occurs when the elapsed angle from a timing pulse is equal to the instantaneous value of the alpha order. The alpha order is a command variable received from the convertor controller. The controller modelled here is a constant current control of the proportional integral type (figure 3.6), which will respond to harmonics in the dc current. From figure 3.6, the alpha order can be expressed as a sum of harmonic

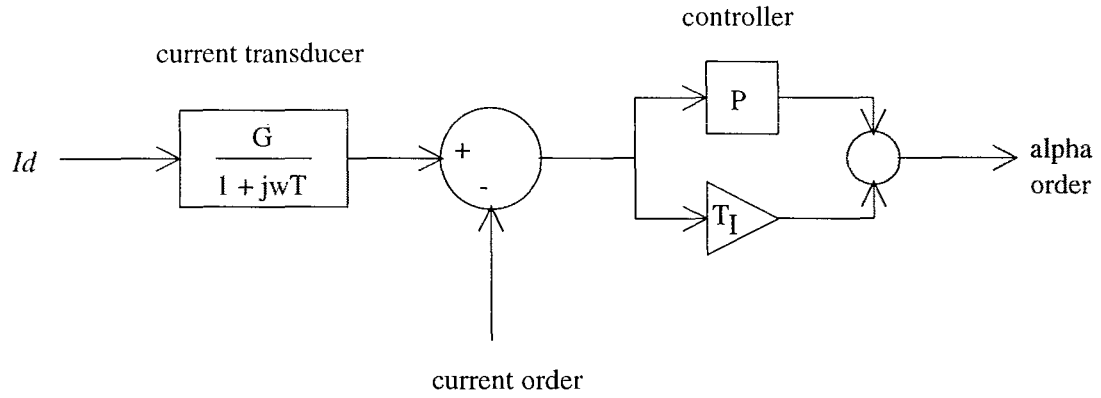

Figure 3.6 Current controller

phasors:

$$\alpha = \mathcal{I}\left\{ j\alpha_0 + \sum_{k=1}^{n_h} \alpha_k e^{jk\omega t} \right\}, \tag{3.9}$$

where

$$\alpha_k = \frac{G}{1 + jk\omega T}\left(P + \frac{1}{jk\omega T_I}\right) I_{d_k}. \tag{3.10}$$

With reference to figure 3.7, it can be seen that firing occurs when the elapsed angle from the equidistant timing reference is equal to the instantaneous value of the alpha order ie $\alpha = \theta_i - \beta_i$. The equidistant timing references are represented by $\beta_i = (i-1)\pi/3$. The firing mis-match equation is therefore:

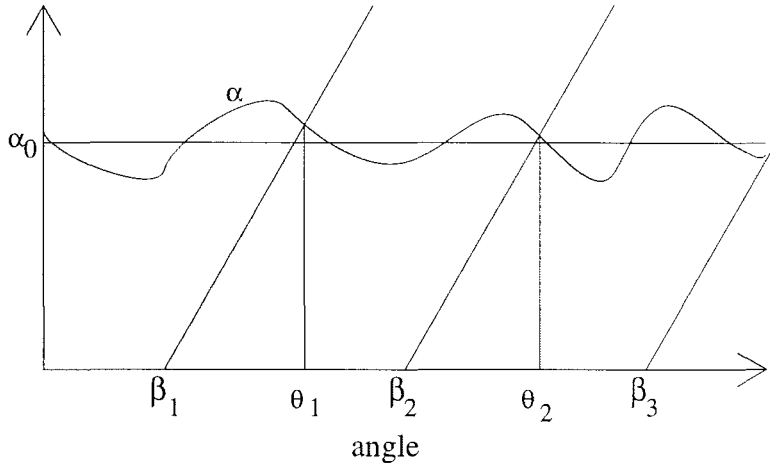

Figure 3.7 Method of finding the firing instants. The timing instants are assumed perfectly equidistant ($\frac{\pi}{3}$).

$$F_{\theta_i} = \mathcal{I}\left\{ j(\beta_i + \alpha_0 - \theta_i) + \sum_{k=1}^{n_h} \alpha_{i_k} e^{jk\theta_i} \right\} = 0. \tag{3.11}$$

This analysis of the firing process is also valid for a bridge connected via a star-g/delta bridge to the ac system, in which case, the equidistant timing references should be advanced by 30°.

3.5 DIRECT VOLTAGE

The six pulse bridge passes through twelve states per cycle. Six of these are commutation states, and six are 'direct' conduction states. During direct conduction the positive and negative rails of the DC side are connected to the ac side via two conducting thyristors. As in the case of the commutation analysis, either state can be modelled by the immediate steady state of a simple linear circuit [1]. The circuit consists of a star or delta connected ac voltage source with inductance, connected to a current source

[1]The linear circuits have no initial transient

representing the dc system. The particular configuration of each circuit depends upon the conduction pattern of the valves in the bridge.

Although it is straightforward to solve the representative linear circuits, the outcome of each steady state solution is a harmonic spectrum, which when transformed into the time domain, matches the dc voltage during the appropriate conduction interval only. The objective is a single spectrum that is valid for one complete cycle of dc voltage, not twelve spectra each valid for only one twelfth of a cycle. The complete spectrum is obtained by convolving each of the twelve 'sample' spectra with the spectrum of a periodic square pulse that has value of one during the corresponding conduction interval, and a value of zero everywhere else. This yields twelve dc voltage sample spectra, the sum of which is the spectrum of the dc voltage across the bridge.

3.5.1 Star Connection Voltage Samples

During normal conduction the positive and negative rails of the DC side are directly connected to different phases of the AC terminal via the commutating reactance in each phase. The kth harmonic component of the DC voltage is therefore:

$$V_{dp_k} = V_+ - V_- - j\omega k(L_+ + L_-)I_{d_k}. \tag{3.12}$$

During a commutation on the positive rail, analysis of figure 3.4 yields:

$$V_{dp_k} = \frac{L_e V_b + L_b(V_e - jk\omega L_e I_{d_k})}{L_e + L_b} - V_o - jk\omega L_o I_{d_k}, \tag{3.13}$$

and

$$V_{dp_k} = V_o - jk\omega L_o I_{d_k} - \frac{L_e V_b + L_b(V_e + jk\omega L_e I_{d_k})}{L_e + L_b} \tag{3.14}$$

for a commutation on the negative rail. In these equations e refers to phase ending conduction, b to a phase beginning conduction, and o to the other phase.

From the known conduction pattern in each of the twelve states, equations 3.12, 3.13 and 3.14 are used to assemble the twelve samples of the DC voltage. These samples are summarised in table 3.1.

3.5.2 Delta Connection Voltage Samples

The dc voltage during a particular commutation has already been derived in section 3.3.2 with reference to figure 3.5. The general result is

$$V_{dpk} = P_{a_{pk}} V_{ak} + P_{b_{pk}} V_{bk} + P_{c_{pk}} V_{ck} + P_{d_{pk}} I_{dk}, \tag{3.15}$$

sample (p)	Phase Currents			DC Voltage (V_{dp})					
	A	B	C	e	b	o	+	-	eqn
1	I_{c1}	$-I_d$	$I_d - I_{c1}$	A	C	B	.	.	(3.13)
2	I_d	$-I_d$	0	.	.	.	A	B	(3.12)
3	I_d	$-I_{c2} - I_d$	I_{c2}	C	B	A	.	.	(3.14)
4	I_d	0	$-I_d$	.	.	.	A	C	(3.12)
5	$I_d - I_{c3}$	I_{c3}	$-I_d$	B	A	C	.	.	(3.13)
6	0	I_d	$-I_d$	.	.	.	B	C	(3.12)
7	I_{c4}	I_d	$-I_{c4} - I_d$	A	C	B	.	.	(3.14)
8	$-I_d$	I_d	0	.	.	.	B	A	(3.12)
9	$-I_d$	$I_d - I_{c5}$	I_{c5}	C	B	A	.	.	(3.13)
10	$-I_d$	0	I_d	.	.	.	C	A	(3.12)
11	$-I_{c6} - I_d$	I_{c6}	I_d	B	A	C	.	.	(3.14)
12	0	$-I_d$	I_d	.	.	.	C	B	(3.12)

Table 3.1 Construction of DC voltage and AC phase current samples

where $p = 1, 3, 5, 7, 9, 11$ refers to the conduction interval number. The coefficient matrix P is constant, and need only be calculated once. During a commutation on the positive rail

$$P_{epk} = \frac{X_{co}}{X_{co} + X_{ce}} \tag{3.16}$$

$$P_{opk} = \frac{-X_{ce}}{X_{co} + X_{ce}} \tag{3.17}$$

$$P_{bpk} = 0 \tag{3.18}$$

$$P_{dpk} = \frac{-jkX_{co}X_{ce}}{X_{co} + X_{ce}}, \tag{3.19}$$

where if $i\epsilon\{1 \cdots 6\}$ is the number of a commutation on the positive rail, $p = 2i - 1$, then the subscripts $\{e, b, o\}$ are a permutation of $\{a, b, c\}$ according to i. A similar result holds for a commutation on the negative rail.

During a normal conduction period all three phases of the voltage source contribute to the dc voltage. Figure 3.8 shows the representative linear circuit of a particular conduction period. This circuit is analysed by first writing nodal and loop equations at harmonic k:

$$\begin{aligned} i_{ak} - i_{ck} - I_{dk} &= 0 \\ I_{dk} - i_{ak} + i_{bk} &= 0 \\ i_{ck} &= i_{bk} \\ V_{ak} - ji_{ak}X_{ak} - V_{dk} &= 0 \\ V_{bk} - ji_{bk}X_{bk} + V_{dk} + V_{ck} - ji_{ck}X_{ck} &= 0. \end{aligned} \tag{3.20}$$

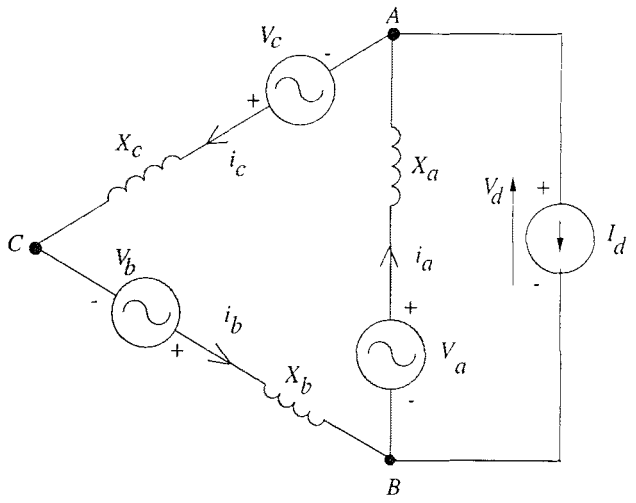

Figure 3.8 Representative linear circuit for a particular conduction period with a delta connected source.

This system is readily solved for the dc voltage sample at harmonic k:

$$V_{dk} = \frac{(V_{ak} - jX_{ak}I_{dk})(X_{bk} + X_{ck}) - X_{ak}(V_{bk} + V_{ck})}{X_{ak} + X_{bk} + X_{ck}} \tag{3.21}$$

As for the star connected source, the solution for the dc voltage samples is generalised over all twelve conduction periods into a matrix of coefficients of the dc and ac sources, ie

$$V_{dlk} = P_{a_{lk}}V_{ak} + P_{b_{lk}}V_{bk} + P_{c_{lk}}V_{ck} + P_{d_{lk}}I_{dk}, \tag{3.22}$$

where $l = 2, 4, 6, 8, 10, 12$.

3.5.3 Convolution of the Samples

Having obtained twelve dc voltage samples as a function of dc and ac side sources, the overall solution for the dc voltage spectrum is constructed by convolving each sample with a square pulse sampling function (figure 3.9). Calculation of harmonic transfers across the convertor using the discrete convolution is not new, having been implemented recently by Sakui *et al.* [1989], Jalali and Lasseter [1991], Rajagopal and Quaicoe [1993], Xu *et al.* [1994], and Ritteger and Kulicke [1995]. The convolution described here is positive frequency only, and so generates phase conjugated terms. The square pulse is periodic at the fundamental frequency, and delimited alternately by the firing and end of commutation angles as listed in table 3.2. The complex Euler coefficient for the

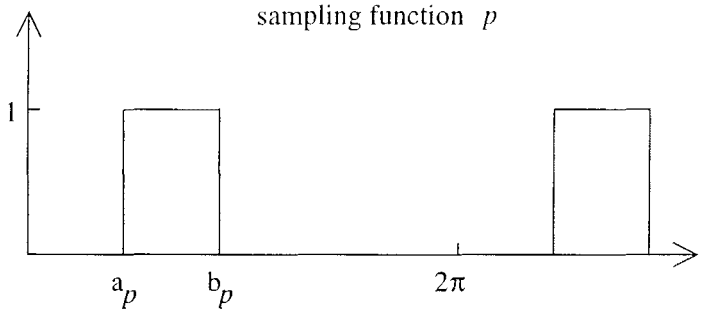

Figure 3.9 Sampling functions used for convolutions.

sampling function at harmonic k is

$$\Psi_{p_k} = \frac{1}{k\pi}[\cos(ka_p) - \cos(kb_p)] + j\frac{1}{k\pi}[\sin(kb_p) - \sin(ka_p)]. \tag{3.23}$$

$$\Psi_{p_0} = \begin{cases} j\frac{b_p - a_p}{2\pi} & b_p > a_p \\ j\left[1 - \frac{a_p - b_p}{2\pi}\right] & \text{otherwise} \end{cases} \tag{3.24}$$

Since the end of one conduction interval is the beginning of the next, all of the trigonometric evaluations are used in two consecutive sampling functions, thus halving the number of calculations. The dc voltage can now be written as:

sample (p)	a_p	b_p
1	θ_1	ϕ_1
2	ϕ_1	θ_2
3	θ_2	ϕ_2
4	ϕ_2	θ_3
5	θ_3	ϕ_3
6	ϕ_3	θ_4
7	θ_4	ϕ_4
8	ϕ_4	θ_5
9	θ_5	ϕ_5
10	ϕ_5	θ_6
11	θ_6	ϕ_6
12	ϕ_6	θ_1

Table 3.2 Limits of convertor states for use in sampling functions

$$V_d = \sum_{p=1}^{12} V_{dp} \otimes \Psi_p. \tag{3.25}$$

The convolution of two phasors is given by,

$$A_k \otimes B_l = \begin{cases} \frac{1}{2}j(A_k B_l^*)_{(k-l)} - \frac{1}{2}j(A_k B_l)_{(k+l)} & \text{if } k \geq l \\ \frac{1}{2}j(A_k B_l^*)^*_{(l-k)} - \frac{1}{2}j(A_k B_l)_{(k+l)} & \text{otherwise} \end{cases} \tag{3.26}$$

as described in Appendix A.

The conjugate operator makes the convolution non-analytic, and so not differentiable in the complex form. It avoids the need for negative harmonics however, and it is still possible to obtain partial derivatives by decomposing into real and imaginary parts. Sum and difference harmonics are generated by the convolution, and since it is required to calculate voltage harmonics up to n_h, the sampling function spectra must be evaluated up to $2n_h$. Since the convolution operator is linear, the twelve convolutions in equation 3.25 can be decomposed into convolutions of the component phasors:

$$V_{dp} \otimes \Psi_p = \sum_{k=1}^{n_h} \sum_{l=0}^{2n_h} V_{dp_k} \otimes \Psi_{p_l}. \tag{3.27}$$

This equation generates voltage harmonic components of order above n_h which are discarded. By using equations 3.25, 3.26, and 3.27, the kth harmonic phasor component of V_d is

$$V_{d_k} = \frac{1}{2}j \sum_{p=1}^{12} \left\{ \sum_{l=k}^{n_h} (V_{dp_l} \Psi^*_{p_{l-k}}) + \sum_{l=1}^{n_h} (V_{dp_l} \Psi^*_{p_{l+k}})^* - \sum_{l=0}^{k} (V_{dp_l} \Psi_{p_{k-l}}) \right\} \quad , k > 0. \tag{3.28}$$

$$V_{d_0} = \frac{1}{2}j \sum_{p=1}^{12} \left\{ \sum_{l=0}^{n_h} (V_{dp_l} \Psi^*_{p_l}) - 2j(V_{dp_0} \Psi_{p_0}) \right\} \tag{3.29}$$

This completes the derivation of the dc voltage harmonics in terms of a dc side harmonic source, and a three phase ac side voltage source connected in star or delta, with source inductance. The process of sampling and convolution to obtain the dc voltage is demonstrated graphically in figure 3.10. This sequence of plots was obtained by first simulating a 6 pulse rectifier to the steady state in the time domain. The spectra of the terminal voltage and dc current were then used to calculate the dc voltage, allowing a validation against the time domain solution.

3.6 SECONDARY PHASE CURRENTS

The derivation of the DC voltage involves the convolution of twelve different DC voltage samples, so by using the same sampling functions, 36 convolutions would be required to obtain the three phase currents. However referring to table 3.1, and using the linearity

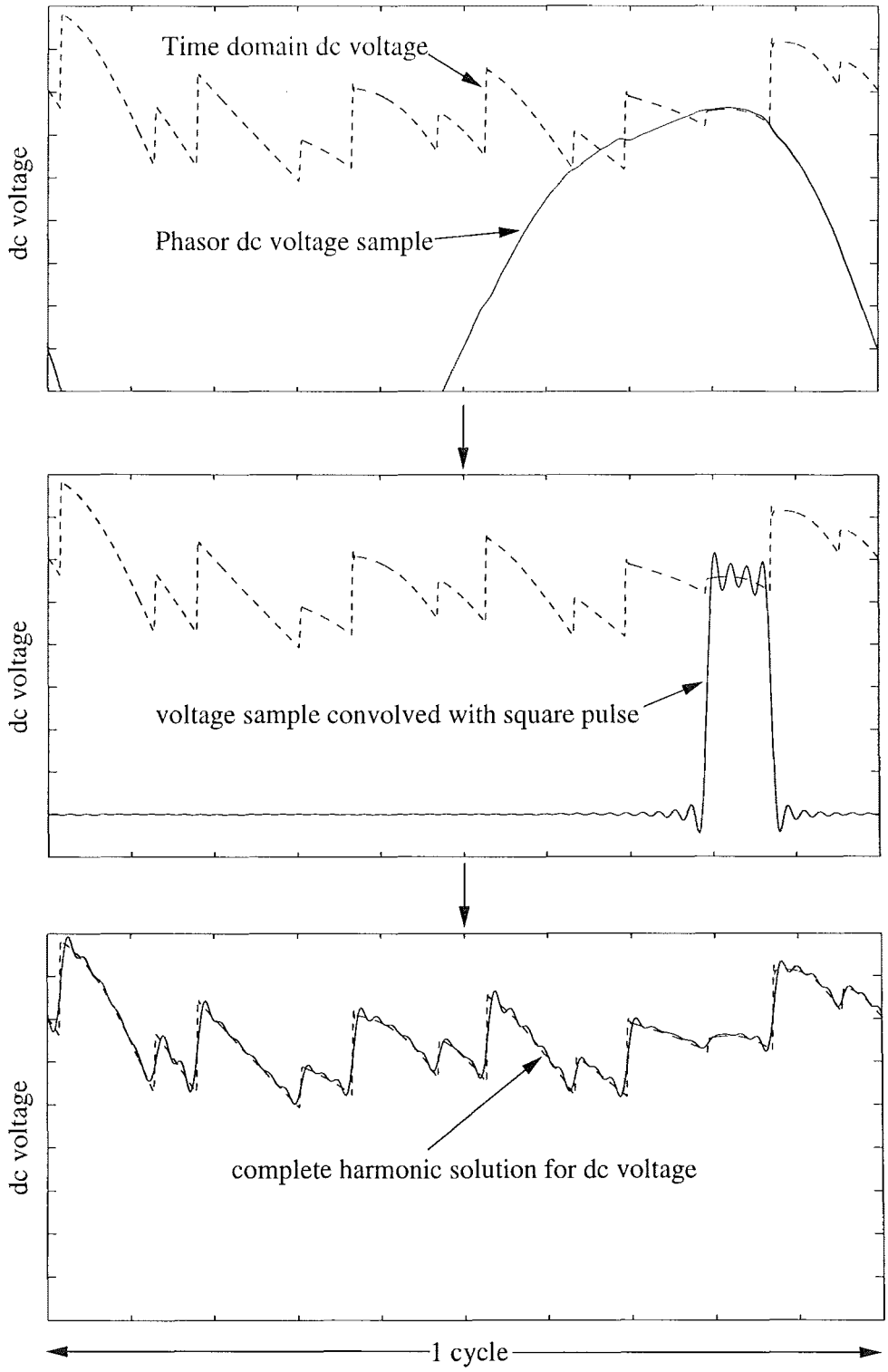

Figure 3.10 Construction of the dc voltage, and validation against time domain solution.

of the convolution, the phase A secondary current can be written as:

$$\begin{aligned} I_a &= I_d \otimes \{\Psi_2 + \Psi_3 + \Psi_4 + \Psi_5 - \Psi_8 - \Psi_9 - \Psi_{10} - \Psi_{11}\} \\ &\quad + I_{c_1} \otimes \Psi_1 - I_{c_3} \otimes \Psi_5 - I_{c_4} \otimes \Psi_7 + I_{c_6} \otimes \Psi_{11} \end{aligned} , \tag{3.30}$$

and similarly for one of the other two phases. The third phase must always be the negative sum of the first two, since there is no path for zero sequence into a bridge. This leads to a total of 8 convolutions to calculate the three phase currents. As evident in equation 3.30, the periodic samples for the phase current calculation are just the dc side current, and the commutation currents derived in section 3.3. The calculation of the phase current flowing into the transformer primary is addressed in the next section. The derivation of a phase current is illustrated graphically in figure 3.11.

3.7 TRANSFORMER MODELLING

The convertor transformer is a critical element in a HVdc convertor, simultaneously performing several useful tasks. Apart from altering the potential of the dc link to a level suitable for efficient transmission of energy, the convertor transformer is also part of a control loop that minimises the reactive power consumption by means of tap changer control of the secondary voltage. The star-g/delta connection, in phase shifting the fundamental by 30°, also shifts the negative sequence fifth, and positive sequence seventh by 180° with respect to a star-g/star connection. This phase shift causes the cancellation of low order harmonics that would otherwise require filtering. Finally, the transformer leakage reactance, via the commutation process, substantially reduces harmonics in the phase currents.

To the extent that these functions are not performed in an ideal manner, the injection of harmonic currents by the convertor will be larger at both characteristic and noncharacteristic harmonics. Unbalance in the tap changer setting between the two six pulse groups will lead to imperfect cancellation of six pulse harmonics on the ac and dc sides of the convertor. If the impedances in each phase of a three phase bank are not all equal, the convertor will generate positive and negative sequence odd triplen harmonics. The unbalanced star-g/delta connected transformer also acts as a sequence transformer, causing the convertor to both respond to, and generate zero sequence harmonics.

No attempt is made to model nonlinear transformer effects such as core saturation or hysteresis. The transformer is to be modelled as a series connection of ideal tap changing transformers on the primary and secondary sides, a conduction resistance, a leakage reactance, and a star/delta connection. The resistance and reactance may be unbalanced, but the tap settings are assumed to be the same on all phases. The tap change controller is not modelled as it does not respond to harmonics. The magnetising current injection is approximated by a shunt to ground at the primary terminal.

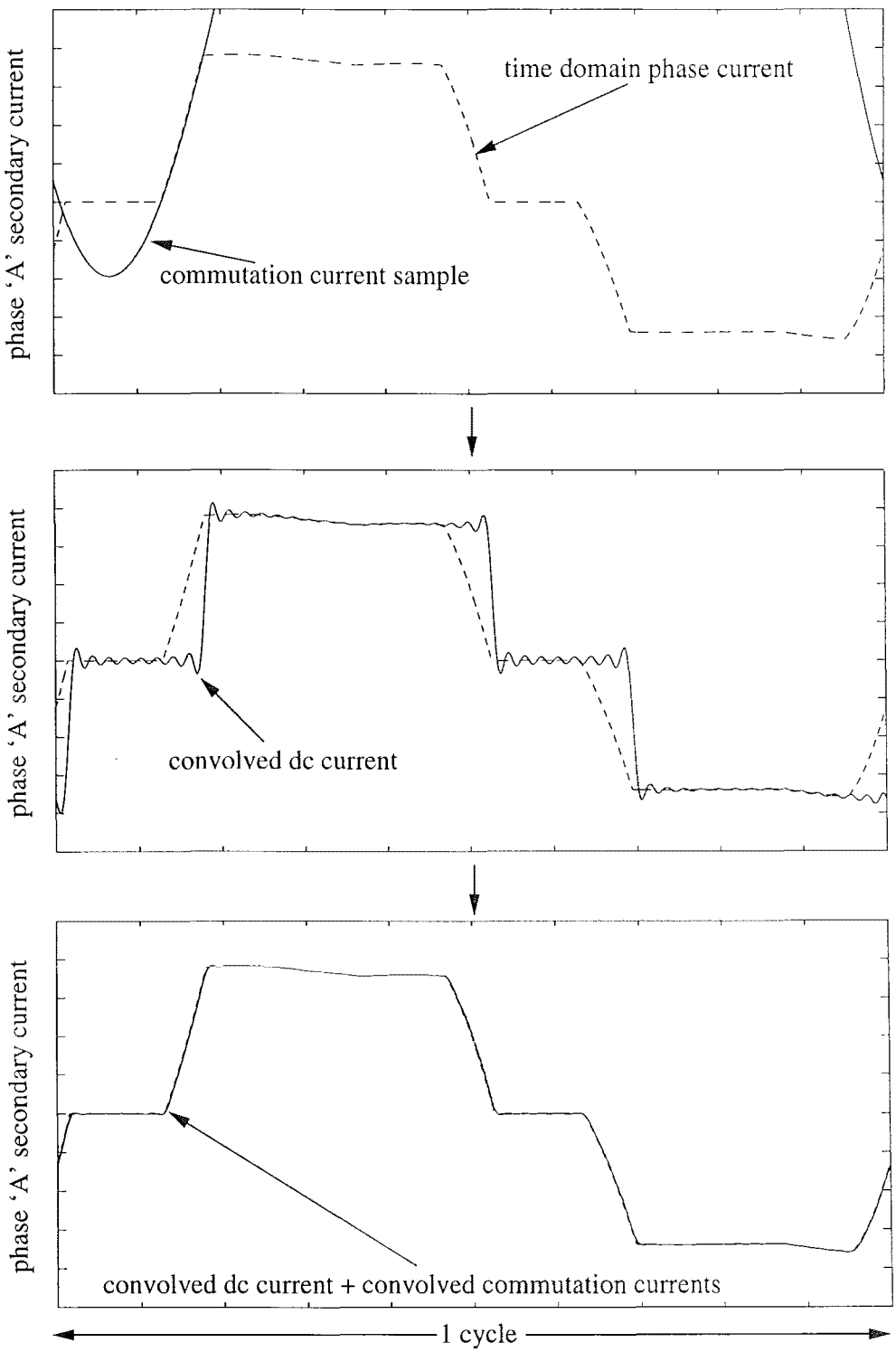

Figure 3.11 Construction of the phase current, and validation against time domain solution.

The outcome of this analysis is a transfer model of the transformer; the primary currents are related directly to the secondary currents, and the secondary voltage to the primary voltage. This is easily achieved for the star-g/star connection, shown as a single line diagram in figure 3.12. The transformer and thyristor resistances have been referred to an equivalent ac side resistance, R_{ac}:

$$R_{ac} = a_1^2 \left(\frac{R_t}{a_2^2} + R_c \right). \tag{3.31}$$

The leakage reactance has been referred to an equivalent on the secondary side:

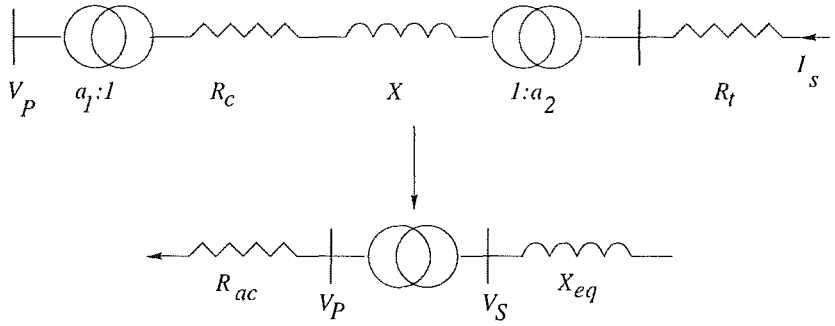

Figure 3.12 Equivalent circuit for star-g/star transformer.

$$X_{eq} = a_2^2 X. \tag{3.32}$$

Since all impedance has been removed from the transformer, the secondary voltage is now independent of the current through the transformer:

$$V_S = \frac{a_2}{a_1} V_P, \tag{3.33}$$

and similarly for the phase current:

$$I_P = \frac{a_2}{a_1} I_S. \tag{3.34}$$

These equations are repeated over all harmonics, and all three phases.

The star-g/delta connected transformer is considerably more difficult to model, and in fact requires two separate analyses for transfers from the star to delta side and vice versa. As shown in figure 3.13, the transfer from star to delta is primarily concerned with setting up the delta connected source for the voltage sampling and commutation analyses. The secondary side delta connected voltage source is scaled by:

$$V_S = \sqrt{3} \frac{a_2}{a_1} V_P, \tag{3.35}$$

and the equivalent reactance is:

$$X_{eq} = 3a_2^2 X. \tag{3.36}$$

The $\sqrt{3}$ scaling for the delta winding does not affect the transfer of thyristor resistance through the transformer, since it is not connected in delta. Thus, the referred ac system resistance is the same as equation 3.31.

Calculation of the primary side phase currents in terms of the secondary currents is complicated by the circulating current in the delta winding. If the transformer is unbalanced, some of this appears as a positive or negative sequence current on the primary side.

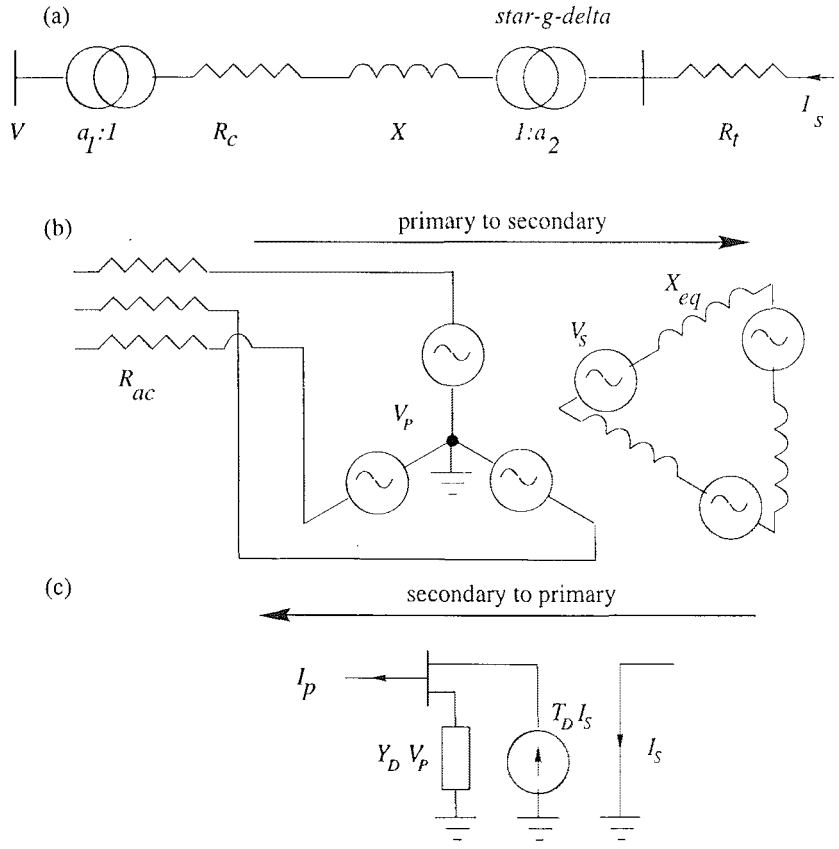

Figure 3.13 a) Equivalent circuit for star-g/delta transformer. b) transfer from star to delta. c) transfer from delta to star.

The admittance matrix for an unbalanced star-g/delta transformer is readily obtained:

$$\begin{bmatrix} I_{Pa} \\ I_{Pb} \\ I_{Pc} \\ I_{Sa} \\ I_{Sb} \\ I_{Sc} \end{bmatrix} = \begin{bmatrix} \alpha^2 Y_a & 0 & 0 & -\alpha\beta Y_a & \alpha\beta Y_a & 0 \\ 0 & \alpha^2 Y_b & 0 & 0 & -\alpha\beta Y_b & \alpha\beta Y_b \\ 0 & 0 & \alpha^2 Y_c & \alpha\beta Y_c & 0 & -\alpha\beta Y_c \\ -\alpha\beta Y_a & 0 & \alpha\beta Y_c & \beta^2(Y_a + Y_c) & -\beta^2 Y_a & -\beta^2 Y_c \\ \alpha\beta Y_a & -\alpha\beta Y_b & 0 & -\beta^2 Y_a & \beta^2(Y_a + Y_b) & -\beta^2 Y_b \\ 0 & \alpha\beta Y_b & -\alpha\beta Y_c & -\beta^2 Y_c & -\beta^2 Y_b & \beta^2(Y_b + Y_c) \end{bmatrix} \begin{bmatrix} V_{Pa} \\ V_{Pb} \\ V_{Pc} \\ V_{Sa} \\ V_{Sb} \\ V_{Sc} \end{bmatrix} \tag{3.37}$$

where:

$$Y = \frac{1}{R_c + jX} \tag{3.38}$$

$$\alpha = \frac{1}{a_1} \tag{3.39}$$

$$\beta = \frac{1}{\sqrt{3}a_2}. \tag{3.40}$$

Equation 3.37 is used to calculate the primary current, by assuming that V_P and I_S are known, and eliminating V_S. The admittance matrix in equation 3.37 is not invertible, as the delta winding is floating; there are an infinite number of possible potentials of the delta winding which are consistent with a given current injection into the transformer. One such potential is that obtained by grounding phase 'c' on the secondary so that $V_{Sc} = 0$. This permits the removal of the last row and column from equation 3.37:

$$\begin{bmatrix} I_{Pa} \\ I_{Pb} \\ I_{Pc} \\ I_{Sa} \\ I_{Sb} \end{bmatrix} = \begin{bmatrix} A & B \\ C & D \end{bmatrix} \begin{bmatrix} V_{Pa} \\ V_{Pb} \\ V_{Pc} \\ V_{Sa} \\ V_{Sb} \end{bmatrix}, \tag{3.41}$$

where:

$$A = \begin{bmatrix} \alpha^2 Y_a & 0 & 0 \\ 0 & \alpha^2 Y_b & 0 \\ 0 & 0 & \alpha^2 Y_c \end{bmatrix}, \tag{3.42}$$

$$B = \begin{bmatrix} -\alpha\beta Y_a & \alpha\beta Y_a \\ 0 & -\alpha\beta Y_b \\ \alpha\beta Y_c & 0 \end{bmatrix}, \tag{3.43}$$

$$C = \begin{bmatrix} -\alpha\beta Y_a & 0 & \alpha\beta Y_c \\ \alpha\beta Y_a & -\alpha\beta Y_b & 0 \end{bmatrix}, \tag{3.44}$$

$$D = \begin{bmatrix} \beta^2(Y_a + Y_c) & -\beta^2 Y_a \\ -\beta^2 Y_a & \beta^2(Y_a + Y_b) \end{bmatrix}. \tag{3.45}$$

Eliminating V_s, the primary phase currents are:

$$I_P = [A - BD^{-1}C]V_P + BD^{-1}I_S, \tag{3.46}$$

$$\stackrel{\text{def}}{=} Y_D V_P + T_D I_S. \tag{3.47}$$

Y_D is a shunt admittance to ground at the convertor terminal that is added to the filter shunt. T_D is a transfer matrix across the transformer, of size 3×2, indicating that there is no zero sequence current on the secondary side, and that only the phase 'a' and 'b' currents need be calculated. If the transformer is balanced, then Y_D is a zero sequence shunt, and so is not invertible. This also implies that if the transformer is nearly balanced, Y_D has a high condition number, and should not be inverted into an impedance without first being combined with an admittance that offers a path to positive and negative sequence currents.

3.8 CONSTANT CURRENT CONTROL

The constant current controller typically responds to harmonic ripple in the dc current causing a modulation of the firing angles. This effect has been modelled in section 3.4, where the firing order was written as a Fourier series:

$$\alpha = \mathcal{I}\left\{ j\alpha_0 + \sum_{k=1}^{n_h} \alpha_k e^{jk\omega t} \right\}. \tag{3.48}$$

The α_k in this equation are obtained from the harmonic transfer function of the constant current PI controller. The constant component of the alpha order, α_0, cannot be solved for directly, as the PI control has a pole at zero frequency. However in the steady state, the average delay angle, α_0, takes on a value that causes the dc component of the dc current to be equal to the current order. This requirement is easily expressed as mismatch equation that has a zero crossing at the current order:

$$(V_{d0} - V_{dc})Y_{d0} - I_{d0} = 0. \tag{3.49}$$

This equation states that the the dc voltage, when applied to the dc system, causes the current order to flow in the dc system. The dc voltage is obtained from equation 3.29. Note that equation 3.49 is not a function of α_0, the average delay angle does however

feature in the firing angle mismatch equations 3.11. When the convertor is solved in chapter 4, the average alpha order will emerge from the Newton solution.

3.9 CONSTANT POWER CONTROL

The constant power controller passes a current order to the current controller that leads to the rectified power being the power order for the link. The time constant of the power controller is assumed to be long enough that it is unresponsive to harmonics in the instantaneous dc power. The power controller is therefore easily modelled by:

$$P_{measured} - P_{order} = 0. \tag{3.50}$$

The measured power is the constant component of the convolution of the measured dc voltage with the measured dc current, where the measured quantity is a harmonic weighting of the actual quantity due to the linear frequency response of the measurement transducer:

$$I^m_{dk} = C_{Ik} I_{dk}, \tag{3.51}$$

$$V^m_{dk} = C_{Vk} V_{dk}, \tag{3.52}$$

and

$$P_{measured} = \mathcal{I}\left\{\frac{1}{2}j\left[\sum_{l=0}^{n_h}(V^m_{dl} I^{m*}_{dl}) - 2j(V^m_{d0} I^m_{d0})\right]\right\}. \tag{3.53}$$

Typically the harmonics contribute little to the real power, and the measured power can be simplified to:

$$P_{measured} = V_{do} I_{d0}. \tag{3.54}$$

3.10 STATION LOAD AND FILTERS

This section describes the modelling of shunts at the convertor terminal. The shunts can be filters, a $P + jQ$ type load, a delta winding shunt, or a magnetising current injection. Only the first three have been properly modelled here, as they are by far the most significant. The filters and delta winding shunt are represented by three phase harmonic admittances, while the load is modelled by a current injection at the fundamental, and a shunt admittance at harmonics.

Given a per phase station load of $S = P + jQ$, the current injection is related to the load by

$$I_l = 2S^*/V^*. \tag{3.55}$$

The harmonic impedance of loads for harmonic studies is an area that requires further work, it is modelled here as an admittance:

$$Y_{lk} = P - j\frac{Q}{k}. \tag{3.56}$$

3.11 AC AND DC SYSTEM MODELLING

The interaction of the convertor with the ac and dc systems requires a transfer representation of these systems. For example, the terminal voltage of the convertor can be calculated from the phase current injection into the ac system, and knowledge of the ac system. Similarly, on the dc side, the dc current can be found by impressing the dc voltage upon a representation of the dc system.

The linear part of the ac system is readily modelled using existing harmonic software. Three phase harmonic penetration programs can model with relative ease the passive transmission system, and include approximate complex admittance models of loads, transformers, and synchronous machines. The resulting three phase harmonic admittance matrix of the power system can then be simplified to an equivalent admittance at the convertor bus by means of the Kron reduction. This step is essentially a linearisation of the power system from the convertor bus, as a complicated network can be converted into a Norton equivalent using the equivalent admittance. The Norton current would then be the calculated short circuit current at the convertor bus. If the system admittance matrix is invertible, a three phase Thevenin equivalent exists as well.

A high condition number, or linear dependence in the system equivalent admittance matrix will result if there is little or no path for zero, positive, or negative sequence current into the ac system. The most likely case would be a convertor bus, connected via a short transmission line to a delta, or ungrounded star connection. In this instance, zero sequence is blocked, and there is no equivalent impedance matrix for the ac system Thevenin equivalent. Generally this scenario is unlikely, shunt paths for zero sequence are provided wherever possible to reduce transmission of interference producing zero sequence. In addition, the convertor filters, load, or transformer delta may provide a zero sequence path. It is therefore assumed that the ac system can be represented by a Thevenin equivalent. If a case did arise where there was no zero sequence path, the convertor model could be modified to use a different type of mismatch on the ac side. This possibility is discussed in section 4.2.2.

Chapter 4

SOLUTION OF THE CONVERTOR BY NEWTON'S METHOD

4.1 INTRODUCTION

In this chapter a sparse Newton solution for the steady state interaction of a controlled convertor with the ac and dc systems is developed. The objective is to solve the system of figure 4.1. In this system the ac network is modelled by a three phase Thevenin

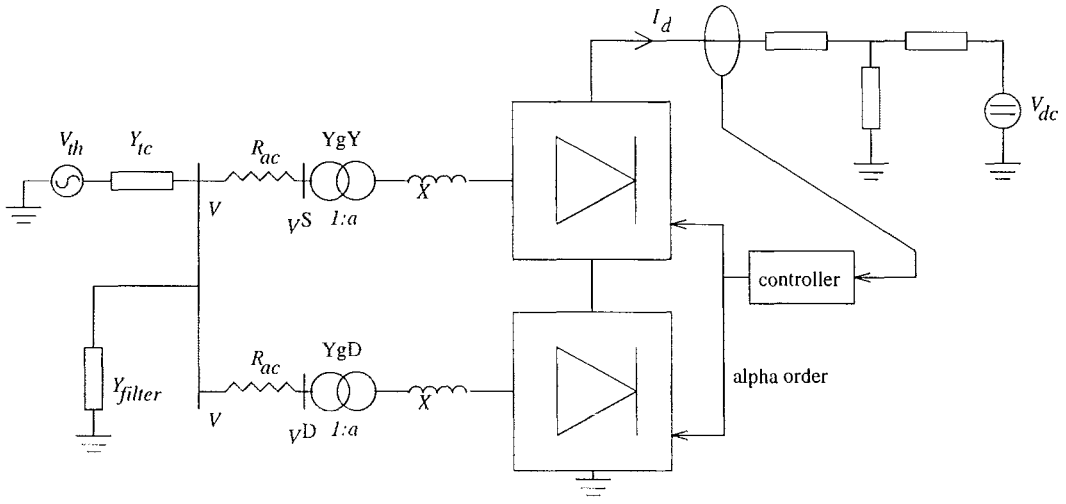

Figure 4.1 Twelve pulse convertor model to be solved.

equivalent, while the dc system is modelled by a T-circuit equivalent with a dc source representing the invertor end of a dc link. The six pulse version of this circuit has been solved in [Smith *et al.* 1995] for a system in which the ac system is infinite, and with a known harmonic voltage distortion.

The variables to solve for in figure 4.1 are the terminal voltage harmonic phasors, V^S and V^D, the dc current harmonics I_d, the twelve firing instants, θ, the twelve end of commutation instants, ϕ, the average delay angle, α_0, and, in the case of constant power control, the average dc current, I_{d0}. For a solution of every harmonic up to the

50th, there are therefore 726 unknowns, as each harmonic requires two variables to be specified. Being three phase and 2-port, a full specification of the terminal voltage requires six hundred variables. If the commutating resistance, R_c, is removed from the circuit, the number of unknowns reduces to 426 since the two six pulse rectifiers share the same ac terminal voltage. A solution for this system is developed by using the inter-relationships of chapter 3 to write a set of simultaneous mismatch equations, the simultaneous zero of which corresponds to the desired steady state solution. This nonlinear problem is solved by Newton's method with sparsity, and validated against a time domain simulation of a test system to the steady state.

4.1.1 Test System

The particular system used for the harmonic domain analysis and its time domain validation, is the rectifier end of the model developed by the CIGRE working group 14-02, 'Control in HVdc systems', for the purpose of comparing different controllers and simulation techniques [Szechtman *et al.* 1991]. The benchmark system is operationally difficult in that it consists of a weak ac system resonant at the 2nd harmonic, coupled via the convertor to a fundamental resonance on the dc side. Although designed for time domain and simulator studies, the benchmark is also ideal for testing the harmonic model, as a composite ac/dc resonance at the 2nd and 1st harmonics has a larger effect on the modulation of switching angles than other harmonics. The inverter in the CIGRE benchmark has been removed, and modelled in the dc circuit as a dc voltage source. Full parameters for the test system are given in appendix B.

4.2 MISMATCH EQUATIONS

The objective of this section is to develop mismatch equations suitable for use in Newton's method. It is necessary first to define all the quantities that will be used by reference to figure 4.1, to recast the relationships of chapter 3 in terms of these quantities, and finally to compose these relationships into a minimal set of variables and mismatch functions. The convertor circuit of figure 4.1 will be described by the following quantities:

- V, the three phase harmonic series convertor terminal voltage.
- V_P^D, the voltage at the equivalent star-g/delta transformer primary, on the convertor side of the lumped commutation resistance. As shown in figure 4.1 the transformer and thyristor conduction resistances have been lumped into an equivalent resistance between each bridge transformer and the ac terminal of the twelve pulse convertor.
- V_P^S, as above for for the star-g/star transformer.

- I_S^S, I_S^D the phase currents flowing into the secondary windings of the star-g/star and star-g/delta transformers, respectively.
- I_P^S, I_P^D the primary phase currents for the two transformers.
- V_{dk}, V_{d0} the dc voltage harmonics and dc component, respectively.
- I_{dk}, I_{d0} the dc current harmonics and dc component, respectively.
- $F_{\alpha 0}$ the average delay angle mismatch equation.
- $F_{\theta i}^D$, $F_{\theta i}^S$, the firing angle mismatches of the thyristors in the bridges attached to the star-g/delta and star-g/star transformers, respectively.
- $F_{\phi i}^D$, $F_{\phi i}^S$, the end of commutation mismatches in the bridges attached to the star-g/delta and star-g/star transformers, respectively.

4.2.1 Functional Description of the Twelve Pulse Convertor

Chapter 3 developed various equations to relate quantities around the components of a rectifier. The relationships derived are central to the convertor model, but are quite detailed. In this chapter, those relationships are used to solve the convertor, and it is only necessary to refer to the relationships of chapter 3 expressed in terms of variables relevant to figure 4.1. A functional notation is therefore introduced to describe relationships between the quantities that describe the convertor in the steady state. The starting point will be a relationship between the convertor phase currents, and the convertor terminal voltage.

Given the primary phase currents, the terminal voltage can be found by;

$$[V]_k = [Y_{cc}]_k^{-1}(-[I_P^S + I_P^D]_k + [Y_{ct}]_k[V_{th}]_k), \tag{4.1}$$

where the square brackets denote a three phase quantity. The AC system impedance, $[Y_{cc}]_k^{-1}$, is calculated by inverting the sum of the admittances attached to the convertor bus. These are the filter admittance, Y_{filter}, and the Thevenin source admittance, Y_{tc}. This equation will be represented over all phases and harmonics by:

$$V = f_1(I_P^S, I_P^D) \tag{4.2}$$

The convertor terminal voltage is then related to the equivalent transformer primary voltages by the voltage drops through the equivalent commutating resistances:

$$[V_P^S]_k = [V]_k - [R^S][I_P^S]_k' \tag{4.3}$$

$$[V_P^D]_k = [V]_k - [R^D][I_P^D]_k'. \tag{4.4}$$

The commutating resistance matrix is assumed frequency independent and diagonal, but possibly unbalanced. The use of phase currents from the previous iteration in equations 4.3 and 4.4, leads to the derivation of a smaller nonlinear system in section 4.2.2. This is denoted by the primed quantities in these equations. Using the function notation again, where phase currents from the previous iteration are treated as parameters, not variables:

$$V_P^S = f_2(V), \tag{4.5}$$
$$V_P^D = f_3(V). \tag{4.6}$$

Chapter 3 described how to calculate the dc voltage across a six pulse bridge attached to either a star or delta connected ac source, with inductive source impedance. Using the transformer models of section 3.7, the primary voltages, V_P^S and V_P^D, can be transformed into equivalent star or delta connected inductive sources on the secondary side. The dc voltages across each group are then added to obtain the total dc voltage, and the constant forward voltage drop associated with each group is subtracted from the total dc side voltage direct component. The calculation of the dc voltage is again represented in functional notation:

$$V_{dl} = f_4(V_P^S, V_P^D, I_{dk}, \theta_i^S, \theta_i^D, \phi_i^S, \phi_i^D), \tag{4.7}$$
$$V_{d0} = f_5(V_P^S, V_P^D, I_{dk}, \theta_i^S, \theta_i^D, \phi_i^S, \phi_i^D). \tag{4.8}$$

The dc voltage is functionally dependent on the switching angles since they define the limits of the convolution analysis used to calculate the dc side voltage across each group. The dc current harmonics are present in the calculation of the voltage samples which are convolved with the sampling functions. The dc voltage, when applied to the dc system, yields the dc side current. For example:

$$I_{dk} = V_{dk} Y_{dk} \tag{4.9}$$
$$I_{d0} = (V_{d0} - 4V_{fwd} - E_d) Y_{d0}. \tag{4.10}$$

summarised for any topology as:

$$I_{dk} = f_6(V_{dk}) \tag{4.11}$$
$$I_{d0} = f_7(V_{d0}). \tag{4.12}$$

The dc current, switching angles, and primary transformer voltage can be used to calculate the transformer secondary phase currents applying the analysis of section 3.6

to each bridge:

$$I_S^S = f_8(V_P^S, I_{dk}, I_{d0}, \theta_i^S, \phi_i^S) \quad (4.13)$$
$$I_S^D = f_9(V_P^D, I_{dk}, I_{d0}, \theta_i^D, \phi_i^D). \quad (4.14)$$

The transformer analysis of section 3.7 then describes how the primary currents are obtained:

$$I_P^S = f_{10}(I_S^S) \quad (4.15)$$
$$I_P^D = f_{11}(V_P^D, I_S^D). \quad (4.16)$$

Implicit equations have been derived in chapter 3 for the convertor switching angles, the power control, and the average delay angle. These equations, written in the form of mismatch equations which equal zero at the solution, are summarised below and in table 4.1.

$$M_\phi^S = f_{12}(V_P^S, I_{dk}, \theta_i^S, \phi_i^S) \quad (4.17)$$
$$M_\phi^D = f_{13}(V_P^D, I_{dk}, \theta_i^D, \phi_i^D) \quad (4.18)$$
$$M_\theta^S = f_{14}(I_{dk}, I_{d0}, \theta_i^S, \alpha_0) \quad (4.19)$$
$$M_\theta^D = f_{15}(I_{dk}, I_{d0}, \theta_i^D, \alpha_0) \quad (4.20)$$
$$M_S = f_{16}(V_{d0}, I_{d0}) \quad (4.21)$$
$$M_{\alpha 0} = f_{17}(V_{d0}, I_{d0}) \quad (4.22)$$

A total of seventeen functional relationships have been described, representing 2328 equations in as many unknowns, for a solution up to the 50th harmonic. The functional relationships are summarised in table 4.1.

4.2.2 Composition of Mismatch Functions

There is a great deal of redundancy in the system of equations summarised in table 4.1. By a variety of substitutions of functions for variables, the number of simultaneous equations and variables can be reduced to 426. For example, taking f_1 and substituting functions for the variables I_P^S and I_P^D:

$$\begin{aligned} V &= f_1(I_P^S, I_P^D) \\ &= f_1\left(f_{10}(I_S^S), f_{11}(V_P^D, I_S^D)\right) \\ &= f_1\left(f_{10}(f_8(V_P^S, I_{dk}, I_{d0}, \theta_i^S, \phi_i^S)), f_{11}(V_P^D, f_9(V_P^D, I_{dk}, I_{d0}, \theta_i^D, \phi_i^D))\right) \\ &= f_1\left(f_{10}(f_8(f_2(V), I_{dk}, I_{d0}, \theta_i^S, \phi_i^S)), f_{11}(f_3(V), f_9(f_3(V), I_{dk}, I_{d0}, \theta_i^D, \phi_i^D))\right) \\ &= f_{18}(V, I_{dk}, I_{d0}, \theta_i^D, \phi_i^D, \theta_i^S, \phi_i^S) \end{aligned} \quad (4.23)$$

Variable	No. of Vars.	Function of
V	300	$f_1(I_P^S, I_P^D)$
V_P^S	300	$f_2(V)$
V_P^D	300	$f_3(V)$
V_{dl}	100	$f_4(V_P^S, V_P^D, I_{dk}, \theta_i^S, \theta_i^D, \phi_i^S, \phi_i^D)$
V_{d0}	1	$f_5(V_P^S, V_P^D, I_{dk}, \theta_i^S, \theta_i^D, \phi_i^S, \phi_i^D)$
I_{dk}	100	$f_6(V_{dk})$
I_{d0}	1	$f_7(V_{d0})$
I_S^S	300	$f_8(V_P^S, I_{dk}, I_{d0}, \theta_i^S, \phi_i^S)$
I_S^D	300	$f_9(V_P^D, I_{dk}, I_{d0}, \theta_i^D, \phi_i^D)$
I_P^S	300	$f_{10}(I_S^S)$
I_P^D	300	$f_{11}(V_P^D, I_S^D)$
F_ϕ^S	6	$f_{12}(V_P^S, I_{dk}, \theta_i^S, \phi_i^S)$
F_ϕ^D	6	$f_{13}(V_P^D, I_{dk}, \theta_i^D, \phi_i^D)$
F_θ^S	6	$f_{14}(I_{dk}, I_{d0}, \theta_i^S, \alpha_0)$
F_θ^D	6	$f_{15}(I_{dk}, I_{d0}, \theta_i^D, \alpha_0)$
F_S	1	$f_{16}(V_{d0}, I_{d0})$
$F_{\alpha 0}$	1	$f_{17}(V_{d0}, I_{d0})$

Table 4.1 Functional relationships between 12 pulse rectifier variables

The new function, f_{18}, is a composition of several functions which describe how the dc current and terminal voltage, together with the switching angles are used to calculate the primary phase currents. The primary phase currents are then injected into the ac system impedance to yield the terminal voltage. The relationship

$$V = f_{18}(V, I_{dk}, I_{d0}, \theta_i^D, \phi_i^D, \theta_i^S, \phi_i^S) \tag{4.24}$$

can be written as a mismatch equation suitable for use in Newton's method:

$$F_V = V - f_{18}(V, I_{dk}, I_{d0}, \theta_i^D, \phi_i^D, \theta_i^S, \phi_i^S). \tag{4.25}$$

Equation 4.25 is called the *voltage mismatch equation*, and when decomposed into phases, harmonics, and rectangular components, yields 300 real equations. An exactly similar formulation for the terminal voltage mismatch was used by Valcárcel and Mayordomo [1993] in a three phase harmonic and load flow program. A similar type of mismatch equation can be constructed on the dc side:

$$\begin{aligned} I_{dk} &= f_6(V_{dk}) \\ &= f_6(f_4(V_P^S, V_P^D, I_{dl}, \theta_i^S, \theta_i^D, \phi_i^S, \phi_i^D)) \\ &= f_6(f_4(f_2(V), f_3(V), I_{dl}, \theta_i^S, \theta_i^D, \phi_i^S, \phi_i^D)) \\ &= f_{19}(V, I_{dk}, \theta_i^D, \phi_i^D, \theta_i^S, \phi_i^S) \end{aligned} \tag{4.26}$$

from which the following mismatch equation is constructed:

$$F_{Id} = I_{dk} - f_{19}(V, I_{dk}, I_{d0}, \theta_i^D, \phi_i^D, \theta_i^S, \phi_i^S). \tag{4.27}$$

Equation 4.27 yields 100 equations when decomposed into harmonic real and imaginary components, and is a composition of functions that describe the calculation of the dc voltage and its application to the dc system model, to yield the dc current. A further 26 mismatch equations are obtained in a similar manner, related to the convertor controller and the switching instants:

$$\begin{aligned}
F_\phi^S &= f_{12}(V_P^S, I_{dk}, \theta_i^S, \phi_i^S) \\
&= f_{12}(f_2(V), I_{dk}, \theta_i^S, \phi_i^S) \\
&= f_{20}(V, I_{dk}, \theta_i^S, \phi_i^S) && (4.28)\\
F_\phi^D &= f_{13}(V_P^D, I_{dk}, \theta_i^D, \phi_i^D) \\
&= f_{13}(f_3(V), I_{dk}, \theta_i^D, \phi_i^D) && (4.29)\\
&= f_{21}(V, I_{dk}, \theta_i^D, \phi_i^D) && (4.30)\\
F_\theta^S &= f_{14}(I_{dk}, I_{d0}, \theta_i^S, \alpha_0) && (4.31)\\
F_\theta^D &= f_{15}(I_{dk}, I_{d0}, \theta_i^D, \alpha_0) && (4.32)\\
F_S &= f_{16}(V_{d0}, I_{d0}) \\
&= f_{16}(f_5(V_P^S, V_P^D, I_{dk}, \theta_i^S, \theta_i^D, \phi_i^S, \phi_i^D), I_{d0}) \\
&= f_{16}(f_5(f_2(V), f_3(V), I_{dk}, \theta_i^S, \theta_i^D, \phi_i^S, \phi_i^D), I_{d0}) \\
&= f_{22}(V, I_{dk}, I_{d0}, \theta_i^S, \theta_i^D, \phi_i^S, \phi_i^D) && (4.33)\\
F_{\alpha 0} &= f_{17}(V_{d0}, I_{d0}) \\
&= f_{23}(V, I_{dk}, I_{d0}, \theta_i^S, \theta_i^D, \phi_i^S, \phi_i^D) && (4.34)
\end{aligned}$$

A smaller system of 426 simultaneous mismatch equations in 426 variables has now been developed, and is summarised in table 4.2. The reduced set of variables to be

Variable	No. of Vars.	Function of
F_V	300	$V - f_{18}(V, I_{dk}, I_{d0}, \theta_i^D, \phi_i^D, \theta_i^S, \phi_i^S)$
F_{Id}	100	$I_{dk} - f_{19}(V, I_{dk}, I_{d0}, \theta_i^D, \phi_i^D, \theta_i^S, \phi_i^S)$
F_ϕ^S	6	$f_{20}(V, I_{dk}, \theta_i^S, \phi_i^S)$
F_ϕ^D	6	$f_{21}(V, I_{dk}, \theta_i^D, \phi_i^D)$
F_θ^S	6	$f_{14}(I_{dk}, I_{d0}, \theta_i^S, \alpha_0)$
F_θ^D	6	$f_{15}(I_{dk}, I_{d0}, \theta_i^D, \alpha_0)$
F_S	1	$f_{22}(V, I_{dk}, I_{d0}, \theta_i^S, \theta_i^D, \phi_i^S, \phi_i^D)$
$F_{\alpha 0}$	1	$f_{23}(V, I_{dk}, I_{d0}, \theta_i^S, \theta_i^D, \phi_i^S, \phi_i^D)$

Table 4.2 Mismatches and variables for the 12 pulse rectifier.

solved for consists of the ac terminal voltage, the dc current, the switching angles, and the average delay angle.

It would be possible to solve for a different set of variables, however those chosen have the advantage of being less distorted. In particular, the ac side terminal voltage is less distorted than the phase currents, and the dc side current is less distorted than the dc voltage. In fact, a fundamental frequency ac/dc load flow, will give a very reasonable estimate of the fundamental voltage component on the ac side, and the dc current component on the dc side.

The interaction of the convertor with the ac system has been specified in terms of terminal voltage mismatch. This requires the injection of phase currents into the ac system impedance to obtain a voltage to be compared with the estimated terminal voltage.

The ac system interaction can also be expressed in terms of a current mismatch. The estimated terminal voltage is applied to the ac system admittance to obtain phase currents that are compared with phase currents calculated by the convertor model using the estimated voltage:

$$\begin{aligned} F_I &= [Y_{cc}][V] - [Y_{ct}][V_{th}] - f_8(f_2(V), I_{dk}, I_{d0}, \theta_i^S, \phi_i^S) \\ &\quad - f_9(f_3(V), I_{dk}, I_{d0}, \theta_i^D, \phi_i^D) \end{aligned} \tag{4.35}$$

Note that the current mismatch is still expressed in terms of the same variables as the voltage mismatch. The current mismatch has the advantage that it doesn't require the system admittance to be inverted, a possible difficulty if it has a high condition number. The current mismatch is also the preferred method of modelling the interaction with a purely inductive ac system, such as the unit connection, as the system admittance will decrease with increasing harmonic order.

Only the voltage mismatch will be implemented here, as the ac system admittance is usually invertible, and the ac system impedance is typically much less than one per unit. A hybrid mixture of voltage and current mismatches at different harmonic orders would be the most robust and versatile approach to take; the voltage mismatch would be used at all harmonics where the system impedance is less than one per unit, otherwise the current mismatch would be used. In the hybrid mismatch method, the convertor interacts with a reasonably strong ac system at all harmonic orders, and no admittance or impedance is larger than one per unit.

The dc current mismatch, F_{Id}, defining the interaction with the dc system, can also be written as a dc voltage mismatch, F_{Vd}. This mismatch is obtained by injecting the estimated dc current into the dc system impedance and comparing the resulting

voltage with the calculated dc voltage:

$$F_{Vd} = \frac{I_{dk}}{Y_{dk}} - f_4(f_2(V), f_3(V), I_{dk}, \theta_i^S, \theta_i^D, \phi_i^S, \phi_i^D) \tag{4.36}$$

The dc voltage mismatch would be preferred in the unlikely instance of a capacitive dc system. Again, a hybrid current and voltage mismatch on the dc side is the most robust, as a series resonance can be modelled by a small impedance rather than a large admittance as in the dc current mismatch equation. Only the current mismatch has been implemented in this chapter, as the dc side admittance to harmonics is generally less than one per unit due to the presence of a smoothing reactor.

4.3 NEWTON'S METHOD

The mismatch equations and variables obtained in section 4.2 are a mixture of real and complex valued. Newton's method is implemented here entirely in terms of real valued equations and variables. All complex quantities are therefore converted into real form by taking the real and imaginary components. A decomposition into polar components is also possible, and this is investigated in chapter 5. A decomposition into real form is required in any case, since the ac voltage and dc current mismatch equations are not differentiable in complex form. Newton's method is implemented by first assembling the variables to be solved for into a real vector X:

$$X = [\mathcal{R}\{V\}, \mathcal{I}\{V\}, \mathcal{R}\{I_d\}, \mathcal{I}\{I_d\}, \theta, \phi, \alpha_0, I_{d0}]^T. \tag{4.37}$$

The mismatch equations are likewise assembled into a real vector:

$$F(X) = [\mathcal{R}\{F_V\}, \mathcal{I}\{F_V\}, \mathcal{R}\{F_{Id}\}, \mathcal{I}\{Id\}, F_\theta, F_\phi, F_{\alpha 0}, F_{Id0}]^T. \tag{4.38}$$

Given an initial estimate of the solution, X^0, Newton's method is an iterative process for finding the solution vector, $X^\bullet$, that causes the mismatch vector to be zero:

$$F(X^\bullet) = 0. \tag{4.39}$$

The iterative process is defined by;

$$F(X^N) = J^N Y \tag{4.40}$$

$$X^{(N+1)} = X^N - Y, \tag{4.41}$$

with convergence deemed to have occurred when some norm of the residual vector $F(X^N)$ is less than a preset tolerance. Newton's method is not guaranteed to converge, but convergence is likely if the starting point is close to the solution. Central to Newton's method is a Jacobian matrix, J^N, of partial derivatives. For a system of 426

equations, the Jacobian is 426 elements square, as it contains the partial derivative of every mismatch function, with respect to every variable. This is illustrated for the twelve pulse convertor functions and variables in figure 4.2, for a system with constant current control.

There are two methods for obtaining the Jacobian elements; numerical partial differentiation, and the evaluation of analytically derived expressions for the partial derivatives. The numerical method is used here to validate the analytic expressions for the Jacobian elements. Numerical calculation of the Jacobian has the advantage of ease of coding, but is quite slow. Each column of the Jacobian requires an evaluation of all the mismatch equations, and the resulting calculation is only an approximation to the partial derivative. The *numerical Jacobian* is obtained by sequentially perturbing each element of X, and calculating the change in all the mismatches: $J_{ij} = \frac{\Delta F_i}{\Delta X_j}$. Provided ΔX_j is small enough, this gives a good approximation to the Jacobian.

The analytical method of calculating the Jacobian matrix requires considerable effort to obtain all the partial derivatives in analytic form, but is exceptionally fast. Frequently, the amount of computation required to calculate the *analytic Jacobian* is of the same order as that required to calculate the complete set of mismatches just once. For the convertor system of 426 mismatch equations, the analytic Jacobian can be calculated in about one second, as opposed to twenty seconds for the numerical Jacobian. The numerical Jacobian for the test system has been plotted in figure 4.3, for a solution up to the thirteenth harmonic. This Jacobian was calculated at the solution, and so represents a linearisation of the system of equations in table 4.2 around the convertor operating point.

Referring to figure 4.3, the elements of the Jacobian have been ordered in blocks corresponding to the three phases of terminal voltage, the dc current, the end of commutation angles, the firing angles, and the average delay angle. The blocks associated with interactions between the dc current harmonics, and the ac voltage harmonics comprise the *ac/dc partition*, which is 104 elements square. All other parts of the Jacobian are called the *switching terms*. Within the ac/dc partition, elements have been arranged within each block in ascending harmonic order, with the real and imaginary parts of each harmonic alternating. Each block in the ac/dc partition is therefore 26 elements square in figure 4.3, but 100 elements square for a solution to the fiftieth harmonic.

The Jacobian displays several important structural features:

A The test system contains a parallel resonance in the ac system at the second harmonic. This leads to rows of large terms in the Jacobian aligned with the second harmonic terminal voltage mismatch (the *resonance terms*).

B A change in harmonic k on one side of the convertor affects harmonics $k+1$ and $k-1$ on the other side of the convertor, causing the double diagonal structures

$$
J = \begin{bmatrix}
\frac{\partial \mathcal{R}\{F_{V_k^a}\}}{\partial \mathcal{R}\{V_m^a\}} & \frac{\partial \mathcal{R}\{F_{V_k^a}\}}{\partial \mathcal{I}\{V_m^a\}} & \frac{\partial \mathcal{R}\{F_{V_k^a}\}}{\partial \mathcal{R}\{V_m^b\}} & \frac{\partial \mathcal{R}\{F_{V_k^a}\}}{\partial \mathcal{I}\{V_m^b\}} & \frac{\partial \mathcal{R}\{F_{V_k^a}\}}{\partial \mathcal{R}\{V_m^c\}} & \frac{\partial \mathcal{R}\{F_{V_k^a}\}}{\partial \mathcal{I}\{V_m^c\}} & \frac{\partial \mathcal{R}\{F_{V_k^a}\}}{\partial \mathcal{R}\{I_{d_m}\}} & \frac{\partial \mathcal{R}\{F_{V_k^a}\}}{\partial \mathcal{I}\{I_{d_m}\}} & \frac{\partial \mathcal{R}\{F_{V_k^a}\}}{\partial \phi_i} & \frac{\partial \mathcal{R}\{F_{V_k^a}\}}{\partial \theta_i} & 0 \\
\frac{\partial \mathcal{I}\{F_{V_k^a}\}}{\partial \mathcal{R}\{V_m^a\}} & \frac{\partial \mathcal{I}\{F_{V_k^a}\}}{\partial \mathcal{I}\{V_m^a\}} & \frac{\partial \mathcal{I}\{F_{V_k^a}\}}{\partial \mathcal{R}\{V_m^b\}} & \frac{\partial \mathcal{I}\{F_{V_k^a}\}}{\partial \mathcal{I}\{V_m^b\}} & \frac{\partial \mathcal{I}\{F_{V_k^a}\}}{\partial \mathcal{R}\{V_m^c\}} & \frac{\partial \mathcal{I}\{F_{V_k^a}\}}{\partial \mathcal{I}\{V_m^c\}} & \frac{\partial \mathcal{I}\{F_{V_k^a}\}}{\partial \mathcal{R}\{I_{d_m}\}} & \frac{\partial \mathcal{I}\{F_{V_k^a}\}}{\partial \mathcal{I}\{I_{d_m}\}} & \frac{\partial \mathcal{I}\{F_{V_k^a}\}}{\partial \phi_i} & \frac{\partial \mathcal{I}\{F_{V_k^a}\}}{\partial \theta_i} & 0 \\
\frac{\partial \mathcal{R}\{F_{V_k^b}\}}{\partial \mathcal{R}\{V_m^a\}} & \frac{\partial \mathcal{R}\{F_{V_k^b}\}}{\partial \mathcal{I}\{V_m^a\}} & \frac{\partial \mathcal{R}\{F_{V_k^b}\}}{\partial \mathcal{R}\{V_m^b\}} & \frac{\partial \mathcal{R}\{F_{V_k^b}\}}{\partial \mathcal{I}\{V_m^b\}} & \frac{\partial \mathcal{R}\{F_{V_k^b}\}}{\partial \mathcal{R}\{V_m^c\}} & \frac{\partial \mathcal{R}\{F_{V_k^b}\}}{\partial \mathcal{I}\{V_m^c\}} & \frac{\partial \mathcal{R}\{F_{V_k^b}\}}{\partial \mathcal{R}\{I_{d_m}\}} & \frac{\partial \mathcal{R}\{F_{V_k^b}\}}{\partial \mathcal{I}\{I_{d_m}\}} & \frac{\partial \mathcal{R}\{F_{V_k^b}\}}{\partial \phi_i} & \frac{\partial \mathcal{R}\{F_{V_k^b}\}}{\partial \theta_i} & 0 \\
\frac{\partial \mathcal{I}\{F_{V_k^b}\}}{\partial \mathcal{R}\{V_m^a\}} & \frac{\partial \mathcal{I}\{F_{V_k^b}\}}{\partial \mathcal{I}\{V_m^a\}} & \frac{\partial \mathcal{I}\{F_{V_k^b}\}}{\partial \mathcal{R}\{V_m^b\}} & \frac{\partial \mathcal{I}\{F_{V_k^b}\}}{\partial \mathcal{I}\{V_m^b\}} & \frac{\partial \mathcal{I}\{F_{V_k^b}\}}{\partial \mathcal{R}\{V_m^c\}} & \frac{\partial \mathcal{I}\{F_{V_k^b}\}}{\partial \mathcal{I}\{V_m^c\}} & \frac{\partial \mathcal{I}\{F_{V_k^b}\}}{\partial \mathcal{R}\{I_{d_m}\}} & \frac{\partial \mathcal{I}\{F_{V_k^b}\}}{\partial \mathcal{I}\{I_{d_m}\}} & \frac{\partial \mathcal{I}\{F_{V_k^b}\}}{\partial \phi_i} & \frac{\partial \mathcal{I}\{F_{V_k^b}\}}{\partial \theta_i} & 0 \\
\frac{\partial \mathcal{R}\{F_{V_k^c}\}}{\partial \mathcal{R}\{V_m^a\}} & \frac{\partial \mathcal{R}\{F_{V_k^c}\}}{\partial \mathcal{I}\{V_m^a\}} & \frac{\partial \mathcal{R}\{F_{V_k^c}\}}{\partial \mathcal{R}\{V_m^b\}} & \frac{\partial \mathcal{R}\{F_{V_k^c}\}}{\partial \mathcal{I}\{V_m^b\}} & \frac{\partial \mathcal{R}\{F_{V_k^c}\}}{\partial \mathcal{R}\{V_m^c\}} & \frac{\partial \mathcal{R}\{F_{V_k^c}\}}{\partial \mathcal{I}\{V_m^c\}} & \frac{\partial \mathcal{R}\{F_{V_k^c}\}}{\partial \mathcal{R}\{I_{d_m}\}} & \frac{\partial \mathcal{R}\{F_{V_k^c}\}}{\partial \mathcal{I}\{I_{d_m}\}} & \frac{\partial \mathcal{R}\{F_{V_k^c}\}}{\partial \phi_i} & \frac{\partial \mathcal{R}\{F_{V_k^c}\}}{\partial \theta_i} & 0 \\
\frac{\partial \mathcal{I}\{F_{V_k^c}\}}{\partial \mathcal{R}\{V_m^a\}} & \frac{\partial \mathcal{I}\{F_{V_k^c}\}}{\partial \mathcal{I}\{V_m^a\}} & \frac{\partial \mathcal{I}\{F_{V_k^c}\}}{\partial \mathcal{R}\{V_m^b\}} & \frac{\partial \mathcal{I}\{F_{V_k^c}\}}{\partial \mathcal{I}\{V_m^b\}} & \frac{\partial \mathcal{I}\{F_{V_k^c}\}}{\partial \mathcal{R}\{V_m^c\}} & \frac{\partial \mathcal{I}\{F_{V_k^c}\}}{\partial \mathcal{I}\{V_m^c\}} & \frac{\partial \mathcal{I}\{F_{V_k^c}\}}{\partial \mathcal{R}\{I_{d_m}\}} & \frac{\partial \mathcal{I}\{F_{V_k^c}\}}{\partial \mathcal{I}\{I_{d_m}\}} & \frac{\partial \mathcal{I}\{F_{V_k^c}\}}{\partial \phi_i} & \frac{\partial \mathcal{I}\{F_{V_k^c}\}}{\partial \theta_i} & 0 \\
\frac{\partial \mathcal{R}\{F_{I_{d_k}}\}}{\partial \mathcal{R}\{V_m^a\}} & \frac{\partial \mathcal{R}\{F_{I_{d_k}}\}}{\partial \mathcal{I}\{V_m^a\}} & \frac{\partial \mathcal{R}\{F_{I_{d_k}}\}}{\partial \mathcal{R}\{V_m^b\}} & \frac{\partial \mathcal{R}\{F_{I_{d_k}}\}}{\partial \mathcal{I}\{V_m^b\}} & \frac{\partial \mathcal{R}\{F_{I_{d_k}}\}}{\partial \mathcal{R}\{V_m^c\}} & \frac{\partial \mathcal{R}\{F_{I_{d_k}}\}}{\partial \mathcal{I}\{V_m^c\}} & \frac{\partial \mathcal{R}\{F_{I_{d_k}}\}}{\partial \mathcal{R}\{I_{d_m}\}} & \frac{\partial \mathcal{R}\{F_{I_{d_k}}\}}{\partial \mathcal{I}\{I_{d_m}\}} & \frac{\partial \mathcal{R}\{F_{I_{d_k}}\}}{\partial \phi_i} & \frac{\partial \mathcal{R}\{F_{I_{d_k}}\}}{\partial \theta_i} & 0 \\
\frac{\partial \mathcal{I}\{F_{I_{d_k}}\}}{\partial \mathcal{R}\{V_m^a\}} & \frac{\partial \mathcal{I}\{F_{I_{d_k}}\}}{\partial \mathcal{I}\{V_m^a\}} & \frac{\partial \mathcal{I}\{F_{I_{d_k}}\}}{\partial \mathcal{R}\{V_m^b\}} & \frac{\partial \mathcal{I}\{F_{I_{d_k}}\}}{\partial \mathcal{I}\{V_m^b\}} & \frac{\partial \mathcal{I}\{F_{I_{d_k}}\}}{\partial \mathcal{R}\{V_m^c\}} & \frac{\partial \mathcal{I}\{F_{I_{d_k}}\}}{\partial \mathcal{I}\{V_m^c\}} & \frac{\partial \mathcal{I}\{F_{I_{d_k}}\}}{\partial \mathcal{R}\{I_{d_m}\}} & \frac{\partial \mathcal{I}\{F_{I_{d_k}}\}}{\partial \mathcal{I}\{I_{d_m}\}} & \frac{\partial \mathcal{I}\{F_{I_{d_k}}\}}{\partial \phi_i} & \frac{\partial \mathcal{I}\{F_{I_{d_k}}\}}{\partial \theta_i} & 0 \\
\frac{\partial F_{\phi_i}}{\partial \mathcal{R}\{V_m^a\}} & \frac{\partial F_{\phi_i}}{\partial \mathcal{I}\{V_m^a\}} & \frac{\partial F_{\phi_i}}{\partial \mathcal{R}\{V_m^b\}} & \frac{\partial F_{\phi_i}}{\partial \mathcal{I}\{V_m^b\}} & \frac{\partial F_{\phi_i}}{\partial \mathcal{R}\{V_m^c\}} & \frac{\partial F_{\phi_i}}{\partial \mathcal{I}\{V_m^c\}} & \frac{\partial F_{\phi_i}}{\partial \mathcal{R}\{I_{d_m}\}} & \frac{\partial F_{\phi_i}}{\partial \mathcal{I}\{I_{d_m}\}} & \frac{\partial F_{\phi_i}}{\partial \phi_i} & \frac{\partial F_{\phi_i}}{\partial \theta_i} & 0 \\
\frac{\partial F_{\theta_i}}{\partial \mathcal{R}\{V_m^a\}} & \frac{\partial F_{\theta_i}}{\partial \mathcal{I}\{V_m^a\}} & \frac{\partial F_{\theta_i}}{\partial \mathcal{R}\{V_m^b\}} & \frac{\partial F_{\theta_i}}{\partial \mathcal{I}\{V_m^b\}} & \frac{\partial F_{\theta_i}}{\partial \mathcal{R}\{V_m^c\}} & \frac{\partial F_{\theta_i}}{\partial \mathcal{I}\{V_m^c\}} & \frac{\partial F_{\theta_i}}{\partial \mathcal{R}\{I_{d_m}\}} & \frac{\partial F_{\theta_i}}{\partial \mathcal{I}\{I_{d_m}\}} & 0 & \frac{\partial F_{\theta_i}}{\partial \theta_i} & \frac{\partial F_{\theta_i}}{\partial \alpha_0} \\
\frac{\partial \mathcal{I}\{F_{\alpha_0}\}}{\partial \mathcal{R}\{V_m^a\}} & \frac{\partial \mathcal{I}\{F_{\alpha_0}\}}{\partial \mathcal{I}\{V_m^a\}} & \frac{\partial \mathcal{I}\{F_{\alpha_0}\}}{\partial \mathcal{R}\{V_m^b\}} & \frac{\partial \mathcal{I}\{F_{\alpha_0}\}}{\partial \mathcal{I}\{V_m^b\}} & \frac{\partial \mathcal{I}\{F_{\alpha_0}\}}{\partial \mathcal{R}\{V_m^c\}} & \frac{\partial \mathcal{I}\{F_{\alpha_0}\}}{\partial \mathcal{I}\{V_m^c\}} & \frac{\partial \mathcal{I}\{F_{\alpha_0}\}}{\partial \mathcal{R}\{I_{d_m}\}} & \frac{\partial \mathcal{I}\{F_{\alpha_0}\}}{\partial \mathcal{I}\{I_{d_m}\}} & \frac{\partial \mathcal{I}\{F_{\alpha_0}\}}{\partial \phi_i} & \frac{\partial \mathcal{I}\{F_{\alpha_0}\}}{\partial \theta_i} & 0
\end{bmatrix}
$$

Figure 4.2 Assembly of the Jacobian matrix from partial derivatives.

in the ac to dc, and dc to ac blocks. These are the *three port terms*, after [Larson *et al.* 1989].

C The end of commutation mismatch is very sensitive to harmonics in the terminal voltage and dc current.

D The individual firing instants are sensitive to harmonics in the dc current.

E The average delay angle mismatch, since it relates to the average dc current, is extremely sensitive to changes in the fundamental terminal voltage. There is also some sensitivity to harmonics coupled to the fundamental; ie the 11th and 13th harmonics on the ac side.

F As would be expected, there is strong coupling between the switching angles and the switching mismatches.

G The Jacobian contains a strong diagonal, approximately equal to one in the ac/dc partition. A large diagonal is often beneficial when the linear system corresponding to the Jacobian is solved.

There is also apparently no dependence of the terminal voltage mismatches on the end of commutation angles, even though there is a sensitivity to the firing angles. This seemingly anomalous result is due to the formulation of the mismatch equations. A change in θ moves the entire commutation current curve, whereas a change in ϕ moves only the end of commutation, consequently having a negligible effect. This is demonstrated in figure 4.4, and it is apparent that different behaviour would be observed with a different formulation of the mismatch equations.

The most useful feature of the Jacobian however, is the large number of small elements. Since the Jacobian is only an estimate of the behaviour of the nonlinear system in response to small perturbations, it is acceptable to approximate elements in the Jacobian, without affecting the convergence of Newton's method. Small elements may therefore be approximated by zero, making the Jacobian sparse. The sparsity structure of the Jacobian is illustrated in figure 4.5, and again the structural elements described above are evident. For a solution up to the fiftieth harmonic, the Jacobian is typically 96% sparse. The sparsity structure of figure 4.5 was obtained by scanning through the Jacobian, analytically calculating selected elements, and retaining those elements in the ac/dc partition larger than 0.05, and switching elements larger than 0.02.

In scanning the Jacobian, it is not necessary to calculate all elements. On the ac or dc side of the convertor, an odd harmonic never couples to an even harmonic, while for transfers across the convertor, an odd harmonic only couples to an even harmonic. The total time to scan the ac/dc partition can therefore be halved by scanning with the checkerboard pattern of figure 4.6. For a case with 50 harmonics, the bulk of

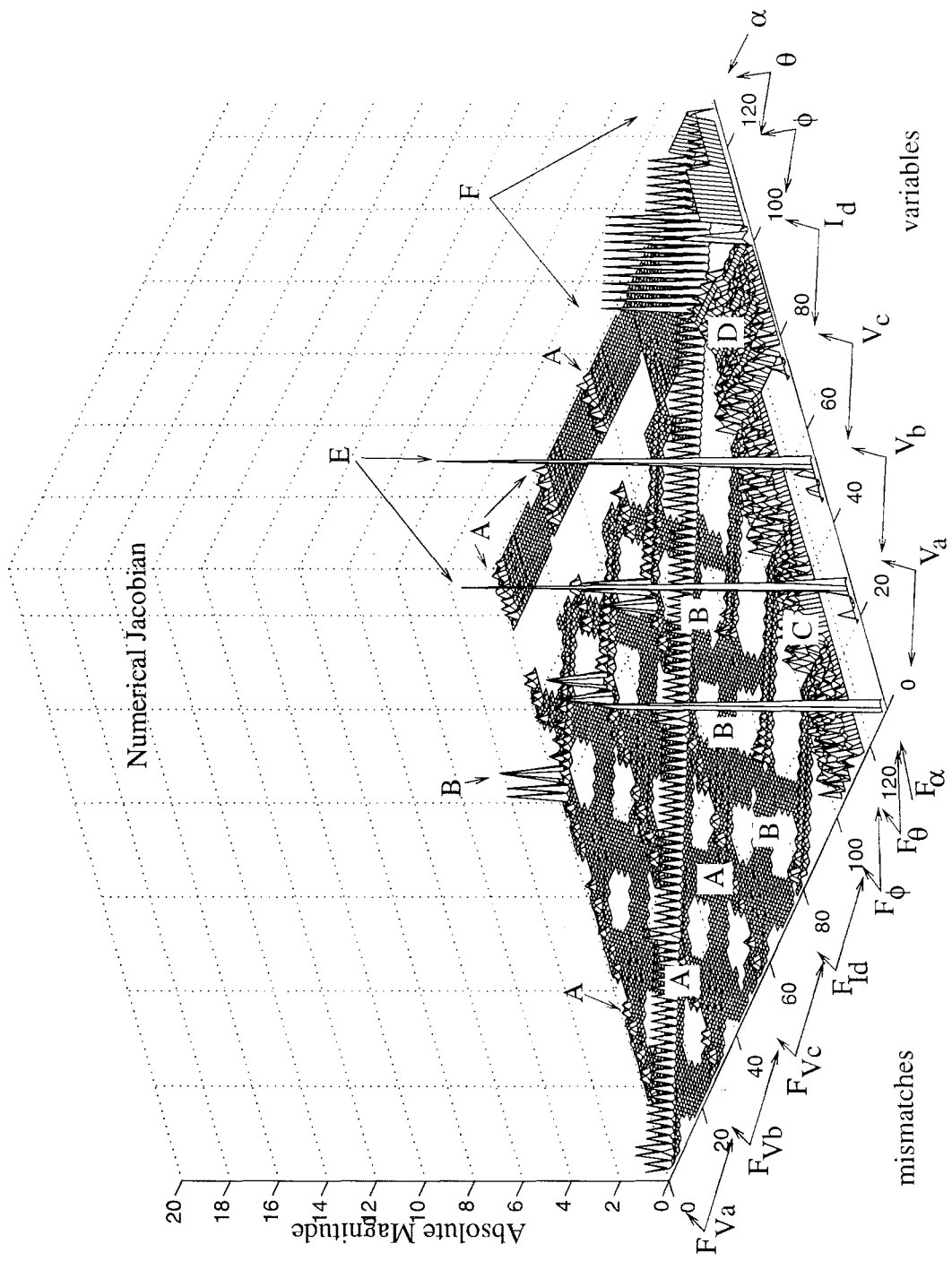

Figure 4.3 Numerically calculated Jacobian for the test system; 13 harmonics.

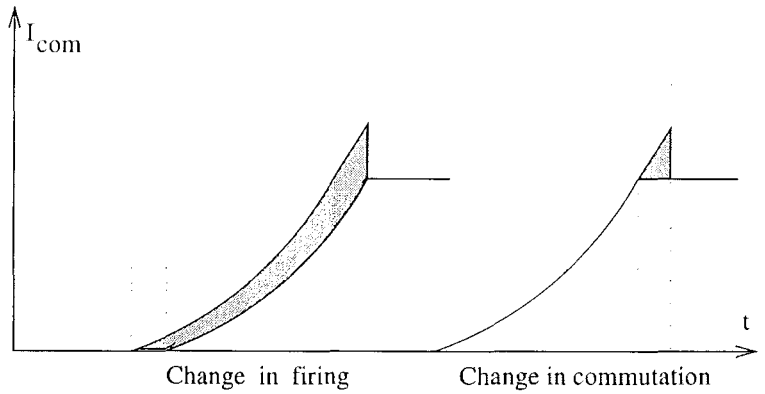

Figure 4.4 Effect of variation in firing angle versus end of commutation angle.

the Jacobian consists of the ac/dc partition, and clearly it would be worthwhile to develop more sophisticated scan algorithms. For example, scanning only the 3-port and resonance terms.

Analytic expressions for the partial derivatives that comprise the Jacobian elements are derived in appendix C. In order to simplify the derivation and notation, partial derivatives for a six pulse current controlled rectifier with a star-g/star connected transformer are obtained. The extension to twelve pulse partial derivatives is relatively straightforward, the twelve pulse ac/dc Jacobian partition being the sum of the ac/dc partitions for the two six pulse star and delta convertors, minus the identity matrix. The switching terms associated with each group are the same.

The partial derivative analytic expressions have been verified by calculating the sparse matrix of differences between the analytic Jacobian and the numerical Jacobian. The difference matrix is sparse, since it is only calculated at the sparse locations of the analytic Jacobian. As illustrated in figure 4.7, the two Jacobians agree to within 5×10^{-4}. Since convergence is not affected by a scan tolerance of 0.02, these differences are inconsequential, and are inherent to a numerical calculation of the Jacobian.

4.4 IMPLEMENTATION

In this section the application of Newton's method to the case at hand is described in detail. Several issues are addressed that have not yet been discussed. Of particular importance is the method of determining a suitable starting point for the Newton method, the updating of the Jacobian matrix, the sparse solution of the linear Jacobian system, and the stopping criteria for the iterative process. These points are illustrated in the flow diagram for the solution (figure 4.8), where it can be seen that a two stage process is employed to calculate the starting point. A first estimate of the convertor is obtained by using a classical analysis, followed by a Newton solution of the *switching*

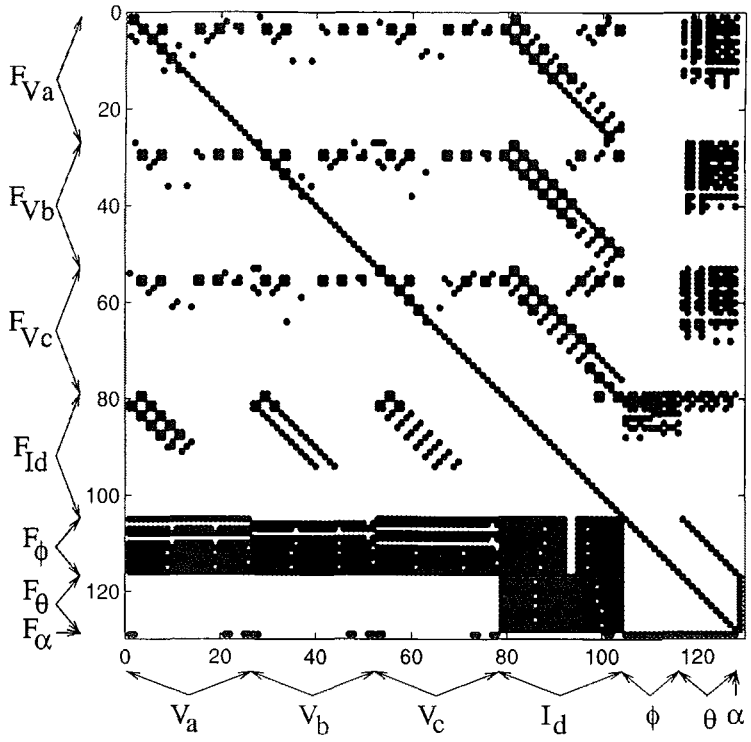

Figure 4.5 Sparsity structure of the Jacobian; 13 harmonics.

system, with no harmonics. If the switching system converges, a full harmonic solution follows, after which the results are printed to output files.

4.4.1 Initialisation

An initial estimate for the convertor delay angle is obtained from the equation:

$$V_{d0} = \frac{2 \cdot 3\sqrt{2 \cdot 3}}{\pi} |V_{th1}| \cos \alpha - \frac{3X}{\pi} I_{d0}, \tag{4.42}$$

ignoring voltage magnitude drop through the ac system impedance. The dc voltage is estimated from the voltage drop through the dc system and the dc source:

$$V_{d0} = E + \frac{I_{d0}}{Y_{d0}} \tag{4.43}$$

The average commutation angle is obtained from:

$$V_{d0} = \frac{3\sqrt{2}}{\pi} |V_{th}| [\cos \alpha + \cos (\alpha + \mu)] \tag{4.44}$$

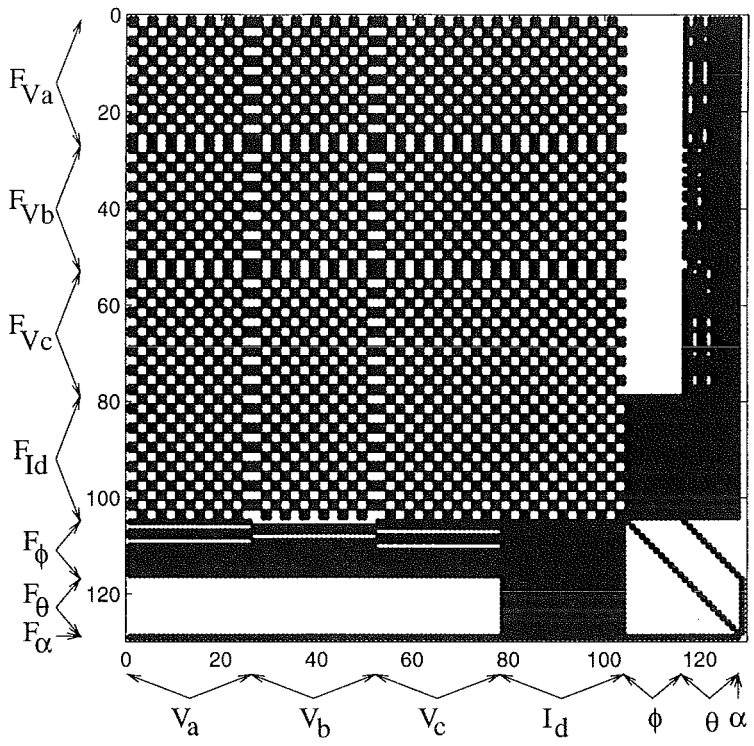

Figure 4.6 Scan structure of the sparse Jacobian; 13 harmonics.

These angles are then used to assemble the individual firing and end of commutation angles:

$$\theta_i = \beta_i + \alpha \tag{4.45}$$

$$\phi_i = \theta_i + \mu \tag{4.46}$$

These calculations yield a very rough estimate of the convertor switching angles, which is subsequently improved substantially by a Newton solution of the switching system.

4.4.2 The Switching System

The purpose of the switching system is to solve the relationships between the fundamental terminal voltage, the DC current, and the switching angles for both bridges. The switching system is thus a complete model of the twelve pulse convertor in the presence of constant terminal voltage and DC current harmonics, since the harmonic quantities appear as constant parameters. The mismatch equations and partial derivatives for the twelve pulse switching system have all been derived previously. The set of

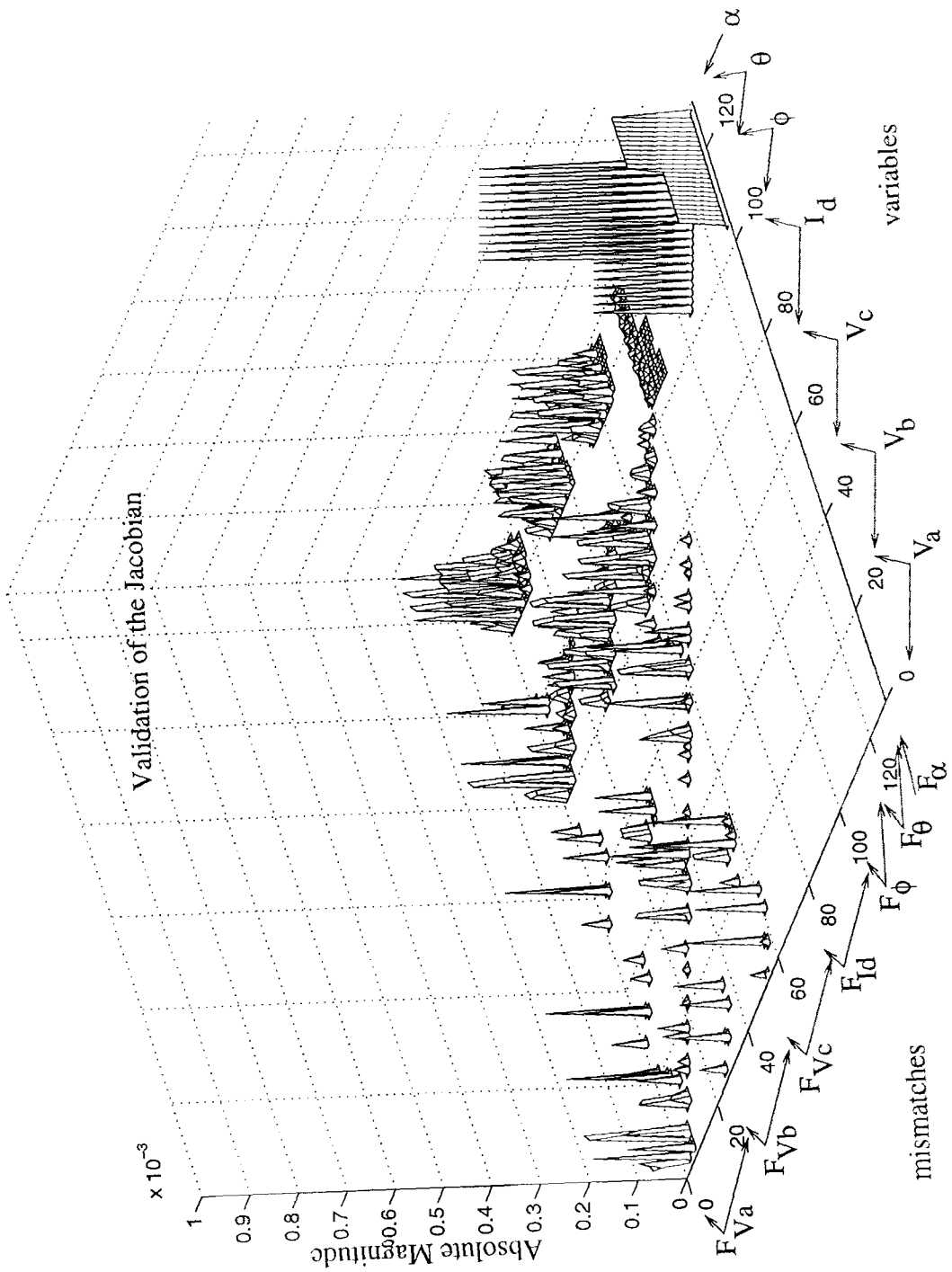

Figure 4.7 Difference between numerical and analytic Jacobians; 13 harmonics.

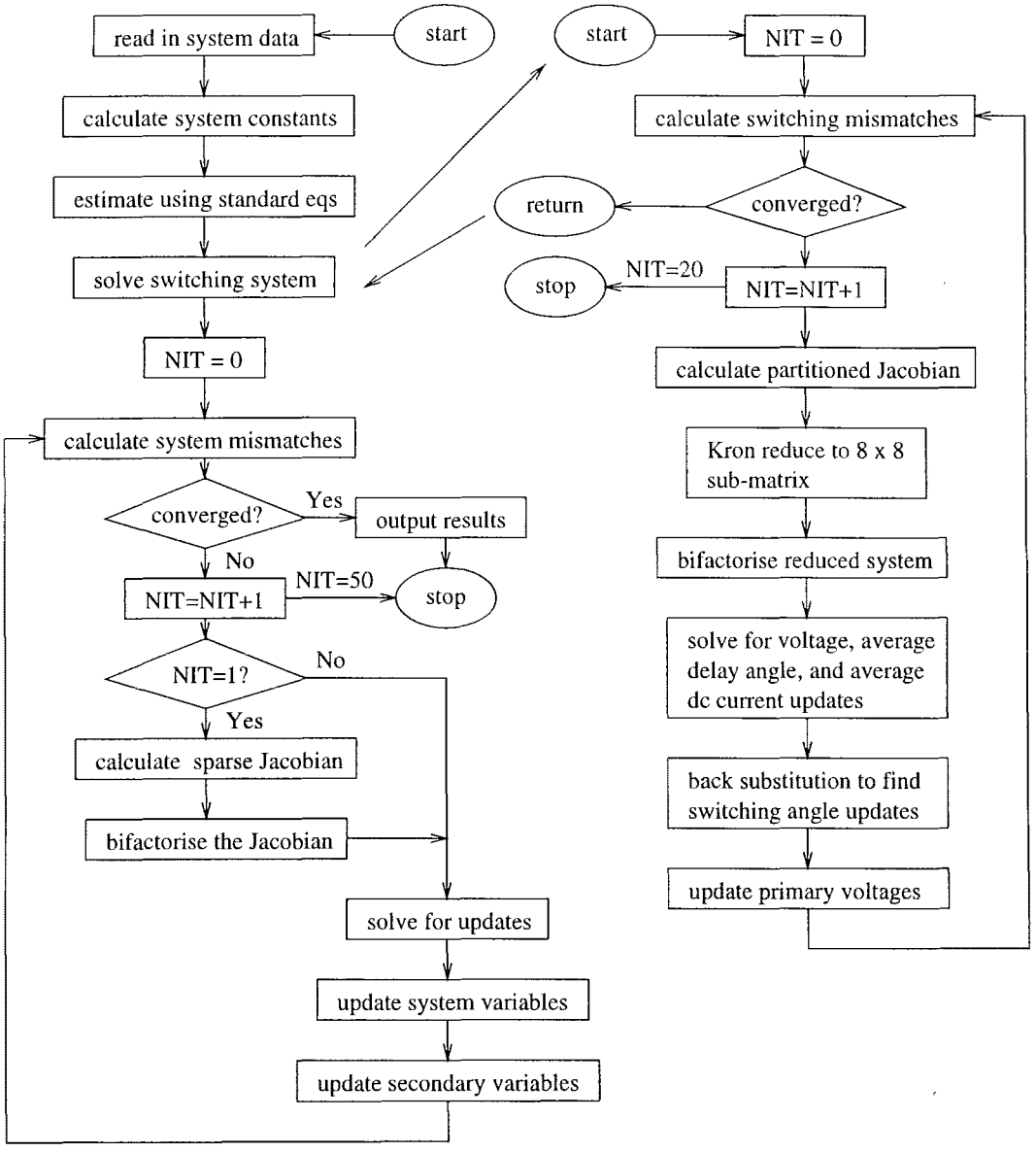

(a) main harmonic system (b) switching system

Figure 4.8 Flow chart for the sparse Newton solution.

equations to be solved in the switching system (for constant current control) are:

$$\begin{aligned} F^S_{\phi_i}(\phi^S_i, \theta^S_i, V, I_d) &= 0 \\ F^D_{\phi_i}(\phi^D_i, \theta^D_i, V, I_d) &= 0 \\ F^S_{\theta_i}(\theta^S_i, V, I_d) &= 0 \\ F^D_{\theta_i}(\theta^D_i, I_d, \alpha_0) &= 0 \\ F_{V_1}(\phi^S_i, \theta^S_i, V, I_d) &= 0 \\ F_{\alpha_0}(\phi^S_i, \theta^S_i, V, I_d) &= 0. \end{aligned} \tag{4.47}$$

A flow diagram for the switching system is shown in figure 4.8, part (b), while the structure of the switching Jacobian can be seen in figure 4.9. Those elements corresponding to the partial derivatives of voltage mismatch with respect to end of commutation angle have been set equal to zero, since they are always insignificant.

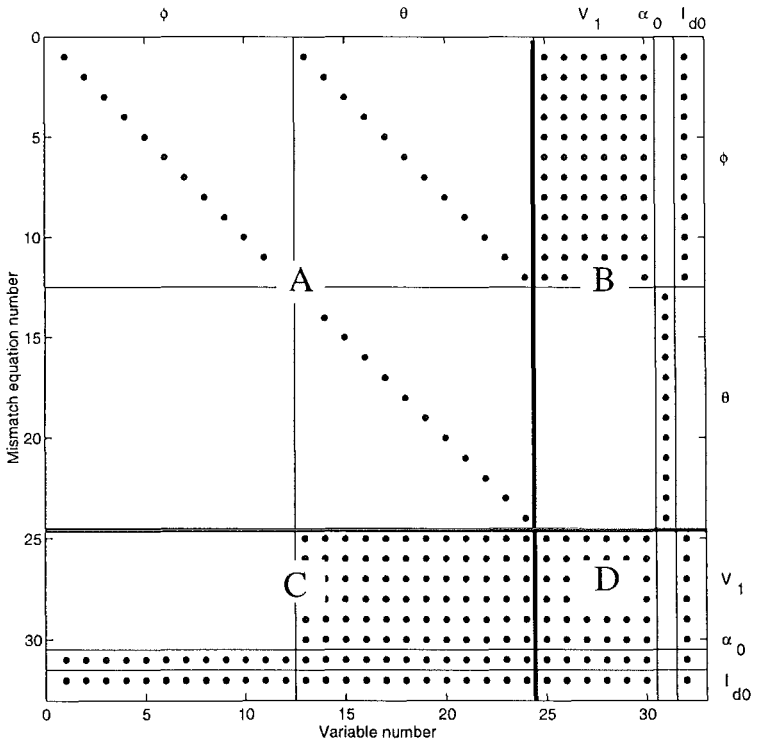

Figure 4.9 Sparsity structure of the switching Jacobian matrix (power control).

This Jacobian is quite sparse, and always has the same sparsity structure, however it is of an intermediate size, being too small for a general purpose sparse solution, and yet large enough to be significant. In the case of an interharmonic model, the switching Jacobian would be of size $24n+8$, where n is the number of cycles over which the steady state is defined. It is therefore worthwhile to develop an 'ad hoc' sparse solution of the

switching Jacobian, and the best way to do this is to employ a partitioning method.

With reference to figure 4.9, the partitioning method exploits the fact that the top left hand part of the switching Jacobian, A, is almost diagonal, and can easily be reduced to the identity matrix. It is then straightforward to create a reduced system of size 8×8 by multiplying the rectangular cross coupling partitions, C and B, to give $D - CB$. In this case the cross coupling matrix multiplication is very fast, since the variables have been ordered so that most of the nonzero elements of each of the cross coupling partitions correspond to the zeros of the other. Using this method, the linear system can be solved in approximately 1000 flops, instead of some 10 000. Indexing overheads have been virtually eliminated by storing partial derivatives directly into specific vectors, and then using 'ad hoc' code for the partitioning method. The reduced 8×8 system is solved by LU decomposition for the terminal voltage, average delay angle, and dc current order updates. These are then backsubstituted to find the switching angle updates.

The switching Jacobian is updated every iteration of the Newton method, and convergence has been found to be rapid and robust. The convergence criteria for the switching system is:

$$\begin{aligned}
\frac{|F_{V_1}|}{|V_1|} &< 0.001 \\
\frac{|F_{I_1}|}{|I_1|} &< 0.001 \\
\frac{|F_{\alpha_0}|}{|I_{d0}|} &< 0.001 \\
\frac{|F_{Id0}|}{|P|} &< 0.001 \\
|F_{\theta_i}| &< 5 \times 10^{-8} \\
|F_{\phi_i}| &< 5 \times 10^{-8}.
\end{aligned} \tag{4.48}$$

Convergence typically occurs in 4 to 10 iterations, for starting terminal voltages ranging from 0.3 to 7 p.u. A case with a system impedance of 1.3 p.u. at the fundamental has been solved (which required 11 iterations). A failure to converge in 20 iterations has so far always implied that the system has no solution. An invalid solution (eq negative firing angle) has never occurred, nor have multiple valid solutions been observed. If the dc voltage source is negative, the system will solve as for a current controlled inverter.

The solution obtained with the switching system is an excellent starting point for the full harmonic solution, as the switching angles are largely determined by interactions at the fundamental frequency. Since the switching system is three phase, it includes the effect of any unbalance. The switching system is utilised in chapter 5 as part of a fast decoupled convertor solution, and has also been interfaced to a three phase load flow.

4.4.3 The Harmonic Solution

The system of harmonic phasor and switching angle equations is quite large (426 elements square), and at each iteration of Newton's method, a linear system this size must be solved for the update vector: $F(X^N) = J^N Y^N$. This step represents the bulk of the computation required in Newton's method, and so techniques for speeding up the overall solution are concerned with details of the Jacobian linear system, and its solution method. The Jacobian has been made sparse, and it is essential that this sparsity is exploited in an efficient manner.

Three types of sparse linear solver have been implemented. One of these, the sparse symmetric bifactorisation [Zollenkopf 1970] method was found to be quite unsuitable, as it requires the Jacobian to be diagonally row dominant. Although the Jacobian has a large diagonal, it is not diagonally row dominant. The method of Zollenkopf pivots for sparsity, not numerical stability, and does not yield the correct solution when applied to the Jacobian system. The Zollenkopf method is essentially optimised for solving admittance matrix systems, which are necessarily symmetric in structure, and diagonally row dominant. The two other sparse solvers that have been implemented are an asymmetric sparse bifactorisation that pivots for a compromise between numerical stability and sparsity, and the iterative conjugate gradient method [Press *et al.* 1992]. The sparse bifactorisation employed is the *y12m* solver from the *netlib*[1]. Both methods have been found to be satisfactory, but suited to different types of solution algorithm.

Frequently, the Newton method can be improved by calculating the Jacobian matrix only once, on the first iteration, and keeping it constant throughout the solution. In this case, the sparse bifactorisation method is fastest, as the bifactorisation need only be calculated once. On subsequent iterations the linear system is solved using the factorised Jacobian from the first iteration. This method also avoids many of the indexing overheads associated with the sparse bifactorisation, since the sparsity structure is constant. Holding the Jacobian constant, leads to a larger number of faster iterations to obtain the overall solution.

Another method is to update 'important' parts of the Jacobian, holding the bulk of the Jacobian constant. Convergence in the least number of iterations has been obtained by holding the ac/dc partition constant, and updating the switching terms, since they can be recalculated quickly. In this case the Jacobian must be refactorised at each iteration, and the conjugate gradient method is almost as fast. The conjugate gradient method typically requires 100 iterations to converge to an accuracy in the update that does not slow the Newton solution. On the whole, the sparse bifactorisation has been found to be the most versatile. In the special case of the fast decoupled solution implemented in chapter 5, the conjugate gradient method requires on average just 10 iterations to converge, and is therefore faster.

[1] accessible on the World Wide Web at http://netlib.att.com/netlib/y12m/index.html

There are better iterative methods than the conjugate gradient, such as the preconditioned biconjugate gradient, that have not been implemented. The preconditioned biconjugate gradient method can be used efficiently if a sparse approximation to the inverse of the Jacobian can be created. This is very likely, as the inverse of the Jacobian contains many small elements. A final advantage of the conjugate gradient methods is that they can be easily implemented on a parallel processor, as the algorithm is based on successive sparse multiplications of the Jacobian by a vector.

4.4.4 Convergence Tolerance

The basic requirement of convergence is that all of the mismatches $F(X)_i$ are small enough. The mismatches however, are of several types, entailing a different convergence requirement for each type of mismatch. The convergence tolerances are listed below:

$$\begin{aligned}
\frac{|F_{Vk}|}{|V_k|} &< 0.001 \\
\frac{|F_{Ik}|}{|I_k|} &< 0.001 \\
\frac{|F_{Id}|}{|Id|} &< 0.001 \\
\frac{|F_{\alpha_0}|}{|I_{d0}|} &< 0.001 \\
\frac{|F_{Id0}|}{|P|} &< 0.001 \\
|F_{\theta_i}| &< 5 \times 10^{-8} \\
|F_{\phi_i}| &< 5 \times 10^{-8}.
\end{aligned} \tag{4.49}$$

Note that convergence tolerance for the complex mismatches, F_V, F_I, F_{Id} is expressed in terms of the magnitude of the mismatch. This means that the error in an estimated value for a variable , for example V_{11}, is smaller than 0.1% of its own length. The advantage of a relative mismatch of this type, is that it treats all harmonics equally. However to prevent an attempt to converge to an absolute error of zero for harmonics that are not present (eg even harmonics in some cases), this convergence test is only applied to harmonics that have a size larger than 10^{-5} per unit. These convergence tolerances can be made tighter to obtain more accurate solutions if necessary. A relative convergence tolerance of 2×10^{-6} has been used in the impedance calculations of chapter 6.

The tolerance set for the switching mismatches of 5×10^{-8} corresponds to 1.4×10^{-4} degrees at the 50th harmonic, or 0.1 nsec. This high tolerance has been used in the calculation of the convertor impedance, and does not require any extra iterations. Another type of convergence tolerance that can be used, is to calculate a norm of the

real mismatch vector; for example, the 1-norm:

$$|X|_1 = \sum_{i=1}^{n} |X_i| \tag{4.50}$$

A tolerance of $|X|_1 < 10^{-5}$ is suitable for general purpose use. This type of convergence test is fast and easy to apply, but does not imply that all harmonics have converged to a satisfactory accuracy.

4.5 VALIDATION AND PERFORMANCE

The model was verified against time domain simulation of the test system described in appendix B, using the program PSCAD/EMTDC. The steady state solution was obtained by simulating for one second, with a time step of 20μs, and then obtaining waveforms over one cycle for subsequent comparison with the harmonic domain solution. The results of four tests are given here, comparing the dc voltage and ac phase current waveforms and spectra, since these quantities are the most distorted. The tests are designed to highlight any modelling, and convergence deficiencies. The tests carried out were:

Test 1: A base case solution with no harmonic sources in the ac system.

Test 2: The Thevenin voltage source in the ac system was distorted by 5% positive sequence second harmonic. This excites the composite ac/dc system resonance, leading to noncharacteristic harmonics, and a high degree of interaction between convertor switching angles and the ac/dc harmonics.

Test 3: The leakage reactance of the phase 'b' star-g/delta transformer was increased from 0.18 to 0.3 per unit. This imbalance causes the generation of odd harmonics, and a relatively large coupling to the zero sequence, which is illustrated in figure 4.14.

Test 4: A 0.1 per unit resistance was placed in series with the star-g/delta transformer, and the secondary tap changer of that transformer was set to 1.1 p.u. Convergence with such a large series resistance indicates that the effect on convergence of not representing commutation resistance in the Jacobian is acceptable. Setting the tap changer on one transformer but not the other introduces six pulse unbalance. It was necessary to increase the ac system fundamental source from 1.10976 to 1.20976 p.u. to enable the current order to be satisfied.

The results of test one, the base case, are shown in figures 4.10 and 4.11. It can be seen from the spectra that only the characteristic harmonics are present, and that there is a close match between the time and harmonic domain solutions. The time domain solution yielded small residual non-characteristic harmonics in the spectra,

which were suppressed in the phase graphs. The dc voltage waveform was generated from the harmonic domain solution by plotting the Fourier series for each dc voltage sample during the appropriate interval, rather than inverse transforming the dc voltage spectra. This eliminates Gibbs phenomena associated with the step changes in voltage, but gives overly sharp voltage spikes. These are not present in the time domain solution due to modelling of the snubber circuits, which limit the $\frac{dV}{dt}$. The time domain derived dc voltage waveform is therefore more rounded. Clearly, if an accurate time domain waveform was required from the harmonic domain solution, it would be necessary to post process the waveshape using knowledge of the snubber circuit time domain response. The comparison of the waveshapes indicates that all the switching angles are correct.

When a second order harmonic voltage source was placed in the ac system, the composite resonance was excited, resulting in non-characteristic harmonics. Referring to figures 4.12 and 4.13, odd harmonics are present on the dc side, and even harmonics on the ac side. In particular, the fundamental resonance on the dc side is excited, and there is a large fundamental component in the dc voltage.

Unbalancing the star-g/delta transformer leakage reactance (figures 4.14 and 4.15), caused the generation of many harmonics, and a large zero sequence on the ac primary side. This is due to sequence transformation by the transformer, irrespective of its connection to a convertor. The zero sequence has been plotted in figure 4.14, and the close agreement with the time domain solution is evident. The final set of results, figures 4.16 and 4.17, shows the expected generation of six pulse harmonics due to imbalance between the two six pulse groups.

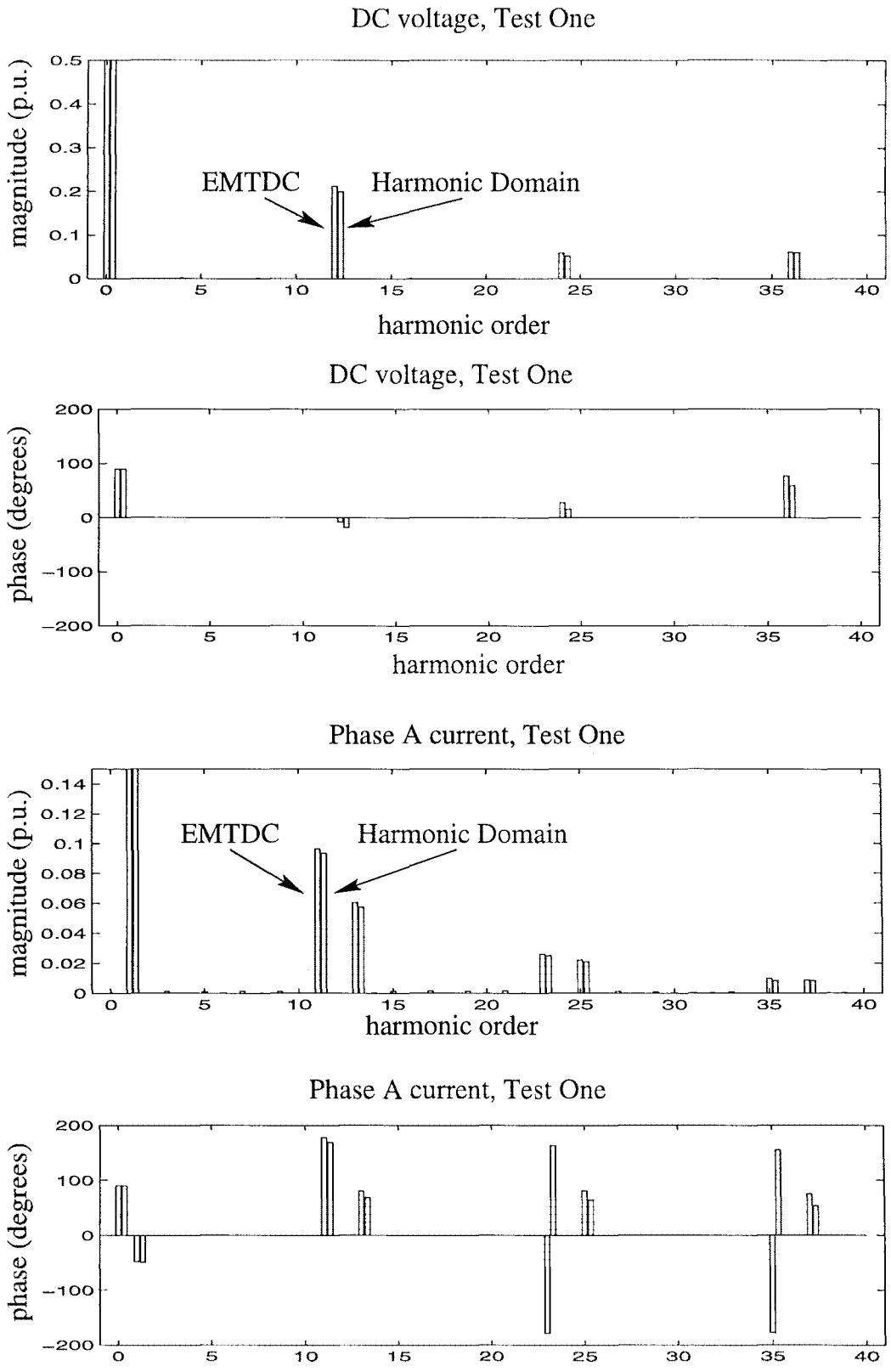

Figure 4.10 Comparison of time and harmonic domain solutions for phase currents and dc voltage spectra: Base Case

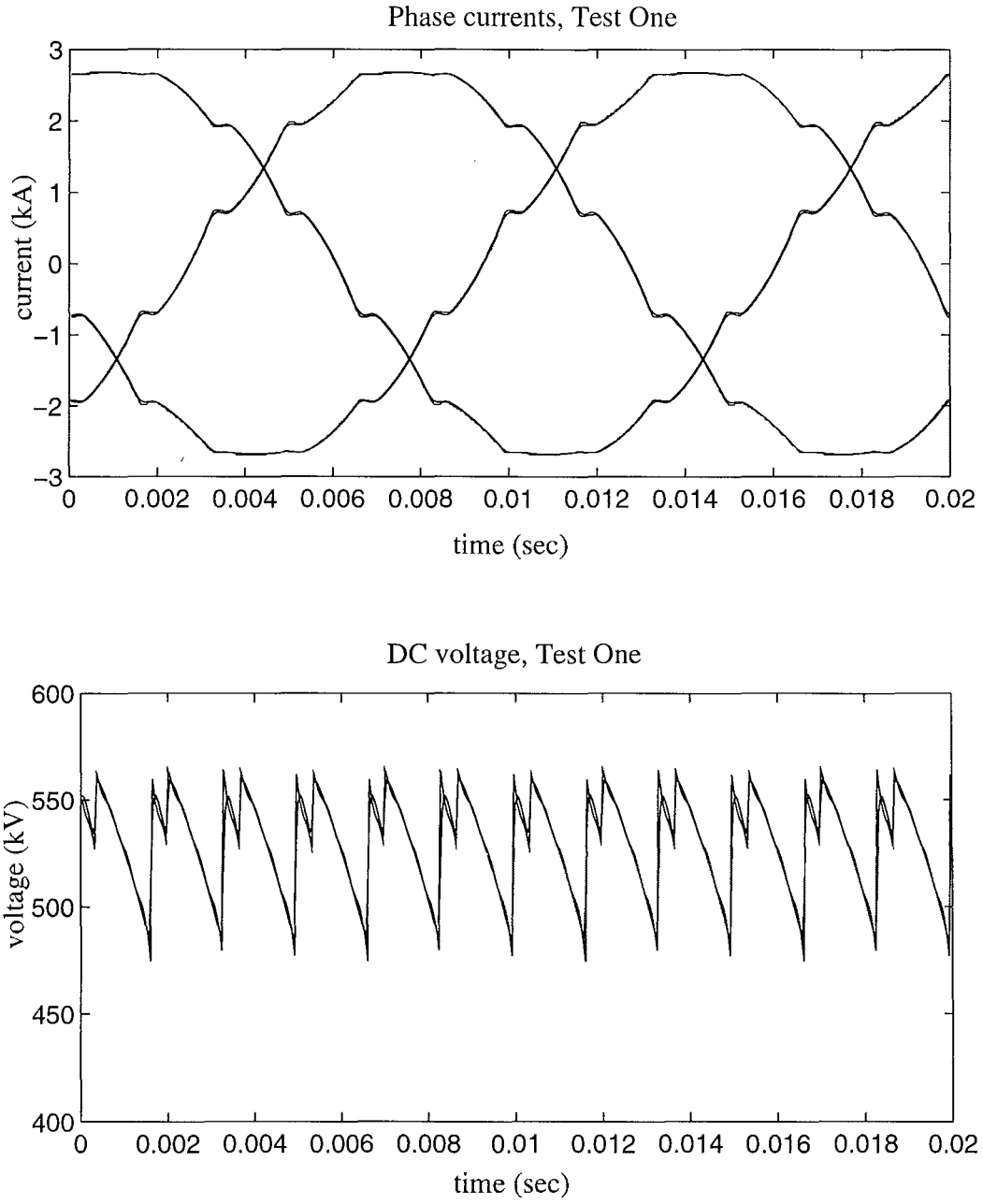

Figure 4.11 Comparison of time and harmonic domain solutions for phase current and dc voltage waveforms: Base Case.

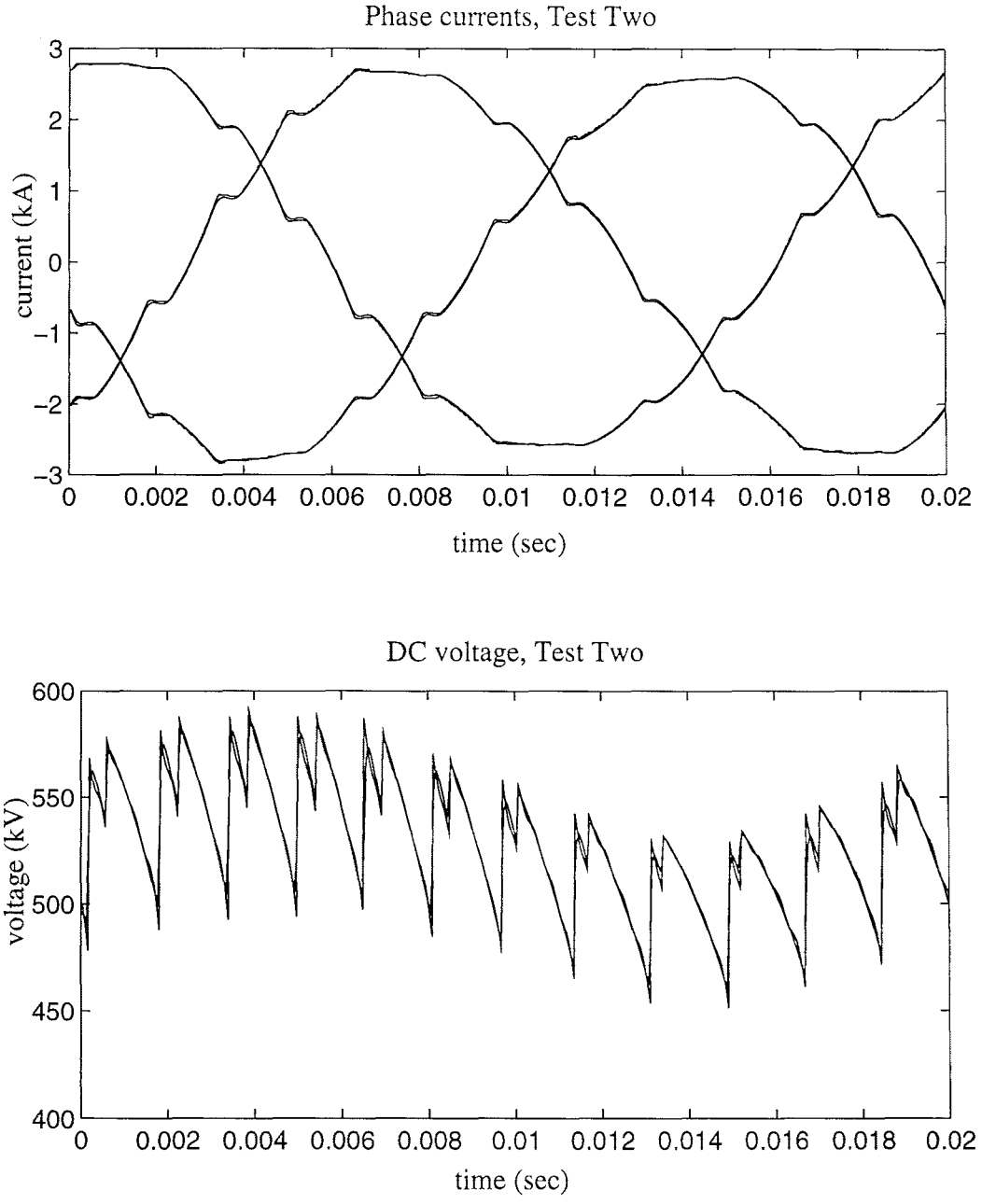

Figure 4.12 Comparison of time and harmonic domain solutions for phase current and dc voltage waveforms: Test 2.

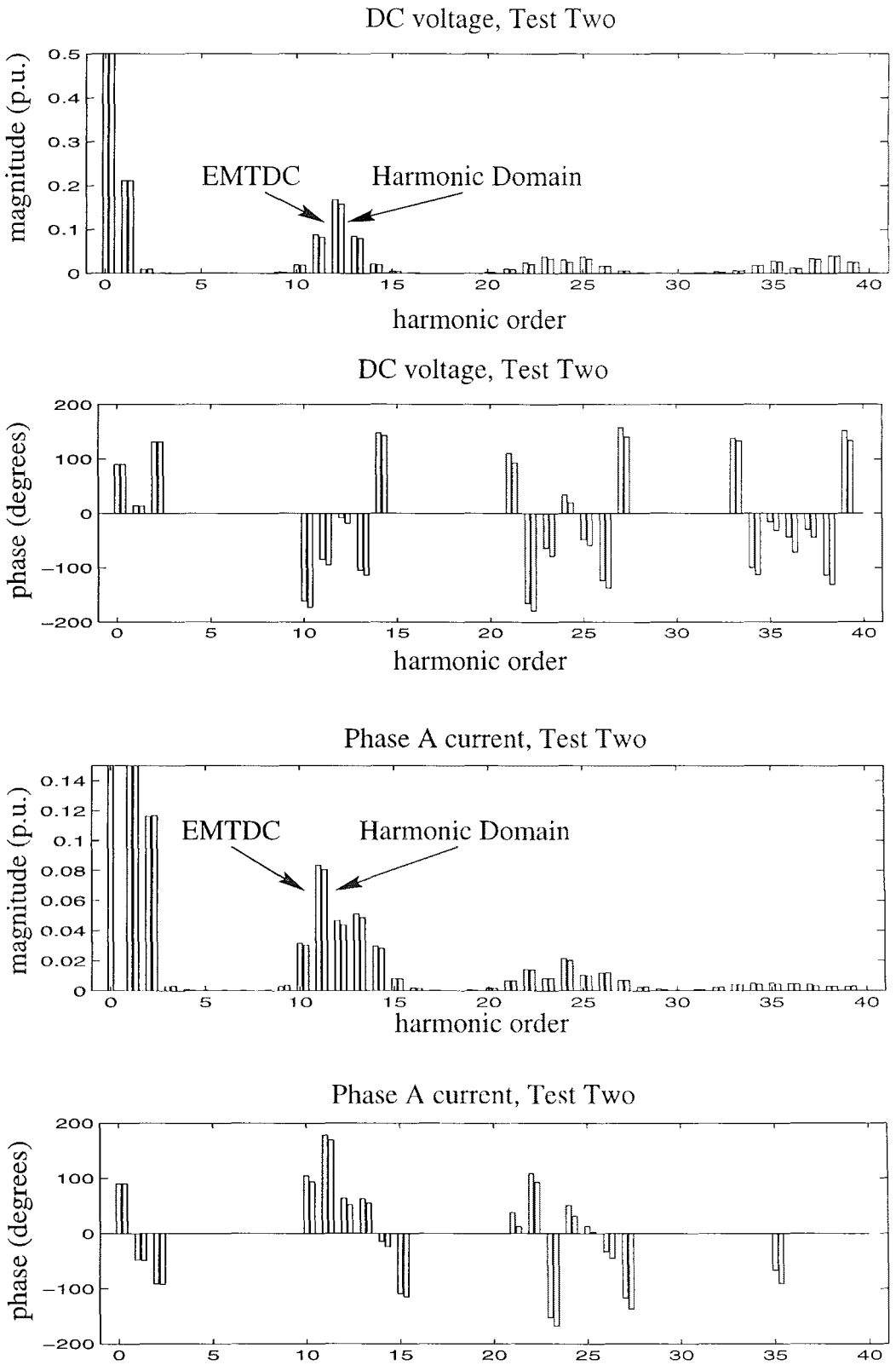

Figure 4.13 Comparison of time and harmonic domain solutions for phase currents and dc voltage spectra: Test 2.

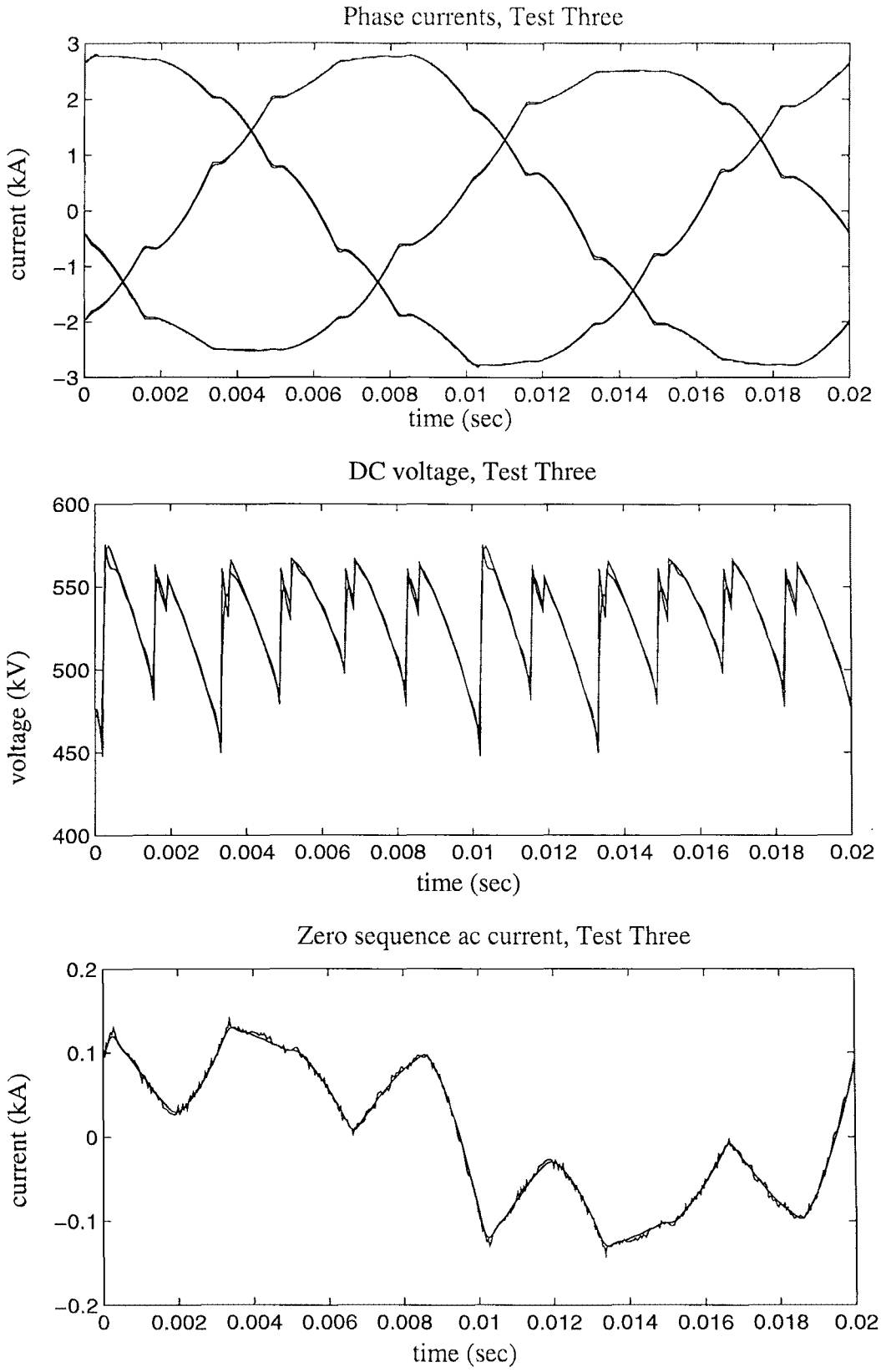

Figure 4.14 Comparison of time and harmonic domain solutions for phase current and dc voltage waveforms: Test 3.

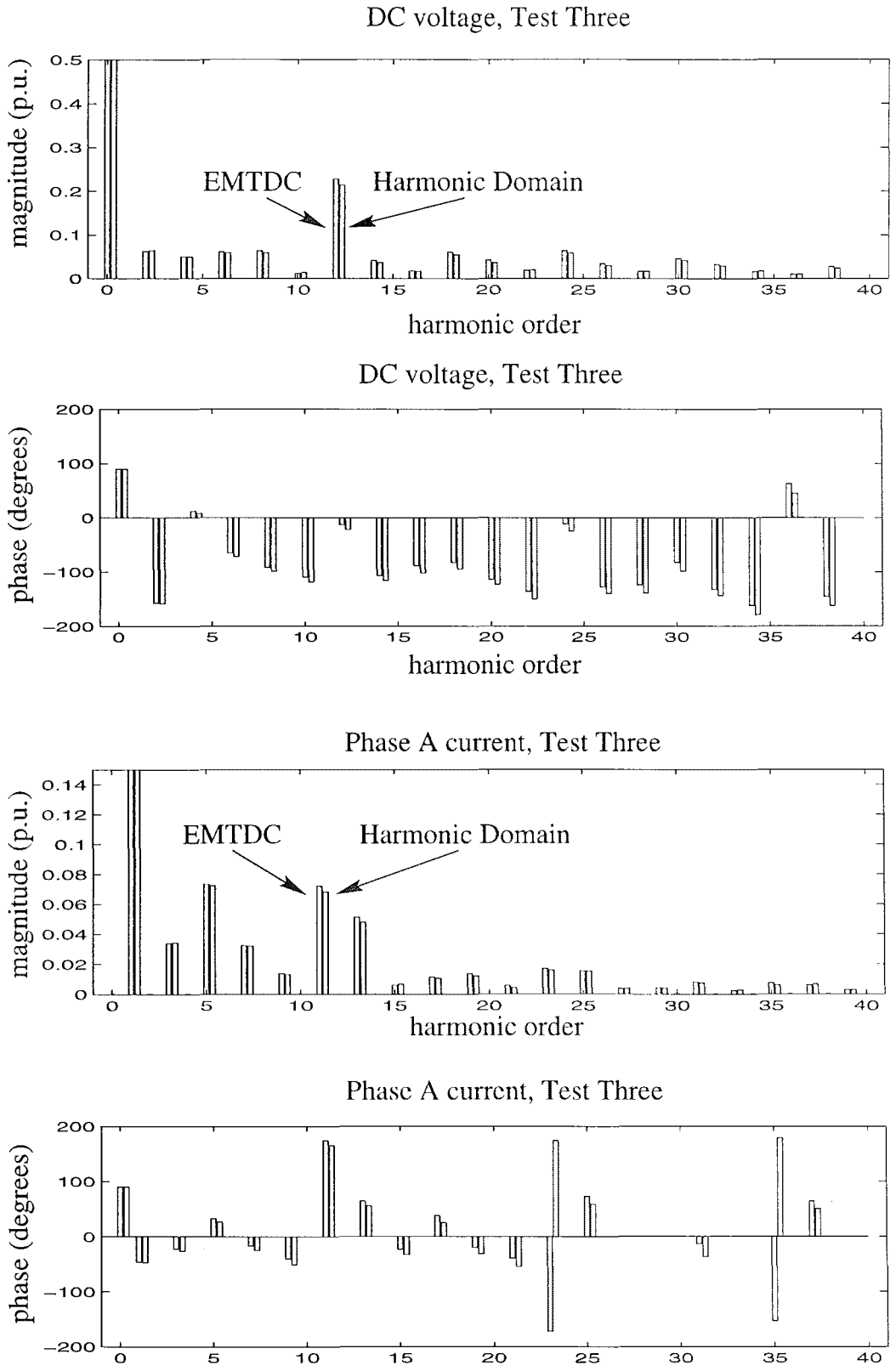

Figure 4.15 Comparison of time and harmonic domain solutions for phase currents and dc voltage spectra: Test 3.

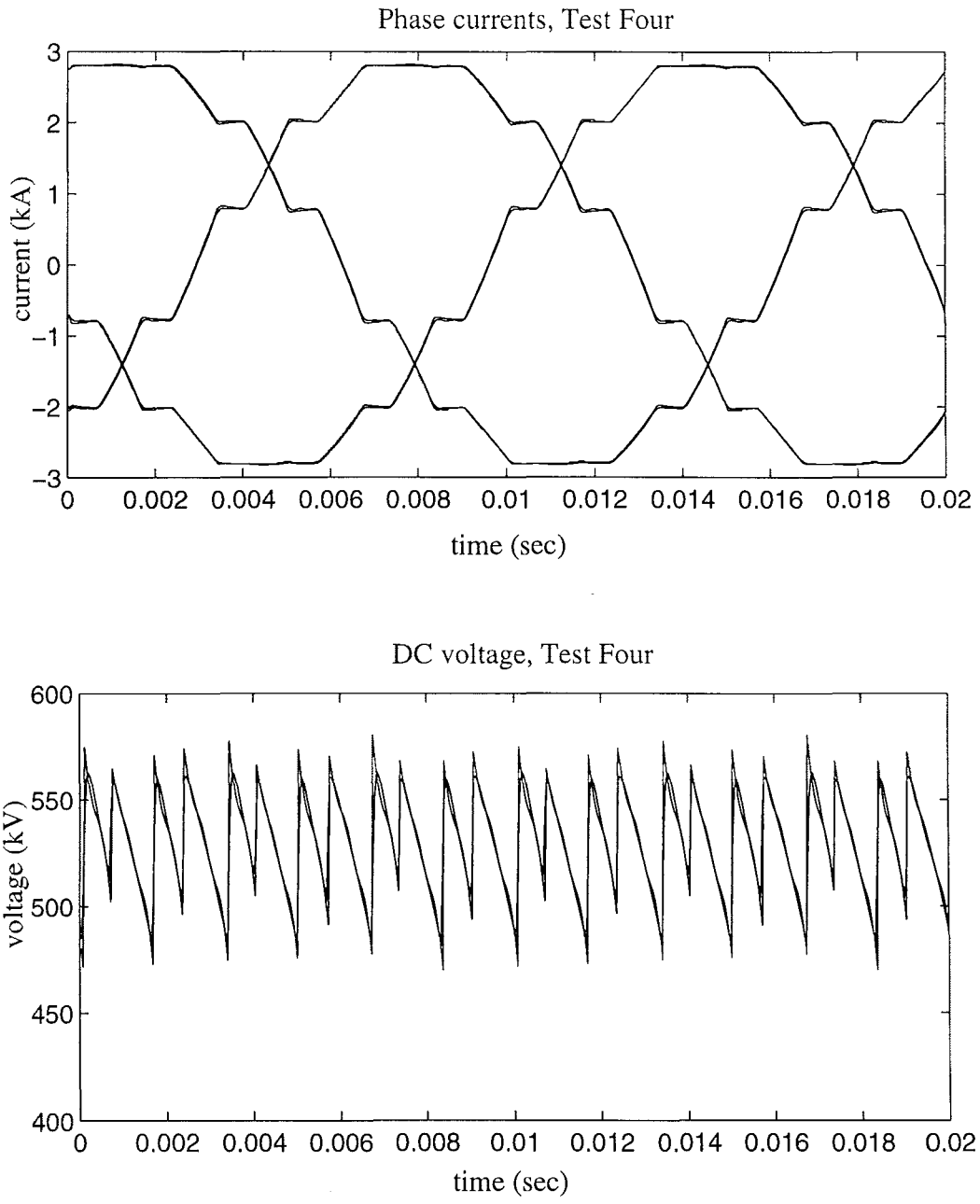

Figure 4.16 Comparison of time and harmonic domain solutions for phase current and dc voltage waveforms: Test 4.

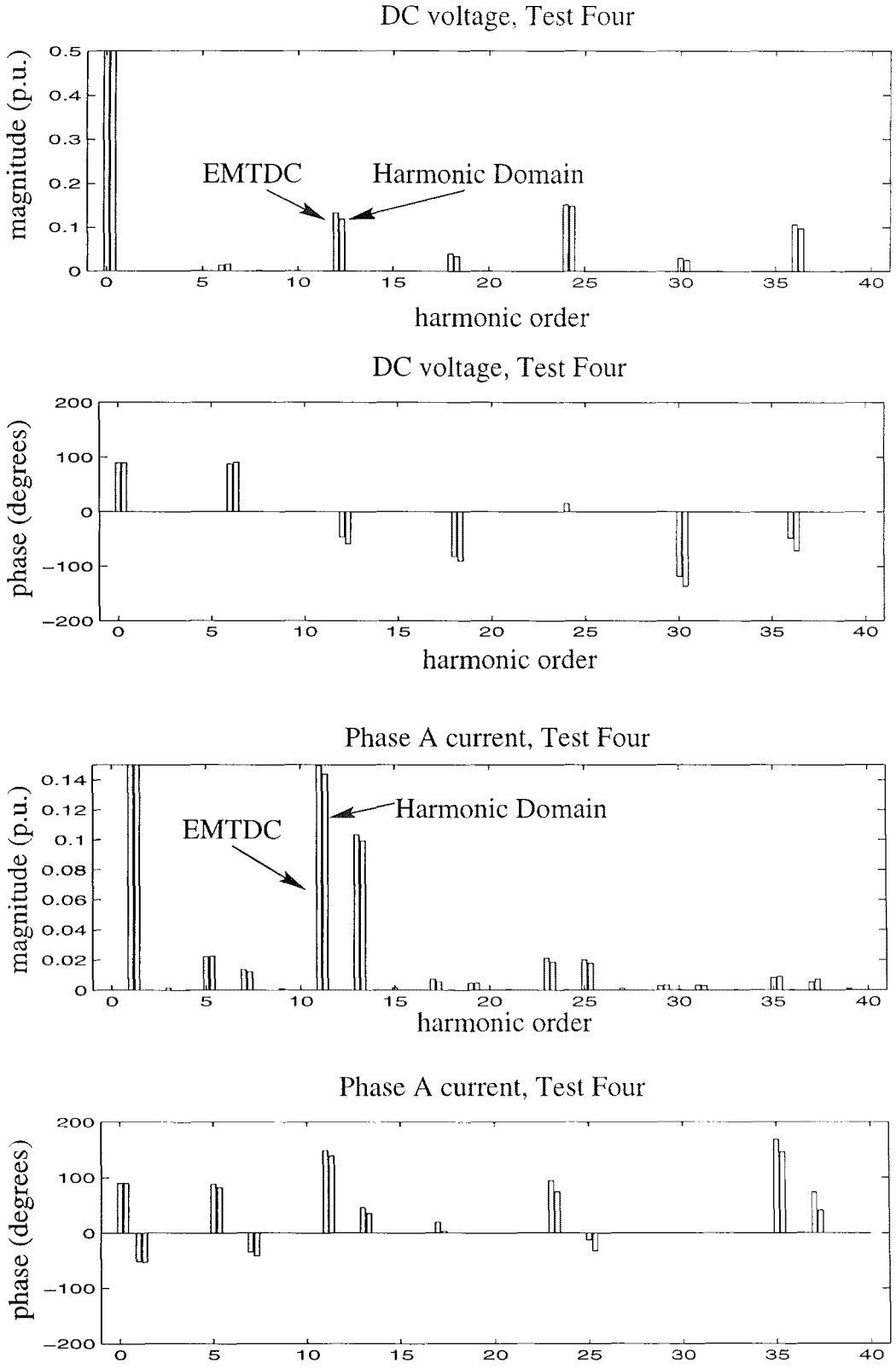

Figure 4.17 Comparison of time and harmonic domain solutions for phase currents and dc voltage spectra: Test 4.

Convergence of the sparse Newton solution is fast and robust, even if the Jacobian matrix is held constant. A convenient measure of the convergence is the 1-norm, the sum of the magnitudes of all the mismatches. At each iteration the 1-norm is reduced by an approximately constant *convergence factor*, λ, depending upon the difficulty of the system, and whether the switching terms are updated. The constant convergence factor is evident in figures 4.18 and 4.19, which show the decreasing 1-norm as a function of iteration number for all five test cases. Note that the final 1-norm at convergence varies according to the test, as the required convergence of a particular small noncharacteristic harmonic may require more iterations. An additional test has also been plotted, test five, where a 20% second order harmonic source was placed in the ac system. As indicated in table 4.3, a smaller convergence factor (and hence fewer iterations to convergence) is obtained if the switching terms are updated (rows with subscript 'a'). However the constant Jacobian method is always faster as each iteration takes approximately 0.6 seconds as opposed to 2.3 seconds. The constant Jacobian method is only slower if it requires more than four times as many iterations to converge. The only situation in which this has been observed is when the composite resonance is excited by a very large (0.3 p.u.) second harmonic source. The constant Jacobian method is therefore likely to be faster in any realistic case.

Test No.	CPU time (seconds)	Switch Iterations	Main Iterations	λ
1a	15.5	6	4	0.1314
1b	11.1	6	6	0.1712
2a	24.9	6	8	0.1440
2b	14.8	6	11	0.2562
3a	17.7	6	5	0.1069
3b	12.3	6	7	0.1130
4a	22.7	9	7	0.2498
4b	14.1	9	9	0.3129
5a	31.5	6	11	0.3068
5b	20.8	6	21	0.5382

Table 4.3 Convergence and performance of the solution a) updating switching terms, b) constant Jacobian.

It is evident from table 4.3 that convergence is slowed by the low harmonic order composite resonance, and by the presence of a large commutating resistance. The second order harmonic composite resonant is particularly difficult for the constant Jacobian method, as there is a higher coupling between low order harmonics and the switching angles. This is evident in the convergence of Test 5, which required 21 iterations. For more realistic systems, convergence in eight iterations using a constant Jacobian might be expected. The execution times listed in table 4.3 are for a Sun Sparcstation IPX.

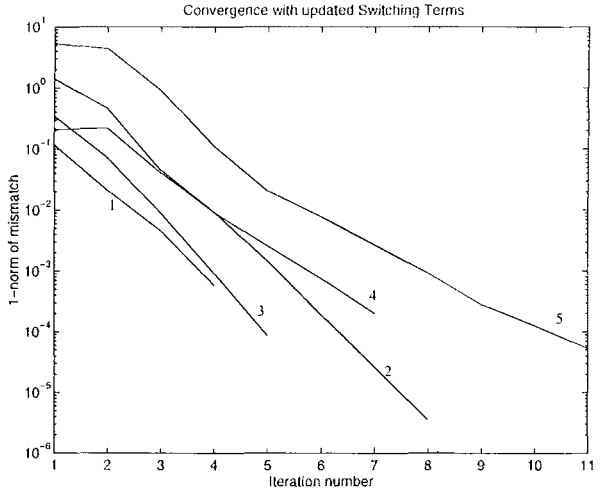

Figure 4.18 Convergence with the switching terms updated each iteration.

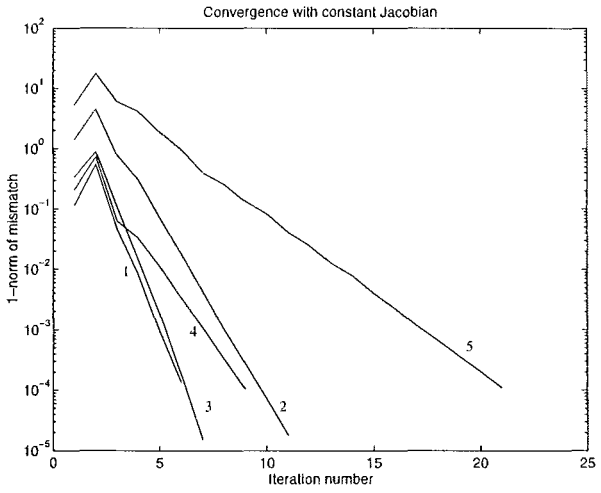

Figure 4.19 Convergence with the Jacobian held constant.

4.6 NEW ZEALAND SOUTH ISLAND SYSTEM

The results of the previous section show that the harmonic convertor model yields essentially the same solution as an EMTP based simulation to the steady state. One of the main advantages of harmonic domain analysis is that the frequency dependence of the ac system impedance can be calculated with relative ease. It is therefore possible to use the harmonic convertor model to calculate the interaction with any ac system for which a harmonic penetration is available. For this next study, the ac system of the CIGRE benchmark was replaced by the three phase harmonic impedance of the

New Zealand South Island system, looking from the Benmore 220kV bus (since there is a HVdc link convertor station there). The use of per unit quantities in the convertor model allows a direct connection, despite the difference in voltage levels. The hybrid CIGRE/NZ test system is described in appendix B

Since the New Zealand South Island system is stronger than the CIGRE system, and lacks difficult composite resonances, solution of the unified method was rapid, converging in 7 iterations to a 1-norm residual of 6×10^{-6}p.u. The system impedance used at each harmonic was a full 3×3 matrix, and so the effect of intersequence coupling and impedance unbalance was modelled in this solution. To determine the nature of this effect, the off diagonal impedance matrix terms were set to zero to remove intersequence coupling, and the remaining diagonal terms were made equal (balanced). The solution obtained with a balanced impedance is representative of what may be expected from a single phase harmonic model. The terminal voltage and phase current harmonics are compared in figure 4.20.

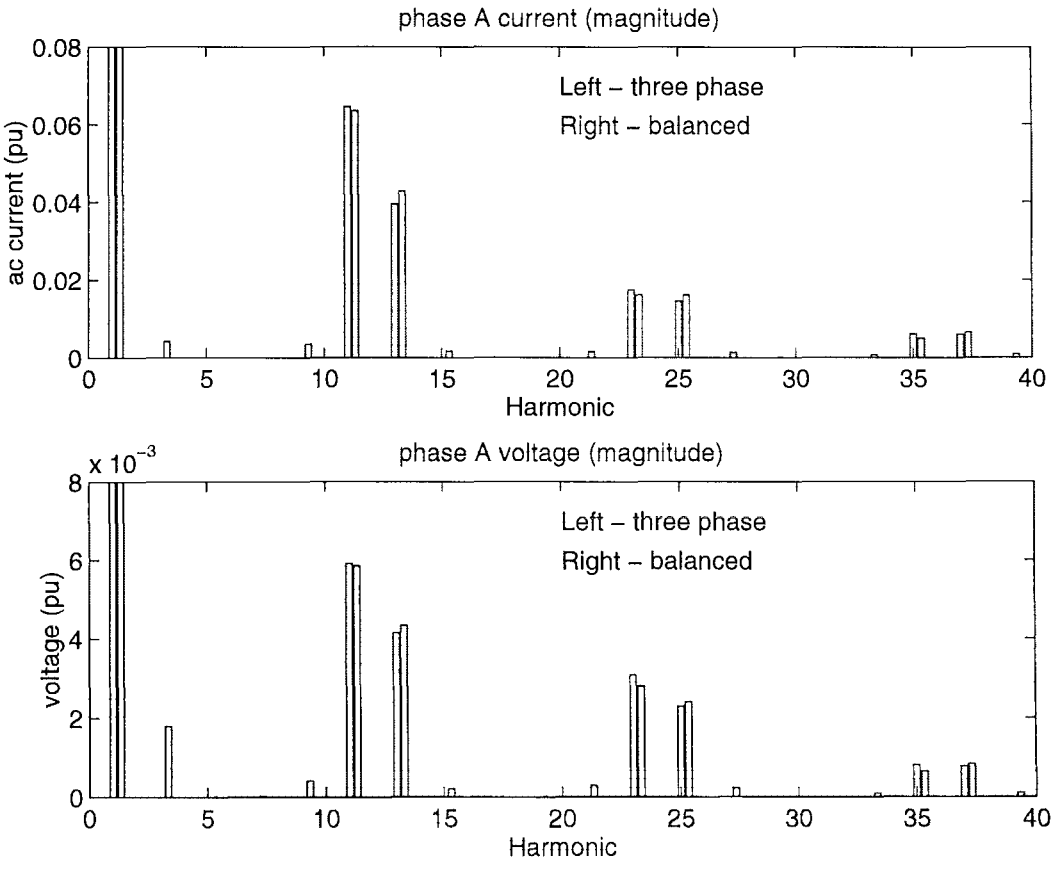

Figure 4.20 Comparison of solutions for the South Island system with full and balanced ac system impedance.

The effect of unbalance in the ac system impedance is to promote the injection of

triplen harmonics by the convertor. The triplens are primarily positive and negative sequence, and of a substantial magnitude.

4.7 CONCLUSION

Using the interelationships of chapter 3 a functional description, of the twelve pulse controlled rectifier, with ac and dc system representation, has been made. This functional description has been used to assemble a reduced set of mismatch equations suitable for use in Newton's method. The Newton's method solution was then described, and the Jacobian matrix of partial derivatives used in this method analysed. The Jacobian matrix displays several structural features, such as resonance terms and three port terms that are related to the interaction of the convertor with the ac and dc systems. The Jacobian matrix can be made sparse by setting small elements to zero.

The implementation of Newton's method for the case at hand has been described, with particular attention given to the starting point for the Newton procedure, and the convergence criteria. A Newton solution at the fundamental frequency, has been shown to provide a good estimate of the switching angles even with an unbalanced and weak ac system. Two methods of solving the sparse Jacobian system were described, with a direct sparse bifactorisation method preferred at present, given that the Jacobian is held constant.

The convertor model was verified against time domain solutions using the program PSCAD/EMTDC, for the rectifier end of the CIGRE benchmark model. Excellent agreement was obtained between the two solutions even in the presence of unbalance in the convertor transformer, and excitation of a composite ac/dc system resonance. Convergence was rapid, although slowed slightly by a large commutating resistance. Despite requiring more iterations, fastest convergence was obtained when the Jacobian was held constant.

Interaction of the CIGRE benchmark rectifier with the New Zealand South Island system was solved by using a suite of harmonic penetration software to calculate the South Island system equivalent impedance at the BENMORE–220 bus. The solution was obtained rapidly, and predicted the generation of noncharacteristic triplen harmonics by the rectifier due to unbalance in the ac system impedance.

Neither invalid, nor multiple solutions have been observed with the convertor model to date. However in general, multiple solutions must exist, and an example of an unstable periodic solution for a nonlinear system is given by Aprille and Trick [1972]. There is therefore some incentive to develop a postprocessing stage to check the validity of the solution. To date, the model has simply diverged if no solution is possible (for example the current order is too large for the strength of the ac system).

The model described here can be made more robust with respect to commutating

resistance by using 726 mismatch equations instead of 426, as this allows a full representation of the commutating resistance in the Jacobian. In this case both ac system terminals would be represented, and the solution would be for V^D and V^S. This approach would allow the modelling of skin effect in the transformers, and its effect on the convertor impedance for example, although would be slightly slower for systems with little commutating resistance. It is suggested that a hybrid voltage and current mismatch implementation would also better handle large impedances in the ac system.

The description of the system in terms of functions affords a modular implementation of the model. For example, the functions that describe transfer through the convertor transformer could readily be extended to cover other transformer connections. The Jacobian matrix itself retains the same structure, even in multiconvertor systems or when interfaced to a load flow. In either case, the Jacobian matrix described here would be a block in a block diagonal system Jacobian with linear coupling terms to other nonlinearities.

Other methods of improving the convertor model are possible, such as a polar coordinates implementation, a fast decoupled solution, or a sequence components solution. These possibilities are investigated in the next chapter, where only the latter is found to be worthwhile.

Chapter 5

ALTERNATIVE IMPLEMENTATIONS

In this chapter three alternative implementations of the convertor model are investigated, with a view to obtaining faster, or more robust solutions. Existing practice with the load flow problem suggests two possible modifications to the convertor model; a polar components specification of the mismatch equations and variables, and a fast decoupled solution method. With the polar components method it is hoped to find little coupling between mismatch angles and variable magnitudes and vice versa. This would enable the implementation of a decoupled solution, where two decoupled Jacobians are used to update magnitudes and phase angles separately. Even without the polar components representation of ac/dc harmonics, a decoupled solution is still possible, and is implemented below by decoupling the convertor switch system variables and the ac/dc side harmonics.

Any alternative to a rectangular phase components model is achieved by an appropriate transformation of the existing variables and mismatch equations. This means that the analyses of chapters 3 and 4, and the derivation of the Jacobian in appendix C are all still useful. An example is the sequence components transformed model, derived in section 5.3, where the Newton solution algorithm can be written in terms of the existing phase components solution using a matrix, T, based on the sequence transform matrix:

$$\begin{aligned} U^N &= TX^N \\ V^N &= TF(X^N) \\ V^N &= TJT^{-1}Z^N \\ U^{(N+1)} &= U^N - Z^N \\ X^{(N+1)} &= T^{-1}U^{(N+1)} \end{aligned} \tag{5.1}$$

The quantity TJT^{-1} is the *transformed Jacobian*, obtained in this case by means of linear transformation. The transformation to polar coordinates is not linear, however a very similar approach, using the chain rule, is described below.

5.1 POLAR TRANSFORMS

The motivation for developing a polar transformed solution is the expectation that a change in the magnitude of a harmonic will affect mainly the magnitude of harmonics coupled to it, and similarly for the phase. It is thus hoped to make the ac/dc partition more sparse by eliminating coupling between phase angles and magnitudes. A polar transform has the additional advantage of being simple to implement and calculate.

In order to simplify the notation, the polar method is described with reference to a 'generic' non-analytic complex function G, which is a function of the complex variable x. The following notation is also useful in referring to their rectangular or polar parts:

$$\begin{aligned} G_R &= \text{real part of G} \\ G_I &= \text{imaginary part of G} \\ G_M &= \text{magnitude of G} \\ G_\theta &= \text{angle of G} \\ x_R &= \text{real part of x} \\ x_I &= \text{imaginary part of x} \\ x_M &= \text{magnitude of x} \\ x_\theta &= \text{angle of x} \end{aligned}$$

The quantities G_R, G_I, x_R, x_I are assumed known, as are the partial derivatives $\frac{\partial G_R}{\partial x_R}$, $\frac{\partial G_R}{\partial x_I}$, $\frac{\partial G_I}{\partial x_R}$, and $\frac{\partial G_I}{\partial x_I}$. G_M and G_θ are readily derived:

$$G_M = \sqrt{(G_R^2 + G_I^2)} \tag{5.2}$$

and

$$G_\theta = \arctan \frac{G_I}{G_R} \tag{5.3}$$

G_R and G_I can be considered to be functions of the real and imaginary parts of x, which in turn are functions of the polar parts of x:

$$G_R(x_R(x_M, x_\theta), x_I(x_M, x_\theta)) \tag{5.4}$$

$$G_I(x_R(x_M, x_\theta), x_I(x_M, x_\theta)) \tag{5.5}$$

The rectangular and polar parts of x are related by:

$$x_R = x_M \cos x_\theta \tag{5.6}$$

$$x_I = x_M \sin x_\theta \tag{5.7}$$

The following partial derivatives are also required:

$$\frac{\partial x_R}{\partial x_M} = \cos x_\theta \tag{5.8}$$

$$\frac{\partial x_R}{\partial x_\theta} = -x_I \tag{5.9}$$

$$\frac{\partial x_I}{\partial x_M} = \sin x_\theta \tag{5.10}$$

$$\frac{\partial x_I}{\partial x_\theta} = x_R \tag{5.11}$$

$$\tag{5.12}$$

Differentiating equation 5.2 partially with respect to x_M:

$$\begin{aligned}\frac{\partial G_M}{\partial x_M} &= \frac{1}{G_M}\left[G_R\left(\frac{\partial G_R}{\partial x_I}\frac{\partial x_I}{\partial x_M}+\frac{\partial G_R}{\partial x_R}\frac{\partial x_R}{\partial x_M}\right)+G_I\left(\frac{\partial G_I}{\partial x_I}\frac{\partial x_I}{\partial x_M}+\frac{\partial G_I}{\partial x_R}\frac{\partial x_R}{\partial x_M}\right)\right]\\ &= \frac{1}{G_M}\left[G_R\left(\sin x_\theta\frac{\partial G_R}{\partial x_I}+\cos x_\theta\frac{\partial G_R}{\partial x_R}\right)+G_I\left(\sin x_\theta\frac{\partial G_I}{\partial x_I}+\cos x_\theta\frac{\partial G_I}{\partial x_R}\right)\right]\end{aligned} \tag{5.13}$$

The other partial derivatives are obtained in a similar manner to yield:

$$\begin{aligned}\frac{\partial G_M}{\partial x_\theta} &= \frac{1}{G_M}\left[G_R\left(x_R\frac{\partial G_R}{\partial x_I}-x_I\frac{\partial G_R}{\partial x_R}\right)+G_I\left(x_R\frac{\partial G_I}{\partial x_I}-x_I\frac{\partial G_I}{\partial x_R}\right)\right]\\ \frac{\partial G_\theta}{\partial x_M} &= \frac{1}{1+(\frac{G_I}{G_R})^2}\frac{1}{G_R}\left[\sin x_\theta\frac{\partial G_I}{\partial x_I}+\cos x_\theta\frac{\partial G_I}{\partial x_R}-\frac{G_I}{G_R}\left(\sin x_\theta\frac{\partial G_R}{\partial x_I}+\cos x_\theta\frac{\partial G_R}{\partial x_R}\right)\right]\\ \frac{\partial G_\theta}{\partial x_\theta} &= \frac{1}{1+(\frac{G_I}{G_R})^2}\frac{1}{G_R}\left[x_R\frac{\partial G_I}{\partial x_I}-x_I\frac{\partial G_I}{\partial x_R}-\frac{G_I}{G_R}\left(x_R\frac{\partial G_R}{\partial x_I}-x_I\frac{\partial G_R}{\partial x_R}\right)\right]\end{aligned} \tag{5.14}$$

Both the voltage and current mismatches are expressed as the difference between an estimate of a harmonic phasor, and a calculation of that phasor using the estimate. For example the voltage mismatch is:

$$\begin{aligned}F_V &= V - f_{18}(V, I_{dk}, I_{d0}, \theta_i^D, \phi_i^D, \theta_i^S, \phi_i^S)\\ &= V - V'(X),\end{aligned} \tag{5.15}$$

which is readily transformed to a pair of real polar mismatches:

$$\begin{aligned}F_{V1} &= V_M - V'_M,\\ F_{V2} &= V_\theta - V'_\theta.\end{aligned} \tag{5.16}$$

For polar Jacobian elements off the diagonal, it is necessary to differentiate f_{18}, for

example:

$$\begin{aligned}\frac{\partial F_{V1k}}{\partial V_{Ml}} &= -\frac{\partial V'_{Mk}}{\partial V_{Ml}} \\ &= \frac{\partial |f_{18k}|}{\partial V_{Ml}}.\end{aligned} \tag{5.17}$$

Retaining the notation $V' \equiv f_{18}$, the polar partial derivatives can be expressed in terms of the rectangular components partial derivatives by substituting $G \leftarrow V'$ and $x \leftarrow V$ in equation 5.13, and equations 5.14:

$$\begin{aligned}\frac{\partial V'_{Mk}}{\partial V_{Ml}} &= \cos\left(V'_{\theta k}\right)\left(\sin V_{\theta l}\frac{\partial V'_{Rk}}{\partial V_{Il}} + \cos V_{\theta l}\frac{\partial V'_{Rk}}{\partial V_{Rl}}\right) + \\ &\quad \sin\left(V'_{\theta k}\right)\left(\sin V_{\theta l}\frac{\partial V'_{Ik}}{\partial V_{Il}} + \cos V_{\theta l}\frac{\partial V'_{Ik}}{\partial V_{Rl}}\right) \\ \frac{\partial V'_{Mk}}{\partial V_{\theta l}} &= \cos\left(V'_{\theta k}\right)\left(V_{Rl}\frac{\partial V'_{Rk}}{\partial V_{Il}} - V_{Il}\frac{\partial V'_{Rk}}{\partial V_{Rl}}\right) + \sin\left(V'_{\theta k}\right)\left(V_{Rl}\frac{\partial V'_{Ik}}{\partial V_{Il}} - V_{Il}\frac{\partial V'_{Ik}}{\partial V_{Rl}}\right) \\ \frac{\partial V'_{\theta k}}{\partial V_{Ml}} &= \frac{1}{1+\tan\left(V'_{\theta k}\right)^2}\frac{1}{V'_{Rk}}\left[\sin V_{\theta l}\frac{\partial V'_{Ik}}{\partial V_{Il}} + \cos V_{\theta l}\frac{\partial V'_{Ik}}{\partial V_{Rl}} - \right. \\ &\quad \left. \tan\left(V'_{\theta k}\right)\left(\sin V_{\theta l}\frac{\partial V'_{Rk}}{\partial V_{Il}} + \cos V_{\theta l}\frac{\partial V'_{Rk}}{\partial V_{Rl}}\right)\right] \\ \frac{\partial V'_{\theta k}}{\partial V_{\theta l}} &= \frac{1}{1+\tan\left(V'_{\theta k}\right)^2}\frac{1}{V'_{Rk}}\left[V_{Rl}\frac{\partial V'_{Ik}}{\partial V_{Il}} - V_{Il}\frac{\partial V'_{Ik}}{\partial V_{Rl}} - \right. \\ &\quad \left. \tan\left(V'_{\theta k}\right)\left(V_{Rl}\frac{\partial V'_{Rk}}{\partial V_{Il}} - V_{Il}\frac{\partial V'_{Rk}}{\partial V_{Rl}}\right)\right]\end{aligned} \tag{5.18}$$

The polar derivatives suffer from scaling problems not observed in the polar coordinates load flow, where the voltage magnitudes are typically close to one per unit. The problem here is that the harmonic voltage or current magnitudes are likely to be in the range 10^{-8} to 10^{-2}, and that some of the polar derivatives are scaled either by the harmonic magnitude, or the inverse of the magnitude. The rectangular coordinates partial derivatives lie in the range 0.1 to 10; using a value of one, approximating the sine or cosine of any angle to one, and making $|V'_k| \approx |V_l| \approx 10^{-4}$ in the above equations yields the following estimate for the size of the polar derivatives:

$$\begin{aligned}\frac{\partial V'_{Mk}}{\partial V_{Ml}} &\approx 1 \\ \frac{\partial V'_{Mk}}{\partial V_{\theta l}} &\approx 10^{-4} \\ \frac{\partial V'_{\theta k}}{\partial V_{Ml}} &\approx 10^{4} \\ \frac{\partial V'_{\theta k}}{\partial V_{\theta l}} &\approx 1.\end{aligned} \tag{5.19}$$

Equations 5.19 are a fairly conservative estimate of the deficiencies of the polar Jacobian. The partial derivatives are evidently extremely sensitive to the magnitude and phase angles of the harmonic phasors on both sides of the convertor. Truncating the Jacobian at 0.05, will still lead to more than five orders of magnitude variation in the size of the remaining elements, which will be numerous. One way around the scaling problem is to use radius, G_M, and arc length, $G_M G_\theta$ coordinates instead of polar coordinates. This preserves any decoupling of magnitude and phase angles (even under a rotation of the coordinate system). Application of the chain rule yields the *arc length* partial derivatives in terms of the polar partial derivatives:

$$\begin{aligned}
\frac{\partial V'_{Mk}}{\partial V_{Ml}} &\approx 1 \text{ as before} \\
\frac{\partial V'_{Mk}}{\partial (V_{Ml} V_{\theta l})} &= \frac{1}{V_{Ml}} \frac{\partial V'_{Mk}}{\partial V_{\theta l}} \approx 1 \\
\frac{\partial (V'_{Mk} V'_{\theta k})}{\partial V_{Ml}} &= V'_{Mk} \frac{\partial V'_{\theta k}}{\partial V_{Ml}} + V'_{\theta k} \frac{\partial V'_{Mk}}{\partial V_{Ml}} \approx 1 \\
\frac{\partial (V'_{Mk} V'_{\theta k})}{\partial (V_{Ml} V_{\theta l})} &= \frac{V'_{Mk}}{V_{Ml}} \frac{\partial V'_{\theta k}}{\partial V_{\theta l}} + \frac{V'_{\theta k}}{V_{Ml}} \frac{\partial V'_{Mk}}{\partial V_{\theta l}} \approx 1,
\end{aligned} \tag{5.20}$$

all of which are well scaled. Unfortunately however, decoupling is not evident when the arc length Jacobian is calculated. There is therefore no justification for developing a Newton solution for the convertor in this coordinate system, given the extra processing overheads associated with the coordinate transform.

5.2 DECOUPLED SOLUTION

A decoupled solution for the convertor is developed by first noting that the operating point of the convertor is essentially fixed by interactions between the switching angles, the fundamental frequency on the ac side, and the average dc current on the dc side. It is likely therefore, that a solution can be obtained by iterating between a solution of the switching system as described in subsection 4.4.2, and a Newton solution of harmonic interactions between the ac and dc systems (with the convertor switching instants held constant). Such a solution is a type of *fixed point iteration*, for which there is a theoretical analysis of the convergence criteria.

The fixed point iteration can also be called a decoupled solution, since all those switching terms in the Jacobian which represent the effect of harmonics on switching angles, or vice versa, have been set equal to zero. This is analogous to the decoupled load flow, where terms relating magnitudes and phase angles are eliminated. Removing the cross coupling terms from the Jacobian matrix effectively partitions the mismatch

and variable vectors into the switch system,

$$X_{Switch} = [V_1, I_{d0}, \phi, \theta, \alpha_0]^T \quad (5.21)$$
$$F_{Switch} = [F_{V1}, F_{Id0}, F_\phi, F_\theta, F_{\alpha_0}]^T, \quad (5.22)$$

and the ac/dc harmonic system,

$$X_{ACDC} = [V_k, I_{dl}]^T, \ k > 1, l > 0 \quad (5.23)$$
$$F_{ACDC} = [F_{Vk}, F_{Idl}]^T, \ k > 1, l > 0. \quad (5.24)$$

The mismatch equations associated with the variables in each vector contain the variables of the other vector as constant parameters. Each vector of equations can be solved by Newtons method:

$$X_{ACDC}^{(N+1)} = X_{ACDC}^N - (J^N)_{ACDC}^{-1} F_{ACDC}^N \quad (5.25)$$
$$X_{Switch}^{(N+1)} = X_{Switch}^N - (J^N)_{Switch}^{-1} F_{Switch}^N \quad (5.26)$$

Restricting the domain of the variables in each vector to the region of convergence of Newtons method to the correct solution, the Newton solution provides a one to one mapping from an initial estimate, to the actual root. The position of the root however is perturbed slightly by the parameter set corresponding to the other vector of variables. Since the Newton solution defines a one to one mapping, it can be represented by a function:

$$G_{ACDC} \stackrel{\text{def}}{=} X_{ACDC}^\bullet \quad (5.27)$$
$$G_{Switch} \stackrel{\text{def}}{=} X_{Switch}^\bullet \quad (5.28)$$

where $X^\bullet$ is the converged Newton solution for the root. These last equations can be used to define a fixed point iterative solution for the complete set of variables:

$$X_{ACDC}^{(N+1)} = G_{ACDC}(X_{ACDC}^N, X_{Switch}^N) \quad (5.29)$$
$$X_{Switch}^{(N+1)} = G_{Switch}(X_{ACDC}^N, X_{Switch}^N) \quad (5.30)$$

This fixed point iteration will converge provided the partial derivatives of G are sufficiently small. For the self terms

$$\frac{\partial G_{ACDC_i}}{\partial X_{ACDC_j}} = 0, \quad (5.31)$$
$$\frac{\partial G_{Switch_i}}{\partial X_{Switch_j}} = 0, \quad (5.32)$$

since the Newton procedure that defines G must, by assumption, converge to the same

root, $X^\bullet$, if the parameter vector is held constant. The size of the cross coupling partial derivatives $\frac{\partial G_{ACDC_i}}{\partial X_{Switch_j}}$ and $\frac{\partial G_{Switch_i}}{\partial X_{ACDC_j}}$, depends upon the degree of coupling between the two partitions of the overall solution. The largest such coupling exists between dc current harmonics and the switching angles.

The cross coupling partial derivatives mentioned above can be evaluated numerically by sequentially perturbing each of the elements of one of the variable vectors, converging the other Newton system with the perturbed parameter set, and calculating the change in the solution vector, ie:

1. Perturb $X'_{Switch_j} = X_{Switch_j} + \Delta X_{Switch_j}$,
2. Converge the Newton system $F'_{ACDC}(X_{ACDC}) = G_{ACDC}$, in which X'_{Switch} is a parameter.
3. A column of cross coupling partial derivatives is thereby defined by

$$\frac{\partial G_{ACDC_i}}{\partial X_{Switch_j}} \approx \frac{F'_{ACDC} - F_{ACDC}}{\Delta X_{Switch_j}}$$

Cross coupling partial derivatives obtained by this method have been plotted for the CIGRE benchmark rectifier in figure 5.1. A greater degree of coupling between the fixed point functions and the convertor variables is evident in this plot than in the Jacobian matrix. Convergence criteria for the fixed point iteration method is stated in [Burden *et al.* 1981], and is clearly not met for this system. The convergence criteria for a solution initiated in the neighbourhood of the solution is that

$$\left|\frac{\partial G_i}{\partial X_j}\right| \leq \frac{K}{n_v} \tag{5.33}$$

for some $K < 1$. For a system of 129 equations (corresponding to 13 harmonics), each partial derivative must therefore have a magnitude less than 0.00775. Although the decoupled solution is not guaranteed to converge in this case, it may still converge in practice. This is a much worse situation than the pure Newton method which is guaranteed to converge quadratically from a good starting point.

Even more so than the Jacobian matrix, the cross coupling matrix reveals the relative magnitude of inter-relationships between some of the convertor variables. Referring to features labelled on figure 5.1;

A The ac and dc side harmonics are affected to a similar degree by changes in individual firing instants, or end of commutation instants.

B Dc side current harmonics have a larger effect on switching and commutation angles, than do ac side voltage harmonics. This is because the switching angles

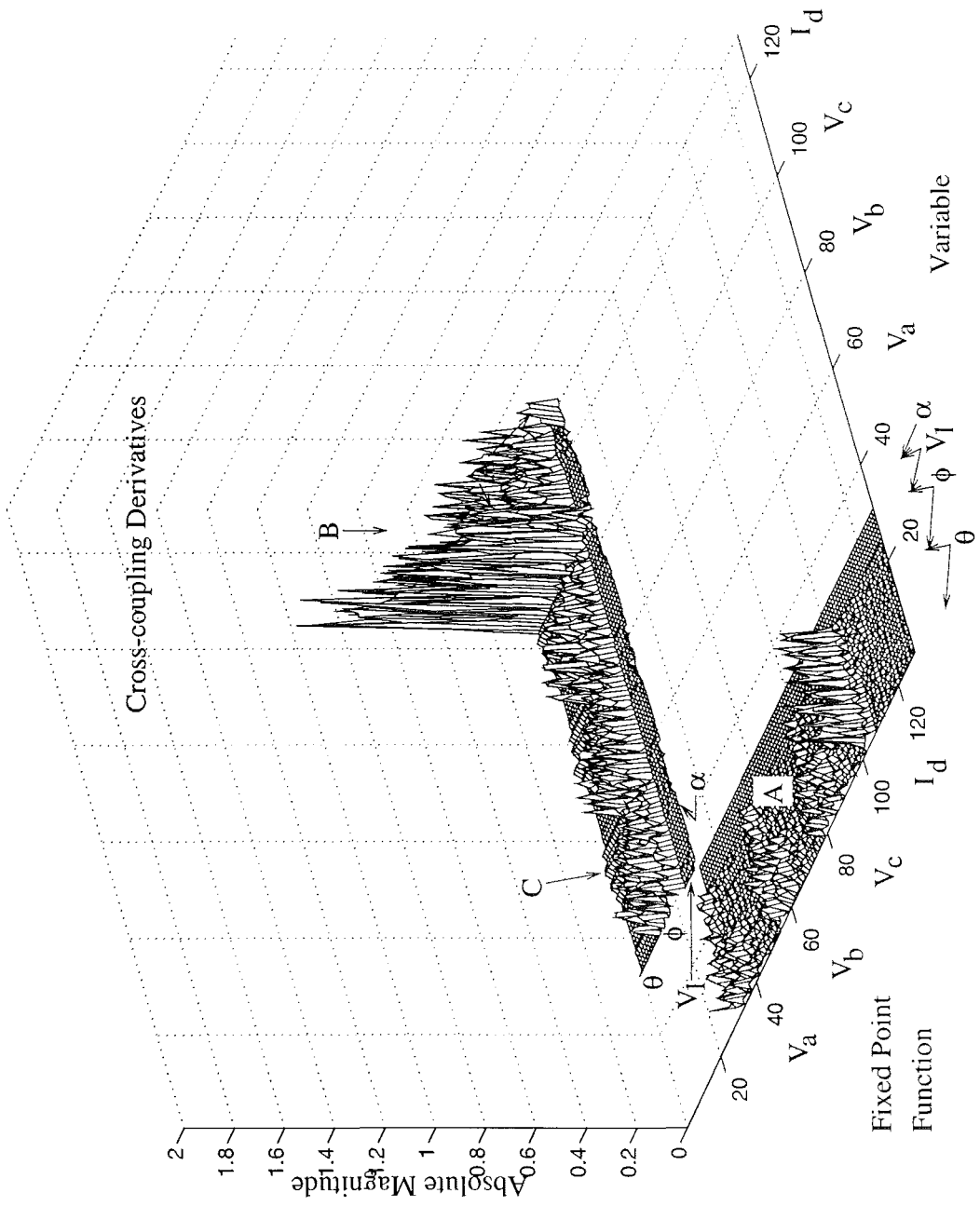

Figure 5.1 Numerically calculated cross coupling partial derivatives for the CIGRE benchmark; 13 harmonics.

depend on instantaneous values of the dc current, whereas the end of commutation angles depend on the terminal voltage harmonics integrated over the short commutation interval.

C Controller action causes the firing angles to be affected by terminal voltage harmonics coupled to the fundamental. For example a negative sequence 11th harmonic on the ac side is converted to dc on the dc side, which is compensated for by the current controller to maintain the current order.

Rather than use a converged Newton solution in the definition of G_{ACDC}, it is possible to use just a single iteration of Newton's method. This yields a speed improvement in the overall solution, since it is wasteful to solve intermediate steps in the fixed point iteration accurately. As there are many variables in the ac/dc partition, but only 32 in the switching partition, the fixed point iteration equations are:

$$G_{ACDC} \stackrel{\text{def}}{=} X_{ACDC} - J_{ACDC}^{-1} F_{ACDC} \tag{5.34}$$

$$G_{Switch} \stackrel{\text{def}}{=} X_{Switch}^{\bullet} \tag{5.35}$$

At each iteration, the variables in the ac/dc partition are updated by a single step of Newton's method, while the switching angles are solved exactly. As in the unified solution developed in chapter 4, the Jacobian of the ac/dc partition is held constant after the first iteration. The overall fixed point solution method is illustrated in figure 5.2. When the decoupled method was applied to the four test systems of chapter 4,

Test No.	CPU time (seconds)	Switch Iterations	Main Iterations	λ
1b	11.1	6	6	0.1712
1c	10.4	9	4	0.0926
2b	14.8	6	11	0.2562
2c	37.2	60	26	0.6048
3b	12.3	6	7	0.1130
3c	16.5	22	9	0.2918
4b	14.1	9	9	0.3129
4c	16.2	33	5	0.1808

Table 5.1 Convergence and performance of the convertor model, b) constant unified Jacobian, c) decoupled solution.

convergence was obtained in all cases. The performance of the decoupled method is summarised in table 5.1, and figure 5.3. The decoupled method is typically slower than the constant unified Jacobian method, especially when the composite resonance is excited in Test Two.

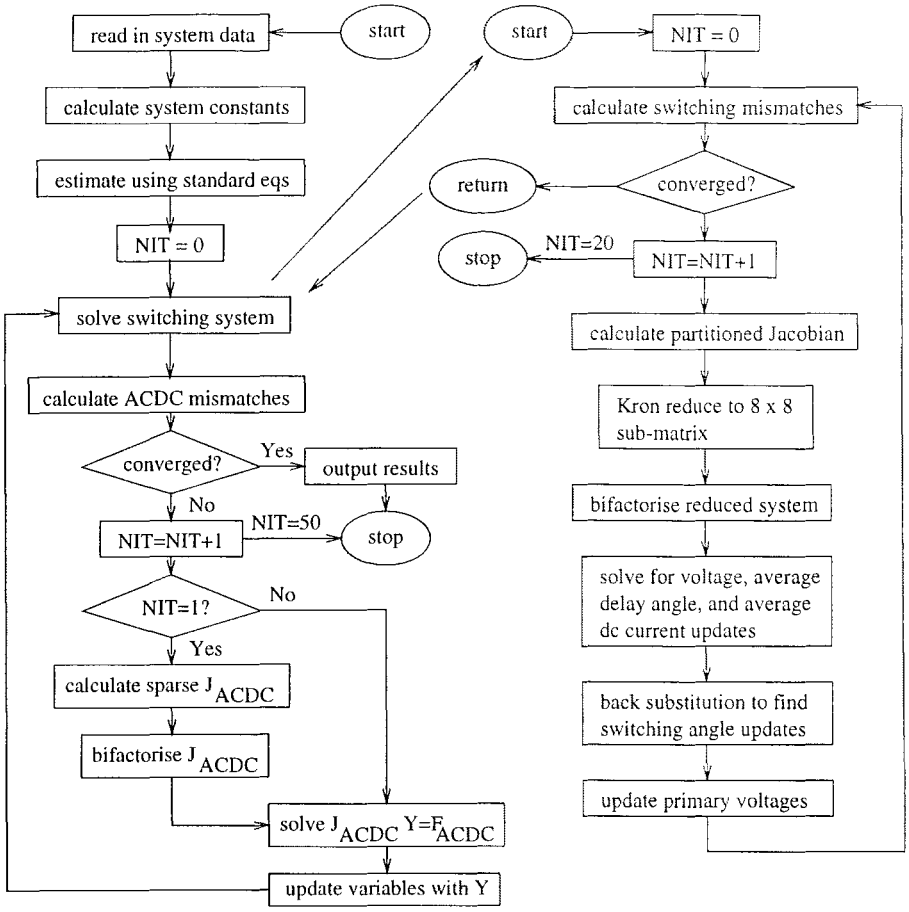

Figure 5.2 Overall algorithm for the fixed point solution.

One reason for the longer execution time of the decoupled method is the large number of iterations of the switching system, as it is converged at every iteration of the overall method. An improvement in execution time and convergence, could possibly be obtained by performing only one iteration of the switch system instead of converging it. This approach has not been pursued because of the poor performance of the decoupled method when applied to the NZ South Island system equivalent impedance.

When applied to the NZ South Island test system, the decoupled method diverges if there is an even order harmonic voltage source in the ac system, converging only for odd order harmonic sources. This divergence is related to the phase angle of the ac system impedance, as a capacitive impedance leads to slower divergence, or even slow convergence at the fourth harmonic. Making the ac system impedance balanced and without interphase coupling does not affect the divergence of the decoupled method. The decoupled method, to the extent that it has been developed here, is not robust enough for general purpose use, as even order harmonic sources do occur in the ac system.

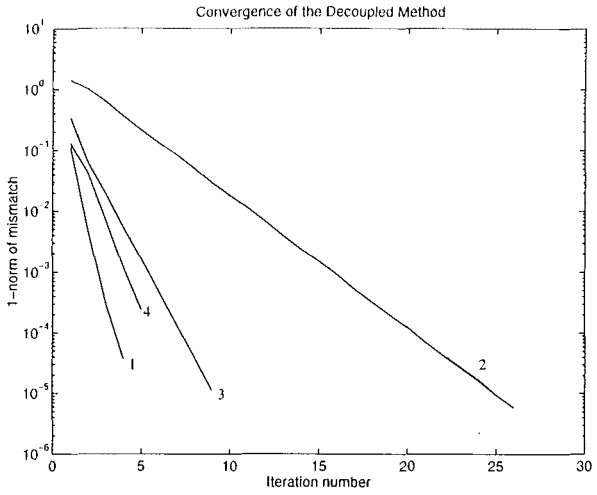

Figure 5.3 Convergence of the decoupled method on the four test systems.

5.3 SEQUENCE COMPONENTS SOLUTION

Until this point the convertor has of necessity been modelled in phase components. This is because individual conduction intervals, related to switchings between the three phases, must be modelled explicitly. Like many power system components, the convertor is best understood in terms of sequence components, as in the steady state the convertor transforms harmonic sequence components on the ac side, to harmonics on the dc side [Larson *et al.* 1989] [Wood 1993],and vice versa. There are therefore fewer harmonic interactions between sequence components than between phase components, indicating that a solution of the convertor in sequence components should be easier. An additional motivation is that there is always going to be little, or no coupling to the zero sequence on the ac side from any of the convertor variables.

A sequence components solution is implemented by using the sequence transform matrix, T, to interface complex phase component calculations to the Newton solution in sequence components. For complex phasors, the complex 3×3 sequence transform is

$$\begin{bmatrix} V^0 \\ V^- \\ V^+ \end{bmatrix} = \begin{bmatrix} 1 & 1 & 1 \\ 1 & a^2 & a \\ 1 & a & a^2 \end{bmatrix} \begin{bmatrix} V^a \\ V^b \\ V^c \end{bmatrix}, \tag{5.36}$$

where $a = e^{j\frac{2\pi}{3}}$. Setting

$$W = \begin{bmatrix} V^0 \\ V^- \\ V^+ \end{bmatrix}$$

as the sequence components voltage yields $W = TV$, and $V = T^{-1}W$. If a three phase quantity has been decomposed in real rectangular components, as in the Jacobian matrix, a real components sequence transform matrix, $\bar{T}$, can be constructed:

$$\bar{W} = \begin{bmatrix} V_R^0 \\ V_I^0 \\ V_R^- \\ V_I^- \\ V_R^+ \\ V_I^+ \end{bmatrix} = \begin{bmatrix} 1 & 0 & 1 & 0 & 1 & 0 \\ 0 & 1 & 0 & 1 & 0 & 1 \\ 1 & 0 & \mathcal{R}a^2 & -\mathcal{I}a^2 & \mathcal{R}a & -\mathcal{I}a \\ 0 & 1 & \mathcal{I}a^2 & \mathcal{R}a^2 & \mathcal{I}a & \mathcal{R}a \\ 1 & 0 & \mathcal{R}a & -\mathcal{I}a & \mathcal{R}a^2 & -\mathcal{I}a^2 \\ 0 & 1 & \mathcal{I}a & \mathcal{R}a & \mathcal{I}a^2 & \mathcal{R}a^2 \end{bmatrix} \begin{bmatrix} V_R^a \\ V_I^a \\ V_R^b \\ V_I^b \\ V_R^c \\ V_I^c \end{bmatrix} = \bar{V} \tag{5.37}$$

The existing phase components mismatch equations summarised in table 4.2 can now be written as sequence component mismatches, in terms of the sequence components terminal voltage, using the sequence transform matrix. Sequence component mismatches for the twelve pulse controlled rectifier are listed in table 5.2 below. The

equation	No. of Eqns.	functional notation
F_W	300	$W - Tf_{18}(T^{-1}W, I_{dk}, I_{d0}, \theta_i^D, \phi_i^D, \theta_i^S, \phi_i^S)$
F_{Id}	100	$I_{dk} - f_{19}(T^{-1}W, I_{dk}, I_{d0}, \theta_i^D, \phi_i^D, \theta_i^S, \phi_i^S)$
F_ϕ^S	6	$f_{20}(T^{-1}W, I_{dk}, \theta_i^S, \phi_i^S)$
F_ϕ^D	6	$f_{21}(T^{-1}W, I_{dk}, \theta_i^D, \phi_i^D)$
F_θ^S	6	$f_{14}(I_{dk}, I_{d0}, \theta_i^S, \alpha_0)$
F_θ^D	6	$f_{15}(I_{dk}, I_{d0}, \theta_i^D, \alpha_0)$
F_S	1	$f_{22}(T^{-1}W, I_{dk}, I_{d0}, \theta_i^S, \theta_i^D, \phi_i^S, \phi_i^D)$
$F_{\alpha 0}$	1	$f_{23}(T^{-1}W, I_{dk}, I_{d0}, \theta_i^S, \theta_i^D, \phi_i^S, \phi_i^D)$

Table 5.2 Mismatches and variables for the 12 pulse rectifier with the terminal voltage in sequence components.

chain rule readily yields the modifications that must be made to the phase components partial derivatives, to yield the sequence components partial derivatives:

$$\begin{aligned} \left[\frac{\partial F_W}{\partial W}\right] &= \left[\frac{\partial W_i}{\partial W_j}\right] - \bar{T}\left[\frac{\partial f_{18}}{\partial V}\right]\bar{T}^{-1} \\ \left[\frac{\partial F_W}{\partial x}\right] &= -\bar{T}\left[\frac{\partial f_{18}}{\partial x}\right], \quad x \in \{I_{dk}, I_{d0}, \theta_i^D, \phi_i^D, \theta_i^S, \phi_i^S\} \\ \left[\frac{\partial F_x}{\partial W}\right] &= \left[\frac{\partial F_x}{\partial V}\right]\bar{T}^{-1}, \quad x \in \{I_{dk}, I_{d0}, \theta_i^D, \phi_i^D, \theta_i^S, \phi_i^S\} \end{aligned} \tag{5.38}$$

The resulting Jacobian matrix, calculated using the numerical perturbation method, is plotted in figure 5.5, and shows a greater degree of sparsity. This is primarily due to the absence of any coupling between the zero sequence ac voltage harmonics and any of the other convertor variables. In many cases, it would be possible to decouple zero sequence from the convertor model completely, and solve the zero sequence termi

nal voltage directly after the convertor model had converged. This is because there is usually no nonlinearity due to the convertor in the zero sequence.

Unbalance in the star-g/delta transformer however causes cross sequence coupling in that transformer, with the result that a full three sequence solution is required. This is illustrated in figure 5.6 of the Jacobian matrix, where the leakage reactance in phase 'b' of the star-g/delta transformer has been increased from 0.18 to 0.30 per unit. Coupling between zero sequence and all the other convertor variables is evident in this case.

The overall sequence components solution algorithm is the same as that of figure 4.8, with the switching system solved in phase components, and the harmonic system solved in sequence components. Inspection of table 5.3 shows that convergence of the sequence components method is usually slightly better than the phase components solution. Convergence on a step by step basis for the four test cases is plotted in figure 5.4.

Test No.	CPU time (seconds)	Switch Iterations	Main Iterations	λ
1b	11.1	6	6	0.1712
1d	10.9	6	5	0.0851
2b	14.8	6	11	0.2562
2d	15.0	6	12	0.2973
3b	12.3	6	7	0.1130
3d	11.5	6	6	0.1056
4b	14.1	9	9	0.3129
4d	13.4	9	8	0.2834

Table 5.3 Convergence and performance of the convertor model, b) constant unified Jacobian, d) Constant sequence components Jacobian.

Although the performance of the sequence components method is slightly better than that of the phase components solution, it is not remarkably so. However the storage requirements for the Jacobian elements are reduced by approximately 500 - 1000 elements for a solution up to the 50th harmonic. Sequence components modelling may also have additional advantages when combined with synchronous machine models, or a three sequence load flow.

5.4 CONCLUSION

Three alternative implementations of the convertor model have been investigated. One of these, the polar coordinates implementation, was found to be unsuitable because of poor conditioning of the Jacobian matrix, due to the large range of harmonic mag-

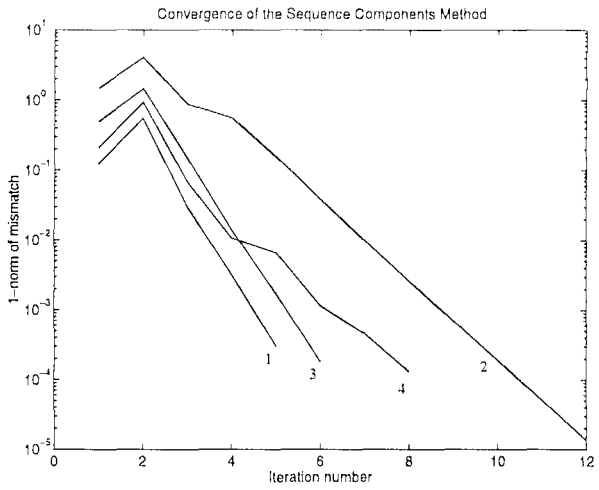

Figure 5.4 Convergence of the constant sequence components Jacobian on the four test systems.

nitudes that are of interest. This conclusion was arrived at by forming analytical expressions for the polar partial derivatives.

A decoupled method was implemented by partitioning each of the vectors of variables and mismatch functions, into two sub-vectors associated with the switching system, and the harmonic interactions between the ac and dc sides of the convertor. Such a decoupling can be viewed as a fixed point iteration, for which there is a simple test on convergence based upon the magnitudes of the partial derivatives of the iterating functions. These partial derivatives were calculated numerically for the CIGRE rectifier, and found to contravene the convergence criteria. The decoupled method nevertheless converges quite well for this system, except when the composite resonance is excited. When applied to the hybrid CIGRE/NZ test system, the decoupled method was found to diverge if even order harmonic sources were present in the ac system. The method is therefore not robust enough for general purpose use.

The sequence components method was implemented by placing sequence/phase transforms at selected stages of the phase components solution. This yielded a Jacobian matrix with little or no coupling to the zero sequence, and therefore fewer terms in the Jacobian. The sequence components method was found to yield slightly better convergence than a solution in phase components. In the long term, the choice between phase or sequence components modelling depends upon whichever is more efficient for the modelling of the power system as a whole.

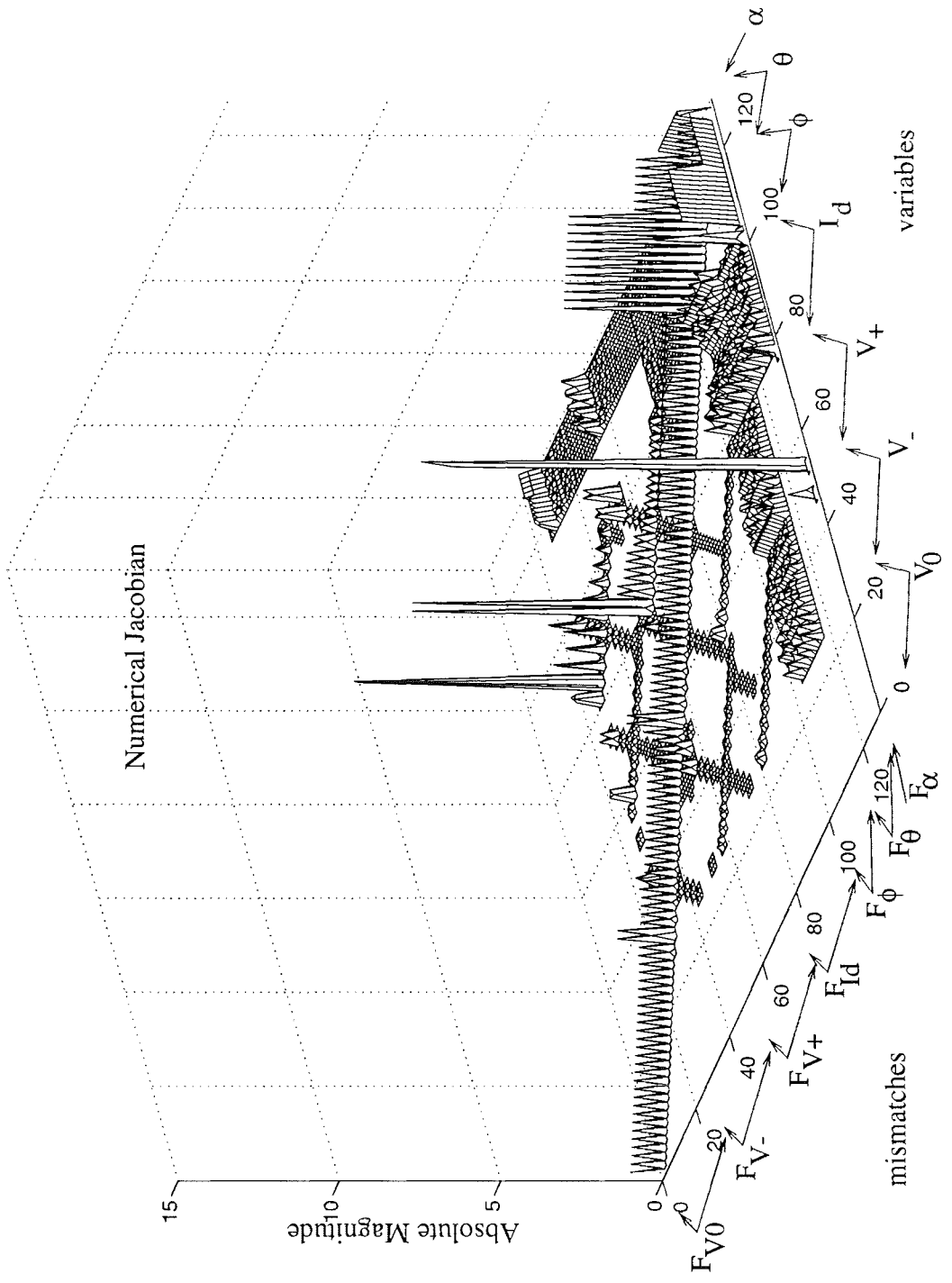

Figure 5.5 Numerically calculated sequence components Jacobian; 13 harmonics.

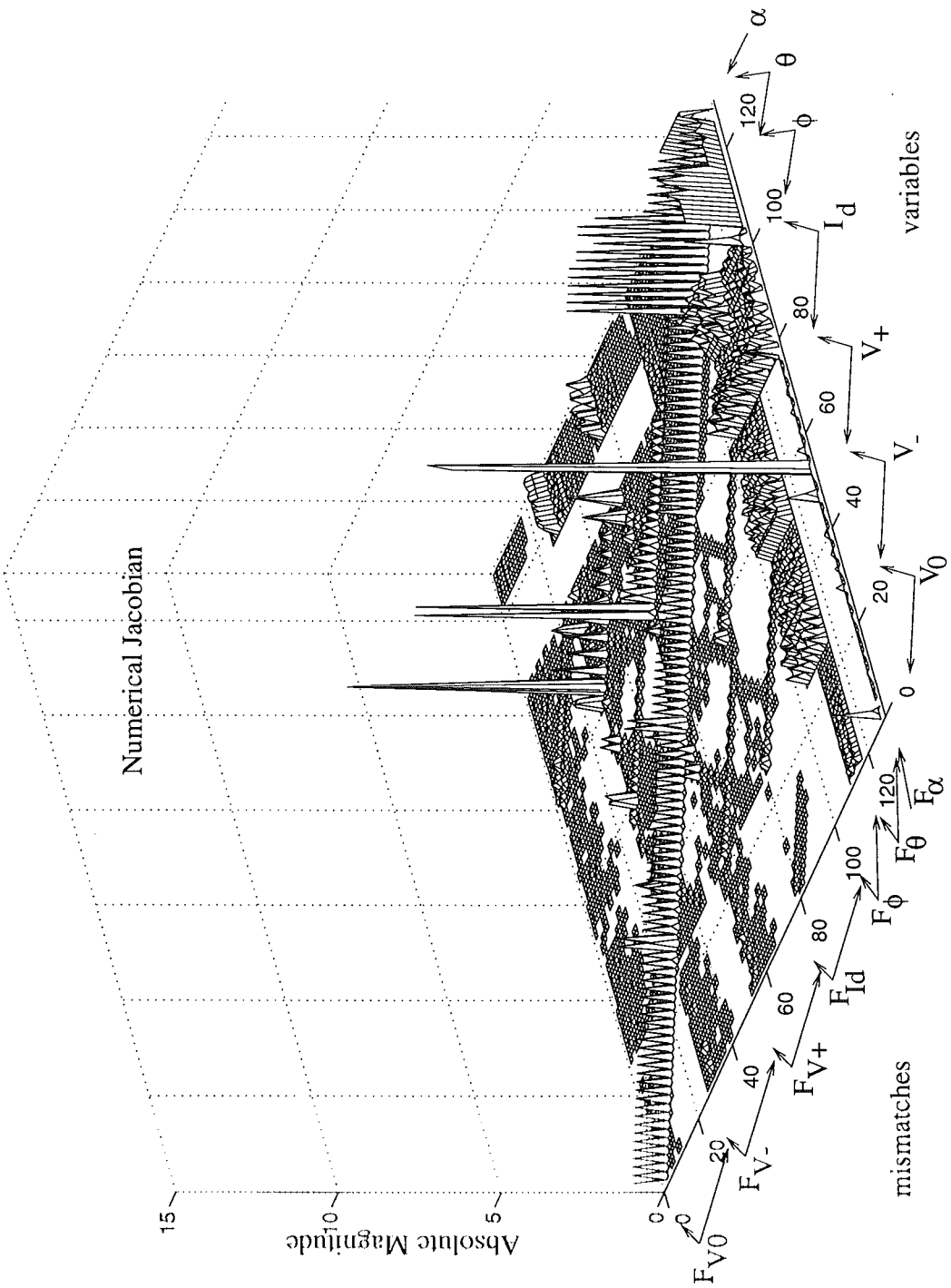

Figure 5.6 Numerically calculated sequence components Jacobian with mbalanced star-g/delta transformer; 13 harmonics.

Chapter 6

TENSOR LINEARISATION USING THE JACOBIAN

6.1 INTRODUCTION

A widely used and powerful technique for analysing nonlinear devices is to linearise around an operating point. If the nonlinearity is a voltage-current relationship, the linearisation yields an admittance. This type of linearisation is particularly relevant to the convertor, as the convertor admittance can be combined with the ac and dc system admittances to analyse resonances, harmonic transfers, and harmonic magnification factors. For example, [Bahrman *et al.* 1986] calculated the dc side impedance of a convertor, including the effect of ac side impedance at coupled harmonics. Dickmander *et al.* [1994] analysed a GIC induced 5th harmonic resonance, and showed that the resonance could only be explained by combining the impedance of the convertor at the 5th harmonic with that of the ac system. The convertor impedance was in turn a function of the dc system impedance.

The linearisation of the convertor to a frequency dependent impedance is a simple, yet powerful tool for solving ac/dc system interactions, that offers greater insight than repeated numerical solutions of the interaction. The linearisation can be extended to include coupling between harmonics on the ac and dc sides of the convertor. This was first proposed by Larson *et al.* [1989], with the linearisation calculated by many small harmonic perturbations of a time domain simulation. More recently Wood and Arrillaga [1995b] developed a frequency domain method for calculating the convertor impedance directly.

The interactions between several nonlinearities can also be linearised, as in the analysis of convertor transformer core saturation [Hammad 1992], [Chen *et al.* 1996]. Relationships other than between voltage and current have been linearised. Persson [1970], Ferreira *et al.* [1987], and Wood and Arrillaga [1995a] have calculated relationships between firing angle modulation and dc current ripple, for modelling of the control loop. Elimination of noncharacteristic harmonics by directly modulating the firing angle, has also required the linearisation of relationships between firing angle modulation harmonics, and phase current harmonics [Farret and Freris 1990], [Hammad 1992].

When linearising general nonlinear devices to an equivalent impedance, representation by a single complex number is not possible. This was noted by Semlyen *et al.* [1988], who proposed the use of either complex or real valued matrices. The fact that the complex value of an impedance can depend upon the phase angle of the current flowing through it, and still be linear, is not widely appreciated. Persson [1970] noted that the linear transfer from firing angle modulation to direct current at the 6th harmonic was phase dependent, and described a circle in the complex plane. The fact that this applied to the convertor linearised impedance was noted by Wood [1], and prompted an investigation of the effect using three different convertor models [Wood *et al.* 1995].

Central to Newton's method for solving nonlinear systems is the Jacobian matrix, which represents a linearisation of the system of equations at every iteration. Although the Jacobian is typically held constant during the solution, it can be re-calculated at convergence. In the context of the convertor model, it should therefore be possible to use the Jacobian matrix to calculate equivalent impedances for the convertor, or indeed any other linearised relationship. The advantage of calculating impedances in this way is that the effect of control, switching instant variation, unbalance, and system impedances are automatically taken into account.

Clearly the utility of this method increases as the generality of the Newton solution is expanded. For example, a unified Newton solution of several ac systems connected by dc links, with load flow and transformer saturation represented, would enable the direct calculation of any desired linear relationship from the Jacobian. In the remainder of this chapter, methods for extracting impedances from the Jacobian matrix, and for performing nodal analysis using phase dependent admittances are developed.

6.2 THE IMPEDANCE TENSOR

In this section a framework for linearising the convertor is established that is able to account for the phase dependent nature of the convertor at some harmonics. This will allow a linearised impedance representation of the convertor suitable for use in a real components nodal analysis, or a complex conjugate type nodal analysis of the convertor interaction with ac and dc system linearisations.

Any power system component can be represented by a voltage controlled current source: $I = F(V)$, where I and V are vectors of harmonic phasors. The function F, is a complex vector function, and may be non-linear, and non-analytic. If F is linear, it may include linear cross-coupling between harmonics, and may be non-analytic, ie harmonic cross coupling and phase dependence do not imply non-linearity in the harmonic domain. It will be shown in section 6.3 that for harmonic perturbations less than 0.2 p.u., the CIGRE current controlled rectifier is a good approximation to such a device.

[1] *pers com*, 1994

The linearised response of F to a single applied harmonic may be calculated by taking the first partial derivatives in rectangular coordinates:

$$\begin{bmatrix} \Delta I_R \\ \Delta I_I \end{bmatrix} = \begin{bmatrix} \frac{\partial F_R}{\partial V_R} & \frac{\partial F_R}{\partial V_I} \\ \frac{\partial F_I}{\partial V_R} & \frac{\partial F_I}{\partial V_I} \end{bmatrix} \begin{bmatrix} \Delta V_R \\ \Delta V_I \end{bmatrix}, \tag{6.1}$$

where F has been expanded into its component parts:

$$I_R + jI_I = F_R(V_R, V_I) + jF_I(V_R, V_I). \tag{6.2}$$

If the Cauchy-Rieman conditions

$$\frac{\partial F_R}{\partial V_R} = \frac{\partial F_I}{\partial V_I} \tag{6.3}$$

$$\frac{\partial F_I}{\partial V_R} = -\frac{\partial F_R}{\partial V_I} \tag{6.4}$$

hold, then the matrix of partial derivatives is of the form

$$\begin{bmatrix} a & -b \\ b & a \end{bmatrix},$$

which is a type of matrix isomorphic with the complex number field. The linearisation then becomes

$$\Delta I = \frac{\partial F}{\partial V}\Delta V. \tag{6.5}$$

The complex admittance representation of a linearisation can therefore only be applied to analytic current injections. Non-analytic injections are quite common, for example in the load flow, $I = S^*/V^*$ for a $P + jQ$ bus, which is also nonlinear. An example of a linear, but nonanalytic injection would be:

$$I = Y_1 V + Y_2 V^*. \tag{6.6}$$

This is linear, since if

$$I_1 = Y_1 V_1 + Y_2 V_1^* \tag{6.7}$$

$$I_2 = Y_1 V_2 + Y_2 V_2^* \tag{6.8}$$

$$V_3 = aV_1 + bV_2 \tag{6.9}$$

then

$$\begin{aligned} I_3 &= Y_1 V_3 + Y_2 V_3^* && (6.10)\\ &= Y_1(aV_1 + bV_2) + Y_2(aV_1 + bV_2)^* && (6.11)\\ &= aY_1V_1 + bY_1V_2 + aY_2V_1^* + bY_2V_2^* && (6.12)\\ &= aI_1 + bI_2. && (6.13) \end{aligned}$$

For such a source, the complex admittance is;

$$\begin{aligned} Y &= \frac{I}{V} && (6.14)\\ &= \frac{Y_1V + Y_2V^*}{V} && (6.15)\\ &= Y_1 + |Y_2| \angle (\angle Y_2 - 2\angle V) && (6.16) \end{aligned}$$

The complex admittance twice traces a circular locus centered at Y_1 in the clockwise direction, as the angle of the applied voltage is varied through 2π. By the inverse mapping, $Z = \frac{1}{Y}$, also traces a circular locus, but in the anti-clockwise direction. Next, it will be shown that any current injection, when linearised, can be written in the form

$$\Delta I = Y_1 \Delta V + Y_2 \Delta V^* \tag{6.17}$$

Expanding equation 6.17 into components,

$$\begin{bmatrix} \Delta I_R \\ \Delta I_I \end{bmatrix} = \begin{bmatrix} Y_{1R} + Y_{2R} & Y_{2I} - Y_{1I} \\ Y_{1I} + Y_{2I} & Y_{1R} - Y_{2R} \end{bmatrix} \begin{bmatrix} \Delta V_R \\ \Delta V_I \end{bmatrix}, \tag{6.18}$$

Equating the matrices on the right hand sides of equations 6.18 and 6.1, the real and imaginary parts of Y_1 and Y_2 are readily expressed in terms of the partial derivatives:

$$\begin{aligned} Y_{1R} &= \frac{1}{2}\left(\frac{\partial F_R}{\partial V_R} + \frac{\partial F_I}{\partial V_I}\right)\\ Y_{1I} &= \frac{1}{2}\left(\frac{\partial F_I}{\partial V_R} - \frac{\partial F_R}{\partial V_I}\right)\\ Y_{2R} &= \frac{1}{2}\left(\frac{\partial F_R}{\partial V_R} - \frac{\partial F_I}{\partial V_I}\right)\\ Y_{2I} &= \frac{1}{2}\left(\frac{\partial F_R}{\partial V_I} + \frac{\partial F_I}{\partial V_R}\right) \end{aligned} \tag{6.19}$$

For nodal analysis, the conjugate operator is eliminated by treating conjugated voltages and currents as additional variables. The conjugation operator then introduces a harmonic cross coupling term between the conjugated variables, and the linearised

admittance of any source can be written:

$$\begin{bmatrix} \Delta I \\ \Delta I^* \end{bmatrix} = \begin{bmatrix} Y_1 & Y_2 \\ Y_2^* & Y_1^* \end{bmatrix} \begin{bmatrix} \Delta V \\ \Delta V^* \end{bmatrix}, \tag{6.20}$$

This is the nodal analysis proposed by Semlyen *et al.* [1988], and used in the HDA program. It has also been used to form ABCD parameter matrices relating harmonics on the ac and dc sides of the convertor [Jalali and Lasseter 1991]. If F is non-analytic, $Y_2 \neq 0$, and the complex admittance will be a circular locus. For positive frequency nodal analysis, the real matrix of partial derivatives is retained, and is henceforth called the admittance or impedance *tensor*:

$$\bar{Y} = \begin{bmatrix} y_{11} & y_{12} \\ y_{21} & y_{22} \end{bmatrix} = \begin{bmatrix} \frac{\partial F_R}{\partial V_R} & \frac{\partial F_R}{\partial V_I} \\ \frac{\partial F_I}{\partial V_R} & \frac{\partial F_I}{\partial V_I} \end{bmatrix}. \tag{6.21}$$

The nodal analysis is then performed in real components using a Cartesian vector representation of voltage and current phasors on the Argand plane, and a second rank tensor representation of admittances and impedances. Tensors are widely used in physics to represent a relationship between vectors that is invariant under rotation of the coordinate axes [Arfkin 1985]. In this case, the coordinate axes are the real and imaginary components of the complex voltage phasor, which rotate under a shift in phase reference. The components of the voltage therefore transform like the elements of a vector under this rotation. Since the current is a vector function of the voltage, the matrix of partial derivatives can be written as the direct product of the gradient operator with the current vector, yielding a second rank tensor

$$\bar{Y} = \nabla \hat{I}^T, \tag{6.22}$$

Although the elements of the tensor admittance are modified by a change in phase reference, they transform in such a way that the relationship described by the tensor, dependence of current on voltage, is invariant. When the tensor admittance is extended to three phases and multiple harmonics, the dimension will be $6n_h$, but the rank of the tensor will still be two.

Given an admittance tensor $\bar{Y}$, the impedance tensor is

$$\bar{Z} = \bar{Y}^{-1} = \begin{bmatrix} z_{11} & z_{12} \\ z_{21} & z_{22} \end{bmatrix} \tag{6.23}$$

The impedance tensor corresponds to a circular impedance locus on the complex plane, of radius r, x-position a, y-position b, and *rotation* γ. The rotation of the impedance locus is defined to be the angular position on the circular locus corresponding to an applied current of phase 0. These quantities are illustrated in figure 6.1. In Appendix D,

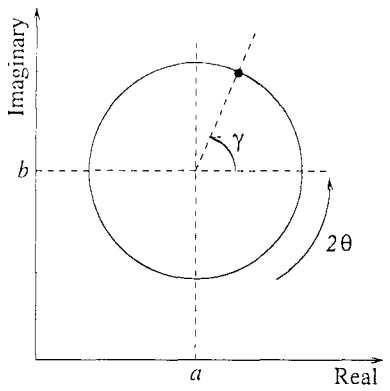

Figure 6.1 Complex impedance locus for an impedance tensor. The locus point rotates counter clockwise twice, starting from the angle γ, as the current injection ranges in angle from 0 to 2π.

the parameters of the impedance circle are derived entirely in terms of the tensor components, and are listed below.

$$a = \frac{1}{2}(z_{11} + z_{22}) \tag{6.24}$$

$$b = \frac{1}{2}(-z_{12} + z_{21}) \tag{6.25}$$

$$r = \frac{1}{2}\sqrt{(z_{11} - z_{22})^2 + (z_{12} + z_{21})^2} \tag{6.26}$$

$$\gamma = \tan^{-1}\frac{z_{12} + z_{21}}{z_{22} - z_{11}} \tag{6.27}$$

Since the impedance tensor is a matrix, it may not be invertible, in which case the determinant is zero. However

$$\begin{aligned} a^2 + b^2 - r^2 &= \frac{1}{4}\left[(z_{11} + z_{22})^2 + (-z_{12} + z_{21})^2 - (z_{11} - z_{22})^2 - (z_{12} + z_{21})^2\right] \\ &= z_{11}z_{22} - z_{12}z_{21} \\ &= det(\bar{Z}), \end{aligned} \tag{6.28}$$

and the tensor is invertible if and only if the complex circular locus does not intersect the origin. The x-axis intercepts of the circular locus correspond to a resistive impedance, so that

$$\bar{Z}I = RI. \tag{6.29}$$

The eigenvalues of $\bar{Z}$ are therefore the values of resistance where the locus intersects

the x-axis. The characteristic equation is

$$\begin{vmatrix} (z_{11}-R) & z_{12} \\ z_{21} & (z_{22}-R) \end{vmatrix} = R^2 - R(z_{11}+z_{22}) - z_{12}z_{21} + z_{11}z_{22} \quad (6.30)$$

$$= 0, \quad (6.31)$$

which is a quadratic in R, and it is easy to show that a real solution for R is only possible if $r^2 > b^2$, ie the circular locus is close enough to the x-axis. If the x-axis intercepts are considered as being a type of resonance, then the eigenvectors of $\bar{Z}$ are those currents that have the correct angle to excite the resonance.

6.3 CALCULATION OF THE CONVERTOR IMPEDANCE

In general the convertor impedance for small distortions will be phase dependent, and therefore best represented by a tensor. The impedance tensor can be directly calculated from the convertor Jacobian, since the Jacobian is a linearisation of the convertor around an operating point. Firstly however, the phase and magnitude dependence of the convertor complex impedance to an applied harmonic voltage distortion is investigated by applying a variety of small harmonic distortions to the convertor terminal.

6.3.1 Perturbation Analysis

An approximation to the convertor impedance to small harmonic distortions applied to the ac terminal can be determined by solving the convertor model for perturbations around an initial solution. For example, to solve the 7th harmonic positive sequence impedance, the convertor base case is first solved (Test One in Chapter 4). A sequence transform is then applied to the 7th harmonic voltage and phase current at the ac terminal to yield base values:

$$V_{7b}^{+} = [TV_{7b}]^{+} \quad (6.32)$$

$$I_{7b}^{+} = [TI_{7b}]^{+} \quad (6.33)$$

Next, a small positive sequence 7th harmonic voltage source is added to the ac system Thevenin voltage source, and the convertor model is re-converged. The perturbed positive sequence 7th harmonic ac terminal quantities are then calculated, as above:

$$V_{7p}^{+} = [TV_{7p}]^{+} \quad (6.34)$$

$$I_{7p}^{+} = [TI_{7p}]^{+} \quad (6.35)$$

A value of 7th harmonic impedance is then obtained from the ratio of change in voltage, to change in current:

$$Z_7^+ = \frac{V_{7p}^+ - V_{7b}^+}{I_{7p}^+ - I_{7b}^+} \tag{6.36}$$

The variation of the impedance with magnitude or phase, is determined by applying several different magnitudes or phase of voltage to the ac system Thevenin equivalent voltage source. For most harmonics, the series combination of filters and system impedance in the CIGRE model acts as a voltage divider to any applied harmonic voltage in the ac system, so that it is difficult to obtain a large voltage distortion at the convertor terminal. Accordingly, for the purpose of determining the response of the convertor impedance to a large harmonic distortion, the ac system and filter impedances at every harmonic were made equal to their impedances at the fundamental. The effect of harmonic magnitude was then determined by applying a voltage source in the ac system that resulted in approximately 0.001 p.u. change in voltage distortion at the convertor terminal, and then a source that resulted in 0.12 p.u. voltage distortion. The small source yields a good approximation to the 'slope' convertor impedance, whereas the 0.12 p.u. distortion resulting from the large source is larger than would be encountered in practice.

Forty phase angles, from 0 to 2π, of voltage distortion were applied at both magnitudes, and at every harmonic order from 2 to 37, in positive and negative sequence. The resulting impedance loci have been plotted in figure 6.2.

To obtain accurately the value of small current and voltage perturbations, the convergence tolerance for the model was reduced to:

$$\begin{aligned}
\frac{|F_V|}{|V|} &< 2 \times 10^{-6} \\
\frac{|F_I|}{|I|} &< 2 \times 10^{-6} \\
\frac{|F_{Id}|}{|Id|} &< 2 \times 10^{-6} \\
\frac{|F_{\alpha_0}|}{|I_{d0}|} &< 2 \times 10^{-6} \\
|F_{\theta_i}| &< 5 \times 10^{-8} \\
|F_{\phi_i}| &< 5 \times 10^{-8},
\end{aligned} \tag{6.37}$$

and thresholding was removed for the impedance harmonic under consideration. Since the system was the same for every perturbation, the Jacobian was held constant for all 5760 runs. The main features to be observed in figure 6.2 are the phase dependence of the convertor impedance at 6-pulse characteristic harmonics, and the independence of impedance with magnitude of applied voltage. At the 12-pulse characteristic harmonics,

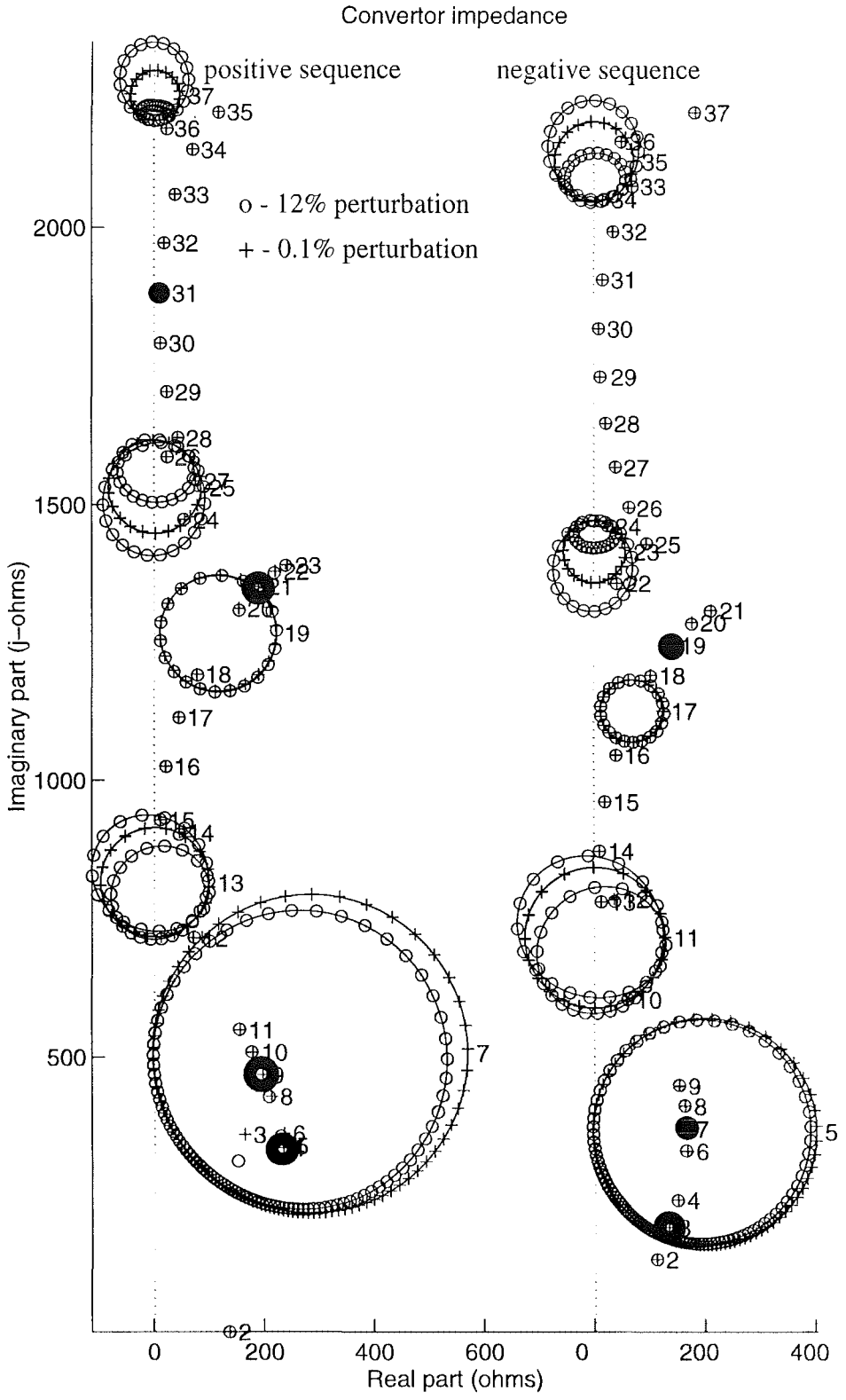

Figure 6.2 Dependence of convertor impedances on magnitude of applied voltage perturbation.

a large value of distortion leads to an epicyclic phase dependent locus, due to the coupling of these harmonics to the average dc current, and hence control action. At all other harmonics and sequences, the convertor impedance is essentially completely linear over the range of magnitudes likely to be encountered. In practice, there will also be filters at the characteristic and high order harmonics, and high levels of voltage distortion will not be encountered.

Despite a uniform progression of voltage phase angles applied to the 5th and 7th harmonics, the associated circular loci display a clustering of impedance points near the origin. This is a consequence of the perturbation method used, rather than the impedance itself, and is best explained by considering the locus of the returned current perturbations, as plotted in figure 6.3 for the positive sequence 7th harmonic.

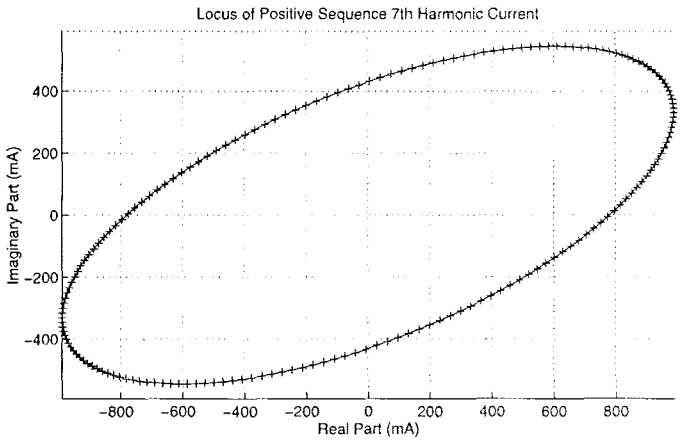

Figure 6.3 Locus of the perturbed fifth harmonic current.

As the applied voltage phase progresses uniformly through 2π, the returned current is determined by a uniform double rotation around the admittance locus. The admittance locus is not concentric with the origin, and so the returned current is small only for those few points on the admittance locus close to the origin. This results in the clustering of points on the extrema of the elliptical current locus. When points on the impedance locus are calculated, this clustering effect is compounded by the radial distance from the origin on the impedance plane, since the current locus is clustered at large values of current, which correspond to small impedances. If the voltage perturbation method is used to calculate the admittance locus instead, the points are equi-spaced. If the impedance locus is centered a long way from the origin, relative to the radius of the locus, the clustering is insignificant.

In relation to the earlier discussion on phase dependence, it is evident that the convertor impedance can be described by complex numbers at all harmonics, apart from $h = 6n \pm 1$. At these harmonics the impedance should be a tensor representation, or a coupling to the conjugate of the applied voltage. The generation of harmonic

currents by the convertor related to the conjugate of an applied voltage distortion is predicted by the modulation theory analysis of Wood and Arrillaga [1995b]. The impedance of the convertor is calculated in this model by superimposing the effect of several small amplitude waveform distortion transfers, each calculated by modulation theory. Although this model predicts many relationships involving multiples of the modulation frequency, these higher order terms are very small, and it suffices for a qualitative understanding of the convertor impedance to consider only the relationships described below.

Modulation Theory of the Impedance The application of either a positive sequence harmonic voltage of order $(k+1)$ angle δ, or a negative sequence harmonic $(k-1)\angle\delta$ on the ac side of the convertor is directly transferred to a dc side voltage $k\angle(a_1+\delta)$ and a small $(12-k)\angle(a_2-\delta)$, where a_i is a constant angle. If $k=6$ then the first reflected term, $(12-k)$, is at the same harmonic, but phase conjugated. This mechanism of phase conjugation occurs quite generally for all the distortion transfers through the convertor. The dc ripple at harmonic k, resulting from the voltage ripple, will be transferred to the ac side currents $(k+1)\angle(a_3+\delta)$ in positive sequence, and $(k-1)\angle(a_4+\delta)$ in negative sequence. There will also be ac side currents $(11-k)\angle(a_5-\delta)$ in positive sequence, and $(13-k)\angle(a_6-\delta)$ in negative sequence. The reflected terms, $(11-k)$ and $(13-k)$, are very small, but demonstrate one mechanism whereby there is a phase conjugation of applied voltage to returned current on the ac side.

Commutation Period Modulation The application of harmonic voltage orders of either $(k+1)\angle\delta$ in positive sequence, or $(k-1)\angle\delta$ in negative sequence on the ac side will directly modulate the end of commutation angles at harmonic $k\angle(a_7+\delta)$. This has a very significant effect on ac side impedances, since the full dc current will be modulated. The end of commutation modulation leads to a range of modulation products on the ac side, including the harmonic orders $(k+1)\angle(a_8+\delta)$ in positive sequence, $(k-1)\angle(a_9+\delta)$ in negative sequence, $(11-k)\angle(a_{10}-\delta)$ in negative sequence, and $(13-k)\angle(a_{11}-\delta)$ in positive sequence. The reflected terms in this case are significant, and are scaled by the product of two sinc functions: $\mathrm{sinc}(k\mu/2)\mathrm{sinc}(m\mu/4)$, where $m=1,11,13,23...$ Setting $k=6$, indicates that the 5th negative, and 7th positive sequence impedances of the convertor are substantially phase dependent. If a 6th positive sequence voltage is applied to the convertor there will be a negative sequence current returned, and vice versa. A similar analysis holds for all 6-pulse order harmonics, reflecting as appropriate from higher order multiples of the modulating frequency.

Having established that the convertor impedance is magnitude independent, and best represented by a tensor at particular harmonics, it is not necessary to calculate the complex impedance for a full 2π of applied voltage distortions. In fact, just two perturbations yield four equations in the four unknown tensor elements. However the

perturbation method is essentially a numerical partial differentiation, rife with potential problems. For example, it is difficult to know if the perturbation is definitely small enough, and whether the convergence tolerance specified has yielded suitably accurate data points. In the next section, the Jacobian matrix is modified to yield directly any desired tensor relationship. Anticipating this result, figure 6.14 is a comparison of the CIGRE rectifier impedance loci calculated analytically from the Jacobian (continuous circles), and by perturbation (data points on circles), for every harmonic order from 2 to 37 in positive and negative sequence. The perturbation calculation of the convertor impedance has been further intervalidated against perturbation of an EMTDC model, and a direct 6-port analytic calculation using the above described analytic model in [Wood *et al.* 1995].

6.3.2 The Lattice Tensor

Several authors, most notably [Larson *et al.* 1989], have noted that from the point of view of the ac system, the convertor presents a stable and quite linear set of interrelationships between harmonics and sequences. For example, the application of a positive sequence voltage distortion at harmonic order $k+1$, leads to the injection of harmonic currents $(11 \pm k)$, $(23 \pm k)$, etc in negative sequence, and $(1 \pm k)$, $(13 \pm k)$, $(25 \pm k)$ etc in positive sequence. The difference terms are always phase conjugated, unless the harmonic would be negative, in which case the sequence is reversed. In fact the analysis of [Wood and Arrillaga 1995a] predicts many other multiple reflections that usually, but not always, decay with order (for example $12m \pm nk \pm 1$). This 'numerology of the convertor' is succinctly summarised by a lattice-like diagram of connections between harmonics and sequences, as shown in figure 6.4, for $n = 1$.

Points on figure 6.4 marked with a '+', can be represented by a complex admittance. Points marked by a 'o' represent couplings between positive and negative harmonics, and can be represented either by a circular admittance locus centered on the origin in the complex admittance plane, or by a tensor. Points with both markers, at lattice vertices, indicate that the total current returned consists of two components, related to the voltage applied, and its conjugate. Such points correspond to a circular locus in the complex plane shifted away from the origin. Figure 6.14 is a plot of impedances along the diagonal of figure 6.4, with circular loci occurring at the 6-pulse characteristic harmonics. Also marked on figure 6.4 is the special case of a sixth harmonic positive sequence distortion. A current is returned at the same harmonic in both positive and negative sequence, and it can be seen that the convertor transforms between positive and negative sequence for all harmonics $k = 6n$.

If the convertor is unbalanced, or there are large harmonic distortions, the cross coupling lattice will fill in to some extent, especially at low order harmonics. There will also be current injections related to the conjugate of applied harmonic voltages at

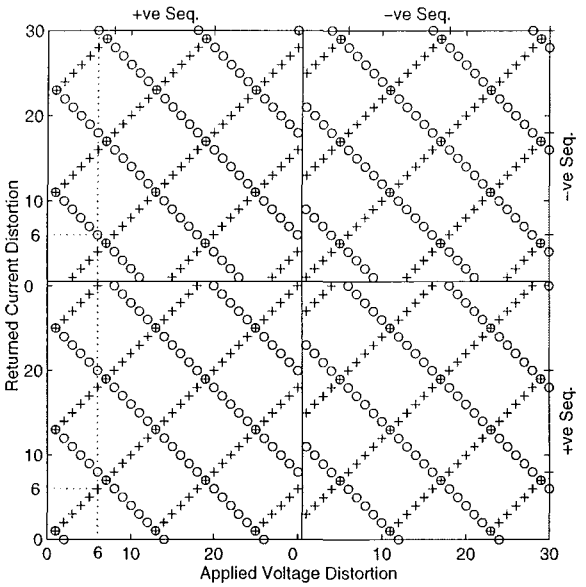

Figure 6.4 Principle harmonic currents returned by a twelve pulse convertor in response to an applied voltage distortion. '+'- current phase related to phase of applied voltage, 'o' - current phase related to conjugate of applied voltage.

most harmonics. In general then, the lattice is most accurately represented by a large *lattice tensor*, of second rank, but of size $4n_h \times 4n_h$ (unless there is coupling to the zero sequence). The lattice tensor can be calculated from the Jacobian matrix by first noting that partial derivatives of the voltage mismatch are of the form:

$$\frac{\partial F_V}{\partial X} = \frac{\partial V}{\partial X} - \frac{\partial f_{18}}{\partial X} \tag{6.38}$$

where f_{18} is the calculated terminal voltage, obtained by injecting the phase currents into the ac system impedance:

$$f_{18k}(X) = [Y_{cc}]_k^{-1}([I_P^S + I_P^D]_k + [Y_{ct}]_k[V_{ih}]_k) \tag{6.39}$$

consequently

$$\frac{\partial f_{18}}{\partial X} = [Y_{cc}]_k^{-1}\frac{\partial [I_P^S + I_P^D]}{\partial X} \tag{6.40}$$

Those rows of the Jacobian that contain partial derivatives of the voltage mismatch are therefore easily modified to contain partial derivatives of the phase currents with respect to the system variables (terminal voltage, dc current, switching angles). The

matrix equation defined by the new matrix, J', is now:

$$\begin{bmatrix} \Delta I \\ \Delta F_{Id} \\ \Delta F_{\phi} \\ \Delta F_{\theta} \\ \Delta F_{\alpha 0} \end{bmatrix} = \begin{bmatrix} \frac{\partial I}{\partial V} & \frac{\partial I}{\partial I_d} & \frac{\partial I}{\partial \phi} & \frac{\partial I}{\partial \theta} & \frac{\partial I}{\partial \alpha_0} \\ \frac{\partial F_{Id}}{\partial V} & \frac{\partial F_{Id}}{\partial I_d} & \frac{\partial F_{Id}}{\partial \phi} & \frac{\partial F_{Id}}{\partial \theta} & \frac{\partial F_{Id}}{\partial \alpha_0} \\ \frac{\partial F_{\phi}}{\partial V} & \frac{\partial F_{\phi}}{\partial I_d} & \frac{\partial F_{\phi}}{\partial \phi} & \frac{\partial F_{\phi}}{\partial \theta} & \frac{\partial F_{\phi}}{\partial \alpha_0} \\ \frac{\partial F_{\theta}}{\partial V} & \frac{\partial F_{\theta}}{\partial I_d} & \frac{\partial F_{\theta}}{\partial \phi} & \frac{\partial F_{\theta}}{\partial \theta} & \frac{\partial F_{\theta}}{\partial \alpha_0} \\ \frac{\partial F_{\alpha 0}}{\partial V} & \frac{\partial F_{\alpha 0}}{\partial I_d} & \frac{\partial F_{\alpha 0}}{\partial \phi} & \frac{\partial F_{\alpha 0}}{\partial \theta} & \frac{\partial F_{\alpha 0}}{\partial \alpha_0} \end{bmatrix} \begin{bmatrix} \Delta V \\ \Delta Id \\ \Delta \phi \\ \Delta \theta \\ \Delta \alpha_0 \end{bmatrix} \tag{6.41}$$

At the convertor solution, all the mismatches are equal to zero. When a harmonic voltage perturbation is applied, it is required that all the mismatches in equation 6.41 remain zero, ie $\Delta F = 0$. Partitioning J' around I, and V, equation 6.41 can be written:

$$\begin{bmatrix} \Delta I \\ 0 \end{bmatrix} = \begin{bmatrix} A & B \\ C & D \end{bmatrix} \begin{bmatrix} \Delta V \\ \Delta X' \end{bmatrix}. \tag{6.42}$$

Eliminating $\Delta X'$:

$$\Delta I = (A - BD^{-1}C)\Delta V \tag{6.43}$$

The large matrix D is not actually inverted, instead columns, y_i of $D^{-1}C$ are obtained from solutions to the linear system

$$Dy_i = c_i, \tag{6.44}$$

where c_i are columns of C. This procedure is much faster as it avoids the matrix multiplication and storage of D^{-1}, and the LU decomposition of D is only calculated once.

Since I and V have been decomposed into real valued components, the matrix $Y_{cp} = A - BD^{-1}C$ is a second rank tensor. It is actually a phase components version of the lattice network, connecting harmonics and phases, rather than harmonics and sequences. The phase components cross coupling tensor has been plotted in figure 6.5, for harmonic interactions up to the 21st harmonic. Only admittances larger than 0.005 p.u. have been retained, and only magnitudes have been plotted. The tensor is 126 elements square ($2 \times 3 \times 21$).

Application of the sequence components transform yields the same tensor in sequence components, plotted in figure 6.6. In sequence components the lattice tensor clearly contains far fewer terms, and the zero sequence part has been diagonalized by the transform. The lattice tensor has also been calculated around the operating points of Test 2 in figure 6.7, and Test 3 in figure 6.8. The presence of 2nd harmonic terminal voltage distortion in figure 6.7 has increased the number of significant cross harmonic couplings. As expected, unbalance of the star-g/delta transformer in figure 6.8 has re-

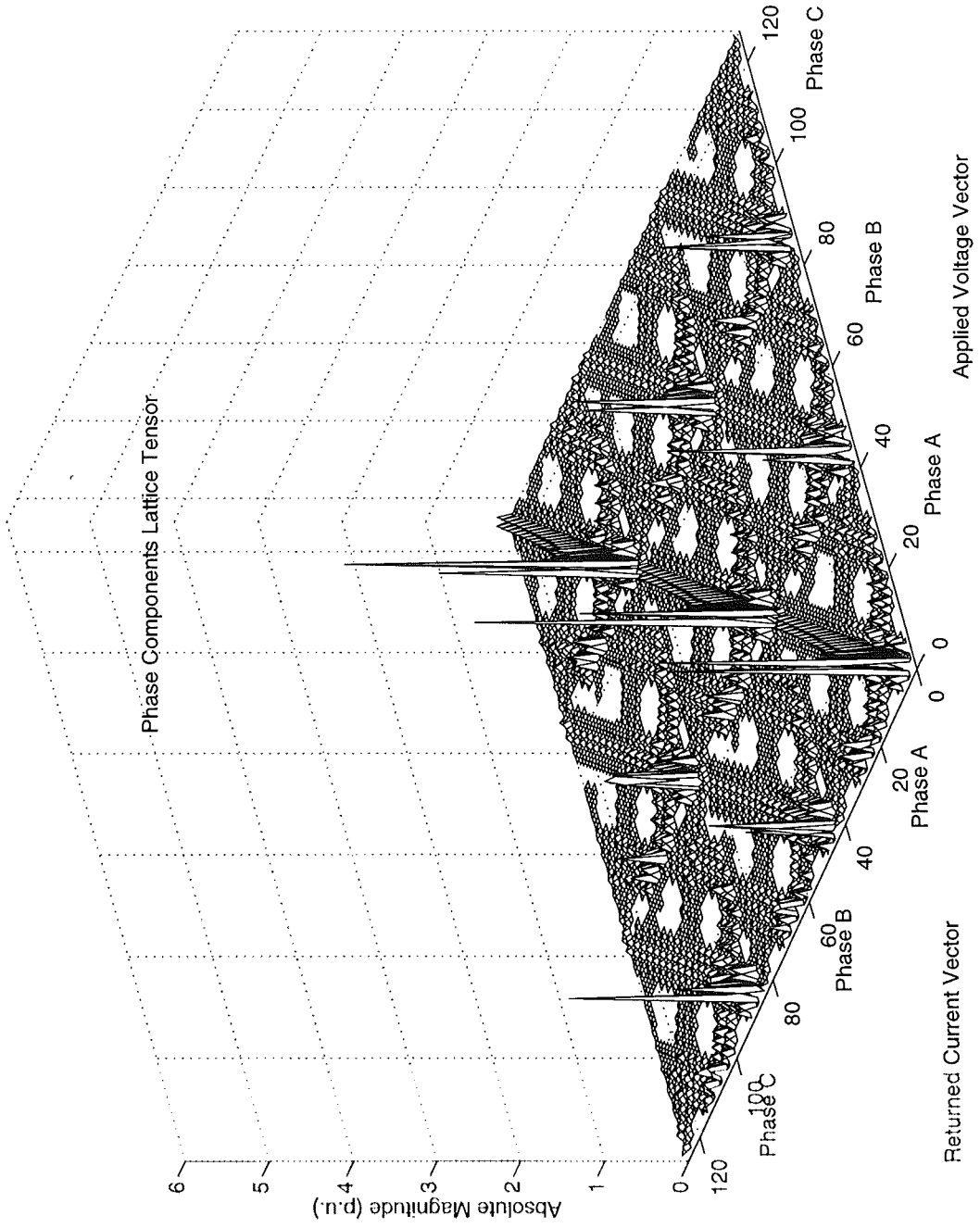

Figure 6.5 Phase components lattice tensor calculated at the solution of Test1.

sulted in substantial coupling to the zero sequence, due to sequence transformation by that transformer. As in Test 2, the unequal commutation periods and voltage samples lead to many more significant admittance terms.

Ignoring now the zero sequence, since there is usually little or no coupling to it in the convertor, the lattice diagram of figure 6.4 is verified against the lattice tensor calculated above. Each '+' or 'o' in figure 6.4 represents four real elements in the lattice tensor, corresponding to variations in the real and imaginary parts of the returned current distortion in response to variations in the real and imaginary parts of the applied voltage distortion (which may be at a different harmonic and sequence). These four elements constitute a tensor cross coupling term that can be represented by a circular locus in the complex admittance plane. By considering sequentially every such cross coupling tensor, figure 6.9 is the result of applying the following plotting rules to the lattice tensor calculated at the solution of Test 1:

1. If the center of the locus is farther than 0.005 p.u. from the origin, plot a '+'.
2. If the radius of the circular locus is greater than 0.005, plot a 'o'.
3. If a '+' has been plotted, and the radius is greater than 1% of the distance of the center of the locus from the origin, plot a 'o' as well.
4. If an 'o' has been plotted, and the distance of the center of the locus from the origin is greater than 1% of the radius of the locus, plot a '+' as well.

The purpose of the plotting rules is to sift out very small admittances, but to still show the nature of admittances that have been retained. The result is a classification of the crosscoupling tensors into direct '+', and phase conjugating 'o' admittances, that essentially recreates the lattice diagram of figure 6.4 in figure 6.9. However, if the same process is applied to the lattice tensor calculated at the solution of Test 2, the result is a lattice diagram, figure 6.10, with a considerable amount of fill-in. A more realistic case is plotted in figure 6.11, where the ac system source was distorted by 1% negative sequence fundamental, resulting in 0.8% negative sequence fundamental at the convertor ac terminal. The conclusion to be drawn is that the lattice diagram is only valid in balanced, undistorted conditions.

The lattice tensor can be used to form a Norton equivalent for the convertor. However given that the convertor model developed in Chapters 3 to 5 converges rapidly, it is not necessary to approximate the convertor by a linearised equivalent in order to solve ac system interactions.

Several authors have proposed the use of ABCD parameter matrices to characterise the harmonic interaction of the ac and dc systems, ie

$$\begin{bmatrix} I \\ V_d \end{bmatrix} = \begin{bmatrix} A & B \\ C & D \end{bmatrix} \begin{bmatrix} V \\ I_d \end{bmatrix} \tag{6.45}$$

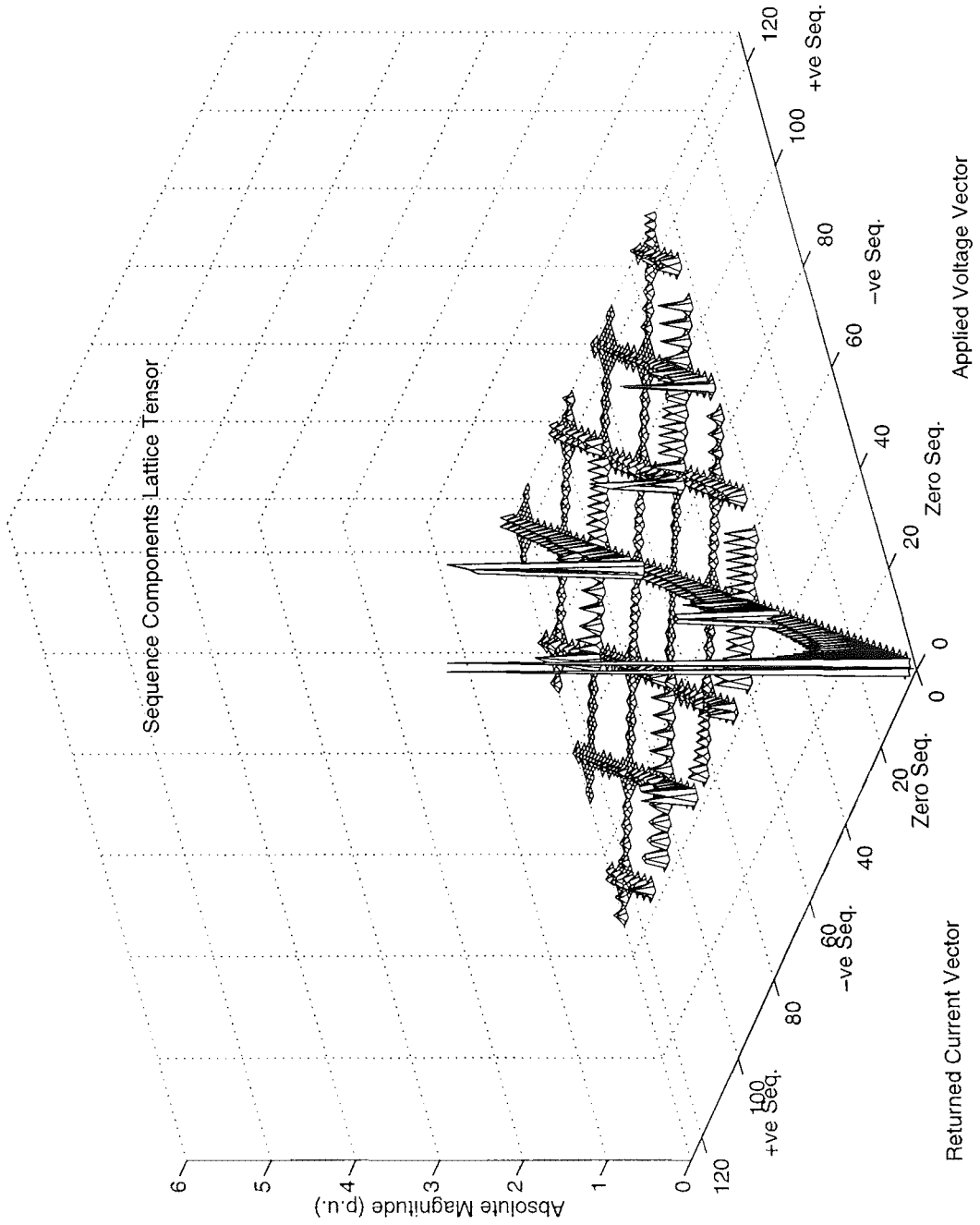

Figure 6.6 Sequence components lattice tensor calculated at the solution of Test 1.

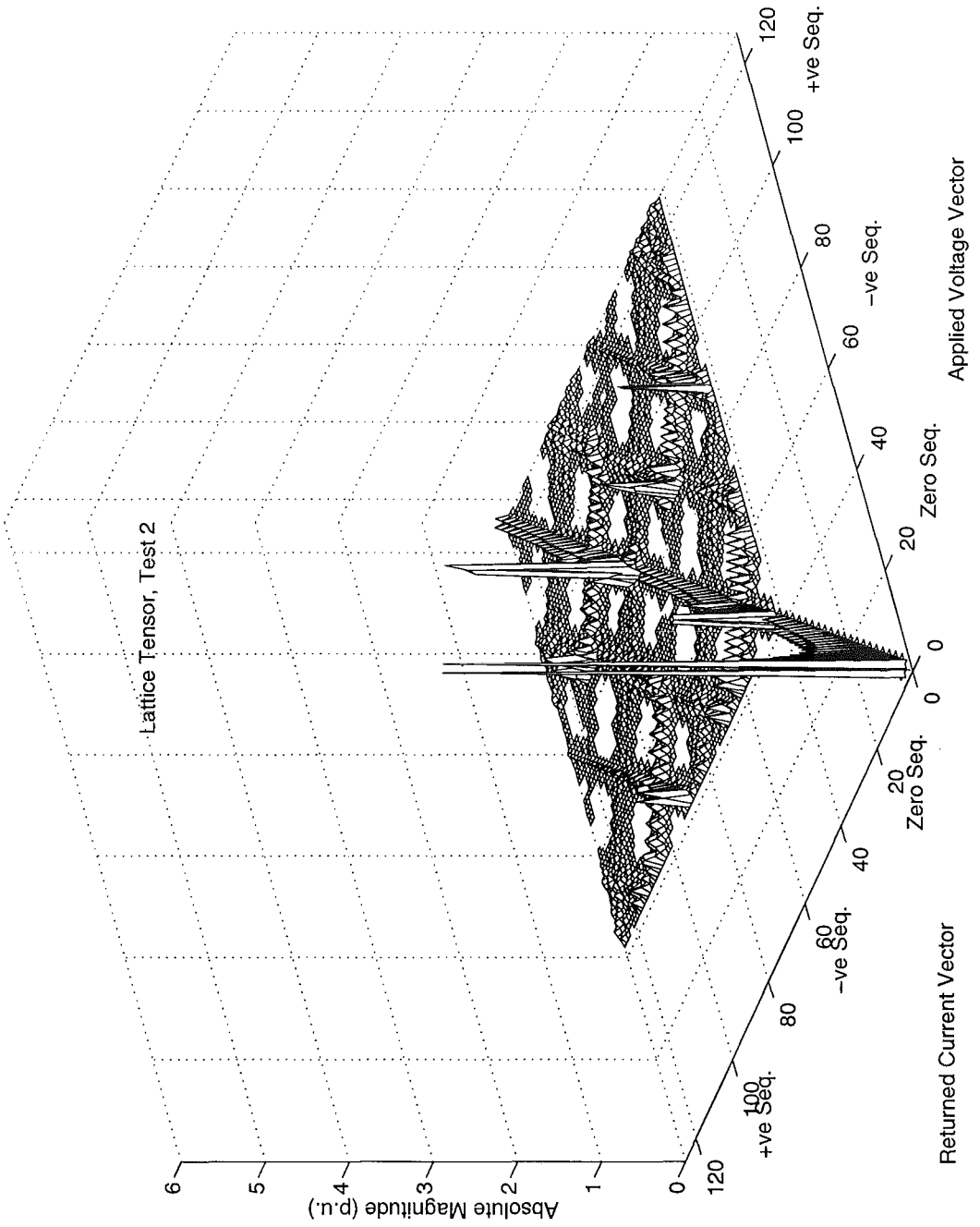

Figure 6.7 Sequence components lattice tensor calculated at the solution of Test 2.

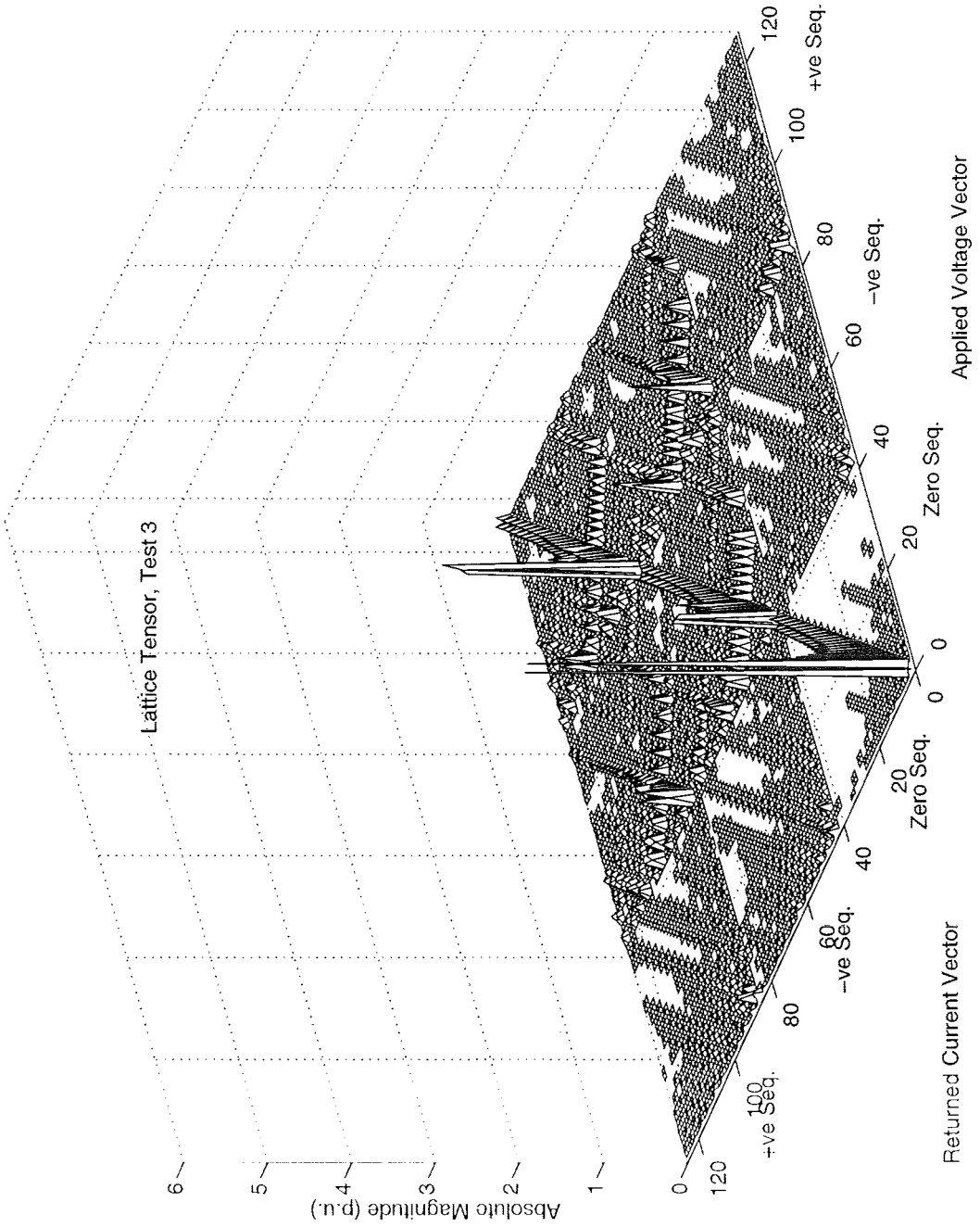

Figure 6.8 Sequence components lattice tensor calculated at the solution of Test 3.

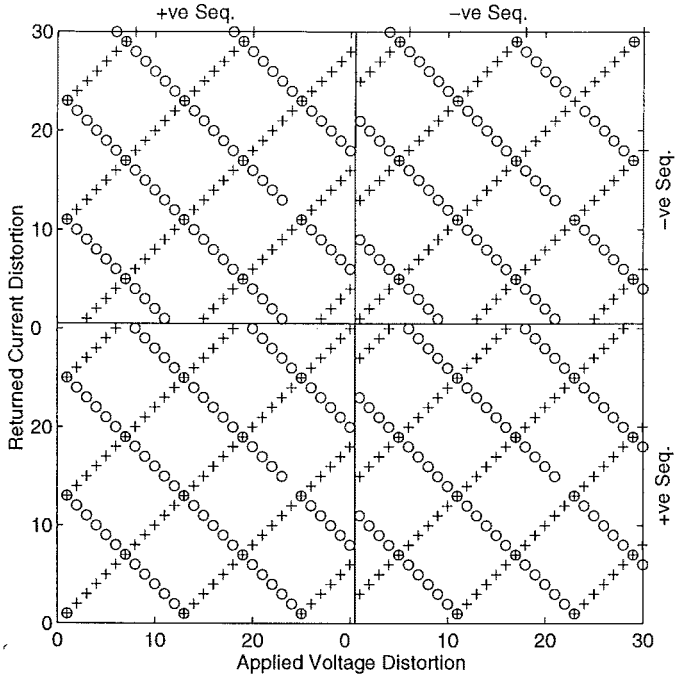

Figure 6.9 Lattice diagram calculated at the solution of Test 1.

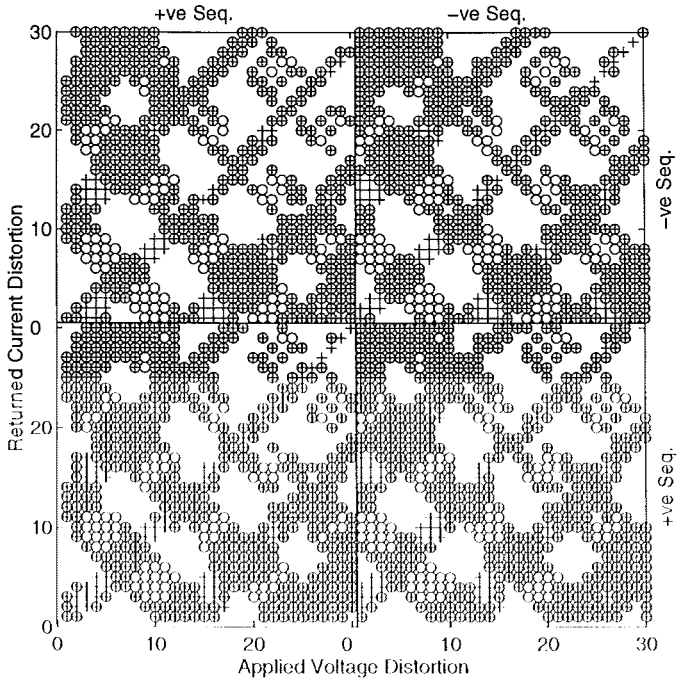

Figure 6.10 Lattice diagram calculated at the solution of Test 2.

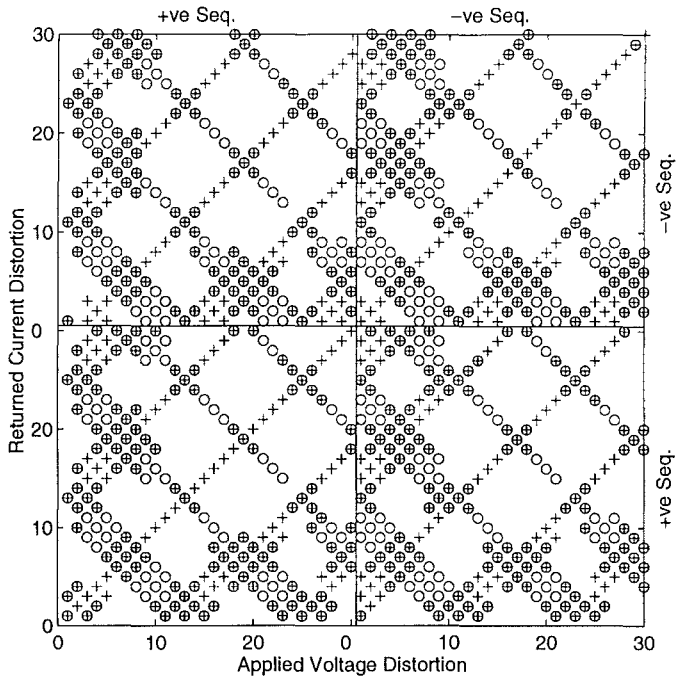

Figure 6.11 Lattice diagram calculated at a solution with 0.85% negative sequence fundamental voltage distortion at the convertor terminal

with the ABDC parameters calculated by means of the perturbation of time domain simulations, or perturbation of a switching function approach. The ABCD matrix (or tensor in positive frequency analysis), can be calculated directly from the Jacobian matrix by modifying the dc mismatch derivatives to be derivatives of the dc voltage, and then performing a Kron reduction to eliminate the switching angle perturbations, as for the lattice tensor above. Once again however, this is of limited use in ac/dc system harmonic analysis, since the full interaction can be solved quickly by the convertor model.

In the next section, the lattice tensor is combined with the ac system tensor admittance, and then used to calculate the impedance of the convertor at selected harmonics and sequences.

6.3.3 Derivation of the Convertor Impedance by Kron Reduction

Calculation of equivalent, or driving point impedances is widely used in system analysis to derive Norton or Thevenin equivalents. For example, the nodal analysis method is used in harmonic penetration and load flow programs, with each node corresponding to a physical node in phase components. When a Kron reduction is applied to a complex admittance matrix, the result is a matrix of reduced size, fully representing the interaction between sources connected to the remaining nodes.

In the harmonic domain, every harmonic of a particular sequence is a node, and provided there are no phase conjugating current injections, a positive frequency complex admittance matrix can be formed to represent the system. Thus an 'off the shelf' harmonic penetration program can analyse a network in which there are cross harmonic couplings, simply by duplicating every bus at every harmonic. If there are phase conjugating admittances in the network, it would be necessary to create additional buses representing conjugate current injections and voltages.

Alternatively, creating vectors of the real and imaginary parts of voltage and current harmonic phasors, the system admittance matrix becomes a real valued tensor. The system tensor can include the linearisation of any device in the system, including voltage controlled buses, convertors, and load flow buses. In general then, the system tensor, when Kron reduced to a single three phase bus, will be a matrix $2 \times 3 \times n_h$ square. In phase components, the system tensor derived from a conventional equivalent complex admittance, will be block diagonal, with each 6×6 block being the three phase tensor corresponding to each three phase harmonic admittance. Assuming that there is no cross coupling between harmonics in the ac system, the connection of the convertor to the ac system may be visualized as in figure 6.12.

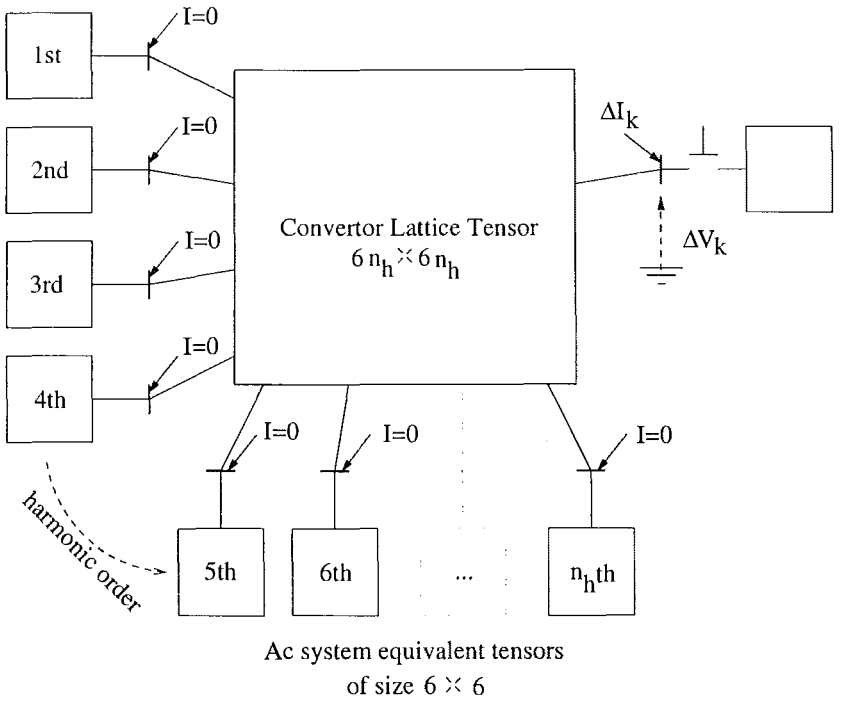

Figure 6.12 Linearised connection of the convertor to an ac system.

In this figure a harmonic current is injected into the three phase harmonic k node. In general currents will flow at every harmonic order into the ac system, causing harmonic voltages that influence the harmonic voltage at the kth node. The ac system has

been disconnected from the convertor at the kth harmonic, since we want to calculate the convertor impedance only. The nodal equation corresponding to this scenario is:

$$\begin{bmatrix} [0] \\ \Delta I_k \end{bmatrix} = \begin{bmatrix} A + \mathrm{diag}(\bar{Y}_{sys}) & B \\ C & D \end{bmatrix} \begin{bmatrix} \Delta V_j \\ \Delta V_k \end{bmatrix} \tag{6.46}$$

The matrices A, B, C, and D are obtained by moving the six rows and columns of the lattice tensor associated with harmonic order k, to the end of the tensor, and then partitioning off these last six rows and columns. The matrix A is therefore of size $6(n_h - 1) \times 6(n_h - 1)$. A current injected at any of the three phase harmonic nodes marked in figure 6.12 will see the system and convertor tensor admittances in parallel, consequently the system 6×6 equivalent admittance tensors are added as a block diagonal matrix to partition A of the convertor lattice tensor. The system admittance at the kth harmonic has been disconnected from the convertor, and so is not added to the D partition.

Applying the Kron reduction to equation 6.46, yields the equivalent 6×6, kth harmonic three phase tensor admittance at the convertor ac terminal:

$$\Delta I_k = (D - C(A + \mathrm{diag}(\bar{Y}_{sys}))^{-1}B)\Delta V_k \tag{6.47}$$

$$\stackrel{\mathrm{def}}{=} Y_{ck}\Delta V_k \tag{6.48}$$

This tensor admittance is a linearisation of the convertor response to applied kth harmonic three phase voltage perturbations, and includes the effect of control, switching angle variation, and coupling to the ac and dc systems at other harmonics. Once again, the large matrix $A + \mathrm{diag}(\bar{Y}_{sys})$ is not actually inverted, but rather bifactorised to LU form, and then columns of $(A + \mathrm{diag}(\bar{Y}_{sys}))^{-1}B$ are obtained by solving the linear system

$$(A + \mathrm{diag}(\bar{Y}_{sys}))y_i = B(:, i), \tag{6.49}$$

where the y_i are the columns of $(A + \mathrm{diag}(\bar{Y}_{sys}))^{-1}B$. Sequence transforming Y_{ck}, it is possible to apply another Kron reduction to obtain a single sequence equivalent. The situation here is more complicated than in figure 6.12, as in general the ac system admittance at a particular harmonic will contain intersequence coupling. The situation is illustrated in figure 6.13, where we wish to find the equivalent positive sequence 7th harmonic admittance of the convertor, under the assumption that both the convertor and ac system convertor transform between sequences at this harmonic. The following

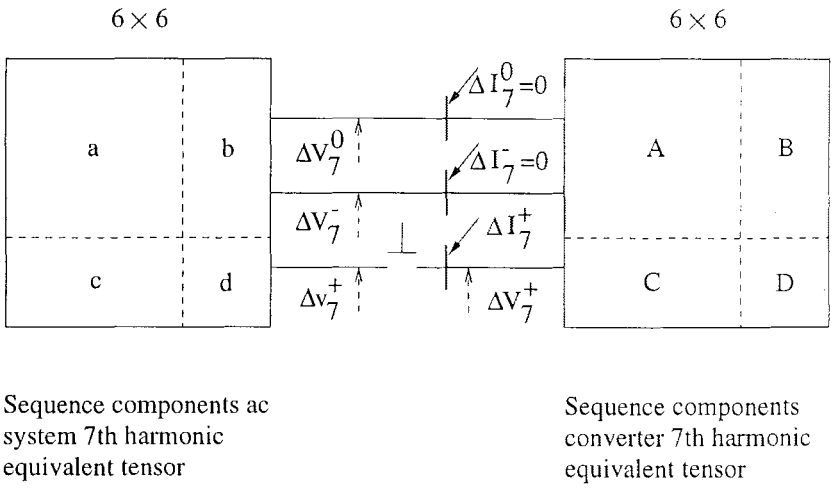

Figure 6.13 Linearised connection of the convertor to an ac system at the 7th harmonic.

equations describe the nodal voltages and currents of figure 6.13:

$$\begin{bmatrix} \Delta I_7^0 \\ \Delta I_7^- \end{bmatrix} = A \begin{bmatrix} \Delta V_7^0 \\ \Delta V_7^- \end{bmatrix} + B\Delta V_7^+ \tag{6.50}$$

$$-\begin{bmatrix} \Delta I_7^0 \\ \Delta I_7^- \end{bmatrix} = a \begin{bmatrix} \Delta V_7^0 \\ \Delta V_7^- \end{bmatrix} + b\Delta v_7^+ \tag{6.51}$$

$$\Delta I_7^+ = C \begin{bmatrix} \Delta V_7^0 \\ \Delta V_7^- \end{bmatrix} + D\Delta V_7^+ \tag{6.52}$$

$$0 = c \begin{bmatrix} \Delta V_7^0 \\ \Delta V_7^- \end{bmatrix} + d\Delta v_7^+ \tag{6.53}$$

$\Delta V_7^0, \Delta V_7^-$ and Δv_7^+ are readily eliminated to yield

$$\Delta I_7^+ = \left(D - C[A + a - bd^{-1}c]^{-1}B\right) \Delta V_7^+ \tag{6.54}$$

$$\stackrel{\text{def}}{=} Y_{c7}^+ \Delta V_7^+ \tag{6.55}$$

Equation 6.54 indicates that the positive sequence 7th harmonic admittance of the convertor is obtained by reducing the ac system admittance to a zero and negative sequence equivalent, adding this to the convertor three sequence equivalent, and Kron reducing to the positive sequence. Inverting Y_{c7}^+ and multiplying by the impedance base yields the impedance tensor in ohms. For the rectifier end of the CIGRE benchmark, at the Test 1 solution,

$$Z_{c7}^+ = \begin{bmatrix} 465.39 & -306.22 \\ 719.96 & 93.47 \end{bmatrix} \Omega.$$

Repeating these calculations for every harmonic from 2 to 37, in positive and negative sequence, the resulting circular impedance loci have been plotted in figure 6.14. Data points obtained by the perturbation method have also been plotted on this diagram.

The method developed here for calculating the convertor impedance is somewhat circuitous, as it is not necessary to first calculate the lattice tensor, and then reduce to a single harmonic equivalent. For example to calculate the 7th harmonic impedance from the Jacobian, it would be possible to retain voltage mismatches for every harmonic except the 7th, and then Kron reduce the Jacobian to the 7th harmonic partition. This method would be faster for calculating a single harmonic impedance, but slower for calculating many. Another method would be to repeatedly Kron reduce to small lattice tensors covering a limited range of frequencies. Typically we are interested in harmonics below the 11th, and could therefore retain voltage mismatches in the Jacobian above the 10th harmonic, reduce to a ten harmonic lattice tensor, and then sequentially reduce this tensor to harmonic equivalents. This method would offer a $(49/9)^3 = 161$-fold improvement in speed for the calculation of each harmonic, after the initial calculation of the lattice tensor, but would give the same results. Nevertheless, by obtaining exact agreement with the perturbation method, the lattice tensor itself, and the nodal analysis utilizing that tensor, have been validated.

In Chapter 7 the possibility of extending the convertor model to integrate several ac systems, loadflows, and dc links etc, is discussed. The solution method would be by means of a single sparse, but unified Jacobian. At the solution, it would be useful to calculate the full Jacobian matrix, and use it to calculate impedances, transfer coefficients, stability factors etc. Since the system Jacobian is likely to be extremely large, the possibility of utilizing sparse methods for calculating linearised relationships is explored next.

6.3.4 Sparse Implementation of the Kron Reduction

The motivation for developing a sparse Kron reduction, is the assumption that small elements in the Jacobian will have little, or no effect on the calculated admittance. Having calculated the full Jacobian matrix at the convertor solution, elements larger than a preset tolerance are copied into sparse storage arrays. The Kron reduction to a single harmonic can then be performed using the same sparse routines as were employed in the Newton solution. Since this is a feasibility study only, the method will be implemented for the dc side impedance, as it is single phase.

The starting point is to calculate the full and unmodified Jacobian matrix at the convertor solution. Next, elements larger in absolute size than η, are retained and copied into sparse storage. The full Jacobian is stored in a two dimensional array, and $\eta = 0.001$ initially. The sparse Jacobian is represented by a list of elements, row indices, and column indices. In order to perform a Kron reduction, rows and columns

where the dc side admittance, Y_{dk}, has been written as a tensor. The multiplication by $\bar{Y}_{dk}^{-1}$, and subtraction of I, reverse the Jacobian calculations whereby the dc mismatch partial derivatives are written in terms of the calculated dc voltage partial derivatives.

The dc side impedance calculated by the sparse method may contain errors due to the large number of small Jacobian elements that are neglected. The effect of the small terms on the impedance can be determined, without sacrificing sparsity, by means of the iterative refinement method. When the linear system described by equation 6.56 is solved, the error due to the Jacobian terms less than η is determined by multiplying the solution x_i by the full matrix J_A:

$$r = J_A x_i - b_i \tag{6.58}$$

where r is the residual, and J_A is the full partition of J corresponding to A. Since A has already been bifactorised, it is easy to calculate a correction vector, Δx_i, by solving a sparse linear system with the residual on the RHS:

$$A\Delta x_i = r, \tag{6.59}$$

so that $x_i' = x_i - \Delta x_i$ will be a much better approximation to the solution of $J_A x_i = b_i$. This process could, if desired, be repeated for several iterations, however a single iteration of the refinement method is more than adequate. The main overhead associated with the refinement is the matrix multiplication of a vector, $J_A x_i$, which requires n^2 flops. The solution of the linear system is less than n^2, since A has already been reduced.

The calculated dc side impedances for the CIGRE rectifier are plotted as loci in figure 6.16 for harmonics 1 to 12. Figure 6.16 indicates that in this case the neglected Jacobian terms have had virtually no effect on the dc side impedance, as the loci have been plotted twice, first with no refinement, and then with one iteration of the refinement method.

The sparse calculation of the dc side impedance is validated against a direct frequency domain calculation in figure 6.17 for harmonics up to the 10th. The frequency domain calculation of convertor impedances is described in detail in [Wood 1993], and was there validated against time domain calculations of the convertor dc side impedance using the perturbation method.

6.4 VARIATION OF THE CONVERTOR IMPEDANCE

As indicated by figures 6.6 to 6.8, the convertor lattice tensor is affected by ac terminal distortions, consequently the equivalent impedance of the convertor at a particular harmonic and sequence is likely to vary also. This effect is evident in figure 6.18, where

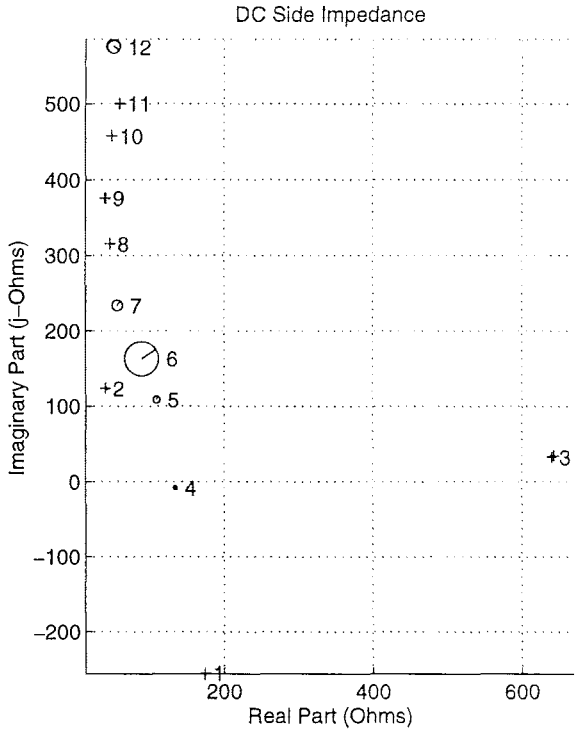

Figure 6.16 Calculated dc side impedances of the CIGRE rectifier using the sparse Kron reduction technique, with and without refinement.

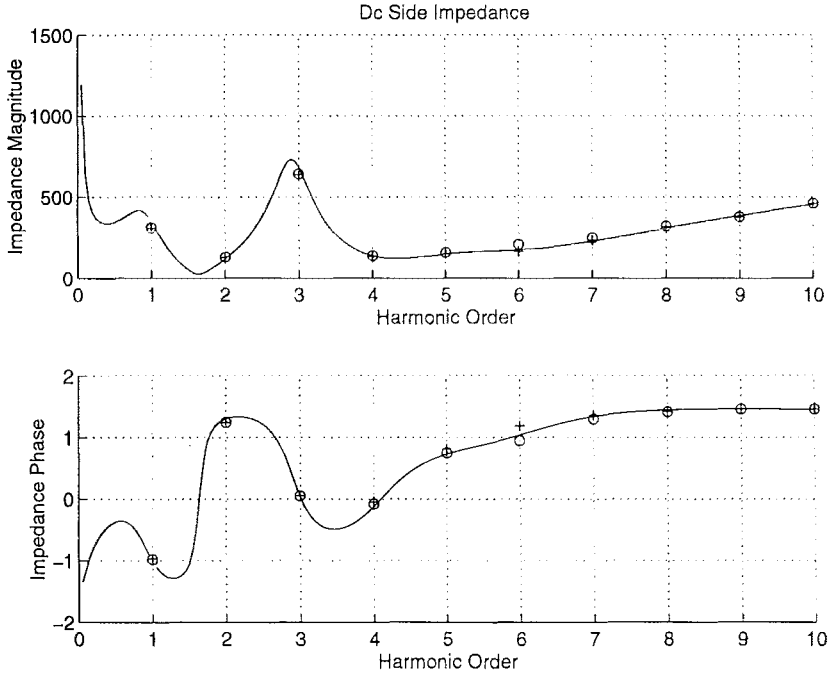

Figure 6.17 Comparison of harmonic and frequency domain solutions to the CIGRE rectifier dc side impedance. '+' and 'o' mark the range of the complex locus at each harmonic.

the negative sequence impedances at low order harmonics have been plotted in the presence of third harmonic positive sequence terminal voltage distortion. The terminal voltage distortion was obtained by adding a third harmonic voltage component to the ac system Thevenin equivalent, and varying the magnitude from 0 to 0.2 p.u., which resulted in a maximum of 0.12 p.u. distortion at the convertor terminal. Figure 6.19 is a similar plot of the positive sequence impedances, with a negative sequence fifth harmonic terminal voltage distortion of up to 0.1 p.u. Clearly, the main effect of an existing distortion is to introduce phase dependence into most of the convertor impedances. If the effect of harmonic distortion at the convertor terminal is ignored, the calculated impedance at other harmonics will be incorrect, but not greatly so.

The convertor impedance is affected to a much larger extent by the operating point of the convertor. In a real dc link, as the current order is reduced, the firing order is held approximately constant by tap change control, and reactive power compensation banks are switched out. Both of these activities will alter the ac side impedance of the convertor, however since the test system does not contain tap change control, or reactive compensation switching, these effects were not investigated.

At lower dc current orders, the commutation periods will be shorter, and an applied voltage distortion will affect the commutation less. It can therefore be expected that the convertor impedance will increase as the current order is reduced. In fact, the analysis of [Wood 1993] predicts a sinc function envelope for the convertor impedance magnitude as a function of commutation angle. Figures 6.20 to 6.23 plot the variation in the convertor positive sequence impedance loci as a function of the current order. The current order was reduced in one hundred steps from 2000A to 200A, which resulted in a variation of firing angle from 14° to 50°, and commutation duration from 23° to 0.7°. The large variation in firing angle was due to a combination of factors; there was no tap change control, the inverter was represented by a constant dc voltage source, and since there was no reduction in reactive power compensation, the fundamental component of the terminal voltage increased. Clearly, a comprehensive study of the convertor impedance variation would require additional steady state control equations to be integrated with the Jacobian matrix. Nevertheless, the procedure for calculating the convertor impedance would remain the same, and the results obtained demonstrate the convertor impedance is a strong function of the operating state.

6.5 CONCLUSION

The representation of phase dependent admittances by second rank tensors has been proposed, and interpreted geometrically as a circular admittance locus on the complex plane. The Jacobian of the convertor model has been used to directly calculate tensor admittances for the convertor on the ac side. A nodal analysis of the cross coupling convertor lattice tensor attached to an ac system was applied to obtain equiv-

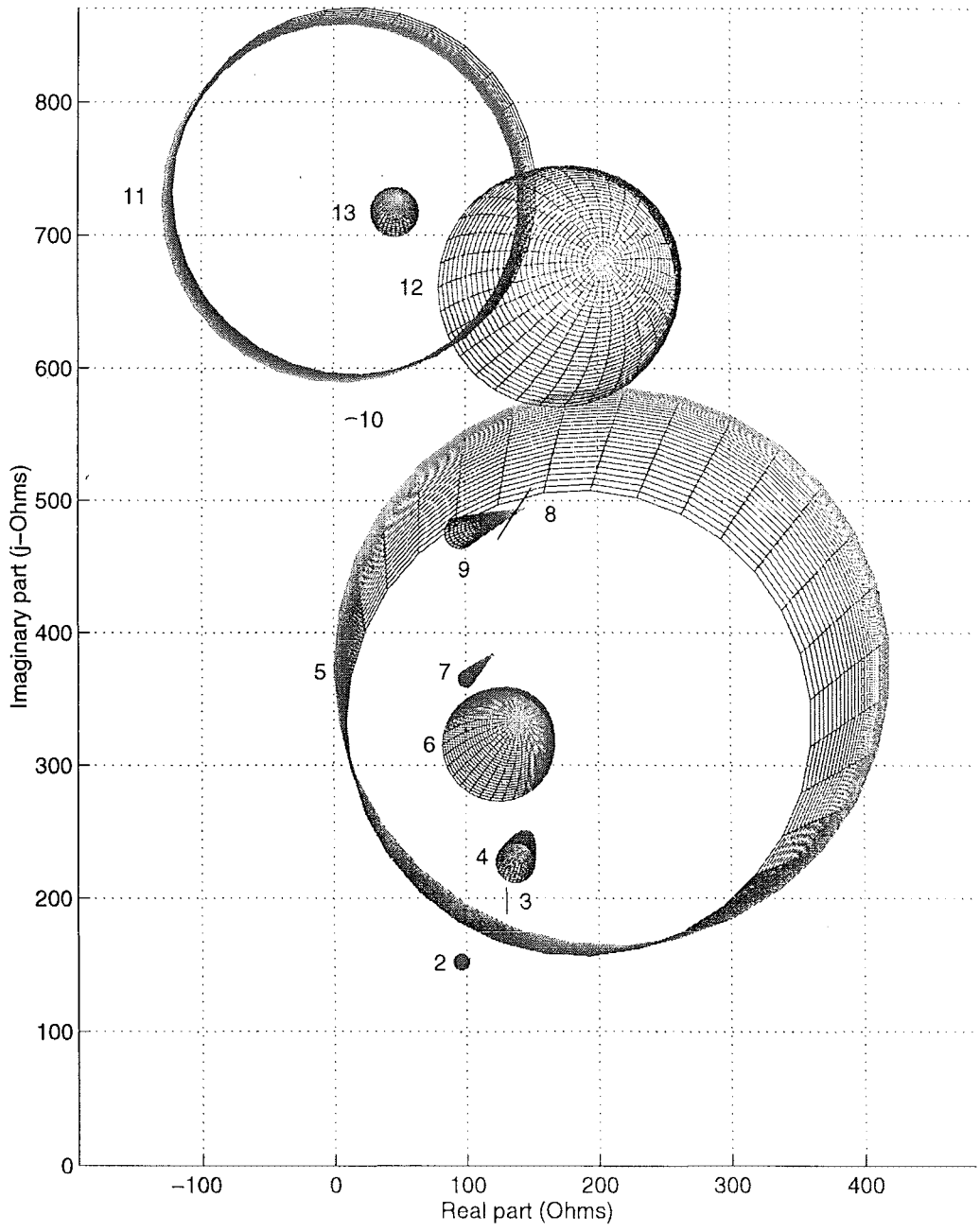

Figure 6.18 Variation in the negative sequence impedance of the CIGRE rectifier as the third harmonic positive sequence terminal voltage distortion is increased from 0 to 0.12 p.u.

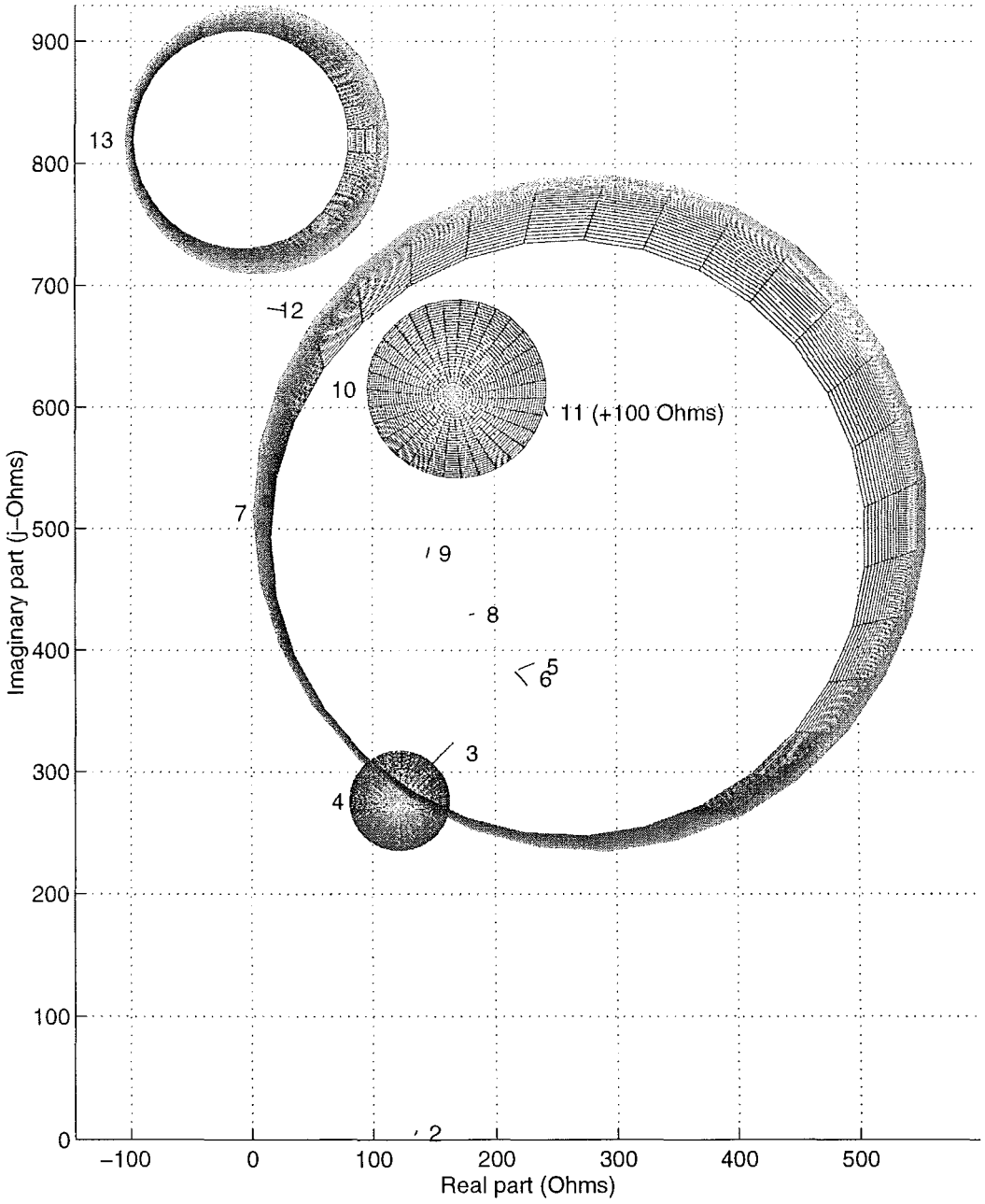

Figure 6.19 Variation in the positive sequence impedance of the CIGRE rectifier as the fifth harmonic negative sequence terminal voltage distortion is increased from 0 to 0.12 p.u.

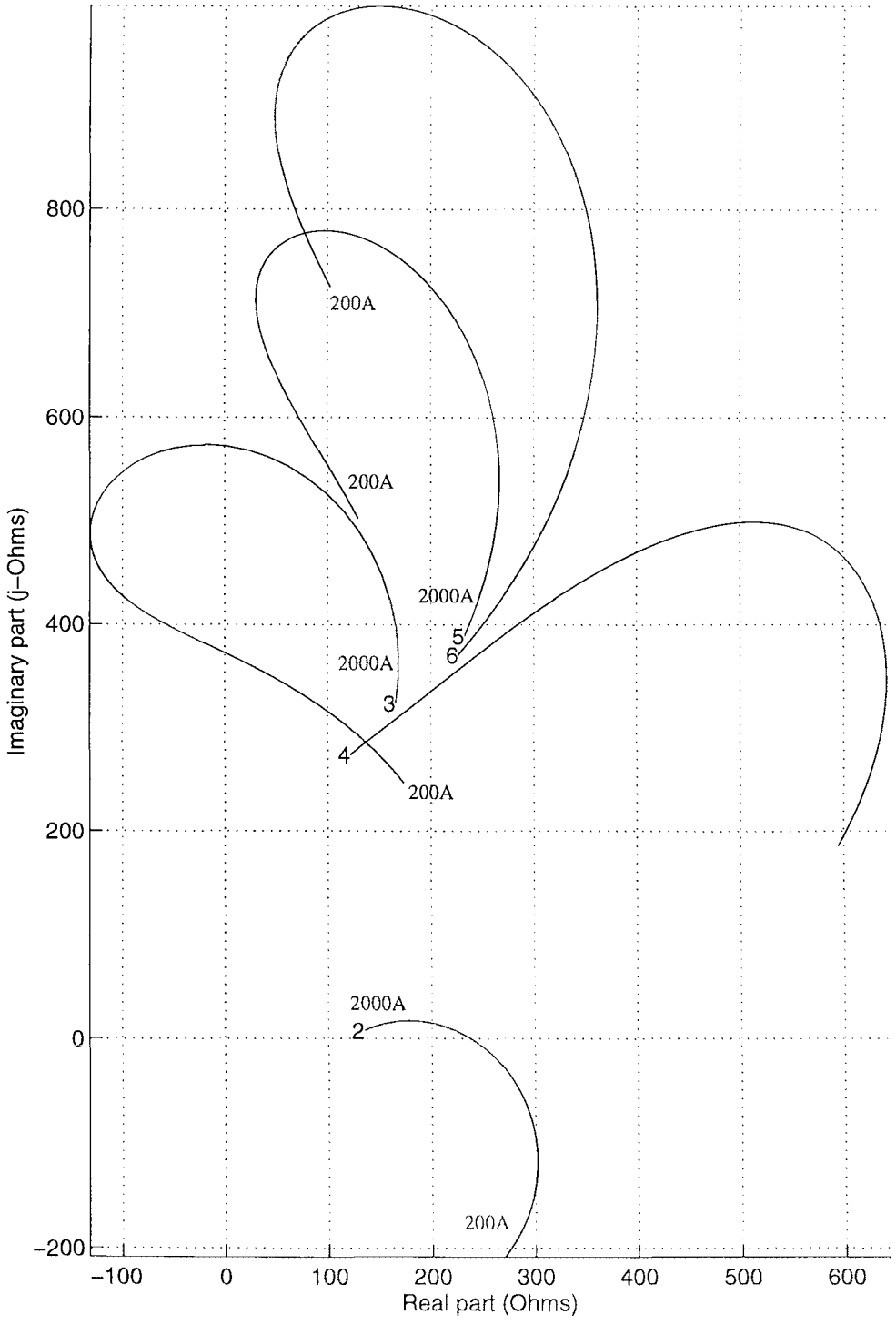

Figure 6.20 Variation in the positive sequence impedance of the CIGRE rectifier as the current order is decreased from 2000A to 200A. Harmonics 2 to 6.

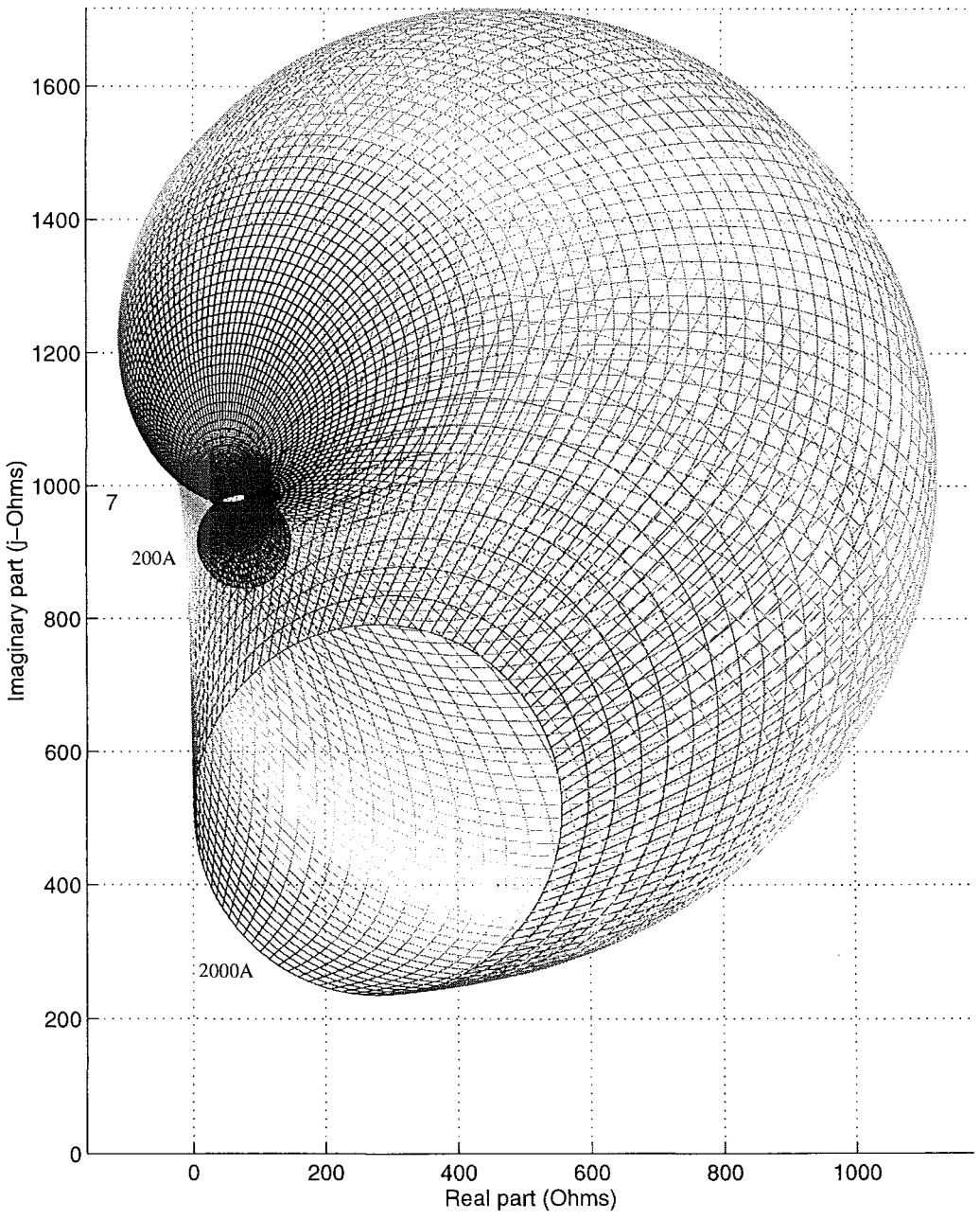

Figure 6.21 Variation in the positive sequence impedance of the CIGRE rectifier as the current order is decreased from 2000A to 200A. Harmonic 7.

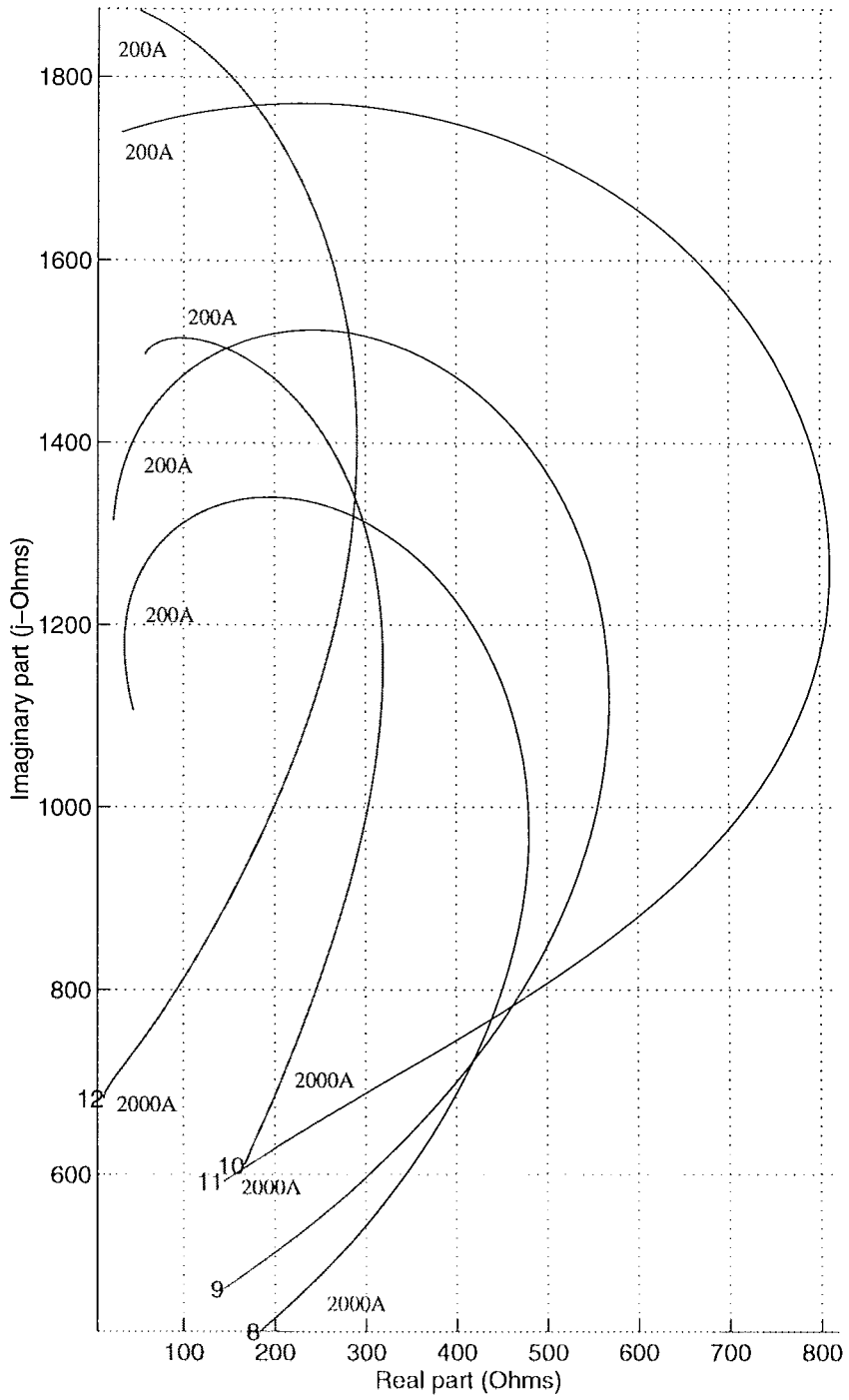

Figure 6.22 Variation in the positive sequence impedance of the CIGRE rectifier as the current order is decreased from 2000A to 200A. Harmonics 8 to 12.

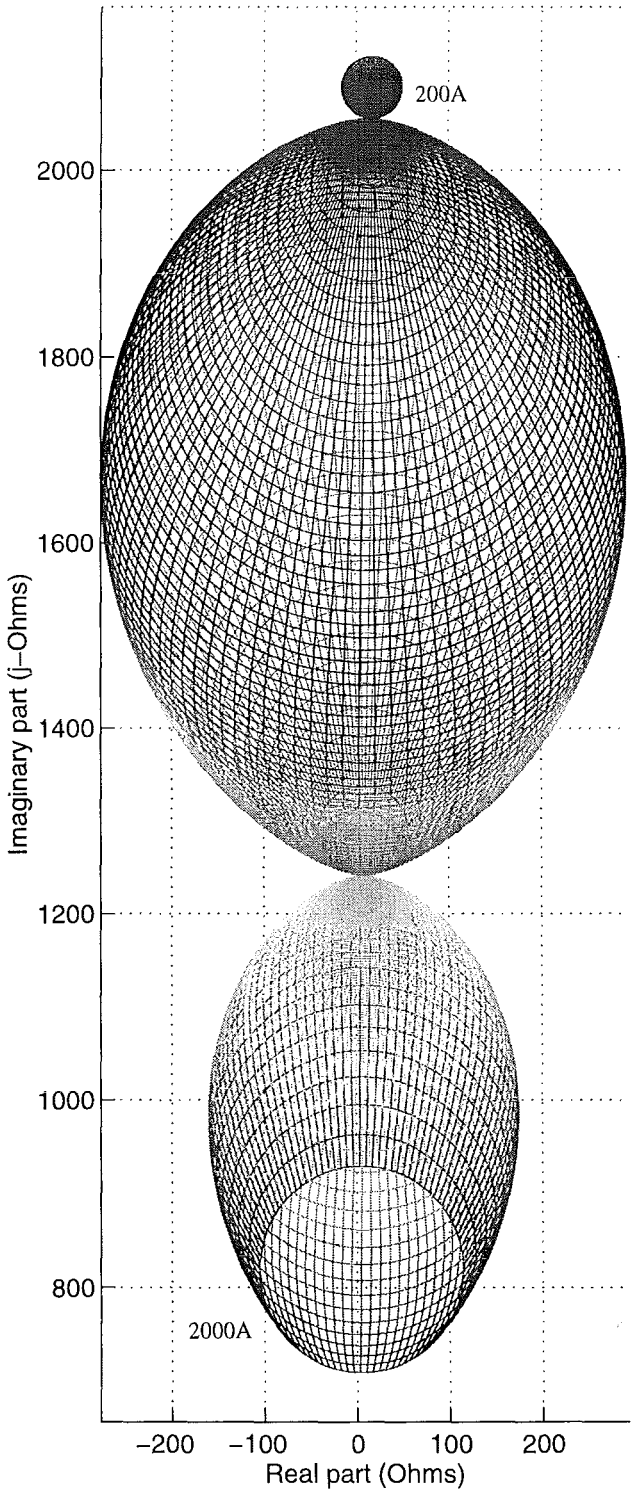

Figure 6.23 Variation in the positive sequence impedance of the CIGRE rectifier as the current order is decreased from 2000A to 200A. Harmonic 13.

alent impedances at the convertor bus. The impedances thus obtained were verified against impedances calculated by a perturbation study at the convertor bus. A sparse calculation of convertor impedances on the dc side was implemented, and employed the iterative refinement method. The dc side impedances were verified against those obtained from a frequency domain convertor model.

The convertor impedances were found to be affected by terminal voltage distortion. Characteristic harmonic impedances were found to be the most strongly phase dependent, as predicted by a frequency domain convertor model. None of the convertor impedances were magnitude dependent, indicating that the convertor is quite linear in the harmonic domain. The convertor impedance was found to be a strong function of the convertor operating point. A detailed study of this dependence would require more general modelling of a full dc link.

Chapter 7

CONCLUSIONS AND FUTURE WORK

7.1 CONCLUSIONS

The proliferation of power electronic devices throughout the power system brings with it a requirement for the modelling of these devices in the steady state, and the propogation of the harmonic currents which they inject. Such an analysis is difficult, since it involves both time and frequency dependent factors. Time domain analysis methods have modelled the convertor well, but the ac system poorly. The reverse is true of harmonic domain analysis methods. The primary objective of the research described in this thesis was to develop a convertor model in the harmonic domain as accurate as the time domain convertor model.

The first step in the development was to derive a new set of equations that fully describe a twelve pulse controlled rectifier in the steady state. The equations developed in Chapter 3 describe harmonic transfer through the 6-pulse bridge, and star-g/star or star-g/delta connected transformers. The commutation process, and unbalance in the convertor transformers have also been fully modelled. Interaction of the convertor with circulating current in an unbalanced delta connection has been analysed for the first time.

To solve the equations that describe the convertor, a set of mismatch equations were constructed, suitable for solution by Newton's method. By utilising positive frequency harmonic phasors in the harmonic model, a decomposition to real components in Chapter 4 permitted a fully unified solution of the harmonic interaction between the ac and dc systems, and the convertor switching instants. This is the first such unified solution to be developed, and by introducing sparsity into the system Jacobian matrix, the system of convertor equations was solved quickly.

The solution obtained was verified against time domain simulations of the rectifier end of the CIGRE benchmark system. Rapid convergence was obtained even if a composite ac/dc resonance was excited. Excellent correlation was obtained with time domain simulations under a variety of severe unbalances. The model was also interfaced to a three phase frequency dependent Thevenin equivalent of the New Zealand South

Island system.

Alternative implementations of the convertor model in phase and sequence components were reported in Chapter 5. A polar components solution is impractical because of poor conditioning, however a sequence components solution displays a much higher degree of sparsity in the Jacobian matrix. A decoupled solution, iterating between solutions of the ac/dc system harmonic interaction, and updates to the switching angles was implemented. This method was found to diverge if even order harmonic sources were present in the ac system.

The Jacobian matrix employed in the Newton solution represents a linearisation of all the equations that describe the convertor controller, harmonic interaction between the ac and dc systems, and the commutation process. A powerful and useful method of extracting linearised relationships from the Jacobian matrix was developed, and described in Chapter 6, with reference to the convertor harmonic impedance. Since the convertor impedance is phase dependent, a more general representation of impedance, the second rank tensor, was developed. Properties of the tensor, and a geometric interpretation of the tensor in the complex impedance plane was described. A nodal analysis using a tensor admittance representation was then applied to the convertor, to derive the convertor impedance at a particular harmonic and sequence. The impedance tensor so obtained was verified against calculations of the convertor impedance obtained from small harmonic perturbations. A sparse method for deriving linearised relationships from large Jacobians was also described, and then applied to the convertor model to calculate the convertor dc side impedance. The dc side impedance was verified against a frequency domain calculation of the impedance.

Finally, the effect of operating point and terminal voltage distortion on the convertor impedance was investigated. As expected, the convertor impedance was highly dependent on operating conditions, however the tensor calculation of the impedance developed in Chapter 6 provides a valuable tool for rapidly calculating the impedance range.

7.2 FUTURE WORK

The research described in this thesis opens up many opportunities for future research and development. Looking first to the convertor model itself, improvements can be made to both the degree, and extent of modelling. Greater gains however, would be obtained from improving the extent of modelling as follows;

1. **Transformer Connections** The analysis of the convertor transformer should be readily extendable to other transformer types, for example star/delta, star/star, delta/star, and delta/delta. Of all the transformer types, the star-g/delta is the

only connection that converts some of the convertor positive and zero sequence currents to zero sequence if the transformer is unbalanced.

2. **Transformer Saturation** Assuming that each convertor transformer consists of three single phase units, accurate modelling of transformer core saturation requires just three additional variables in the Newton solution. These variables are the direct currents shunted in the transformer secondaries. Three equations that describe the dc bias on the saturation curve would also be required. Harmonic domain transformer models are well developed, and could be readily interfaced to the convertor model. The magnetising currents in each phase, and their terminal voltage partial derivatives, would be calculated at each iteration by the time stepping and FFT method.

3. **Current Controller** Any linear current controller could be modelled, since all that is required is the appropriate transfer function from dc ripple to alpha order ripple. An arc-cos lineariser can be accurately modelled by linearising around the average alpha order, on the assumption of a small alpha order ripple.

4. **Inverter Control** If the dc source in the existing model is made negative, the solution obtained corresponds to a current controlled inverter. A minimum gamma controller would require twelve additional equations, very similar to the end of commutation mismatch equations, with roots at the negative going commutating voltage zero crossings. From the twelve measured gamma, the minimum would be selected at every iteration to be the control variable for the minimum gamma mismatch equation: $\gamma_{min} - \gamma_{order} = 0$.

5. **Commutating Capacitance** Extension of the commutation and dc voltage sample analyses to include series and shunt capacitance on the convertor transformer secondary side, would be a valuable improvement to the model. This would allow the modelling of series compensated convertor schemes, and the effects of stray capacitance on dc side harmonics as described by Shore *et al.* [1989]. It would no longer be possible to refer thyristor resistance to the ac system, however the average effect of thyristor resistance could be included as a constant voltage drop on the dc side.

6. **Firing Error** Firing errors can be specified in the model by adding a perturbation to the equidistant timing references, for example setting $\beta_1 = \pi/6 + \Delta\theta_1$ would introduce an error $\Delta\theta_1$ to the first firing. Thus the maximum expected firing error should be supplied to the model as well.

7. **PLO** The effect of terminal voltage harmonics on the phase locked oscillator, is to introduce sampled error in the equidistant timing references. Frequently this is the result of a process very similar to that of the firing pulse generator, but

with a multiple cycle PI time constant. It should be possible therefore to combine the two processes into one, by retaining perfect equidistant firing, but providing a transfer function from sequence components terminal voltage harmonics, to firing order ripple.

8. **Link Control** In the context of a unified harmonic domain model of a bipolar link, several other controls must be modelled. These controls would each contribute one additional equation and unknown to the Newton solution, since tap change control, reactive power compensation control, power control etc do not respond to harmonics. Link controls have already been modelled in existing ac/dc load flow programs.

9. **Discontinuous Current** If the dc current is not continuous, additional equations, similar to the end of commutation mismatches, are required. For each of the twelve current pulses, an equation could readily be constructed that has a zero at the end of the pulse. Applying the dc voltage to the dc system admittance, the resulting continuous current would be convolved with a 12 square pulse sampling function to yield the discontinuous dc current spectra.

The above points describe improvements that can be made to the extent of modelling of a single 12-pulse convertor. The methods employed to solve a single convertor in this thesis, can clearly be used to model more of the power system as a whole. A first step in this direction would be to augment the Jacobian matrix for the convertor with the Jacobian matrix for a unified three phase load flow in rectangular coordinates.

A preliminary decoupled ac/dc load flow and harmonic convertor solution diverged due to interaction between unbalance in the ac system, and triplen harmonic injection from the convertor. A unified solution is therefore recommended, both to improve convergence, and to match the convergence rate between the load flow and convertor model. Although the fast decoupled ac/dc load flow has been found to be very efficient, the large number of iterations required to converge should be avoided if the harmonic model of the convertor is included. This is because the convertor model is more difficult than the load flow, and typically converges in only seven iterations.

The following implementation of a unified load flow and harmonic convertor model is suggested:

- Perform an initial ac/dc load flow, with no harmonics, and utilising the switching system convertor model.
- Calculate a unified load flow and harmonic convertor model Jacobian matrix.
- Solve the load flow and convertor model with constant, but sparse Jacobian.

- Recalculate the full Jacobian at the solution, and calculate any linearised relationships required.

The Jacobian for the unified solution consists of the Jacobians for the load flow and convertor arrayed on the main diagonal, and twelve cross coupling terms for each ac system bus to which the convertor is directly attached.

At some point it will be necessary to extend the convertor model to encompass a full bipolar dc link. In general, the dc current in the two poles will be different, implying 800 harmonic unknowns, 96 switching instants, and several control variables. The structure of the Jacobian however, would be very similar to that developed for the single twelve pulse convertor, and the solution time will scale linearly with the size of the problem. In order to increase availability, dc links have many operating configurations corresponding to different combinations of six pulse groups being blocked. It would therefore be desirable to develop a dc link model that mirrored a similar modular structure so that it could solve each of these configurations.

If the dc link is between two separate ac systems, solutions can be obtained for a variety of phase angles by adding an offset to the angle of the internal emf of the slack bus generator in one of the ac systems. This approach is based on the assumption that the two ac systems are bound to be of very similar frequency, perhaps differing by 0.1Hz. A dc link between systems at 50Hz and 60Hz would require that the fundamental frequency of the model be set to 10Hz, with the primary excitation in the two systems being at the 5th and 6th harmonics respectively. This requires that 5.5 times as many switching angles be solved as well, however once again, the structure of the Jacobian is quite similar to that developed in this thesis.

Eventually it would be desirable to develop a general purpose model with facility for several ac systems, dc systems, and possibly with multiple terminals in each system. This is essentially a software engineering task, as each half pole contributes a block to the main diagonal of the system Jacobian matrix, with diagonal matrices coupling to other harmonic sources in the same system. The main task is to code the program so as to be versatile, easy to use, and modular.

Continuing with this theme, the methods of analysis employed in this thesis to analyse the convertor, are also applicable to FACT devices. It particular, the TCR should be the next device to be modelled in the harmonic domain, since it has similarities with the commutation analysis for the convertor.

The convertor model is at a stage where it could be integrated with the existing Harmonic Domain Analysis (HDA) program by modifying the phase components lattice tensor to a complex conjugate harmonic admittance matrix. By solving the interaction with the dc system at each iteration, the convertor model could be used to construct a Norton equivalent for the convertor. However this is less efficient than a full Newton solution.

Although the range of devices that can be modelled in the harmonic domain has been extended in this thesis, there is no reason to believe that every device that we may wish to model will fall neatly into a set of harmonic domain equations. An example is transformer saturation, for which the time stepping and FFT method is both fast and simple. In proposing a structure for the general modelling of the ac system in the steady state, it is therefore necessary to be as general as possible, and to place no constraints on future models.

As discussed in Chapter 2, there has been an over emphasis on the use of electrical equivalents in the complex conjugate space. This restricts the solution method employed, since it is not possible to include real valued, non-electrical quantities in the solution. Some authors have therefore iterated between an electrical equivalent of the system, and separate procedures, possibly Newton, to solve for the other variables. This type of iteration is inefficient, and displays poor convergence. The overall approach of a Newton solution in real variables, is quite general. As discussed above, the load flow is readily integrated with equations for switching instants, control variables, and harmonic interactions.

The Newton solution method in real variables, is also compatible with any type of device model. For example, a time stepping model of the convertor, with specified terminal voltage, dc current harmonics, and switching angles, could be used to calculate all of the convertor mismatches instead of the harmonic phasor equations used here. Although the Jacobian matrix would be kept the same, the time stepping model could include snubbers, and the conduction characteristic of the thyristors. Although it is not suggested that such a model be developed, it is clearly possible to interface FAST solutions of difficult nonlinearities via a voltage or current mismatch to the overall Newton solution. The required partial derivatives could be obtained from a less general harmonic domain model, or a perturbation method.

A unified load flow and harmonic domain convertor model could therefore provide the core for a general purpose power system steady state solution. Nonlinear device models would be developed separately with a Thevenin equivalent of the ac system, and then interfaced to the system model as a block diagonal in the system Jacobian. The nonlinear device models could be achieved by means of harmonic domain equations, modulation theory analysis, or time domain simulation.

By careful attention to sparsity and efficiency, a general power system steady state solution would be fast, and would scale linearly. Rapid steady state solutions to the power system would provide a basis for stochastic harmonic modelling, previously too difficult. The reliability analysis of the power system at fundamental frequency is now well established, and employs a load flow as the system solution. Reliability analysis has also been applied to the HVdc link, and an interesting possibility for future research would be to integrate a reliability analysis of the power system with a three phase load

flow and harmonic solution of the power system. The present convertor model converges in approximately three seconds for multiple solutions on a Sun Sparcstation V. It would therefore be possible to enumerate a dc link model, with load flow, over several thousand operating conditions and contingencies. The outcome of the enumerated solution would be a probability density function for every harmonic and sequence, at every bus in the power system.

Such a stochastic harmonic system model is the proper framework within which to account for variabilty in the system impedance, random firing errors, background harmonic sources, and highly variable harmonic injections such as the arc furnace. It would therefore provide a valuable tool for assessing the overall harmonic performance of a power system.

Having converged to the system solution, the sparse calculation of impedances from the system Jacobian developed in Chapter 6 becomes a very powerful tool. Any linear relationship between system variables can be extracted from the Jacobian. Examples are harmonic transfers through a back to back dc link, harmonic influence factors, harmonic currents shunted in a filter bank due to another electrically close injection source, voltage stability factors, firing angle modulation transfers etc. Harmonic impedance calculations at nonharmonic frequencies could be obtained by calculating a larger interharmonic Jacobian, for a system with a 10Hz fundamental for example. However a more promising approach is to apply a modulation analysis to the sampling functions calculated at the system harmonic solution.

Of great interest would be the investigation of a phase dependent resonance or harmonic magnification factor, at either the 5th or 7th harmonic, for a twelve pulse convertor.

Apart from research and development directed at enhancing the extent of harmonic modelling, several improvements to the numerical solution of the convertor model should make it considerably faster:

- The initial calculation of the sparse Jacobian is quite slow. Approximately 40% of the total solution time is spent calculating and scanning the full Jacobian in a checkerboard pattern to locate significant elements. This process could almost be eliminated by scanning only the three port terms, and rows associated with a resonance in the ac or dc systems.

- A hybrid use of voltage or current mismatches, depending upon the ac or dc system impedances, should lead to a more robust solution. In this method, a voltage mismatch would be used if the system impedance was less than 1 p.u., otherwise a current mismatch would be used. This ensures that the system impedance or admittance is never greater than 1 p.u., a definite possibility if the group connection is to be modelled, or if there are no filters.

- The decoupled method was found to diverge if even order harmonic sources are present in the ac system. A Kron reduction of the full Jacobian to the ac/dc and switching system Jacobians, should improve the convergence of the decoupled method. Use of the Kron reduction in this manner means that a linearised representation of the ac/dc harmonic interaction is present in the switching system, and vice versa.

- A possibility for future research is to decouple the harmonic analysis of the power system into a set of three harmonic interactions; harmonics $k+1$ and $k-1$, in positive and negative sequence respectively, in the ac system, and harmonic k in the dc system or machine rotors. This decoupling could form the basis of a parallel system solution.

Appendix A

HARMONIC PHASORS

This appendix provides basic background theory on Fourier analysis, harmonic phasors, and discrete convolutions. The phasor representation of a sinusoidally varying quantity is widely used in power systems analysis for undistorted waveforms. Representation of the phasor has been by means of polar co-ordinates (as in the decoupled load flow), or complex rectangular co-ordinates. The complex rectangular representation allows easy addition and multiplication of phasors, and reactive components are easily modelled by an imaginary impedance.

The representation of non-sinusoidal periodic waveforms has commonly used the complex Fourier expansion. The terms in this expansion however, are not complex harmonic phasors. They are complex conjugate pairs associated with the positive and negative harmonic components of the expansion. The complex Fourier series has been used because of its compatibility with the Fast Fourier Transform, a central component of the hybrid time stepping and harmonic injection method of analysis. A useful feature of the complex conjugate representation is that it allows the modelling of the phase reversal of some devices by inclusion of a coupling admittance between the positive and negative frequencies.

If frequent transforms into the time domain are not required, a harmonic phasor Fourier expansion offers several advantages; the redundancy of storing and processing complex conjugate pairs is avoided, the harmonic phasor is compatible with existing analysis methods (such as the load flow), and it is easy to decompose the phasor into real components affording compatibility with the large body of numerical solution packages available on the Internet. Finally, the decomposition into real components is necessary in this thesis in order to develop a unified solution of harmonic phasors, which are complex, and switching angles, which are real.

A.1 THE FOURIER SERIES IN PHASOR FORM

Fourier Theory states that a periodic and integrable function can be represented by an infinite series of trigonometric functions:

$$f(t) = \frac{a_0}{2} + \sum_{k=1}^{\infty} [a_k \cos k\omega t + b_k \sin k\omega t], \tag{A.1}$$

where

$$\begin{aligned} a_k &= \frac{1}{\pi} \int_{-\pi}^{\pi} f(\omega t) cos(k\omega t) d(\omega t) \\ b_k &= \frac{1}{\pi} \int_{-\pi}^{\pi} f(\omega t) sin(k\omega t) d(\omega t). \end{aligned} \tag{A.2}$$

This theory forms the basis of harmonic domain analysis. The fundamental frequency, ω, is chosen to correspond to the duration of one cycle of the periodic steady state, usually 50 or 60 Hz. In the case of a back to back link connecting 50/60 Hz systems, a frequency of 10 Hz would be appropriate in order to resolve all the relevant frequencies. A frequency of 1 Hz could be used to analyse subsynchronous and interharmonic phenomena, while 0.1 Hz resolution could be suitable for analysing transient phenomena.

The trigonometric Fourier expansion A.1 can be converted into a complex exponential Fourier expansion by substituting the following identities for the trigonometric terms:

$$\begin{aligned} \sin(k\omega t) &= \frac{e^{jk\omega t} - e^{-jk\omega t}}{2j} \\ \cos(k\omega t) &= \frac{e^{jk\omega t} + e^{-jk\omega t}}{2}. \end{aligned} \tag{A.3}$$

This results in:

$$f(t) = \sum_{-\infty}^{\infty} c_k e^{jk\omega t}, \tag{A.4}$$

where

$$\begin{aligned} c_k &= a_k - jb_k \\ c_{-k} &= c_k^*. \end{aligned} \tag{A.5}$$

The complex Fourier series expansion is compatible with the Fast Fourier Transform, the method of choice for converting time domain data samples into a Nyquist rate limited frequency spectrum. The trigonometric Fourier expansion can also be written

as a series of phase shifted sine terms by substituting

$$a_k \cos k\omega t + b_k \sin k\omega t = d_k \sin (k\omega t + \psi_k) \tag{A.6}$$

into equation A.1, where

$$\begin{aligned} d_k &= \sqrt{a_k^2 + b_k^2} \\ \psi_k &= \tan^{-1} \frac{a_k}{b_k}. \end{aligned} \tag{A.7}$$

Finally, the phase shifted sine terms can be represented as peak value phasors by setting

$$\Psi_k = d_k e^{j\psi_k}, \tag{A.8}$$

so that

$$\begin{aligned} d_k \sin (k\omega t + \psi_k) &= \mathcal{I}\{\Psi_k e^{jk\omega t}\} \\ &= |\Psi_k| \sin (k\omega t + \angle \Psi_k). \end{aligned} \tag{A.9}$$

The harmonic phasor Fourier series is therefore:

$$f(t) = \sum_{k=0}^{\infty} \mathcal{I}\{\Psi_k e^{jk\omega t}\}, \tag{A.10}$$

which does not contain negative frequency components. Note that the dc term becomes

$$\begin{aligned} \Psi_0 &= \frac{a_0}{2} e^{j\frac{\pi}{2}} \\ &= j\frac{a_0}{2} \end{aligned} \tag{A.11}$$

In practice, the upper limit of the summation is set to n_h, the highest harmonic order of interest. The use of peak value phasors means that the complex power is given by;

$$P + jQ = \frac{1}{2} V I^*, \tag{A.12}$$

where V and I are peak values at the fundamental.

A.2 CONVOLUTION OF HARMONIC PHASORS

The point by point multiplication of two time domain waveforms is expressed in the harmonic domain by a discrete convolution of their Fourier series. When two harmonic phasors of different frequencies are convolved the result are harmonic phasors at sum and difference harmonics. This is best explained by multiplying the corresponding sinusoids using the trigonometric identity for the product of sine waves, and then

converting back to phasor form. Given two phasors, A_k and B_m, of harmonic orders k and m, the trigonometric identity for their time domain multiplication is:

$$\begin{aligned}|A_k|\sin(k\omega t+\angle A_k)|B_m|\sin(m\omega t+\angle B_m) = \\ \frac{1}{2}|A_k||B_m|\left[\sin\left((k-m)\omega t+\angle A_k-\angle B_m+\frac{\pi}{2}\right)\right. \\ \left.-\sin\left((k+m)\omega t+\angle A_k+\angle B_m+\frac{\pi}{2}\right)\right].\end{aligned} \tag{A.13}$$

Converting to phasor form:

$$\begin{aligned}A_k\otimes B_m &= \frac{1}{2}|A_k||B_m|\left[e^{j(\angle A_k-\angle B_m+\frac{\pi}{2})}\Big|_{(k-m)}-e^{j(\angle A_k+\angle B_m+\frac{\pi}{2})}\Big|_{(k+m)}\right] \\ &= \frac{1}{2}\left[(|A_k|e^{j\angle A_k}|B_m|e^{-j\angle B_m}e^{j\frac{\pi}{2}})_{k-m}-(|A_k|e^{j\angle A_k}|B_m|e^{j\angle B_m}e^{j\frac{\pi}{2}})_{k+m}\right] \\ &= \frac{1}{2}j\left[(A_kB_m^*)_{k-m}-(A_kB_m)_{k+m}\right]\end{aligned} \tag{A.14}$$

If k is less than m, a negative harmonic can be avoided by conjugating the difference term. This leads to the overall equation:

$$A_k\otimes B_m=\begin{cases}\frac{1}{2}j(A_kB_m^*)_{(k-m)}-\frac{1}{2}j(A_kB_m)_{(k+m)} & \text{if } k\geq m \\ \frac{1}{2}j(A_kB_m^*)^*_{(m-k)}-\frac{1}{2}j(A_kB_m)_{(k+m)} & \text{otherwise}\end{cases}. \tag{A.15}$$

The multiplication of two nonsinusoidal periodic waveforms leads to a discrete convolution of their harmonic phasor Fourier series:

$$\begin{aligned}f_a(t)f_b(t) &= \sum_{k=0}^{n_h}|A_k|\sin(k\omega t+\angle A_k)\sum_{m=0}^{n_h}|B_k|\sin(m\omega t+\angle B_m) \\ &= \sum_{k=0}^{n_h}\sum_{m=0}^{n_h}|A_k|\sin(k\omega t+\angle A_k)|B_k|\sin(m\omega t+\angle B_m).\end{aligned} \tag{A.16}$$

Rewriting this in terms of phasors yields

$$F_A\otimes F_B=\sum_{k=0}^{n_h}\sum_{m=0}^{n_h}A_k\otimes B_m. \tag{A.17}$$

Equation A.17 generates harmonic phasors of order up to $2n_h$, due to the sum terms. Substituting the equation for the convolution of two phasors, equation A.15, into A.17, and solving for the lth order component yields:

$$(A\otimes B)_l=\frac{1}{2}j\left[\sum_{k=l}^{n_h}A_kB_{k-l}^*+\sum_{k=1}^{n_h}(A_kB_{k+l}^*)^*-\sum_{k=0}^{n_h}A_kB_{l-k}^*\right],\ l>0. \tag{A.18}$$

$$(A \otimes B)_l = \frac{1}{2} j \left[-2A_0 B_0 + \sum_{k=0}^{n_h} A_k B_k^* \right], \quad l = 0. \tag{A.19}$$

The convolution equations are non-analytic in the complex plane, but are differentiable by decomposing into two real valued components (typically polar or rectangular).

Appendix B

TEST SYSTEMS

B.1 CIGRE BENCHMARK

The test systems used in this thesis are based on the rectifier end of the CIGRE benchmark model [Szechtman *et al.* 1991]. The inverter side has been replaced by a constant dc voltage source, E, as illustrated in figure B.1. The benchmark model

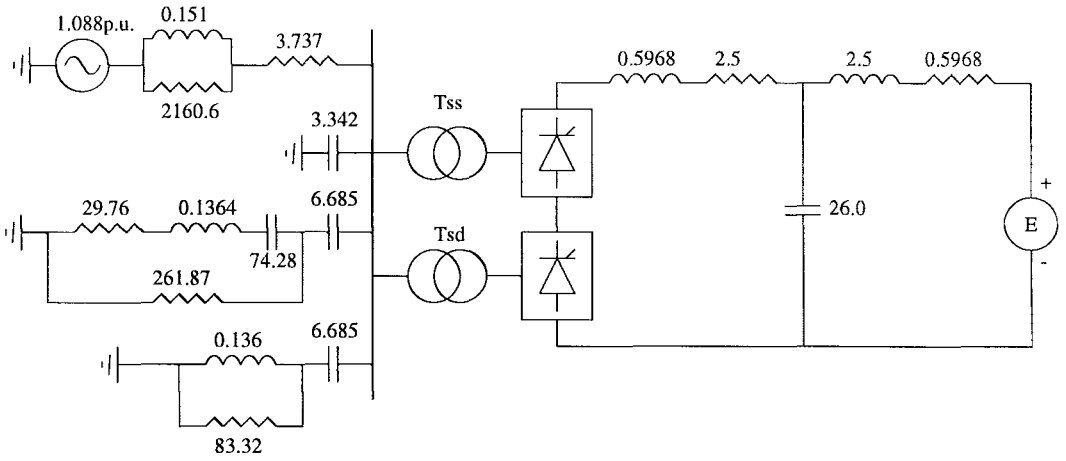

Figure B.1 Rectifier end of the CIGRE benchmark model. Components values in Ω, H, and μF.

consists of a weak ac system, parallel resonant at the second harmonic, coupled via the rectifier to a dc system that is series resonant at the fundamental frequency. These features are shown in the impedance plots of figures B.2 and B.3. The system therefore displays a composite resonance between the ac and dc systems. The ac system is balanced, and is connected in grounded star, as are both converter transformers on the ac side. Additional parameters for the system are listed in table B.1.

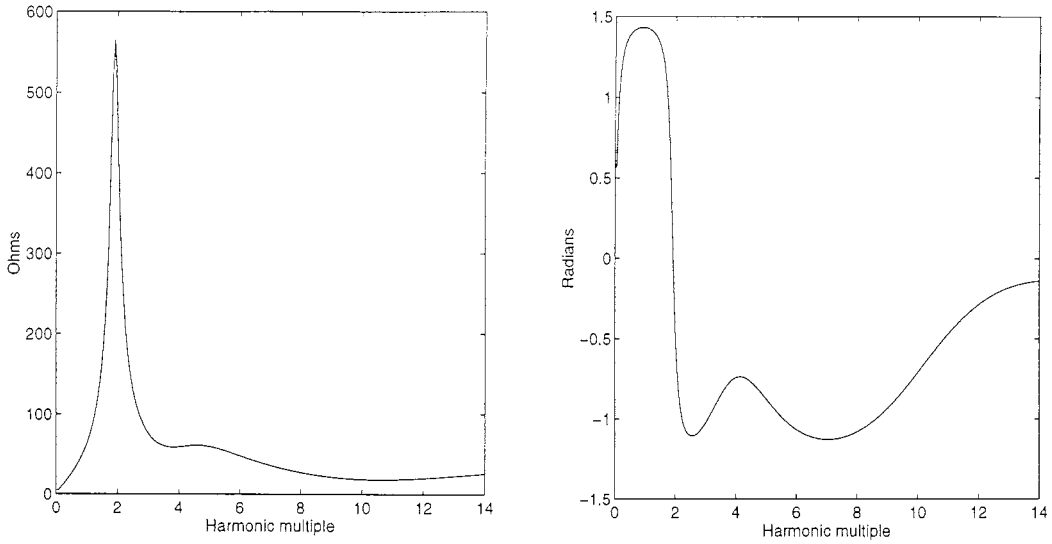

(a) Impedance magnitude (b) Impedance phase

Figure B.2 Frequency scan of the CIGRE rectifier ac system impedance.

B.2 NEW ZEALAND SOUTH ISLAND SYSTEM

In order to construct a more realistic test system, the CIGRE rectifier has been attached to a harmonic representation of the New Zealand South Island looking from the BENMORE–220 busbar. The use of per unit quantities in the convertor model allows a direct connection, despite the difference in voltage levels, however if actual values are used, ideal interconnecting transformers must be present, as in figure B.4. Referring to figure B.4, the equivalent system impedance is three phase, and includes interphase coupling and unbalance. The harmonic impedance at Benmore 220kV was calculated using a suite of harmonic penetration software, that calculated the admittance matrix for the South Island system at every harmonic up to the 50th, and then reduced the admittance matrix to a single system admittance looking from that bus. This admittance was then combined with the filter and delta shunt admittances, and inverted to yield the ac three phase system impedance at each harmonic. The harmonic model of the South Island system includes 138 busbars and 90 transmission lines. The magnitude and phase angle of the phase 'A' ac system impedance, looking from the CIGRE rectifier bus (ie at 345kV) has been plotted in figure B.5.

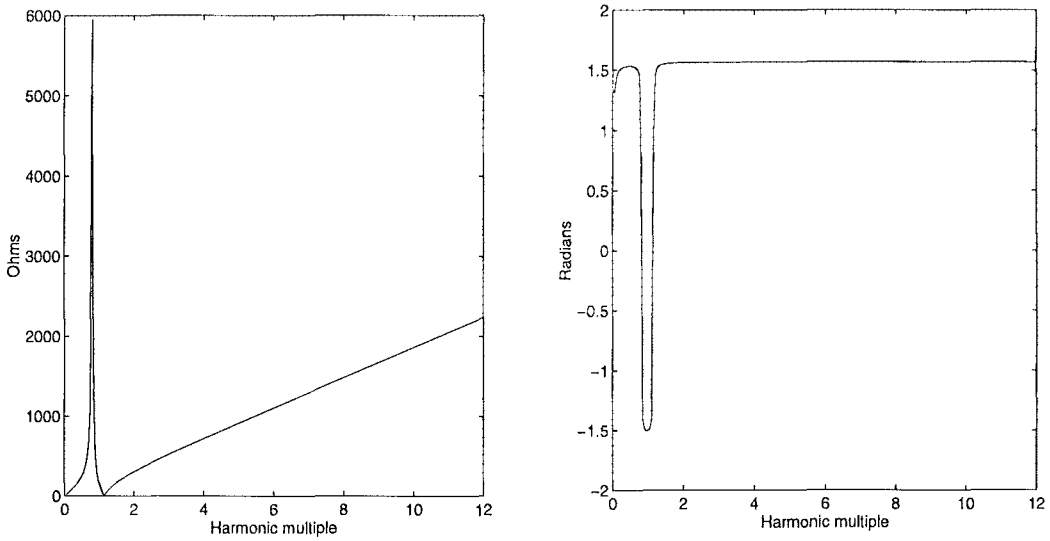

(a) Impedance magnitude (b) Impedance phase

Figure B.3 Frequency scan of the CIGRE rectifier dc system impedance.

power base	603.73 MVA
primary voltage base	345 kV
secondary voltage base	213.4557 kV
nominal dc current	2000 A
nominal firing angle	15°
dc voltage source	4.179 p.u.
transformer leakage reactance	0.18 p.u.
transformer series resistance	0.01 p.u.
thyristor forward voltage drop	8.11E-6 p.u.
thyristor on resistance	0.001325 p.u.
dc current transducer time constant	0.001 s/rad
PI controller proportional gain	1.0989 rad/A(p.u.)
PI controller time constant	0.0091 s/rad

Table B.1 Parameters for the CIGRE benchmark rectifier.

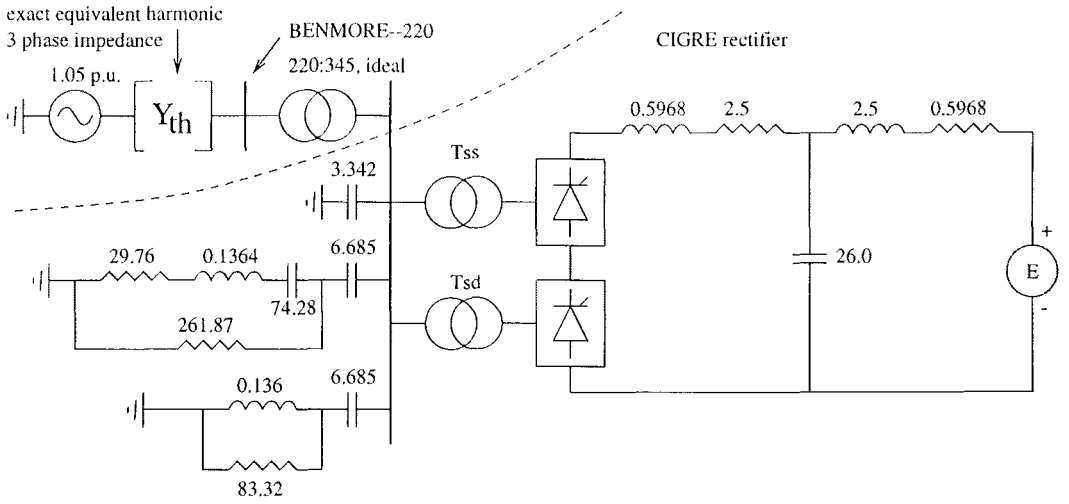

Figure B.4 Rectifier end of the CIGRE benchmark model attached to New Zealand South Island system. Components values in Ω, H, and μF.

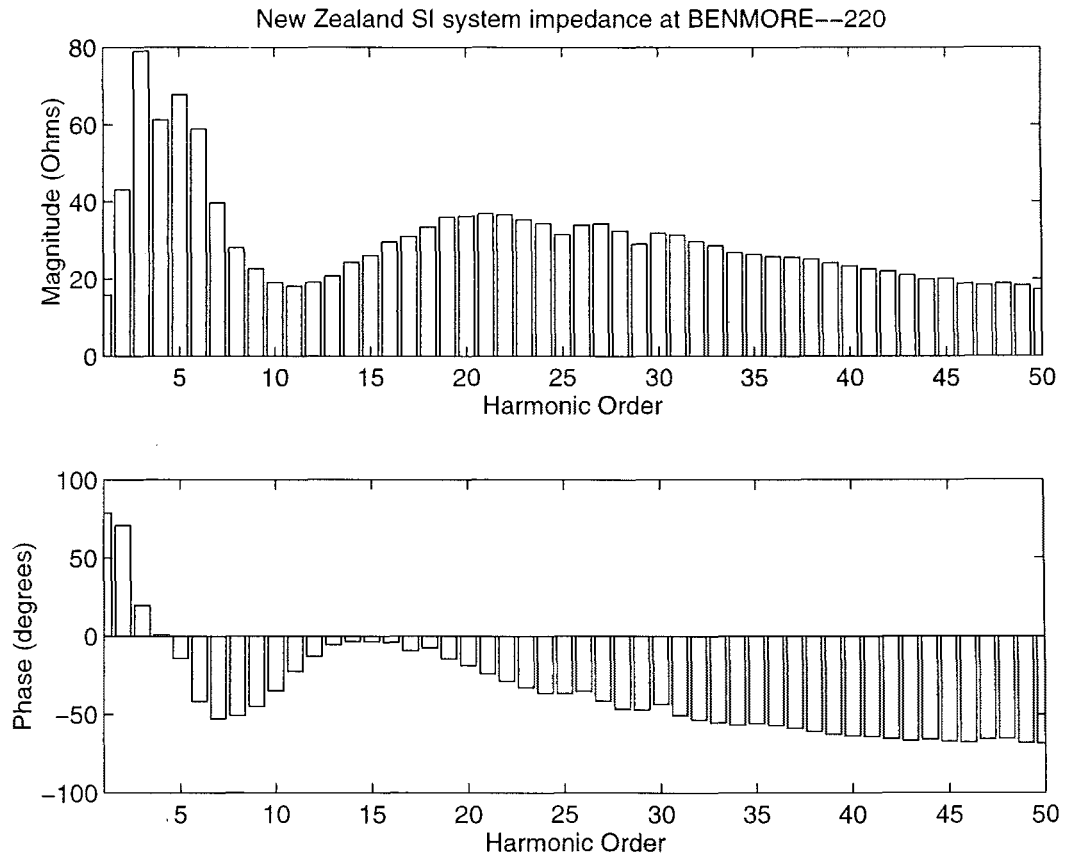

Figure B.5 Phase 'A' of the calculated New Zealand South Island system impedance looking from the CIGRE rectifier bus, under conditions of 100% load and generation.

Appendix C

DERIVATION OF THE JACOBIAN

In this appendix, the full Jacobian matrix is derived for a six pulse rectifier attached to the ac system via a star-g/star transformer. The elements of the Jacobian are the partial derivatives of the mismatch functions with respect to the variables that are being solved for by Newton's method. An important distinction is made in Newtons method between functions and variables. A variable is never a function of something else. A function is only a function of the variables being solved for, and never another mismatch function. The variables that are being solved for are defined to be $V_k^a, V_k^b, V_k^c, I_{d_k}, \phi_i, \theta_i, \alpha_0$. Thus I_{d_k}, the dc current harmonics, are defined not to be a function of V_k, the terminal voltage harmonics. In the analysis to follow, any other quantity is either a function of these variables or a constant.

In finding the partial derivative of a mismatch function with respect to one of these variables, all other variables are held constant. Thus the chain rule is never applied to give a derivative of one variable with respect to another. For example, in the dc current mismatch equations, the partial derivative with respect to the average delay angle is always zero. Intuitively this is incorrect, as we expect a change in delay angle to change all the dc harmonics. However, in terms of the convertor mismatch equations, this requires several applications of the chain rule to quantities that have been defined as variables, not functions. The overall network of interdependency between all the convertor quantities is only fully represented in the inversion of the Jacobian matrix, and in the definition of the mismatch functions.

All of the partial derivatives obtained below have been confirmed by comparison with the numerical partial derivative obtained from the corresponding mismatch equation. That is;

$$\frac{\partial F}{\partial x} \simeq \frac{F(x + \Delta x) - F(x)}{\Delta x} \tag{C.1}$$

C.1 VOLTAGE MISMATCH PARTIAL DERIVATIVES

The voltage mismatch partial derivatives are obtained by first deriving the phase current partial derivatives, and then applying the differential current to the three phase system impedance. The phase current partial derivatives are derived in turn by considering the partial derivatives of the sampled commutation and dc currents of which they are composed.

C.1.1 With Respect to Ac Phase Voltage Variation

First, the partial derivative of the terminal voltage mismatch with respect to terminal voltage variation is obtained. In this analysis all other variables are held constant. The commutation current, sampled dc current, and phase currents are all functions, and require an application of the chain rule. The phase voltage mismatch equation, which represents the interaction of the calculated phase currents with the ac system impedance is

$$F_{V_k^\alpha} = V_k^\alpha - \left[Z_k^{\alpha\alpha}(I_k^\alpha + [Y_{tc}V_{th}]_k^\alpha) + Z_k^{\alpha\beta}(I_k^\beta + [Y_{tc}V_{th}]_k^\beta) + Z_k^{\alpha\gamma}(I_k^\gamma + [Y_{tc}V_{th}]_k^\gamma)\right] \tag{C.2}$$

In order to generalise over all phases, $[\alpha\ \beta\ \gamma]$ is a permutation of $[a\ b\ c]$. $Z = Y_{cc}^{-1}$ is the ac system impedance, and I^α etc are the phase currents. Note that $I(V_k^a, V_k^b, V_k^c, I_{d_k}, \phi_i, \theta_i)$ is a function of the convertor variables. Since the terminal voltages are represented as complex phasors, it is necessary to differentiate with respect to the real and imaginary parts separately. Differentiating equation C.2 partially with respect to a variation in one of the phase voltages:

$$\frac{\partial\mathcal{R}\{F_{V_k^\alpha}\}}{\partial\mathcal{R}\{V_m^\delta\}} = \mathcal{R}\begin{cases} -Z_k^{\alpha\alpha}\frac{\partial I_k^\alpha}{\partial\mathcal{R}\{V_m^\delta\}} - Z_k^{\alpha\beta}\frac{\partial I_k^\beta}{\partial\mathcal{R}\{V_m^\delta\}} - Z_k^{\alpha\gamma}\frac{\partial I_k^\gamma}{\partial\mathcal{R}\{V_m^\delta\}}, & \alpha \neq \delta \text{ or } k \neq m \\ 1 - Z_k^{\alpha\alpha}\frac{\partial I_k^\alpha}{\partial\mathcal{R}\{V_m^\delta\}} - Z_k^{\alpha\beta}\frac{\partial I_k^\beta}{\partial\mathcal{R}\{V_m^\delta\}} - Z_k^{\alpha\gamma}\frac{\partial I_k^\gamma}{\partial\mathcal{R}\{V_m^\delta\}}, & \alpha = \delta \text{ and } k = m \end{cases}, \tag{C.3}$$

$$\frac{\partial\mathcal{R}\{F_{V_k^\alpha}\}}{\partial\mathcal{I}\{V_m^\delta\}} = \mathcal{I}\left\{-Z_k^{\alpha\alpha}\frac{\partial I_k^\alpha}{\partial\mathcal{I}\{V_m^\delta\}} - Z_k^{\alpha\beta}\frac{\partial I_k^\beta}{\partial\mathcal{I}\{V_m^\delta\}} - Z_k^{\alpha\gamma}\frac{\partial I_k^\gamma}{\partial\mathcal{I}\{V_m^\delta\}}\right\}, \tag{C.4}$$

$$\frac{\partial\mathcal{I}\{F_{V_k^\alpha}\}}{\partial\mathcal{I}\{V_m^\delta\}} = \mathcal{I}\begin{cases} -Z_k^{\alpha\alpha}\frac{\partial I_k^\alpha}{\partial\mathcal{I}\{V_m^\delta\}} - Z_k^{\alpha\beta}\frac{\partial I_k^\beta}{\partial\mathcal{I}\{V_m^\delta\}} - Z_k^{\alpha\gamma}\frac{\partial I_k^\gamma}{\partial\mathcal{I}\{V_m^\delta\}}, & \alpha \neq \delta \text{ or } k \neq m \\ j - Z_k^{\alpha\alpha}\frac{\partial I_k^\alpha}{\partial\mathcal{I}\{V_m^\delta\}} - Z_k^{\alpha\beta}\frac{\partial I_k^\beta}{\partial\mathcal{I}\{V_m^\delta\}} - Z_k^{\alpha\gamma}\frac{\partial I_k^\gamma}{\partial\mathcal{I}\{V_m^\delta\}}, & \alpha = \delta \text{ and } k = m \end{cases}, \tag{C.5}$$

$$\frac{\partial \mathcal{I}\{F_{V_k^\alpha}\}}{\partial \mathcal{R}\{V_m^\delta\}} = \mathcal{I}\left\{-Z_k^{\alpha\alpha}\frac{\partial I_k^\alpha}{\partial \mathcal{R}\{V_m^\delta\}} - Z_k^{\alpha\beta}\frac{\partial I_k^\beta}{\partial \mathcal{R}\{V_m^\delta\}} - Z_k^{\alpha\gamma}\frac{\partial I_k^\gamma}{\partial \mathcal{R}\{V_m^\delta\}}\right\}, \tag{C.6}$$

Since the ac phase currents are calculated by sampling the dc and commutation currents, the effect of phase voltage variation on phase current is determined from the effect of phase voltage variation on the sampled commutation currents alone. This is because the dc current and switching angles are variables which are held constant, while the commutation currents are functions of the terminal voltage. Four commutations contribute to one cycle of ac current, consequently

$$\frac{\partial I_k^\alpha}{\partial \mathcal{R}\{V_m^\delta\}} = \sum_{i=1}^{6} C_{\alpha\delta_i}\frac{\partial I_{ci}}{\partial \mathcal{R}\{V_m^\delta\}}, \tag{C.7}$$

and

$$\frac{\partial I_k^\alpha}{\partial \mathcal{I}\{V_m^\delta\}} = \sum_{i=1}^{6} C_{\alpha\delta_i}\frac{\partial I_{ci_k}^s}{\partial \mathcal{I}\{V_m^\delta\}}, \tag{C.8}$$

where I_{ci}^s is the ith commutation current, I_{ci}, sampled over the commutation period. $C_{\alpha\delta_i} \in [-1, 0, 1]$ is a coefficient matrix that defines whether for the ith commutation the phase α current is a function of the phase β terminal voltage, and if so, in which sense. C is defined in the following table where i indexes each set of data: The commutation

		δ		
		a	b	c
α	a	$\{-1,0,-1,-1,0,-1\}$	$\{0,0,1,0,0,1\}$	$\{1,0,0,1,0,0\}$
	b	$\{0,0,1,0,0,1\}$	$\{0,-1,-1,0,-1,-1\}$	$\{0,1,0,0,1,0\}$
	c	$\{1,0,0,1,0,0\}$	$\{0,1,0,0,1,0\}$	$\{-1,-1,0,-1,-1,0\}$

Table C.1 The coefficient matrix $C_{\alpha\delta_i}$ which specifies the dependence between commutation current i, terminal voltage phase, and ac current phase.

current is given by

$$I_{ci}(t) = D + \sum_{k=1}^{n_h} I_{ci_k} e^{jk\omega t}, \tag{C.9}$$

where

$$D = -\mathcal{I}\{\sum_{k=1}^{n_h} I_{ci_k} e^{jk\theta_i}\}, \tag{C.10}$$

$$I_{ci_k} = \frac{jk\omega L_e I_{d_k} - V_{eb_k}}{jk\omega L_{eb}}. \tag{C.11}$$

In equation C.11, e and b are subscript functions of i, and refer to the phases ending and beginning conduction respectively. Sampling the commutation current requires a convolution with the relevant sampling function:

$$I^s_{ci} = \left[D + \sum_{k=1}^{n_h} I_{c_k} \right] \otimes \Psi_{(2i-1)}. \tag{C.12}$$

Setting $I_{ci_0} = D$, expanding the convolution, and taking the kth component yields

$$I^s_{ci_k} = \frac{1}{2} j \left\{ \sum_{l=k}^{n_h} (I_{ci_l} \Psi^*_{(2i-1)_{l-k}}) + \sum_{l=0}^{n_h} (I_{ci_l} \Psi^*_{(2i-1)_{l+k}})^* - \sum_{l=0}^{k} (I_{ci_l} \Psi_{(2i-1)_{k-l}}) \right\}, \quad k > 0. \tag{C.13}$$

Since the commutation circuit is linear,

$$\frac{\partial I_{ci_l}}{\partial \mathcal{R}\{V^\delta_m\}} = 0 \; \forall \; l, m \text{ such that } l \neq m \text{ and } l > 0.$$

This allows the following partial derivative to be written:

$$\begin{aligned} \frac{\partial I^s_{ci_k}}{\partial \mathcal{R}\{V^\delta_m\}} = & \\ & \frac{1}{2} j \left[-\frac{\partial I_{ci_0}}{\partial \mathcal{R}\{V^\delta_m\}} \Psi_{(2i-1)_k} + \left(\frac{\partial I_{ci_0}}{\partial \mathcal{R}\{V^\delta_m\}} \Psi^*_{(2i-1)_k}\right)^* + \left(\frac{\partial I_{ci_m}}{\partial \mathcal{R}\{V^\delta_m\}} \Psi^*_{(2i-1)_{m+k}}\right)^* \right. \\ & \left. + \begin{cases} -\frac{\partial I_{ci_m}}{\partial \mathcal{R}\{V^\delta_m\}} \Psi_{(2i-1)_{k-m}}, & m \leq k \\ \frac{\partial I_{ci_m}}{\partial \mathcal{R}\{V^\delta_m\}} \Psi^*_{(2i-1)_{m-k}}, & m \geq k \end{cases} \right]. \end{aligned} \tag{C.14}$$

Similarly,

$$\begin{aligned} \frac{\partial I^s_{ci_k}}{\partial \mathcal{I}\{V^\delta_m\}} = & \\ & \frac{1}{2} j \left[-\frac{\partial I_{ci_0}}{\partial \mathcal{I}\{V^\delta_m\}} \Psi_{(2i-1)_k} + \left(\frac{\partial I_{ci_0}}{\partial \mathcal{I}\{V^\delta_m\}} \Psi^*_{(2i-1)_k}\right)^* + \left(\frac{\partial I_{ci_m}}{\partial \mathcal{I}\{V^\delta_m\}} \Psi^*_{(2i-1)_{m+k}}\right)^* \right. \\ & \left. + \begin{cases} -\frac{\partial I_{ci_m}}{\partial \mathcal{I}\{V^\delta_m\}} \Psi_{(2i-1)_{k-m}}, & m \leq k \\ \frac{\partial I_{ci_m}}{\partial \mathcal{I}\{V^\delta_m\}} \Psi^*_{(2i-1)_{m-k}}, & m \geq k \end{cases} \right]. \end{aligned} \tag{C.15}$$

The calculations required to evaluate equations C.14 and C.15 can be approximately halved by using the Cauchy Reimann equations for the partial derivatives of complex functions. For an analytic function

$$\frac{\partial F(z)}{\partial \mathcal{I}\{z\}} = j \frac{\partial F(z)}{\partial \mathcal{R}\{z\}}. \tag{C.16}$$

For the complex conjugate of an analytic function

$$\frac{\partial F(z)^*}{\partial \mathcal{I}\{z\}} = -j\frac{\partial F(z)^*}{\partial \mathcal{R}\{z\}}. \tag{C.17}$$

Thus, as each term of equation C.14 is evaluated, the corresponding term in equation C.15 is obtained from a simple rearrangement of the real and imaginary parts. The remaining partial derivatives, $\frac{\partial I_{ci_0}}{\partial \mathcal{R}\{V_m^\delta\}}$ and $\frac{\partial I_{ci_m}}{\partial \mathcal{R}\{V_m^\delta\}}$, are obtained from equations C.10 and C.11;

$$\frac{\partial I_{ci_0}}{\partial \mathcal{R}\{V_m^\delta\}} = -j\mathcal{I}\left\{\frac{e^{jk\theta_i}}{jk\omega L_{eb}}\right\}, \tag{C.18}$$

$$\frac{\partial I_{ci_0}}{\partial \mathcal{I}\{V_m^\delta\}} = -j\mathcal{R}\left\{\frac{e^{jk\theta_i}}{jk\omega L_{eb}}\right\}, \tag{C.19}$$

$$\frac{\partial I_{ci_m}}{\partial \mathcal{R}\{V_m^\delta\}} = \frac{1}{jk\omega L_{eb}}. \tag{C.20}$$

It is assumed here that phase δ is beginning conduction; phase δ ending conduction is accounted for in the C matrix. This completes the derivation of the partial derivative of terminal voltage mismatch with respect to terminal voltage.

C.1.2 With Respect to Dc Ripple Current Variation

A variation in the dc ripple at a particular harmonic is sampled by the compound dc current sampling function, and so affects all phase current harmonics. In addition, the commutation currents are functions of the dc ripple, and so the resulting variation in commutation currents are sampled on the ac side by the commutation interval sampling functions. These two effects, when added together, are sufficient to give the variation in phase currents, and by injecting the phase current variation into the ac system, the required mismatch partial derivative for the Jacobian matrix is obtained. The voltage mismatch partial derivatives are therefore

$$\frac{\partial \mathcal{R}\{F_{V_k^\alpha}\}}{\partial \mathcal{R}\{I_{d_m}\}} = \mathcal{R}\left\{-Z_k^{\alpha\alpha}\frac{\partial I_k^\alpha}{\partial \mathcal{R}\{I_{d_m}\}} - Z_k^{\alpha\beta}\frac{\partial I_k^\beta}{\partial \mathcal{R}\{I_{d_m}\}} - Z_k^{\alpha\gamma}\frac{\partial I_k^\gamma}{\partial \mathcal{R}\{I_{d_m}\}}\right\}, \tag{C.21}$$

$$\frac{\partial \mathcal{R}\{F_{V_k^\alpha}\}}{\partial \mathcal{I}\{I_{d_m}\}} = \mathcal{R}\left\{-Z_k^{\alpha\alpha}\frac{\partial I_k^\alpha}{\partial \mathcal{I}\{I_{d_m}\}} - Z_k^{\alpha\beta}\frac{\partial I_k^\beta}{\partial \mathcal{I}\{I_{d_m}\}} - Z_k^{\alpha\gamma}\frac{\partial I_k^\gamma}{\partial \mathcal{I}\{I_{d_m}\}}\right\}, \tag{C.22}$$

$$\frac{\partial \mathcal{I}\{F_{V_k^\alpha}\}}{\partial \mathcal{R}\{I_{d_m}\}} = \mathcal{I}\left\{-Z_k^{\alpha\alpha}\frac{\partial I_k^\alpha}{\partial \mathcal{R}\{I_{d_m}\}} - Z_k^{\alpha\beta}\frac{\partial I_k^\beta}{\partial \mathcal{R}\{I_{d_m}\}} - Z_k^{\alpha\gamma}\frac{\partial I_k^\gamma}{\partial \mathcal{R}\{I_{d_m}\}}\right\}, \tag{C.23}$$

$$\frac{\partial \mathcal{I}\{F_{V_k^\alpha}\}}{\partial \mathcal{I}\{I_{d_m}\}} = \mathcal{I}\left\{-Z_k^{\alpha\alpha}\frac{\partial I_k^\alpha}{\partial \mathcal{I}\{I_{d_m}\}} - Z_k^{\alpha\beta}\frac{\partial I_k^\beta}{\partial \mathcal{I}\{I_{d_m}\}} - Z_k^{\alpha\gamma}\frac{\partial I_k^\gamma}{\partial \mathcal{I}\{I_{d_m}\}}\right\}. \tag{C.24}$$

The phase currents are composed of commutation currents and the dc current sampled on the ac side:

$$I^\alpha = \sum_{i=1}^{6}[E_i^\alpha I_{ci} \otimes \Psi_{2i-1}] + I_d \otimes \Psi_\alpha. \tag{C.25}$$

Here E_i^α is a coefficient matrix that specifies how the commutation currents contribute to each of the phase currents, and Ψ_α is the phase α dc current compound sampling function. E is listed in table C.2 Differentiating the kth component of equation C.25

		α		
		a	b	c
i	1	1	0	-1
	2	0	-1	1
	3	-1	1	0
	4	1	0	-1
	5	0	-1	1
	6	-1	1	0

Table C.2 Coefficient matrix E_i^α defining the contribution of the commutation currents to each phase current. i is the commutation number.

with respect to $\mathcal{R}\{I_{d_m}\}$ yields

$$\frac{\partial I_k^\alpha}{\partial \mathcal{R}\{I_{d_m}\}} = \frac{\partial\{\sum_i [E_i^\alpha I_{ci} \otimes \Psi_{2i-1}]\}_k}{\partial \mathcal{R}\{I_{d_m}\}} + \frac{\partial\{I_d \otimes \Psi_\alpha\}_k}{\partial \mathcal{R}\{I_{d_m}\}}. \tag{C.26}$$

The first term is similar to the differential with respect to voltage already derived above, as a variation in I_{d_m} affects only I_{ci_m} and I_{ci_0}. Expanding the convolution in the first term, selecting the kth component, and differentiating yields

$$\begin{aligned}\frac{\partial\{\sum_i [E_i^\alpha I_{ci} \otimes \Psi_{2i-1}]\}_k}{\partial \mathcal{R}\{I_{d_m}\}} = \\ \frac{1}{2}j\sum_i E_i^\alpha \left[-\frac{\partial I_{ci_0}}{\partial \mathcal{R}\{I_{d_m}\}}\Psi_{(2i-1)_k} + \left(\frac{\partial I_{ci_0}}{\partial \mathcal{R}\{I_{d_m}\}}\Psi^*_{(2i-1)_k}\right)^*\right. \\ \left. + \left(\frac{\partial I_{ci_m}}{\partial \mathcal{R}\{I_{d_m}\}}\Psi^*_{(2i-1)_{m+k}}\right)^* + \begin{cases} -\frac{\partial I_{ci_m}}{\partial \mathcal{R}\{I_{d_m}\}}\Psi_{(2i-1)_{k-m}}, & m \le k \\ \frac{\partial I_{ci_m}}{\partial \mathcal{R}\{I_{d_m}\}}\Psi^*_{(2i-1)_{m-k}}, & m \ge k \end{cases}\right].\end{aligned} \tag{C.27}$$

Expanding the convolution in the second term of equation C.26 gives the kth component of the sampled dc current:

$$I_{d_k}^{s\alpha} = \frac{1}{2}j\left\{\sum_{l=k}^{n_h}(I_{d_l}\Psi^*_{\alpha_{l-k}}) + \sum_{l=0}^{n_h}(I_{d_l}\Psi^*_{\alpha_{l+k}})^* - \sum_{l=0}^{k}(I_{d_l}\Psi_{\alpha_{k-l}})\right\}, \quad k > 0, \tag{C.28}$$

where $I_{d_k}^{s\alpha}$ is the phase α sample of the dc current. This equation can be differentiated to yield:

$$\frac{\partial\{I_d \otimes \Psi_\alpha\}_k}{\partial\mathcal{R}\{I_{d_m}\}} = \frac{1}{2}j\Psi_{\alpha_{k+m}} + \frac{1}{2}j\begin{cases} -\Psi_{\alpha_{k-m}}, & m \le k \\ \Psi^*_{\alpha_{m-k}}, & m \ge k \end{cases}. \tag{C.29}$$

Applying the above analysis for variations in the imaginary part of I_{d_m} gives

$$\begin{aligned}\frac{\partial\{\sum_i [E_i^\alpha I_{ci} \otimes \Psi_{2i-1}]\}_k}{\partial\mathcal{I}\{I_{d_m}\}} = \\ \frac{1}{2}j\sum_i E_i^\alpha\left[-\frac{\partial I_{ci_0}}{\partial\mathcal{I}\{I_{d_m}\}}\Psi_{(2i-1)_k} + \left(\frac{\partial I_{ci_0}}{\partial\mathcal{I}\{I_{d_m}\}}\Psi^*_{(2i-1)_k}\right)^*\right. \\ \left. + \left(\frac{\partial I_{ci_m}}{\partial\mathcal{I}\{I_{d_m}\}}\Psi^*_{(2i-1)_{m+k}}\right)^* + \begin{cases} -\frac{\partial I_{ci_m}}{\partial\mathcal{I}\{I_{d_m}\}}\Psi_{(2i-1)_{k-m}}, & m \le k \\ \frac{\partial I_{ci_m}}{\partial\mathcal{I}\{I_{d_m}\}}\Psi^*_{(2i-1)_{m-k}}, & m \ge k \end{cases}\right],\end{aligned} \tag{C.30}$$

and

$$\frac{\partial\{I_d \otimes \Psi_\alpha\}_k}{\partial\mathcal{I}\{I_{d_m}\}} = \frac{1}{2}j(j\Psi^*_{\alpha_{k+m}})^* + \frac{1}{2}j\begin{cases} -j\Psi_{\alpha_{k-m}}, & m \le k \\ j\Psi^*_{\alpha_{m-k}}, & m \ge k \end{cases}. \tag{C.31}$$

These equations are then substituted into an equation analogous to equation C.26 and hence into equations C.22 and C.24. The remaining partial derivatives, $\frac{\partial I_{ci_0}}{\partial\mathcal{R}\{I_{d_m}\}}$ and $\frac{\partial I_{ci_m}}{\partial\mathcal{R}\{I_{d_m}\}}$, are obtained from equations C.10 and C.11:

$$\frac{\partial I_{ci_0}}{\partial\mathcal{R}\{I_{d_m}\}} = -j\mathcal{I}\left\{\frac{L_e e^{jk\theta_i}}{L_{eb}}\right\}, \tag{C.32}$$

$$\frac{\partial I_{ci_0}}{\partial\mathcal{I}\{I_{d_m}\}} = -j\mathcal{R}\left\{\frac{L_e e^{jk\theta_i}}{L_{eb}}\right\}, \tag{C.33}$$

$$\frac{\partial I_{ci_m}}{\partial\mathcal{R}\{I_{d_m}\}} = \frac{L_e}{L_{eb}}. \tag{C.34}$$

C.1.3 With Respect to End of Commutation Variation

A variation in the end of commutation angle, ϕ_h, affects the $(2h-1)$th and $2h$th sampling functions. This affects all harmonics of the ac side sampled commutation currents, and dc current. Combining these two effects into the phase current variation, and injecting into the ac system yields the variation in the terminal voltage mismatch;

$$\frac{\partial \mathcal{R}\{F_{V_k^\alpha}\}}{\partial \phi_h} = \mathcal{R}\left\{-Z_k^{\alpha\alpha}\frac{\partial I_k^\alpha}{\partial \phi_h} - Z_k^{\alpha\beta}\frac{\partial I_k^\beta}{\partial \phi_h} - Z_k^{\alpha\gamma}\frac{\partial I_k^\gamma}{\partial \phi_h}\right\}, \tag{C.35}$$

$$\frac{\partial \mathcal{I}\{F_{V_k^\alpha}\}}{\partial \phi_h} = \mathcal{I}\left\{-Z_k^{\alpha\alpha}\frac{\partial I_k^\alpha}{\partial \phi_h} - Z_k^{\alpha\beta}\frac{\partial I_k^\beta}{\partial \phi_h} - Z_k^{\alpha\gamma}\frac{\partial I_k^\gamma}{\partial \phi_h}\right\}. \tag{C.36}$$

Differentiating the kth component of equation C.25 with respect to ϕ_h,

$$\frac{\partial I_k^\alpha}{\partial \phi_h} = \frac{\partial\left\{\sum_i [E_i^\alpha I_{ci} \otimes \Psi_{2i-1}]\right\}_k}{\partial \phi_h} + \frac{\partial\left\{I_d \otimes \Psi_\alpha\right\}_k}{\partial \phi_h} \tag{C.37}$$

A variation in ϕ_h affects only the sampling of the hth commutation current in the first term of equation C.37. Expanding only this convolution from the summation yields

$$I_{ch_k}^s = \frac{1}{2} j E_h^\alpha \left\{\sum_{l=k}^{n_h}(I_{ch_l}\Psi^*_{(2h-1)_{l-k}}) + \sum_{l=0}^{n_h}(I_{ch_l}\Psi^*_{(2h-1)_{l+k}})^* - \sum_{l=0}^{k}(I_{ch_l}\Psi_{(2h-1)_{k-l}})\right\}, \quad k > 0. \tag{C.38}$$

Differentiating this gives

$$\begin{aligned}\frac{\partial\left\{\sum_i [E_i^\alpha I_{ci} \otimes \Psi_{2i-1}]\right\}_k}{\partial \phi_h} = \\ \frac{1}{2} j E_h^\alpha \left\{\sum_{l=k}^{n_h}(I_{ch_l}\frac{\partial \Psi^*_{(2h-1)_{l-k}}}{\partial \phi_h}) + \sum_{l=1}^{n_h}(I_{ch_l}\frac{\partial \Psi^*_{(2h-1)_{l+k}}}{\partial \phi_h})^* - \right. \\ \left. \sum_{l=0}^{k}(I_{ch_l}\frac{\partial \Psi_{(2h-1)_{k-l}}}{\partial \phi_h})\right\}, \quad k > 0,\end{aligned} \tag{C.39}$$

where

$$\frac{\partial \Psi_{(2h-1)_m}}{\partial \phi_h} = -\frac{\partial \Psi_{2h_m}}{\partial \phi_h} = \frac{1}{\pi}\left[\sin(m\phi_h) + j\cos(m\phi_h)\right]. \tag{C.40}$$

The compound sampling function in the second term of equation C.37 is affected by variation in four of the six end of commutation angles. This is because the transfer of dc current to the ac side is defined by two conduction periods per cycle; the beginning and end of each conduction period corresponding to an end of commutation angle. The effect of a variation in ϕ_h therefore depends upon whether it corresponds

to the beginning or end of a positive or negative conduction period for phase α. This information is already collated as the coefficient matrix $-E_{\alpha_i}$.

A similar analysis to the above for the second term of equation C.37 results in

$$\frac{\partial \{I_d \otimes \Psi_\alpha\}_k}{\partial \phi_h} = -\frac{1}{2} j E_h^\alpha \left\{ \sum_{l=k}^{n_h} (I_{d_l} \frac{\partial \Psi^*_{2h_{l-k}}}{\partial \phi_h}) + \sum_{l=1}^{n_h} (I_{d_l} \frac{\partial \Psi^*_{h_{l+k}}}{\partial \phi_h})^* - \sum_{l=0}^{k} (I_{d_l} \frac{\partial \Psi_{2h_{k-l}}}{\partial \phi_h}) \right\}, \quad k > 0. \tag{C.41}$$

Since the compound sampling function is a sum of constituent sampling functions, it has been replaced in the partial derivative by the only term which is a function of ϕ_h. This is then substituted back into equation C.37 to give the required partial derivative.

C.1.4 With Respect to Firing Angle Variation

The transfer of dc current to the ac side of the convertor is defined entirely with reference to the end of commutation angles. The effect of a variation in the firing instants on the phase currents can therefore be obtained by analysing just the sampling of the commutation currents. The partial derivative of the ac voltage mismatch with respect to a firing angle variation is

$$\frac{\partial \mathcal{R}\{F_{V_k^\alpha}\}}{\partial \theta_h} = \mathcal{R}\left\{ -Z_k^{\alpha\alpha} \frac{\partial I_k^\alpha}{\partial \theta_h} - Z_k^{\alpha\beta} \frac{\partial I_k^\beta}{\partial \theta_h} - Z_k^{\alpha\gamma} \frac{\partial I_k^\gamma}{\partial \theta_h} \right\}. \tag{C.42}$$

Since the ac side sampled dc current is not a function of θ_h

$$-\frac{\partial I_k^\alpha}{\partial \theta_h} = \frac{\partial \left\{ \sum_{i=1}^{6} E_i^\alpha I_{ci}^s \right\}_k}{\partial \theta_h} = \frac{\partial \left\{ \sum_{i=1}^{6} E_i^\alpha I_{ci} \otimes \Psi_{(2i-1)} \right\}_k}{\partial \theta_h} = \frac{\partial \left\{ E_h^\alpha I_{ch} \otimes \Psi_{(2h-1)} \right\}_k}{\partial \theta_h}. \tag{C.43}$$

Noting that a change in θ_h affects I_{ch_0} and $\Psi_{(2h-1)}$, applying the product rule to the expansion of the convolution leads to

$$\frac{\partial I_k^\alpha}{\partial \theta_h} = -\frac{1}{2} j E_h^\alpha \left[\sum_{l=k}^{n_h} (I_{ch_l} \frac{\partial \Psi^*_{(2h-1)_{l-k}}}{\partial \theta_h}) + \sum_{l=0}^{n_h} (I_{ch_l} \frac{\partial \Psi^*_{(2h-1)_{l+k}}}{\partial \theta_h})^* - \frac{\partial I_{ch_0}}{\partial \theta_h} \Psi_{(2h-1)_k} + \left(\frac{\partial I_{ch_0}}{\partial \theta_h} \Psi^*_{(2h-1)_k} \right)^* - \sum_{l=0}^{k} (I_{ch_l} \frac{\partial \Psi_{(2h-1)_{k-l}}}{\partial \theta_h}) \right]. \quad \text{(C.44)}$$

This completes the analysis of the terminal voltage mismatch equation partial derivatives, as there is no dependence upon α_0, the only remaining variable.

C.2 DIRECT CURRENT PARTIAL DERIVATIVES

The direct current partial derivatives are obtained by a process analogous to that used in obtaining the terminal voltage partial derivatives. The dc voltage partial derivatives are obtained and then applied to the dc system admittance to calculate the direct current differential. The direct current mismatch equation is:

$$F_{I_k} = I_{d_k} - V_{d_k} Y_{d_k} = 0. \quad \text{(C.45)}$$

Finding the partial derivatives of this equation is therefore mainly concerned with V_{d_k}, which is a function of all the convertor variables except α_0.

C.2.1 With Respect to Ac Phase Voltage Variation

Differentiating equation C.45 with respect to terminal voltage yields

$$\frac{\partial \mathcal{R}\{F_{I_k}\}}{\partial \mathcal{R}\{V_m^\delta\}} = \mathcal{R}\left\{ -Y_{d_k} \frac{\partial V_{d_k}}{\partial \mathcal{R}\{V_m^\delta\}} \right\}, \quad \text{(C.46)}$$

$$\frac{\partial \mathcal{I}\{F_{I_k}\}}{\partial \mathcal{R}\{V_m^\delta\}} = \mathcal{I}\left\{ -Y_{d_k} \frac{\partial V_{d_k}}{\partial \mathcal{R}\{V_m^\delta\}} \right\}, \quad \text{(C.47)}$$

$$\frac{\partial \mathcal{R}\{F_{I_k}\}}{\partial \mathcal{I}\{V_m^\delta\}} = \mathcal{R}\left\{ -Y_{d_k} \frac{\partial V_{d_k}}{\partial \mathcal{I}\{V_m^\delta\}} \right\}, \quad \text{(C.48)}$$

$$\frac{\partial \mathcal{I}\{F_{I_k}\}}{\partial \mathcal{I}\{V_m^\delta\}} = \mathcal{I}\left\{ -Y_{d_k} \frac{\partial V_{d_k}}{\partial \mathcal{I}\{V_m^\delta\}} \right\}. \quad \text{(C.49)}$$

V_{d_k} is given by:

$$V_{d_k} = \frac{1}{2} j \sum_{i=1}^{12} \left\{ \sum_{l=k}^{n_h} (V_{di_l} \Psi^*_{i_{l-k}}) + \sum_{l=1}^{n_h} (V_{di_l} \Psi^*_{i_{l+k}})^* - \sum_{l=0}^{k} (V_{di_l} \Psi_{i_{k-l}}) \right\}, \quad k > 0. \tag{C.50}$$

The only terms in this equation which are a function of V_m^δ are the twelve pre-convolved dc voltage phasors V_{di_l}. There are three equations which define the twelve pre-convolved dc voltage phasors;

$$V_{d,normal_l} = V_l^+ - V_l^- - j\omega k(L^+ + L^-) I_{d_l} \tag{C.51}$$

for a 'normal' conduction interval,

$$V_{d,commutation_l} = \frac{L_e V_l^b + L_b (V_l^e - jk\omega L_e I_{d_l})}{L_e + L_b} - V_l^o - jk\omega L_o I_{d_l} \tag{C.52}$$

for a commutation on the positive dc rail, and

$$V_{d,commutation_l} = V_l^o - jk\omega L_o I_{d_l} - \frac{L_e V_l^b + L_b (V_l^e + jl\omega L_e I_{d_l})}{L_e + L_b} \tag{C.53}$$

for a commutation on the negative rail. Differentiating these three equations with respect to V_m^δ gives 36 possible values for $\frac{\partial V_{di_l}}{\partial V_m^\delta}$ according to the sample number i, and the phase of δ. The required partial derivatives are summarised in table C.3 by reference to the partial derivatives of equations C.51, C.52, and C.53 listed below:

$$\begin{aligned} \frac{\partial V_{di_l}}{\partial \mathcal{R}\{V_l^+\}} &= 1 \\ \frac{\partial V_{di_l}}{\partial \mathcal{R}\{V_l^-\}} &= -1 \end{aligned} \tag{C.54}$$

for a 'normal' conduction interval,

$$\begin{aligned} \frac{\partial V_{di_l}}{\partial \mathcal{R}\{V_l^e\}} &= \frac{L_b}{L_b + L_e} \\ \frac{\partial V_{di_l}}{\partial \mathcal{R}\{V_l^b\}} &= \frac{L_e}{L_b + L_e} \\ \frac{\partial V_{di_l}}{\partial \mathcal{R}\{V_l^o\}} &= -1 \end{aligned} \tag{C.55}$$

for a commutation on the positive dc rail, and

$$\begin{aligned}\frac{\partial V_{di_l}}{\partial \mathcal{R}\{V_l^e\}} &= -\frac{L_b}{L_b+L_e} \\ \frac{\partial V_{di_l}}{\partial \mathcal{R}\{V_l^b\}} &= -\frac{L_e}{L_b+L_e} \\ \frac{\partial V_{di_l}}{\partial \mathcal{R}\{V_l^o\}} &= 1 \end{aligned} \tag{C.56}$$

for a commutation on the negative rail. The Cauchy Reimann equations can be used to give the partial derivative with respect to the imaginary part of the voltage variation as j times that listed above.

sample (i)	Dc Voltage derivative					
	e	b	o	+	-	eqn
1	A	C	B	.	.	(C.55)
2	.	.	.	A	B	(C.54)
3	C	B	A	.	.	(C.56)
4	.	.	.	A	C	(C.54)
5	B	A	C	.	.	(C.55)
6	.	.	.	B	C	(C.54)
7	A	C	B	.	.	(C.56)
8	.	.	.	B	A	(C.54)
9	C	B	A	.	.	(C.55)
10	.	.	.	C	A	(C.54)
11	B	A	C	.	.	(C.56)
12	.	.	.	C	B	(C.54)

Table C.3 Assembly of dc voltage partial derivatives

The partial derivatives in equations C.54, C.55, and C.56 are then substituted into the partial derivatives of equation C.50 which are given below:

$$\begin{aligned}\frac{\partial V_{d_k}}{\partial \mathcal{R}\{V_m^\delta\}} &= \frac{1}{2} j \sum_{i=1}^{12} \left[\left(\frac{\partial V_{di_m}}{\partial \mathcal{R}\{V_m^\delta\}} \Psi^*_{i_{m+k}} \right)^* \right. \\ &\quad \left. + \left\{ \begin{array}{ll} -\frac{\partial V_{di_m}}{\partial \mathcal{R}\{V_m^\delta\}} \Psi_{i_{k-m}} & m \le k \\ \frac{\partial V_{di_m}}{\partial \mathcal{R}\{V_m^\delta\}} \Psi^*_{i_{m-k}} & m \ge k \end{array} \right] , k > 0, \end{aligned} \tag{C.57}$$

$$\frac{\partial V_{d_k}}{\partial \mathcal{I}\{V_m^\delta\}} = \frac{1}{2} j \sum_{i=1}^{12} \left[\left(\frac{\partial V_{di_m}}{\partial \mathcal{I}\{V_m^\delta\}} \Psi^*_{i_{m+k}} \right)^* + \begin{cases} -\frac{\partial V_{di_m}}{\partial \mathcal{I}\{V_m^\delta\}} \Psi_{i_{k-m}} & m \leq k \\ \frac{\partial V_{di_m}}{\partial \mathcal{I}\{V_m^\delta\}} \Psi^*_{i_{m-k}} & m \geq k \end{cases} \right], k > 0. \quad \text{(C.58)}$$

This completes the derivation of the partial derivative of dc current mismatch equation with respect to terminal voltage.

C.2.2 With Respect to Direct Current Ripple Variation

Apart from being the most significant term in the dc current mismatch equation, the dc ripple affects the commutation currents, and also causes a voltage drop through the commutating reactance. These last two effects mean that the dc voltage is a function of the dc current ripple. It is therefore necessary to obtain partial derivatives of the dc voltage harmonics in a similar manner to that undertaken already for the derivative with respect to terminal voltage. Differentiating the dc current mismatch equation;

$$\frac{\partial \mathcal{R}\{F_{I_k}\}}{\partial \mathcal{R}\{I_{d_m}\}} = \mathcal{R} \begin{cases} -Y_{d_k} \frac{\partial V_{d_k}}{\partial \mathcal{R}\{I_{d_m}\}} & k \neq m \\ 1 - Y_{d_k} \frac{\partial V_{d_k}}{\partial \mathcal{R}\{I_{d_m}\}} & k = m \end{cases}, \quad \text{(C.59)}$$

$$\frac{\partial \mathcal{R}\{F_{I_k}\}}{\partial \mathcal{I}\{I_{d_m}\}} = \mathcal{R} \left\{ -Y_{d_k} \frac{\partial V_{d_k}}{\partial \mathcal{I}\{I_{d_m}\}} \right\}, \quad \text{(C.60)}$$

$$\frac{\partial \mathcal{I}\{F_{I_k}\}}{\partial \mathcal{I}\{I_{d_m}\}} = \mathcal{I} \begin{cases} -Y_{d_k} \frac{\partial V_{d_k}}{\partial \mathcal{I}\{I_{d_m}\}} & k \neq m \\ j - Y_{d_k} \frac{\partial V_{d_k}}{\partial \mathcal{I}\{I_{d_m}\}} & k = m \end{cases}, \quad \text{(C.61)}$$

$$\frac{\partial \mathcal{I}\{F_{I_k}\}}{\partial \mathcal{R}\{I_{d_m}\}} = \mathcal{I} \left\{ -Y_{d_k} \frac{\partial V_{d_k}}{\partial \mathcal{R}\{I_{d_m}\}} \right\}. \quad \text{(C.62)}$$

Differentiating equation C.50 with respect to $\mathcal{R}\{I_{d_m}\}$ yields

$$\frac{\partial V_{d_k}}{\partial \mathcal{R}\{I_{d_m}\}} = \frac{1}{2} j \sum_{i=1}^{12} \left[\left(\frac{\partial V_{di_m}}{\partial \mathcal{R}\{I_{d_m}\}} \Psi^*_{i_{m+k}} \right)^* + \begin{cases} -\frac{\partial V_{di_m}}{\partial \mathcal{R}\{I_{d_m}\}} \Psi_{i_{k-m}} & m \leq k \\ \frac{\partial V_{di_m}}{\partial \mathcal{R}\{I_{d_m}\}} \Psi^*_{i_{m-k}} & m \geq k \end{cases} \right], \text{1ex} k > 0. \quad \text{(C.63)}$$

Similarly,

$$\frac{\partial V_{d_k}}{\partial \mathcal{I}\{I_{d_m}\}} = \frac{1}{2}j\sum_{i=1}^{12}\left[(\frac{\partial V_{di_m}}{\partial \mathcal{I}\{I_{d_m}\}}\Psi^*_{i_{m+k}})^* + \left\{\begin{array}{ll} -\frac{\partial V_{di_m}}{\partial \mathcal{I}\{I_{d_m}\}}\Psi_{i_{k-m}} & m \leq k \\ \frac{\partial V_{di_m}}{\partial \mathcal{I}\{I_{d_m}\}}\Psi^*_{i_{m-k}} & m \geq k \end{array}\right], 1\text{ex}k > 0. \quad \text{(C.64)}$$

The partial derivatives $\frac{\partial V_{di_m}}{\partial \mathcal{I}\{I_{d_m}\}}$ are obtained from equations C.51, C.52, and C.53:

$$\frac{\partial V_{di_m}}{\partial \mathcal{R}\{I_{d_m}\}} = -jk\omega(L_+ + L_-) \quad \text{(C.65)}$$

during normal conduction, and

$$\frac{\partial V_{di_m}}{\partial \mathcal{R}\{I_{d_m}\}} = jk\omega[L_0 + \frac{L_e L_b}{L_e + L_b}] \quad \text{(C.66)}$$

during any commutation. Again, the imaginary partial derivatives are obtained by the Cauchy Reimann equations. The correct phase subscripts can be obtained from table C.3. This completes the linearised dependence of the dc mismatch upon dc ripple variation.

C.2.3 With Respect to End of Commutation Variation

The effect of variation in the end of commutation angle ϕ_h is limited solely to the sampling of relevant dc voltage sections. This is best explained with reference to the following equation for the dc voltage:

$$V_d = \frac{1}{2}j\sum_{i=1}^{12} V_{di} \otimes \Psi_i. \quad \text{(C.67)}$$

In this equation, only two of the twelve Ψ_i are functions of ϕ_h. Table C.4 shows that Ψ_{2h} and Ψ_{2h-1} are functions of ϕ_h. Equation C.50 can therefore be differentiated to yield:

$$\begin{aligned}\frac{\partial V_{d_k}}{\partial \phi_h} = & \\ & \frac{1}{2}j\left(\sum_{l=0}^{k} V_{d(2h-1)_l}\frac{\partial \Psi_{2h_{k-l}}}{\partial \phi_h} - \sum_{l=k}^{n_h} V_{d(2h-1)_l}(\frac{\partial \Psi_{2h_{l-k}}}{\partial \phi_h})^*\right. \\ & - \sum_{l=0}^{n_h}\left[V_{d(2h-1)_l}(\frac{\partial \Psi_{2h_{l-k}}}{\partial \phi_h})^*\right]^* - \sum_{l=0}^{k} V_{d(2h)_l}\frac{\partial \Psi_{2h_{k-l}}}{\partial \phi_h} \\ & \left. + \sum_{l=k}^{n_h} V_{d(2h)_l}(\frac{\partial \Psi_{2h_{l-k}}}{\partial \phi_h})^* + \sum_{l=0}^{n_h}\left[V_{d(2h)_l}(\frac{\partial \Psi_{2h_{l-k}}}{\partial \phi_h})^*\right]^*\right) \end{aligned} \quad \text{(C.68)}$$

sample (i)	a_i	b_i
1	θ_1	ϕ_1
2	ϕ_1	θ_2
3	θ_2	ϕ_2
4	ϕ_2	θ_3
5	θ_3	ϕ_3
6	ϕ_3	θ_4
7	θ_4	ϕ_4
8	ϕ_4	θ_5
9	θ_5	ϕ_5
10	ϕ_5	θ_6
11	θ_6	ϕ_6
12	ϕ_6	θ_1

Table C.4 Limits of convertor states for use in sampling functions

Differentiating the dc ripple mismatch equation C.45 yields:

$$\frac{\partial \mathcal{R}\{F_{I_k}\}}{\partial \phi_h} = \mathcal{R}\left\{-Y_{d_k}\frac{\partial V_{d_k}}{\partial \phi_h}\right\}, \tag{C.69}$$

and

$$\frac{\partial \mathcal{I}\{F_{I_k}\}}{\partial \phi_h} = \mathcal{I}\left\{-Y_{d_k}\frac{\partial V_{d_k}}{\partial \phi_h}\right\}. \tag{C.70}$$

Substituting equation C.68 into C.69 and C.70 gives the required partial derivative of dc ripple mismatch with respect to end of commutation.

C.2.4 With Respect to Firing angle variation

The partial derivatives of dc ripple mismatch with respect to firing angle are obtained in an exactly similar manner. The result is:

$$\frac{\partial \mathcal{R}\{F_{I_k}\}}{\partial \theta_h} = \mathcal{R}\left\{-Y_{d_k}\frac{\partial V_{d_k}}{\partial \theta_h}\right\}, \tag{C.71}$$

and

$$\frac{\partial \mathcal{I}\{F_{I_k}\}}{\partial \theta_h} = \mathcal{I}\left\{-Y_{d_k}\frac{\partial V_{d_k}}{\partial \theta_h}\right\}, \tag{C.72}$$

where

$$\frac{\partial V_{d_k}}{\partial \theta_h} =$$
$$\frac{1}{2}j\left(\sum_{l=0}^{k} V_{d(2h-2)_l}\frac{\partial \Psi_{2h_{k-l}}}{\partial \theta_h} - \sum_{l=k}^{n_h} V_{d(2h-2)_l}(\frac{\partial \Psi_{2h_{l-k}}}{\partial \theta_h})^*\right.$$
$$-\sum_{l=0}^{n_h}\left[V_{d(2h-2)_l}(\frac{\partial \Psi_{2h-1_{l-k}}}{\partial \theta_h})^*)\right]^* - \sum_{l=0}^{k} V_{d(2h-1)_l}\frac{\partial \Psi_{2h-1_{k-l}}}{\partial \theta_h}$$
$$\left.+\sum_{l=k}^{n_h} V_{d(2h-1)_l}(\frac{\partial \Psi_{2h-1_{l-k}}}{\partial \theta_h})^* + \sum_{l=0}^{n_h}\left[V_{d(2h-1)_l}(\frac{\partial \Psi_{2h-1_{l-k}}}{\partial \theta_h})^*)\right]^*\right). \quad \text{(C.73)}$$

C.3 END OF COMMUTATION MISMATCH PARTIAL DERIVATIVES

The end of commutation mismatch is the current in the phase that is commutating off, at the end of the commutation. This current should be zero, and is given by

$$F_{\phi_i} = \mathcal{I}\{j(-D + I_{d_0}) + \sum_{k=1}^{n_h} F_{\phi_{i_k}} e^{jk\phi_i}\} = 0 \quad \text{(C.74)}$$

for a commutation on the positive rail, where

$$D = -\mathcal{I}\{\sum_{k=1}^{n_h} I_{ci_k} e^{jk\theta_i}\} \quad \text{(C.75)}$$
$$F_{\phi_{i_k}} = I_{d_k} - I_{ci_k} \quad \text{(C.76)}$$
$$I_{ci_k} = \frac{jk\omega L_e I_{d_k} - V_k^{eb}}{jk\omega L_{eb}}. \quad \text{(C.77)}$$

The end of commutation mismatch equation is therefore a function of all the variables except the average delay angle α_0. A commutation on the negative rail is accounted for by substituting $-I_{d_m}$ in the above equations for I_{d_m}.

C.3.1 With Respect to Ac Phase Voltage Variation

Differentiating equation C.74 with respect to an arbitrary voltage phase and harmonic yields:

$$\frac{\partial F_{\phi_i}}{\partial \mathcal{R}\{V_m^\delta\}} = \mathcal{I}\{-\frac{\partial D}{\partial \mathcal{R}\{V_m^\delta\}} - \frac{\partial I_{ci_m}}{\partial \mathcal{R}\{V_m^\delta\}} e^{jm\phi_i}\} \quad \text{(C.78)}$$

and

$$\frac{\partial F_{\phi_i}}{\partial \mathcal{I}\{V_m^\delta\}} = \mathcal{R}\{-\frac{\partial D}{\partial \mathcal{I}\{V_m^\delta\}} - \frac{\partial I_{ci_m}}{\partial \mathcal{I}\{V_m^\delta\}} e^{jm\phi_i}\}. \quad \text{(C.79)}$$

The partial derivatives in these equations are obtained from equations C.75 to C.77 as

$$\frac{\partial D}{\partial \mathcal{R}\{V_m^\delta\}} = \frac{1}{jm\omega(L_e + L_b)} e^{jk\theta_i}, \tag{C.80}$$

$$\frac{\partial I_{ci_m}}{\partial \mathcal{R}\{V_m^\delta\}} = \frac{-1}{jm\omega(L_e + L_b)}, \tag{C.81}$$

$$\frac{\partial D}{\partial \mathcal{I}\{V_m^\delta\}} = \frac{j}{jm\omega(L_e + L_b)} e^{jk\theta_i}, \tag{C.82}$$

$$\frac{\partial I_{ci_m}}{\partial \mathcal{I}\{V_m^\delta\}} = \frac{-j}{jm\omega(L_e + L_b)}. \tag{C.83}$$

It is assumed in the above analysis that V_m^δ corresponds to a phase ending conduction. Multiplying by -1 gives the required partial derivative for the case that V_m^δ corresponds to a phase beginning conduction.

C.3.2 With Respect to Direct Current Ripple Variation

The analysis is similar to that for ac phase voltage variation. Differentiating equation C.74 with respect to dc ripple yields

$$\frac{\partial F_{\phi_i}}{\partial \mathcal{R}\{I_{d_m}\}} = \mathcal{I}\{-\frac{\partial D}{\partial \mathcal{R}\{I_{d_m}\}} - \frac{\partial I_{ci_m}}{\partial \mathcal{R}\{I_{d_m}\}} e^{jm\phi_i}\}, \tag{C.84}$$

and

$$\frac{\partial F_{\phi_i}}{\partial \mathcal{I}\{I_{d_m}\}} = \mathcal{R}\{-\frac{\partial D}{\partial \mathcal{I}\{I_{d_m}\}} - \frac{\partial I_{ci_m}}{\partial \mathcal{I}\{I_{d_m}\}} e^{jm\phi_i}\}. \tag{C.85}$$

The partial derivatives in these equations are obtained from equations C.75 to C.77 as

$$\frac{\partial D}{\partial \mathcal{R}\{I_{d_m}\}} = \frac{L_e}{L_e + L_b} e^{jk\theta_i}, \tag{C.86}$$

$$\frac{\partial I_{ci_m}}{\partial \mathcal{R}\{I_{d_m}\}} = \frac{-L_e}{L_e + L_b}, \tag{C.87}$$

$$\frac{\partial D}{\partial \mathcal{I}\{I_{d_m}\}} = \frac{jL_e}{L_e + L_b} e^{jk\theta_i}, \tag{C.88}$$

$$\frac{\partial I_{ci_m}}{\partial \mathcal{I}\{I_{d_m}\}} = \frac{-jL_e}{L_e + L_b}. \tag{C.89}$$

This analysis assumes that the commutation is on the positive rail. A similar analysis holds for a commutation on the negative rail, but with $-I_{d_m}$ substituted into equation C.74.

C.3.3 With Respect to End of Commutation Variation

This partial derivative gives the effect on the 'residual' commutating-off current at the end of the commutation, if the end of commutation is moved. It is obtained simply by differentiating equation C.74 with respect to ϕ_i to yield

$$\frac{\partial F_{\phi_i}}{\partial \phi_i} = \mathcal{I}\{\sum_{k=1}^{n_h} jkF_{\phi_{i_k}} e^{jk\phi_i}\} \tag{C.90}$$

C.3.4 With Respect to Firing Instant Variation

The dc offset to the commutation, D, is a function of the firing instant, and so the only effect of θ_i on F_{ϕ_i} is through D. Differentiating the expression for D, equation C.75, gives the required partial derivative.

$$\frac{\partial F_{\phi_i}}{\partial \theta_i} = \mathcal{I}\{-\sum_{k=1}^{n_h} jkI_{c_k} e^{jk\theta_i}\} \tag{C.91}$$

C.4 FIRING INSTANT MISMATCH EQUATION PARTIAL DERIVATIVES

For the implemented constant current controller, the firing instant mismatch is not a function of the ac terminal voltage. This is because the firing order is obtained solely from monitoring the dc current. This also means that the firing mismatch is not a function of the end of commutation instants. The firing instant mismatch is a function only of the dc ripple, the firing angle, and the average firing order. The firing mismatch equation is

$$F_{\theta_i} = \mathcal{I}\{j(\beta_i + \alpha_0 - \theta_i) + \sum_{k=1}^{n_h} \alpha_{i_k} e^{jk\theta_i}\} = 0, \tag{C.92}$$

where

$$\alpha_{i_k} = \frac{G}{1 + jk\omega T}(P + \frac{1}{jk\omega T_I})I_{dk}. \tag{C.93}$$

The partial derivatives are easily obtained as;

$$\frac{\partial F_{\theta_i}}{\partial \alpha_0} = 1, \tag{C.94}$$

$$\frac{\partial F_{\theta_i}}{\partial \theta_i} = \mathcal{I}\{-j + \sum_{k=1}^{n_h} jk\theta_i \alpha_{i_k} e^{jk\theta_i}\}, \tag{C.95}$$

$$\frac{\partial F_{\theta_i}}{\partial \mathcal{R}\{I_{d_k}\}} = \mathcal{I}\left\{\sum_{k=1}^{n_h} \frac{\partial \alpha_{i_k}}{\partial I_{d_k}} e^{jk\theta_i}\right\}, \tag{C.96}$$

$$\frac{\partial F_{\theta_i}}{\partial \mathcal{I}\{I_{d_k}\}} = \mathcal{R}\left\{\sum_{k=1}^{n_h} \frac{\partial \alpha_{i_k}}{\partial I_{d_k}} e^{jk\theta_i}\right\}, \tag{C.97}$$

where

$$\frac{\partial \alpha_{i_k}}{\partial I_{d_k}} = \frac{G}{1 + jk\omega T}(P + \frac{1}{jk\omega T_I}). \tag{C.98}$$

C.5 AVERAGE DELAY ANGLE PARTIAL DERIVATIVES

The average delay angle, α_0, is obtained by requiring that the average dc voltage, when applied to the dc system, should result in the current order. Thus α_0 is a control variable, required for the case of constant current control. The mismatch equation is

$$F_{\alpha_0} = \mathcal{I}\{I_{d_0} - (V_{d_0} - V_{dc})Y_{d_0}\}, \tag{C.99}$$

where V_{dc} represents a dc voltage source, and

$$V_{d_0} = \frac{1}{2} j \sum_{i=1}^{12} \left\{\sum_{l=0}^{n_h} (V_{di_l} \Psi_{i_l}^*)\right\}. \tag{C.100}$$

Thus F_{α_0} is a function of all the convertor variables, with the exception of α_0 itself. Analysis of the partial derivatives of equation C.99 is similar to that for the partial derivatives of the dc ripple mismatch.

C.5.1 With Respect to Ac Phase Voltage Variation

Differentiating the mismatch equation C.99 with respect to an arbitrary phase and harmonic of ac voltage yields

$$\frac{\partial F_{\alpha_0}}{\partial \mathcal{R}\{V_m^\delta\}} = \mathcal{I}\{-Y_{d_0}\frac{\partial V_{d_0}}{\partial \mathcal{R}\{V_m^\delta\}}\}, \tag{C.101}$$

and

$$\frac{\partial F_{\alpha_0}}{\partial \mathcal{I}\{V_m^\delta\}} = \mathcal{I}\{-Y_{d_0}\frac{\partial V_{d_0}}{\partial \mathcal{I}\{V_m^\delta\}}\}. \tag{C.102}$$

Differentiating equation C.100 yields

$$\frac{\partial V_{d_0}}{\partial \mathcal{R}\{V_m^\delta\}} = \frac{1}{2}j\sum_{i=1}^{12}(\frac{\partial V_{di_m}}{\partial \mathcal{R}\{V_m^\delta\}}\Psi_{i_m}^*), \tag{C.103}$$

and

$$\frac{\partial V_{d_0}}{\partial \mathcal{I}\{V_m^\delta\}} = \frac{1}{2}j\sum_{i=1}^{12}(\frac{\partial V_{di_m}}{\partial \mathcal{I}\{V_m^\delta\}}\Psi_{i_m}^*), \tag{C.104}$$

which when substituted back into equations C.101 and C.102 give the required partial derivatives. The remaining partial derivatives, $\frac{\partial V_{di_m}}{\partial \mathcal{R}\{V_m^\delta\}}$ etc, have already been obtained in equations C.51, C.52, and C.53, and by reference to table C.3.

C.5.2 With Respect to dc Ripple Current Variation

Variation in the dc ripple affects the dc voltage samples in a similar manner to that of a variation in the terminal voltage above. Differentiating the mismatch equation C.99 with respect to an arbitrary phase and harmonic of dc current ripple yields

$$\frac{\partial F_{\alpha_0}}{\partial \mathcal{R}\{I_{d_m}\}} = \mathcal{I}\{-Y_{d_0}\frac{\partial V_{d_0}}{\partial \mathcal{R}\{I_{d_m}\}}\}, \tag{C.105}$$

and

$$\frac{\partial F_{\alpha_0}}{\partial \mathcal{I}\{I_{d_m}\}} = \mathcal{I}\{-Y_{d_0}\frac{\partial V_{d_0}}{\partial \mathcal{I}\{I_{d_m}\}}\}. \tag{C.106}$$

Differentiating equation C.100 yields

$$\frac{\partial V_{d_0}}{\partial \mathcal{R}\{I_{d_m}\}} = \frac{1}{2}j\sum_{i=1}^{12}(\frac{\partial V_{di_m}}{\partial \mathcal{R}\{I_{d_m}\}}\Psi_{i_m}^*), \tag{C.107}$$

and

$$\frac{\partial V_{d_0}}{\partial \mathcal{I}\{I_{d_m}\}} = \frac{1}{2} j \sum_{i=1}^{12} \left(\frac{\partial V_{di_m}}{\partial \mathcal{I}\{I_{d_m}\}} \Psi_{i_m}^* \right), \tag{C.108}$$

which when substituted back into equations C.105 and C.106 give the required partial derivatives. The remaining partial derivatives, $\frac{\partial V_{di_m}}{\partial \mathcal{R}\{I_{d_m}\}}$ etc, have already been obtained in equations C.65, and C.66.

C.5.3 With Respect to End of Commutation Variation

The effect of a variation in the end of commutation is to modify the sampling of the dc voltage sections in equation C.100. Differentiating equation C.99 with respect to ϕ_h yields

$$\frac{\partial F_{\alpha_0}}{\partial \phi_h} = \mathcal{I}\{-Y_{d_0} \frac{\partial V_{d_0}}{\partial \phi_h}\}. \tag{C.109}$$

This requires the partial derivative $\frac{\partial V_{d_0}}{\partial \phi_h}$. Differentiating equation C.100 yields

$$\frac{\partial V_{d_0}}{\partial \phi_h} = \frac{1}{2} j \left\{ \sum_{l=1}^{n_h} \left(V_{d(2h-1)_l} \frac{\partial \Psi_{(2h-1)_l}^*}{\partial \phi_h} \right) + \sum_{l=1}^{n_h} \left(V_{d(2h)_l} \frac{\partial \Psi_{2h_l}^*}{\partial \phi_h} \right) \right\}, \tag{C.110}$$

where use has been made of table C.4 to determine the only two sampling functions that are affected by ϕ_h.

C.5.4 With Respect to Firing Angle Variation

The effect of a change in the firing angle on the average delay angle mismatch equation is similar to that for a change in the end of commutation angle. The sampling of the dc voltage sections is modified, and this changes the average dc voltage. The analysis carried out above for the end of commutation variation is also valid in this case, with only the two affected sampling functions, as determined from table C.4 being different. The result is that

$$\frac{\partial F_{\alpha_0}}{\partial \theta_h} = \mathcal{I}\{-Y_{d_0} \frac{\partial V_{d_0}}{\partial \theta_h}\}, \tag{C.111}$$

where

$$\frac{\partial V_{d_0}}{\partial \theta_h} = \frac{1}{2} j \left\{ \sum_{l=1}^{n_h} \left(V_{d(2h-2)_l} \frac{\partial \Psi_{(2h-2)_l}^*}{\partial \theta_h} \right) + \sum_{l=1}^{n_h} \left(V_{d(2h-1)_l} \frac{\partial \Psi_{(2h-1)_l}^*}{\partial \theta_h} \right) \right\}. \tag{C.112}$$

This completes the derivation of the partial derivatives required for the Jacobian matrix, as the average delay angle mismatch equation is not a function of the average delay angle.

Appendix D

PHASE DEPENDENT IMPEDANCE

The circular complex locus of an impedance tensor is obtained in this appendix by injecting a 2π phase range of currents into the impedance tensor, calculating the resulting voltage, and then showing that the complex impedance defined by the ratio of the voltage to the current, corresponds to a circle in the complex plane. Given a current injected into an impedance tensor, the voltage developed is

$$\begin{bmatrix} V_R \\ V_I \end{bmatrix} = \begin{bmatrix} z_{11} & z_{12} \\ z_{21} & z_{22} \end{bmatrix} \begin{bmatrix} I_R \\ I_I \end{bmatrix} \tag{D.1}$$

which can be written in complex form:

$$V = [(z_{11}I_R + z_{12}I_I) + j(z_{21}I_R + z_{22}I_I)]\,. \tag{D.2}$$

Dividing now to obtain the complex impedance:

$$Z = \frac{[(z_{11}I_R + z_{12}I_I) + j(z_{21}I_R + z_{22}I_I)]}{I_R + jI_R} \tag{D.3}$$

$$= \frac{[(z_{11}I_R + z_{12}I_I) + j(z_{21}I_R + z_{22}I_I)]\,(I_R - jI_I)}{|I|^2} \tag{D.4}$$

Separating out the real and imaginary parts of the complex impedance:

$$Z_R = \frac{z_{11}I_R^2 + z_{12}I_I I_R + z_{21}I_R I_I + z_{22}I_I^2}{|I|^2} \tag{D.5}$$

$$Z_I = \frac{z_{21}I_R^2 + z_{22}I_I I_R - z_{11}I_R I_I - z_{12}I_I^2}{|I|^2} \tag{D.6}$$

Since the objective is to obtain a phase dependent locus, the polar transformation,

$$I_R = |I|\cos\theta \tag{D.7}$$

$$I_I = |I|\sin\theta \tag{D.8}$$

is applied, to yield:

$$\begin{aligned} Z_R &= \frac{z_{11}|I|^2\cos^2\theta + (z_{12}+z_{21})|I|^2\sin\theta\cos\theta + z_{22}|I|^2\sin^2\theta}{|I|^2} \\ Z_I &= \frac{z_{21}|I|^2\cos^2\theta + (z_{22}-z_{11})|I|^2\sin\theta\cos\theta - z_{12}|I|^2\sin^2\theta}{|I|^2} \end{aligned} \tag{D.9}$$

The square magnitude of the current evidently cancels from equations D.9, resulting in a phase dependent impedance:

$$\begin{aligned} Z_R &= z_{11}c^2 + (z_{12}+z_{21})sc + z_{22}s^2 \\ Z_I &= z_{21}c^2 + (z_{22}-z_{11})sc - z_{12}s^2, \end{aligned} \tag{D.10}$$

where for the sake of brevity, the following notation has been defined:

$$s \stackrel{\text{def}}{=} \sin\theta \tag{D.11}$$

$$c \stackrel{\text{def}}{=} \cos\theta \tag{D.12}$$

(D.13)

The following identities are therefore valid:

$$s^2 = 1 - c^2 \tag{D.14}$$

$$s^4 = 1 - 2c^2 + c^4 \tag{D.15}$$

$$s^3c = sc - sc^3 \tag{D.16}$$

$$s^2c^2 = c^2 - c^4 \tag{D.17}$$

To show that the phase dependent impedance corresponds to a circular locus, it is necessary only to show that the real and imaginary parts of the complex impedance satisfy the quadratic form for a circle in the plane:

$$(Z_R - a)^2 + (Z_I - b)^2 = r^2, \tag{D.18}$$

where a and b, are the coordinates of the circle center, and r is the radius. The problem is to determine the values of a, b and r, since Z_R and Z_I have been defined parametrically in terms of θ, the angle of the current injection. A lucky guess gave:

$$a = \frac{1}{2}(z_{11} + z_{22}) \tag{D.19}$$

$$b = \frac{1}{2}(-z_{12} + z_{21}) \tag{D.20}$$

$$r = \frac{1}{2}\sqrt{(z_{11} - z_{22})^2 + (z_{12} + z_{21})^2} \tag{D.21}$$

which is now verified by substitution into equation D.18:

$$\begin{aligned}(Z_R - a)^2 + (Z_I - b)^2 = \\ \left(z_{11}c^2 + (z_{12} + z_{21})sc + z_{22}s^2 - \frac{1}{2}(z_{11} + z_{22})\right)^2 \\ + \left((z_{21}c^2 + (z_{22} - z_{11})sc - z_{12}s^2 - \frac{1}{2}(-z_{12} + z_{21})\right)^2\end{aligned} \tag{D.22}$$

expanding the RHS of equation D.22:

$$\begin{aligned}\text{RHS} = \\ & z_{11}^2c^4 + 2z_{11}(z_{12} + z_{21})sc^3 + 2z_{11}z_{22}s^2c^2 + 2z_{22}(z_{12} + z_{21})cs^3 \\ & + (z_{12} + z_{21})^2s^2c^2 + z_{22}^2s^4 + \frac{1}{4}(z_{11} + z_{22})^2 - z_{11}(z_{11} + z_{22})c^2 \\ & - (z_{11} + z_{22})(z_{12} + z_{21})sc - z_{22}(z_{11} + z_{22})s^2 + z_{21}^2c^4 \\ & + 2z_{21}(z_{22} - z_{11})sc^3 - 2z_{21}z_{12}s^2c^2 + (z_{22} - z_{11})^2s^2c^2 \\ & - 2z_{12}(z_{22} - z_{11})cs^3 + z_{12}^2s^4 + \frac{1}{4}(-z_{12} + z_{21})^2 - z_{21}(-z_{12} + z_{21})c^2 \\ & - (z_{22} - z_{11})(-z_{12} + z_{21})sc + z_{12}(-z_{12} + z_{21})s^2\end{aligned} \tag{D.23}$$

Equation D.23 is a trigonometric polynomial in powers of s and c. In order to simplify it, the identities of equations D.14 to D.17 are substituted, and the coefficients of c^2, sc, sc^3, c^4 and the constant component are collected:

$$\begin{aligned}\text{RHS} = \\ & [z_{11}^2 - 2z_{11}z_{22} - (z_{12} + z_{21})^2 + z_{22}^2 + z_{21}^2 + 2z_{21}z_{12} - (z_{22} - z_{11})^2 + z_{12}^2]c^4 \\ & + [2z_{11}(z_{12} + z_{21}) - 2z_{22}(z_{12} + z_{21}) + 2z_{21}(z_{22} - z_{11}) + 2z_{12}(z_{22} - z_{11})]sc^3 \\ & + [2z_{11}z_{22} + (z_{12} + z_{21})^2 - 2z_{22}^2 + (z_{22} - z_{11})(z_{11} + z_{22}) - 2z_{21}z_{12} \\ & + (z_{22} - z_{11})^2 - 2z_{12}^2 - (z_{12} + z_{21})(-z_{12} + z_{21})]c^2 + [2z_{22}(z_{12} + z_{21}) \\ & - (z_{11} + z_{22})(z_{12} + z_{21}) - 2z_{12}(z_{22} - z_{11}) - (z_{22} - z_{11})(-z_{12} + z_{21})]sc \\ & + [z_{22}^2 + \frac{1}{4}(z_{11} + z_{22})^2 - z_{22}(z_{11} + z_{22}) \\ & + z_{12}^2 + \frac{1}{4}(-z_{12} + z_{21})^2 + z_{12}(-z_{12} + z_{21})] \\ = \quad & \frac{1}{4}\left[(z_{11} - z_{22})^2 + (z_{12} + z_{21})^2\right] \\ = \quad & r^2\end{aligned} \tag{D.24}$$

The trigonometric terms all cancel, leaving only a constant term, which shows that all points on the locus are the same distance, r, from the point $(a + jb)$. It remains

only to show that for a full 2π range of applied current angles, all points on the circular locus are visited by the impedance. This is done by subtracting the locus position, $(a + jb)$, from the complex impedance locus. Considering first the real part:

$$\begin{aligned}
Z_R - a &= z_{11}\cos^2\theta + \frac{1}{2}(z_{12}+z_{21})\sin 2\theta + z_{22}\sin^2\theta - \frac{1}{2}(z_{11}+z_{22}) \\
&= z_{11}\cos^2\theta + \frac{1}{2}(z_{12}+z_{21})\sin 2\theta + z_{22} - z_{22}\cos^2\theta - \frac{1}{2}(z_{11}+z_{22}) \\
&= (z_{11}-z_{22})\cos^2\theta + \frac{1}{2}(z_{12}+z_{21})\sin 2\theta - \frac{1}{2}(z_{11}-z_{22}) \\
&= \frac{1}{2}(z_{11}-z_{22}) + \frac{1}{2}(z_{11}-z_{22})\cos 2\theta + \frac{1}{2}(z_{12}+z_{21})\sin 2\theta - \frac{1}{2}(z_{11}-z_{22}) \\
&= \frac{1}{2}\sqrt{(z_{11}-z_{22})^2+(z_{12}+z_{21})^2}\left[\frac{(z_{11}-z_{22})}{\sqrt{(z_{11}-z_{22})^2+(z_{12}+z_{21})^2}}\cos 2\theta\right. \\
&\quad \left. + \frac{(z_{12}+z_{21})}{\sqrt{(z_{11}-z_{22})^2+(z_{12}+z_{21})^2}}\sin 2\theta\right] \\
&= \frac{1}{2}\sqrt{(z_{11}-z_{22})^2+(z_{12}+z_{21})^2}\cos(2\theta+\gamma) \qquad \text{(D.25)}
\end{aligned}$$

where $\gamma = -\tan^{-1}\frac{z_{12}+z_{21}}{z_{11}-z_{22}}$. The analysis for the imaginary part is similar, yielding:

$$Z_I - b = \frac{1}{2}\sqrt{(z_{11}-z_{22})^2+(z_{12}+z_{21})^2}\sin(2\theta+\gamma) \qquad \text{(D.26)}$$

Equations D.25 and D.26 indicate that as the angle of the applied current is increased from zero to 2π radians, the circular impedance locus is traversed twice in a counter clockwise direction, starting from a point on the locus that makes an angle γ radians to the real axis. This is illustrated in figure D.1 below.

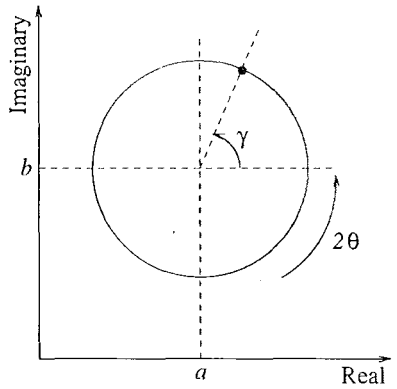

Figure D.1 Complex impedance locus for a tensor impedance. The locus point rotates counter clockwise twice, starting from the angle γ, as the current injection ranges in angle from 0 to 2π.

Appendix E

PUBLISHED PAPERS

The following papers have either been published, or accepted for publication in connection with the research described in this thesis:

1. Smith, B.C., Watson, N.R., Wood, A.R., and Arrillaga, J.(1995), 'Steady state model of the AC/DC convertor in the harmonic domain', IEE Proc.-Gener. Transm. Distrib., Vol 142, No. 2, March 1995, p. 109 - 118

2. Smith, B.C., Watson, N.R., Wood, A.R., and Arrillaga, J.(1995), 'A newton solution for the harmonic phasor analysis of ac/dc converters', IEEE PES Summer Meeting, 95 SM 379-8 PWRD

3. Smith, B.C., Watson, N.R., Wood, A.R., and Arrillaga, J., 'A Newton solution for the steady state interaction of ac/dc systems', accepted for publication with IEE Proc.-Gener. Transm. Distrib.

4. Wood, A.R., Smith, B.C., and Arrillaga, J. (1995) 'The harmonic impedance of an hvdc converter', 6th European Conference on Power Electronics and Applications (EPE 95), Seville, Sept 18-21, p. 1039 - 44

The first paper describes the harmonic domain model of a six pulse convertor, with a hybrid Newton-Raphson, and fixed point iteration solution for the interaction with the dc system. The second paper describes a full Newton solution for the interaction of a six pulse convertor with the dc system, while the third paper extends the solution to include interaction with the ac system. The solution method developed in the third paper employs decoupling between the ac/dc system interactions and the converter switching angles.

The contribution to the fourth paper was to utilise the converter model to calculate convertor impedances by the perturbation method. This enabled an intervalidation of convertor impedance calculations obtained by three different methods.

REFERENCES

AINSWORTH, J.D. (1967), 'Harmonic instability between controlled static convertors and ac networks', *IEE Proceedings*, Vol. 114, No. 7, July, p. 949 to 957.

AINSWORTH, J.D. (1968), 'The phase locked oscillator - a new control system for controlled static convertors.', *IEEE transactions on Power Apparatus and Systems*, Vol. 87, No. 3, May, p. 859 to 865.

APRILLE, T.J. AND TRICK, T.N. (1972), 'Steady state analysis of nonlinear circuits with periodic inputs', *Proceedings of the IEEE*, Vol. 60, No. 1, January, pp. 108–114.

ARFKIN, G. (1985), *Mathematical Methods for Physicists*, Academic Press, Inc., 3rd ed.

ARRILLAGA, J. (1983), *High Voltage Direct Current Transmission*, Vol. 6, Peter Peregrinus Ltd., London, UK.

ARRILLAGA, J., WATSON, N.R., EGGLESTON, J.F. AND CALLAGHAN, C.D. (1987), 'Comparison of steady state and dynamic models for the calculation of ac/dc system harmonics', *IEE Proceedings Pt. C*, Vol. 134, No. 1, January, p. 31 to 37.

ARRILLAGA, J., MEDINA, A., CAVIA, M.L.M. AND SÁNCHEZ, P. (1994), 'The harmonic domain. a frame of reference for power system harmonic analysis', *IEEE Transactions on Power Apparatus and Systems*, Vol. 94 SM 604-9 PWRS.

BAHRMAN, M.P., BROWNELL, G.C., ADIELSON, T., PETERSON, K.J., SHOCKLEY, P. AND LASSETER, R.H. (1986), 'Dc system resonance analysis', *IEEE Transactions on Power Delivery*, Vol. PWRD-2, No. 1, January, p. 156 to 164.

BURDEN, R., FAIRES, J. AND REYNOLDS, A. (1981), *Numerical Analysis*, PWS Publishers, 2 ed.

CALLAGHAN, C. AND ARRILLAGA, J. (1989), 'A double iterative algorthm for the analysis of power and harmonic flows at a.c. - d.c. terminals', *Proc. IEE*, Vol. 136, No. 6, November, pp. 319 – 24.

CALLAGHAN, C. AND ARRILLAGA, J. (1990), 'Convergence criteria for iterative harmonic analysis and its application to static convertors', *ICHPS IV, Budapest*, October, pp. 38 – 43.

CARBONE, R., FANTAUZZI, M., GAGLIARDI, F. AND TESTA, A. (1992), 'Some considerations on the iterative harmonic analysis convergence', *ICHPS V.*

CARPINELLI, G., GAGLIARDI, F., RUSSO, M. AND STURCHIO, A. (1993), 'Steady-state mathematical models of battery storage plants with line-commutated converters', *IEEE Transaction on Power Delivery*, Vol. 8, No. 2, April, p. 494 to 503.

CARPINELLI, G., GAGLIARDI, F., RUSSO, M. AND VILLACCI, D. (1994), 'Generalised converter models for iterative harmonic analysis in power systems', *Proceedings of the IEE Gener. Transm. Distrib.*, Vol. 141, No. 5, September.

CAVALLINI, A., LOGGINI, M. AND MONTANARI, G. (1994), 'Comparison of approximate methods for estimate harmonic currents injected by ac/dc converters', *IEEE Transactions on Industrial Electronics*, Vol. 41, No. 2, April, p. 256 to 262.

CHEN, S., WOOD, A. AND ARRILLAGA, J. (1996), 'Hvdc convertor transformer core saturation instability - a frequency domain analysis', *Accepted for IEE Pt. C. Generation Transmission and Distribution.*

DE JESUS, J.F. (1982), *D.C. Transmission System Harmonic Analysis and Stability using Describing Functions*, PhD thesis, University of London.

DICKMANDER, D., LEE, S., DÉSILETS, G. AND GRANGER, M. (1994), 'Ac/dc harmonic interactions in the presence of gic for the quebec-new england phase ii hvdc transmission', *IEEE Transactions on Power Delivery*, Vol. 9, No. 1, January, p. 68 to 78.

DOMMEL, H.W. (1969), 'Digital computer simulation of electromagnetic transients in single and multiphase networks', *IEEE Transactions on Power Apparatus and Systems*, Vol. PAS-88, No. 4, April, p. 388 to 399.

DOMMEL, H., CHIU, B. AND MEYER, W. (1980), 'Analysing transients in a.c./d.c. systems with the bpa electromagnetic transients program', *IEEE Conference Publication 205, on Thyristor and Variable Static Equipment for a.c. and d.c. Transmission*, pp. 109 – 113.

DOMMEL, H., YAN, A. AND SHI, W. (1986), 'Harmonics from transformer saturation', *IEEE Transactions on Power Delivery*, Vol. 1, No. 2.

EL-BIDWEIHY, E.A. AND AL-BADWAIHY, K. (1982), 'Steady State Analysis of Static Power Convertors', *IEEE Trans on Industry Applications*, Vol. 18, No. 4, July, pp. 405–410.

FARRET, F.A. AND FRERIS, L.L. (1990), 'Minimisation of uncharacteristic harmonics in hvdc convertors through firing angle modulation', *IEE Proceedings Pt. C*, Vol. 137, No. 1, January, p. 45 to 52.

FERREIRA, J.M., FRERIS, L.L. AND PAIVA, J.P.S. (1987), 'Describing function applied to hvdc systems harmonic instability', *IEE Proceedings Pt. C*, Vol. 134, No. 2, March, p. 131 to 137.

GRÖTZBACH, M. AND DRAXLER, B. (1993), 'Effect of dc ripple and commutation on the line harmonics of current-controlled ac/dc converters', *IEEE Transactions on Industry Applications*, Vol. 29, No. 5, September, p. 997 to 1005.

HAMMAD, A. (1992), 'Analysis of second harmonic instability for the chateauguay hvdc/svc scheme', *IEEE Transactions on Power Delivery*, Vol. 7, No. 1, January, p. 410 to 415.

HTSUI., J.S.C. AND SHEPHERD, W. (1971), 'Method of digital computation of thyristor switching circuits', *IEE Proceedings*, Vol. 118, No. 8, August, p. 993 to 998.

HU, L. AND YACAMINI, R. (1992), 'Harmonic transfer through convertors and hvdc links', *IEEE Transactions on Power Electronics*, Vol. 7, No. 3, July, p. 514 to 525.

HU, L. AND YACAMINI, R. (1993), 'Calculation of harmonics and interharmonics in hvdc schemes with low dc side impedance', *IEEE Proceedings-C*, Vol. 140, No. 6, November, p. 469 to 476.

JALALI, S. AND LASSETER, R. (1991), 'Harmonic interaction of power systems with static switching circuits', *22nd Annual IEEE Power Electronics Specialists Conference, Cambridge, MA, USA*, June, p. 330 to 337.

JALALI, S. AND LASSETER, R. (1994), 'A study of nonlinear harmonic interaction between a single phase line-commutated converter and a power system', *IEEE Transactions on Power Delivery*, Vol. 9, No. 3, July, p. 1616 to 1624.

KITCHIN, R.H. (1981), 'New method for digital computer evaluation of convertor harmonics in power systems using state variable analysis.', *IEE Proceedings Pt.C*, Vol. 128, No. 4, July, p. 196 to 207.

LARSON, E.V., BAKER, D.H. AND MCIVER, J.C. (1989), 'Low order harmonic interaction on ac/dc systems', *IEEE Transactions on Power Delivery*, Vol. 4, No. 1, January, p. 493 to 501.

LUCIANO, A.M. AND STROLLO, A.G.M. (1990), 'A fast time-domain algorithm for the simulation of switching power converters', *IEEE Transactions on Power Electronics*, Vol. 5, No. 3, July, pp. 363–370.

MATHUR, R.M. AND SHARAF, A.M. (1977), 'Harmonics on the dc side in hvdc conversion', *IEEE Transactions on Power Apparatus and Systems*, Vol. PAS-96, No. 5, October, p. 1631 to 1638.

OOI, B.T., MENEMENLIS, N. AND NAKRA, H.L. (1980), 'Fast steady state solution for hvdc analysis', *IEEE Transactions on Power Apparatus and Systems*, Vol. 99, No. 6, November, pp. 2453–2459.

PERSSON, E.V. (1970), 'Calculation of transfer functions in grid controlled convertor systems', *IEE Proceedings*, Vol. 117, No. 5, May, p. 989 to 997.

PHADKE, A.G. AND HARLOW, J.H. (1968), 'Generation of abnormal harmonics in high voltage ac/dc power systems', *IEEE Transactions on Power Apparatus and Systems*, Vol. PAS-87, No. 3, March, p. 873 to 883.

PRESS, W., TEUKOLSY, S., VETTERLING, W. AND FLANNERY, B. (1992), *Numerical Recipes in Fortran, The Art Of Scientific Computing*, Cambridge University Press, 2 ed.

RAJAGOPAL, N. AND QUAICOE, J. (1993), 'Harmonic analysis of three-phase ac/dc converters using the harmonic admittance method', *1993 Canadian Conference on Electrical and Computer Engineering, Vancouver, BC, Canada*, Vol. 1, September, pp. 313 – 16.

REEVE, J. AND BARON, J.A. (1970), 'Harmonic dc line voltages arising from hvdc power conversion', *IEEE Transactions on Power Apparatus and Systems*, Vol. PAS-89, No. 7, October, p. 1619 to 1624.

REEVE, J. AND BARON, J.A. (1971), 'Harmonic interaction between hvdc convertors and ac power systems', *IEEE Transactions on Power Apparatus and Systems*, Vol. 90, No. 6, p. 2785 to 2793.

REEVE, J. AND KRISHNAYYA, P.C.S. (1968), 'Unusual current harmonics arising from high voltage dc transmission', *IEEE Transactions on Power Apparatus and Systems*, Vol. PAS-87, No. 3, March, p. 883 to 893.

REEVE, J. AND SUBBA-RAO, T. (1973), 'Dynamic analysis of harmonic interaction between ac and dc power systems', *IEEE Transactions*, p. 640 to 646.

REEVE, J., BARON, J.A. AND KRISHNAYYA, P.C.S. (1969), 'A general approach to harmonic current generation by hvdc convertors', *IEEE Transactions on Power Apparatus and Systems*, Vol. PAS-88, No. 7, July, p. 989 to 995.

RICE, D. (1994), 'A detailed analysis of six-pulse converter harmonic currents', *IEEE Transactions on Industry Applications*, Vol. 30, No. 2, March, p. 294 to 304.

RITTEGER, J. AND KULICKE, B. (1995), 'Calculation of hvdc-converter harmonics in frequency domain with regard to asymmetries and comparison with time domain simulations', *IEEE winter meeting 95 WM 243-6 PWRD.*

SAKUI, M., FUJITA, H. AND SHIOYA, M. (1989), 'A method for calculating harmonic currents of a three phase bridge uncontrolled rectifier with dc filter', *IEEE Transactions on Industrial Electronics*, Vol. 36, No. 3, August, p. 434 to 440.

SEMLYEN, A., ACHA, E. AND ARRILLAGA, J. (1988), 'Newton-type algorithms for the harmonic phasor analysis of non-linear power circuits in periodical steady state with special reference to magnetic non-linearities', *IEEE Transactions on Power Delivery*, Vol. 3, No. 3, July, p. 1090 to 1097.

SHORE, N.L., ANDERSSON, G., CANELHAS, A. AND ASPLUND, G. (1989), 'A three pulse model of dc side harmonic flow in hvdc systems', *IEEE Transactions on Power Delivery*, Vol. 4, No. 3, July, p. 1945 to 1954.

SKELBOE, S. (1982), 'Time–Domain Steady–State Analysis of Nonlinear Electrical Systems', *Proceedings of the IEEE*, Vol. 70, No. 10, October, pp. 1210–1227.

SMITH, B., WATSON, N., WOOD, A. AND ARRILLAGA, J. (1995), 'A newton solution for the harmonic phasor analysis of ac/dc converters', *IEEE PES summer meeting 95 SM 379-8 PWRD.*

STEMMLER, H. (1987), 'Hvdc back to back interties on weak ac systems, second harmonic problems, analyses and solutions', *CIGRE Symposium*, Vol. 09-87, No. 300-08, p. 1 to 5.

SZECHTMAN, M., WEISS, T. AND THIO, C.V. (1991), 'First benchmark model for hvdc control studies.', *Electra*, No. 135, April, p. 55 to 75.

VALCÁRCEL, M. AND MAYORDOMO, J. (1993), 'Harmonic power flow for unbalanced systems', *IEEE PES winter meeting 93 WM 061-2 PWRD.*

WOOD, A.R. (1993), *An analysis of non-ideal HVdc convertor behaviour in the frequency domain, and a new control proposal*, PhD thesis, University of Canterbury, NZ.

WOOD, A.R. AND ARRILLAGA, J. (1994), 'The frequency dependent impedance of an hvdc converter', *ICHPs Conference, 21-24 sept. 1994, Bologna, Italy.*, September.

WOOD, A.R. AND ARRILLAGA, J. (1995a), 'Composite resonance; a circuit approach to the waveform distortion dynamics of an hvdc converter.', *IEEE Transactions on Power Delivery.*

WOOD, A.R. AND ARRILLAGA, J. (1995b), 'Hvdc convertor waveform distortion - a frequency domain analysis.', *IEE proceedings Pt C*, Vol. 142, No. 1, January, p. 88 to 96.

WOOD, A., SMITH, B. AND ARRILLAGA, J. (1995), 'The harmonic impedance of an hvdc converter', *6th European Conference on Power Electronics and Applications (EPE 95), Seville*, September, pp. 1039 – 44.

WOODFORD, D., GOLE, A. AND MENZIES, R. (1983), 'Digital simulation of dc links and ac machines', *IEEE Transactions on Power Apparatus and Systems*, Vol. PAS-102, No. 6, June, p. 1616 to 1623.

XIA, D. AND HEYDT, G. (1982), 'Harmonic power flow studies. part i and ii', *IEEE Transactions on Power Apparatus and Systems*, Vol. PAS 101, No. 6, pp. 1257–70.

XU, W., MARTI, J. AND DOMMEL, H. (1990), 'A multiphase harmonic load flow solution technique', *IEEE PES winter meeting 90 WM 098-4 PWRS.*

XU, W., DRAKOS, J., MANSOUR, Y. AND CHANG, A. (1994), 'A three phase converter model for harmonic analysis of hvdc systems', *IEEE Transactions on Power Delivery*, Vol. 9, No. 3, July, p. 1724 to 1731.

YACAMINI, R. AND DE OLIVEIRA, J.C. (1980), 'Harmonics in multiple convertor systems: a generalised approach.', *IEE Proceedings Pt.B*, Vol. 127, No. 2, March, p. 96 to 106.

YACAMINI, R. AND DE OLIVEIRA, J.C. (1986), 'Comprehensive calculation of convertor harmonics with system impedances and control representation', *IEE Proceedings Pt. B*, Vol. 133, No. 2, March, p. 95 to 102.

ZOLLENKOPF, K. (1970), 'Bi-factorisation–basic computational algorithm and programming techniques', In *Conference on Large Sets of Sparse Linear Equations*, Oxford.